BLM LIBRARY
88000715

PROJECT: AIR QUALITY TECHNICAL REPORT ON THE COSO GEOTHERMAL STUDY AREA

IN SUPPORT OF: COSO GEOTHERMAL DEVELOPMENT ENVIRONMENTAL STATEMENT

U.S. Department of the Interior
Bureau of Land Management
Bakersfield District Office
800 Truxtun Avenue, Room 311
Bakersfield, CA 93301

Rockwell International

Environmental Monitoring & Services Center
Environmental & Energy Systems Division
2421 West Hillcrest Drive
Newbury Park, CA 91320
(805) 498-6771

April 1980

Contract No. YA-512-CT8-216

TD
195
.E4
C67
1980
suppl.
1

88000715

TD
195
.E4
C67
1980
Suppl.
1

BLM Library
D-553A, Building 50
Denver Federal Center
P. O. Box 25047
Denver, CO 80225-0047

PROJECT: AIR QUALITY TECHNICAL REPORT ON THE COSO GEOTHERMAL STUDY AREA

IN SUPPORT OF: COSO GEOTHERMAL DEVELOPMENT ENVIRONMENTAL STATEMENT

U.S. Department of the Interior
Bureau of Land Management
Bakersfield District Office
800 Truxtun Avenue, Room 311
Bakersfield, CA 93301

Rockwell International

Environmental Monitoring & Services Center
Environmental & Energy Systems Division
2421 West Hillcrest Drive
Newbury Park, CA 91320
(805) 498-6771

April 1980

Contract No. YA-512-CT8-216

ACKNOWLEDGEMENTS

This report was prepared by the Environmental Monitoring & Services Center (EMSC). Major participants in the project are:

Project Management:	George Lauer
Air Quality:	Charles E. McDade L. Willard Richards
Climatology:	Brian Winkler Timothy Waldron

Throughout the project many organizations and individuals cooperated generously. We appreciate the contribution these people have made to this report. They include:

BLM, Riverside, Kevin Golden

California Air Resources Board, Ray Tuvell, Andi Ranzieri

U.S. Naval Weapons Center, Tom Dodson, Raymond Kelso, Dick Evert

TABLE OF CONTENTS

Page No.

1.0 ABSTRACT 1-1

2.0 EXECUTIVE SUMMARY. 2-1

3.0 INTRODUCTION 3-1

4.0 EXISTING AIR QUALITY 4-1

- 4.1 METEOROLOGICAL AND CLIMATOLOGICAL DATA. 4-1
- 4.2 AIR QUALITY DATA. 4-7
- 4.3 GOVERNMENT AIR QUALITY REGULATIONS. 4-14
- 4.4 FUGITIVE DUST 4-18

5.0 IMPACTS OF THE PROPOSED ACTION 5-1

- 5.1 EMISSIONS OF THE PROPOSED ACTION. 5-1
  - 5.1.1 Major Gaseous Emissions. 5-1
  - 5.1.2 Minor Emissions and Trace Elements 5-10
  - 5.1.3 Fugitive Dust. 5-10
- 5.2 ATMOSPHERIC DISPERSION MODEL DESCRIPTION. 5-16
- 5.3 AIR QUALITY IMPACT OF THE EMISSIONS 5-18
- 5.4 AIR QUALITY MONITORING PLAN 5-42
- 5.5 VISIBILITY IMPACT 5-44
  - 5.5.1 Visible Spectrum 5-44
  - 5.5.2 Infrared Spectrum. 5-46

6.0 MITIGATION MEASURES. 6-1

7.0 CONCLUSIONS. 7-1

8.0 REFERENCES 8-1

9.0 COSO GEOTHERMAL RESOURCE AREA CLIMATOLOGY. 9-1

- 9.1 GEOGRAPHICAL DESCRIPTION. 9-1
- 9.2 CLIMATOLOGICAL DESCRIPTION. 9-5
- 9.3 TEMPERATURE 9-6
- 9.4 PRECIPITATION 9-55
- 9.5 WINDS 9-78
- 9.6 SEVERE STORMS 9-95
- 9.7 CLIMATE IMPACTS 9-96

LIST OF TABLES

Table No.		Page No.
4.1.1	Coso Area Meteorological Stations	4-2
4.1.2	Seasonal Meteorological Groupings	4-5
4.1.3	Grouped Meteorological Conditions	4-6
4.2.1	Summary of Coso Air Quality Data	4-9
4.2.2	Major Point Emission Sources	4-11
4.2.3	Vehicle Emission Rates for US 395	4-13
4.3.1	Ambient Air Quality Standards	4-15
4.3.2	PSD Regulations	4-17
5.1.1.1	Hourly Average Vehicle Emissions and Locations	5-3
5.1.1.2	Exhaust Emissions During Exploratory Well Development	5-4
5.1.1.4	Exhaust Emissions from Worker Village	5-6
5.1.1.5	Power Plant Locations, Emissions, and Stack Parameters	5-7
5.1.1.6	Total Average Yearly Emissions	5-8
5.3.1	Stage 2 CO From Vehicles	5-19
5.3.2	Stage 2 CO From Exploratory Well Pad Grading	5-21
5.3.3	Stage 2 H_2S From Exploratory Well Flow Testing	5-23
5.3.4	Stage 4 H_2S From Power Plants	5-25
5.3.5	Stage 4 H_2O From Cooling Towers	5-27
5.3.6	Stage 2 Fugitive Dust From Vehicles	5-29
5.3.7	Stage 2 Fugitive Dust From Exploratory Well Past Drilling	5-31
5.3.8	Stage 4 Fugitive Dust From Wind Erosion of Exposed Areas	5-33
5.3.9	Maximum Gaseous Pollutant Concentrations	5-39

LIST OF TABLES

Table No.		Page No.
1	Coso Geothermal Resource Area	9-3
2	Temperature Differences Assuming an Adiabatic Lapse Rate	9-7
3	Monthly Temperature Normals and Extremes, °F, China Lake, California (1946-1976)	9-8
4	Monthly Temperature Extremes, °F, High Desert Stations, August 1977 - Sept. 1978	9-10
5	CGRA Daily Temperature Comparisons	9-11
6	Number of Days per Year the Maximum Temperature Exceed 90 °F or the Minimum Temperature is less than 32°F	9-26
7	Probability of Observing Given Temperatures After Spring Dates or before Fall Dates	9-27
8	Greatest Precipitation in 24 Hours	9-69
9	Mean Number of Days With Precipitation More Than 0.10 Inches	9-70
10	Mean Number of Days with Precipitation More Than 0.01 Inches	9-70
10a	Daily Comparative Rainfall Data for the Coso Geothermal Resource Area	9-72
11	Number of Days per Month per Station of Maximum Daily Rainfall	9-73
12	Data Points Used in the Exponential Curve Fit Equation for Projecting Snowfall Amounts in the CGRA	9-73
13	Projected Average Annual Snowfall Amounts for the CGRA	9-74
14	Mean Monthly Relative Humidity - China Lake (1946-1976)	9-74
15	Mean Number of Days Clear, Partly Cloudy, Cloudy	9-76
16	Prevailing Wind Direction and Mean Wind Speed	9-80
17	Pasquill Stability Classes	9-88
18	Mean Number of Thunderstorm Days, China Lake	9-97

LIST OF FIGURES

Figure No. Page No.

5.3.1 CO From Vehicles - Met Class H 5-20

5.3.2 Stage 2 - CO From Exploratory Well Pad Grading - Met Class J 5-22

5.3.3 H_2S From Exploratory Well Flow Testing - Met Class I 5-24

5.3.4 H_2S From Power Plants - Met Class B 5-26

5.3.5 Stage 4 - H_2O From Cooling Towers - Met Class E 5-28

5.3.6 Stage 2-Fugitive Dust From Vehicles - Met Class D 5-30

5.3.7 Stage 2 - Fugitive Dust From Exploratory Well Pad Drilling - Met Class G 5-32

5.3.8 Stage 4 - Fugitive Dust From Wind Erosion of Exposed Areas - Met Class F 5-34

5.3.9 IMPACT Results, Stage 4 - H_2S From Power Plants - Met Class B 5-38

Coso Geothermal Resource Area Climatology

LIST OF FIGURES

Figure No. Page No.

1 Southern California 9-2

2 Coso Geothermal Resource Area (CGRA) 9-4

3 A Daily Temperature Comparison 9-11A

4a Mean Annual Temperature 9-12

4b Mean January Temperature 9-13

4c Mean February Temperature 9-14

4d Mean March Temperature 9-15

4e Mean April Temperature 9-16

4f Mean May Temperature 9-17

4g Mean June Temperature 9-18

4h Mean July Temperature 9-19

LIST OF FIGURES (CONT.)

Figure No.		Page No.
4i	Mean August Temperature	9-20
4j	Mean September Temperature	9-21
4k	Mean October Temperature	9-22
4l	Mean November Temperature	9-23
4m	Mean December Temperature	9-24
5a	Annual Heating Degree Days Normals	9-29
5b	January Heating Degree Days Normals	9-30
5c	February Heating Degree Days Normals	9-31
5d	March Heating Degree Days Normals	9-32
5e	April Heating Degree Days Normals	9-33
5f	May Heating Degree Days Normals	9-34
5g	June Heating Degree Days Normals	9-35
5h	July Heating Degree Days Normals	9-36
5i	August Heating Degree Days Normals	9-37
5j	September Heating Degree Days Normals	9-38
5k	October Heating Degree Days Normals	9-39
5l	November Heating Degree Days Normals	9-40
5m	December Heating Degree Days Normals	9-41
6a	Annual Cooling Degree Days Normals	9-42
6b	January Cooling Degree Days Normals	9-43
6c	February Cooling Degree Days Normals	9-44
6d	March Cooling Degree Days Normals	9-45
6e	April Cooling Degree Days Normals	9-46
6f	May Cooling Degree Days Normals	9-47
6g	June Cooling Degree Days Normals	9-48
6h	July Cooling Degree Days Normals	9-49

LIST OF FIGURES (CONT.)

Figure No.		Page No.
6i	August Cooling Degree Days Normals	9-50
6j	September Cooling Degree Days Normals	9-51
6k	October Cooling Degree Days Normals	9-52
6l	November Cooling Degree Days Normals	9-53
6m	December Cooling Degree Days Normals	9-54
7a	Average Annual Precipitation	9-56
7b	Average January Precipitation	9-57
7c	Average February Precipitation	9-58
7d	Average March Precipitation	9-59
7e	Average April Precipitation	9-60
7f	Average May Precipitation	9-61
7g	Average June Precipitation	9-62
7h	Average July Precipitation	9-63
7i	Average August Precipitation	9-64
7j	Average September Precipitation	9-65
7k	Average October Precipitation	9-66
7l	Average November Precipitation	9-67
7m	Average December Precipitation	9-68
8	Lake Evaporation	9-77
9	Annual Wind Roses	9-79
10a	Wind Roses August 1978 Hours 01-24	9-81
10b	Wind Roses August 1978 Hours 01-06	9-82
10c	Wind Roses August 1978 Hours 07-12	9-83
10d	Wind Roses August 1978 Hours 13-18	9-84
10e	Wind Roses August 1978 Hours 19-24	9-85

LIST OF FIGURES (CONT.)

Figure No.		Page No.
11	China Lake Annual Wind Rose	9-87
12a	Annual Wind Rose, Stability Class A	9-87
12b	Annual Wind Rose, Stability Class B	9-90
12c	Annual Wind Rose, Stability Class C	9-91
12d	Annual Wind Rose, Stability Class D	9-92
12e	Annual Wind Rose, Stability Class E	9-93
12f	Annual Wind Rose, Stability Class F	9-94

1.0 ABSTRACT

An air quality analysis is performed to assess the impacts of a proposed geothermal power development at the Coso KGRA, California. The present air quality and meteorology are discussed, and a summary of the historical data base is presented. The atmospheric dispersion model RAMR is used to estimate the air quality impacts of both gaseous pollutants (primarily H_2S) and fugitive dust. The effects upon visibility in the visible spectrum as well as in the infrared spectrum are discussed. An air quality monitoring plan is outlined, and a number of mitigation measures are presented.

2.0 EXECUTIVE SUMMARY

The climate of the Coso KGRA is typical of the California high desert. Specific local meteorological conditions, however, tend to differ somewhat from those of the surrounding area. In particular, the prevailing wind direction at Coso tends to be north-northwest or south-southeast (depending upon the season and the time of day), whereas at China Lake it is southwest. Whenever possible in this analysis, local meteorological data from Coso were used in preference to those from China Lake.

From recent source sampling data, it can be concluded that the present air quality in the KGRA is generally quite good, again typical of a non-industrialized desert environment. Visibility is also very good, averaging about 60 miles. The only significant exception is a high ambient H_2S level near some natural fumaroles and old drill holes at Devil's Kitchen. This is, however, a localized problem, not typical of the KGRA as a whole.

The emissions of the proposed geothermal development can be estimated on the basis of the Proposed Action (Chapter One of the Coso Geothermal EIS). Gaseous emissions can come from vehicle and equipment exhausts, well flow testing, and power plant operation. The most prevalent species should be H_2O, CO_2, and H_2S; trace amounts of mercury and other metals may also be present. Fugitive dust can be produced by vehicle traffic on roadways, grading and construction activities, and wind erosion of exposed areas.

Ambient levels of the pollutants of interest have been calculated using the atmospheric dispersion model RAMR. This Gaussian model is one of the UNAMAP series of EPA-approved models, and is particularly suited to multiple point and area sources with multiple receptors under rural dispersion conditions. Meteorological conditions were grouped into 13 separate categories as inputs to the model.

Maximum concentrations of most pollutants were found not to exceed state or Federal air quality standards under most conditions. An exception was

H_2S, which could exceed the state standard in a localized area if new well flow testing were conducted concurrently with full power plant development with wind speeds greater than 5 miles per hour. Also, fugitive dust levels could exceed both state and Federal suspended particulate matter standards under certain conditions.

An air quality monitoring plan is outlined which would check ambient concentrations of both H_2S and total suspended particulate. To correspond with the predicted locations of most probable maximum concentrations, the monitors should be placed approximately 0.5 km and 1.0 km, respectively, downwind of the emission sources, the direction to be determined by the prevailing wind directions. Costs must be considered in designing this system.

H_2S in itself should have no measurable effect upon visibility, but H_2S can be converted in the atmosphere to SO_2 which can undergo further reaction to form sulfate aerosol, an effective visibility-reducing species. The H_2S-to-sulfate conversion half-life is approximately one day under normal atmospheric conditions, so any visibility reduction should be a regional phenomenon due to the dispersion that can occur during this time. Since RAMR is not a regional model, only an upper limit to visibility degradation can be calculated. This upper limit is 10% for H_2S (sulfate), and 16% for fugitive dust, whose effect should be more localized due to lack of long-range transport. Visibility reduction in the infrared as a result of elevated ambient levels of CO_2 and H_2O should be minimal.

The air quality impacts of geothermal development can be reduced to meet government standards by appropriate mitigation measures. Flow testing only during light winds will help to reduce maximum ambient hydrogen sulfide concentrations, while fugitive dust can be mitigated by watering roads and construction sites, graveling exposed area, and reducing traffic on unpaved roads by transporting workers in buses.

3.0 INTRODUCTION

In terms of air quality impacts, the public tends to perceive geothermal development as a clean source of energy. As a relative judgment, this perception is probably not unsound. Many other forms of energy production, such as coal-fired power plants, have been found to have more serious air pollution problems. Nevertheless, there are several potential air quality impacts associated with geothermal systems. This report will address those impacts that can be expected from the proposed geothermal power development at the Coso Known Geothermal Resource Area (KGRA) in Inyo County, California.

There is a great deal of variability worldwide in the chemical composition and source strength of geothermal resources. Thus, one cannot simply extrapolate emission rates from a developed KGRA such as the Geysers, for example, to an undeveloped area such as Coso. In order to provide an analysis which is site-specific for Coso, a number of geologic and hydrologic investigations have been undertaken to characterize the geothermal resource. In addition, an engineering analysis was performed to predict the most likely scenario for energy production. These analyses formed the basis for the pollutant emission predictions in the Proposed Action (Chapter One of the Coso Geothermal EIS). These emission predictions have, in turn, been used as the basis for this report.

In addition to being site-specific in terms of emission rates, the air quality analysis also considers the local meteorology of the Coso KGRA. The study area is located at the eastern base of the Sierra Nevada, between the Owens and Indian Wells Valleys, so it experiences meteorological conditions which can be quite different from those found only 10 or 20 miles away. Thus, local meteorological data were used in this analysis whenever possible. A complete meteorological analysis is included as a separate section of this report.

4.0 EXISTING AIR QUALITY

4.1 METEOROLOGICAL AND CLIMATOLOGICAL DATA

In order to quantitate the sensitivity of an area to air quality degradation, it is necessary to characterize the local meteorology as fully as possible. There are two climatological data bases available for the Coso area. The first is the historical data base compiled by the U.S. Navy at China Lake since the 1940's. These data include wind speed and direction, temperature, precipitation, cloud cover, and air density at China Lake, as well as upper air rawinsonde data on a somewhat irregular basis from Tower 8, which is eight miles northwest of China Lake in Indian Wells Valley. In addition, Pasquill stability classes have been calculated by the National Climatic Center through the STAR program. The second available data base was compiled since August 1977, based on observations at seven meteorological stations either within or adjacent to the Coso KGRA study area. The station locations are listed in Table 4.1.1. These data were collected by the China Lake NWC staff, and include wind speed and direction, precipitation, and temperature. In addition, an acoustic radar system was operated at Rose Valley Ranch during January, February, and March 1979. The acoustic radar data were collected by Aerovironment under contract to the U.S. Navy, and provided a value for the base and top of the lowest inversion, with an upper limit of 1000 meters.

The weather at Coso is not always comparable to that at China Lake. Coso tends to have more cloud cover and overcast conditions than does China Lake, as well as more days with thin, high clouds. Temperatures are generally lower at Coso that at China Lake, particularly at the higher elevations such as Upper Cactus Flat, and there is more snowfall. Perhaps most important, from an air quality standpoint, is the fact that the prevailing wind direction differs at the two sites. China Lake's prevailing wind is from the southwest, whereas the prevailing wind at Coso is either from the south-southeast or from the north-northwest, depending upon the season and the time of day.

Table 4.1.1

Coso Area Meteorological Stations

Station Name	Station Location
Rose Valley Ranch	R37E, T21S, Section 26
Coso Basin	R39E, T22S, Section 10
Red Hill	R38E, T22S, Section 34
Little Lake	R38E, T23S, Section 17
Airport Lake	R39E, T23S, Section 22
Upper Cactus Flat	R39E, T21S, Section 7
Haiwee Reservoir	R37E, T21S, Section 2

For these reasons, meteorological data from Coso were used in this study in preference to those from China Lake wherever possible. Exceptions to this were mixing height, for which only the previously mentioned limited data were available at Coso, and Pasquill stability category, which has never been calculated for Coso. These two parameters were, by necessity, extrapolated from China Lake data.

The meteorological parameters of greatest interest in this air quality analysis are those which are required inputs to RAMR, the EPA-approved atmospheric dispersion model being utilized here. These required inputs are wind speed, wind direction, ambient air temperature, mixing height, and Pasquill stability class. RAMR calculates short term averages (1 hour to 24 hours) of pollutant concentrations and, in an area with a complete meteorological data base, would typically be used to perform a calculation for each hour of a given year based on actual hourly measurements, resulting in a concentration frequency distribution. However, in a region such as Coso which lacks such complete hourly data, it is necessary to construct synthesized typical and extreme meteorological conditions based upon the data available. These synthesized values are then used as dispersion model inputs, and the concentration frequency can be estimated by considering the probability of occurrence of a given synthesized meteorological condition.

Synthesized values for wind speed, wind direction, and temperature were obtained by analysis of the Coso area data collected by the Navy since 1977. For each of the four seasons, data were separated into night (sunset to sunrise), morning (sunrise to approximately three hours after sunrise), and midday (approximately three hours after sunrise to sunset) categories. For each of these categories the data were analyzed to yield typical (average) wind and temperature conditions, as well as high-wind and low-wind extremes. Mixing height and stability class values are largely unavailable for the Coso area, so these parameters were estimated by using the China Lake values observed under similar wind and temperature conditions. The Rose Valley acoustic radar results were utilized, however, during winter periods to estimate mixing height by assuming the inversion base height to be the mixing height. Since RAMR allows only one value of each parameter for an entire region, the synthesized meteorological conditions were constructed primarily for the Coso Hot Springs-Devil's Kitchen area because this is where geothermal development is most likely to occur. Thus, for example, a shallow, ground-based inversion in Rose Valley would not be reflected in these synthesized models because all geothermal emission at Coso Basin would occur above the top of the inversion.

It was found that certain periods could be grouped according to similar meteorological conditions; the 13 groups chosen are shown in Table 4.1.2. The corresponding meteorological conditions are shown in Table 4.1.3. In this table, wind direction is shown in degrees clockwise from the north, the Pasquill stability class is shown as A through F (Turner, 1970), and a ground-based inversion is represented by a mixing height of zero. Wind speed and direction, stability class, and mixing height were the most important factors in choosing the groupings, since the dispersion models are only weakly dependent upon ambient temperature.

It should be noted that RAMR uses a mixing height of zero to represent a ground-based inversion for categories A and B. This is a worst-case estimate and thus results in conservative concentration values. It should be further noted that category B uses F stability with a wind speed of

1 m/sec. This combination is not explicitly listed by Turner (1970), but is nevertheless included as a valid possibility in the RAMR preprocessor (Turner and Novak, 1978).

Categories K, L, and M are special cases which occur rarely but, nevertheless, deserve special attention due to their severity. Category K represents what is known as an Owens Lake Dust Storm. This is characterized by very strong north winds which carry dust from the Owens Lake bed over the Coso Range and into Indian Wells Valley, commonly resulting in markedly decreased visibility. This condition might occur up to a dozen times a year, usually in the winter or spring. Category L is a Sierra Nevada Downdraft, again characterized by strong winds but from the west rather than from the north. This also occurs only a few days per year. Category M represents relatively calm, overcast conditions, and can occur during either day or night. This category is somewhat rare in the desert since overcast conditions are usually associated with frontal systems and their accompanying moderate to strong winds. Calm overcasts can occur, however, and are included here particularly because they can cause adverse air pollution episodes.

Completely calm conditions were not included in any of these synthesized meteorological categories because, as previously mentioned, these parameters were intended to be used as inputs to the atmospheric dispersion models. Since the dispersion calculations include division by the wind speed, a value of zero in the denominator is clearly unacceptable. Thus, a wind speed of 1 meter $\sec^{-1}$ in the prevailing wind direction is used to represent essentially calm conditions.

Table 4.1.2

Seasonal Meteorological Groupings

A - Night, year round, typical
B - Night, year round, low-wind extreme
C - Night, year round, high-wind extreme
D - Morning, winter, typical
E - Morning, year round, low-wind extreme
F - Morning, winter, high-wind extreme
Morning, spring, high-wind extreme
Morning, fall, high-wind extreme
G - Morning, spring, typical
Morning, summer, typical
Morning, fall, typical
H - Midday, year round, typical
I - Midday, year round, low-wind extreme
J - Midday, year round, high-wind extreme
Morning, summer, high-wind extreme
K - Owens Lake Dust Storm
L - Sierra Nevada Downdraft
M - Low-wind overcast (day or night)

Table 4.1.3

Grouped Meteorological Conditions

Group (see Table 4.1.2)	$T(^{o}K)$	Wind Speed (m/sec)	Wind Direction (deg)	Stability Class	Mixing Height (m)
A	280	2	NNW, 337.5	F	0
B	280	1	NNW, 337.5	F	0
C	280	7	NW, 315	D	200
D	280	2	NNW, 337.5	B	75
E	286	1	NNW, 337.5	B	100
F	283	8	NW, 315	D	2500
G	289	4	SSE, 157.5	C	100
H	297	4	SSE, 157.5	B	3000
I	302	1	NNW, 337.5	A	3000
J	291	7	SSE, 157.5	D	3000
K	289	22	N, 0	D	3000
L	289	22	W, 270	D	3000
M	283	1	NNW, 337.5	D	225

4.2 AIR QUALITY DATA

An analysis of the current air quality in the Coso area is a necesary step in predicting the effects of the proposed geothermal development. As the following data will show, the Coso air quality is quite good, being largely typical of the sparsely populated, nonindustrialized areas of the desert southwest. There are few man-made emission sources in the area, and the only natural source that distinguishes Coso from typical desert is the hydrogen sulfide-producing fumarole system in the Devil's Kitchen-Coso Basin area. A growing problem in recent years throughout the California desert has been the influx of photochemical smog from the Los Angeles and San Joaquin Valley areas, particularly during the summer months (Lester and Simon, 1978). This problem is still quite rare in the Coso area, however, because of the distance from major smog-producing areas and because the particular wind conditions required to produce the effect do not occur often. For Los Angeles smog to penetrate the Coso area, for example, the wind must be from the south to southeast, and must be persistent enough to blow the smog up from Los Angeles, yet not so strong (greater than about 5 m/sec) that the smog is funnelled past Coso into the Owens Lake area.

As with meteorological data, air quality data are available at both Coso and China Lake. Long term averages for ozone, light scattering extinction (B_{scat}), and total suspended particulate (TSP) have been compiled at China Lake. Average winter ozone values ranged between 2 and 4 pphm, and average summer ozone values ranged between 4 and 6 pphm, with a peak instantaneous value of 15 pphm and a peak hourly average of 13 pphm. Average B_{scat} over a three year period was approximately 0.4 (10^{-4} m^{-1}), and the latest annual geometric mean (1977) TSP value was 51.3 $\mu g/m^3$.

It is, however, preferable to use air quality data for Coso rather than for China Lake whenever possible, due to the differences in the meteorology and emissions sources between the two areas. The China Lake NWC staff conducted a monitoring program at several locations in the Coso area from August 1977 to May 1978. They measured CO_2, ozone, hydrogen sulfide, total sulfur, and B_{scat}, as well as ambient temperature and dew point. Sampling periods at each site were relatively brief (several weeks each), and the wetter-than-normal winter may have resulted in better air quality than one might find over a sampling period of several years. Nevertheless, the NWC data are the only values available for the Coso area, and will thus be considered representative, keeping in mind the above restrictions. The data are summarized in Table 4.2.1, with the locations of the monitoring stations listed at the end of the table.

Clearly, most of the values listed in Table 4.2.1 lie within the range that one would expect for a nonindustrialized desert region. The major exception is the H_2S concentration at Devil's Kitchen. The average value is over two-thirds of the state standard one-hour average of 30 ppb, and the peak hourly average is almost five times the state standard. Devil's Kitchen is a narrow canyon area with a number of fumaroles, drill holes, and old wells, all of which are potential sources of H_2S. The monitor was located only about 50 feet from the H_2S source, and this, combined with very localized topographical and meteorological effects, seems to account for the high readings at Devil's Kitchen. Excessive ambient H_2S is limited to a small area immediately surrounding Devil's Kitchen. The only other station to record even a trace of H_2S was Coso Resort, which also experiences intermittent fumarole activity within a quarter mile of the monitor.

It is instructive to consider B_{scat} in terms of actual visual range. The Koschmieder formulation (Middleton, 1952) expresses visibility in terms of B_{scat}:

$$V = \frac{24.3}{B_{scat}} \quad ,$$

where V is the visual range in miles and B_{scat} is in units ($10^{-4} m^{-1}$). Referring to Table 4.2.1, this yields a maximum long term average visibility of 90 miles (Coso Resort, 3/78-4/78), and a minimum hourly average visibility of nine miles (Coso Basin). These results indicate generally excellent visibility, with even the lowest long term average visibility being over 50 miles

Table 4.2.1

Summary of Coso Air Quality Data

Species/Location/ Sampling Period	Average Concentration	Peak Hourly Average
CO_2 (ppm)		
Rose Valley Ranch, 9/77	354	380
Coso Basin, 9/77-1/78	346	390
Coso Resort, 2/78-4/78	335	360
Devil's Kitchen, 4/78-5/78	345	370
Ozone (pphm)		
Rose Valley Ranch, 8/77-9/77	4.0	8.0
Coso Basin, 9/77-12/77	3.6	9.0
Coso Resort, 1/78-4/78	3.0	8.0
Devil's Kitchen, 4/78-5/78	4.3	8.0
H_2S (ppb)		
Rose Valley Ranch, 8/77-9/77	0	-
Coso Basin, 10/77	0	-
Coso Resort, 11/77-4/78	0	T
Devil's Kitchen, 4/78-5/78	22	140
Total Sulfur (ppm)		
Rose Valley Ranch, 8/77-9/77	0	-
Coso Basin, 9/77-1/78	T	T
Coso Resort, 2/78-4/78	T	T
Devil's Kitchen, 4/78-5/78	T	0.01
B_{scat} ($\times 10^{-4}$ m^{-1})		
Rose Valley Ranch, 8/77-9/77	0.46	1.40
Coso Basin, 9/77-1/78	0.38	2.65
Coso Resort, 3/78-4/78	0.27	1.40
Devil's Kitchen, 4/78-5/78	0.35	0.80

Station Name	Station Location
Rose Valley Ranch	R37E, T21S, Section 26
Coso Basin	R39E, T22S, Section 10
Coso Resort	R39E, T22S, Section 4
Devil's Kitchen	R39E, T22S, Section 7

(Rose Valley Ranch, 8/77-9/77). It must be cautioned, however, that the Koschmieder formula gives merely an estimated visibility. There is obvious theoretical difficulty in using a point measurement such as B_{scat} to calculate a visual range which may extend up to 90 miles. The value will be exact only if B_{scat} does not vary over the entire visual range.

Although a full range of pollutants such as CO, NO_x, and hydrocarbons (HC) was not measured during the Navy study in the Coso area, ozone is generally considered to be a reasonable indicator of the presence of photochemical smog. The average ozone concentrations were all quite low (only one peak hourly average (Coso Basin) exceeded the old Federal one-hour average standard of 8 pphm). Thus, photochemical smog appears to be, at worst, a minor problem in the Coso area, even at Rose Valley Ranch, which is adjacent to U.S. 395, the only major automobile thoroughfare in the study area.

In attempting to understand the present air quality at Coso, it is useful to consider the major emission sources in the region. The California Air Resources Board (CARB) has surveyed all major point sources in the state (greater than 25 tons per year emissions) through the Emission Inventory Subsystem (EIS). All such point sources in the Coso region are listed in Table 4.2.2, as derived from the EIS Summary of October 16, 1978. The date listed in Table 4.2.2 is the Julian date on which the emissions for each individual source were quantified. Discussions with local air pollution officials revealed that the EIS data are the latest available and that all are valid with the possible exception of the two Kerr-McGee plants in the Trona area. Kerr-McGee has been undergoing expansion during the past several months, and present emissions could be somewhat larger than those listed in Table 4.2.2. Nevertheless, emissions from Kerr-McGee should seldom be a problem at Coso since the prevailing southwest wind at Ridgecrest usually traps the Kerr-McGee emissions in Searles Valley around Trona.

Both the Southern Pacific Railroad and U.S. 395 traverse the study area for about eight miles. Rail traffic is light, but the highway provides a major emission source within the KGRA. According to Caltrans statistics, the

Table 4.2.2

Major Point Emission Sources

Organization	Location	Date	Particulate	SO_2	NO_2	HC	CO
			Tons/year (lbs/hour)				
Big Pine Distributors	Olancha	77088	25 (5.7)		1 (0.2)		
Louisiana Pacific	Inyokern	77098	3 (0.7)	4 (0.9)	26 (5.9)	14 (3.2)	27 (6.2)
Asphalt Construction Co.	Ridgecrest	77173	101 (23.1)	28 (6.4)	14 (3.2)	2 (0.5)	2 (0.5)
NWC	China Lake	78213	7 (1.6)	44 (10.0)	29 (6.6)		6 (1.4)
Kerr-McGee	Trona	77032	425 (97.0)	737 (168)	3905 (892)	79 (18.0)	772 (176)
Kerr-McGee	So. Trona	77074	20 (4.6)	6 (1.4)	229 (52.3)	8 (1.8)	190 (43.4)

average traffic volume along U.S. 395 is 4200 vehicles per day, with a peak volume of 7600 vehicles per day occurring on summer weekends. Using the national average vehicle mix emission factors in Table 3.1.1.1 of EPA Publication AP-42 (EPA, 1977) gives the emission rates listed in Table 4.2.3 for U.S. 395. Due to stricter pollution control standards, emission rates for cars registered in California are slightly lower than the national average rates. Nevertheless, national average values were used here because they are more conservative than the California values, particularly considering that many of the cars in the KGRA belong to transients who are residents of other states.

The Southern Pacific Railroad operates three round-trips per week with one 3600 hoursepower locomotive between Mojave and Lone Pine. The emission rates for this type of equipment, according to Table 3.2.2-2 in AP-42, are: CO 26.2 lb/hr, NO_x 73.0 lb/hr, and hydrocarbons 18.3 lb/hr. The resulting yearly values for the Coso area are: CO 0.8 tons/yr, NO_x 2.3 tons/yr, and hydrocarbons 0.6 tons/yr.

A limited number of vheicles travel on the secondary roads in the Coso area. Naval operations require vehicles to drive to the Coso Basin area, and civilian cars and trucks travel to the pumice mines to the northwest of Cactus Peak. Traffic patterns in both areas are sporadic, and in any case do not account for more than a few cars per day, 20 or less as a general rule. The emissions from these vehicles are essentially insignificant compared to the U.S. 395 emissions.

It is impossible to calculate exactly the emissions from aircraft in the Coso area since flight patterns are not strictly controlled as are automobile and railroad routes. Nevertheless, one can calculate the contribution of military aircraft to the entire China Lake region by considering the traffic volume at Armitage Field, NWC. In 1971, there were 36,680 takeoffs and landings, of which 29,088 were jet operations (Ouimette, 1974). Again, using AP-42 emission factors yields the average emission rates listed in Table 4.2.4. The effective emission rates for Coso are probably much lower than these values since no takeoffs or landings occur in the Coso area, and less than 10% of all flights originating at Armitage Field fly over Coso.

Table 4.2.5 presents the total yearly KGRA emission rate for each pollutant discussed in this section. Each value represents the complete contribution within the study area from highway traffic, railroads, and aircraft. Stationary sources from Table 4.2.2 are not included because none are located within the study area. Only 10% of the aircraft values from Table 4.2.4 are included here to account for the flight patterns in the region.

In addition to all of the emission sources that have been discussed in this section, there are also several existing fugitive dust sources in the Coso study area. The most readily quantifiable source is U.S. 395. The average emission rate for dust entrainment from paved roadways has been shown (EPA, 1978) to be 0.012 lb/vehicle mile. Considering the average traffic volume and the length of U.S. 395 within the KGRA, this yields a yearly average fugitive dust emission rate of 74 tons/year (or 403 lb/day) for the study area. Other fugitive dust sources include the alfalfa ranch in Rose Valley, the pumice mines north of Devil's Kitchen, limited vehicle traffic on dirt roads within the KGRA, and wind erosion of exposed areas; these dust sources tend to be intermittent and/or seasonal.

Table 4.2.3

Vehicle Emission Rates for U.S. 395

Pollutant	Average Emission Rate Tons/year	(lb/mile day)	Peak Emission Rate (lb/mile day)
CO	403	(276)	499
Hydrocarbons	63.5	(43.5)	78.7
NO_x	108	(74.1)	134
Particulate	8.6	(5.6)	10.1
SO_x	3.1	(2.1)	3.9

Table 4.2.4

Aircraft Emission Rates for China Lake

Pollutant	Average Emission Rate Tons/year	(lb/day)
CO	760	(4164)
Hydrocarbons	270	(1480)
NO_x	38.0	(208)
Particulate	90.0	(493)
SO_x	15.0	(82.0)

Table 4.2.5

Total KGRA Emission Rates

Pollutant	Emission Rate Tons/Year
CO	480
Hydrocarbons	92
NO_x	148
Particulate	99
SO_x	18

4.3 GOVERNMENT AIR QUALITY REGULATIONS

The Federal and State of California ambient air quality standards are listed in Table 4.3.1 (CARB, 1977a). The most important of these in terms of geothermal development is hydrogen sulfide, which has a state standard of 30 ppb (42 $\mu g/m^3$). It should be noted that the Federal ozone standard was recently changed from 0.08 to 0.12 ppm.

In addtion to the standards mentioned above, the 1977 Clean Air Act Amendments (PL95-95, November 1977, Part C) specify prevention of significant deterioration (PSD) regulations to insure preservation of current air quality in sensitive areas. According to the regulations, all areas are placed in one of three classes. In Class I areas, only very limited air quality degradation is permitted. In Class II areas, moderate deterioration is allowed in line with somewhat limited growth. Class III regulations specify very liberal allowed increments. In all cases, the total pollutant concentration must not exceed the Federal and state standards listed in Table 4.3.1. Specific allowed increments for particulate matter and sulfur dioxide for each class are listed in the PSD regulations; these are shown in Table 4.3.2. The State of California has been developing a similar plan called the Air Conservation Program (ACP) (CARB, 1977b). This plan would specify four classes (A through D) which would regulate particulate matter and SO_2. Eventually both the Federal PSD and State ACP regulations will regulate all pollutants for which standards have been set (see Table 4.3.1).

The Coso study area currently has a Class II designation, although it is possible that it may be reclassified Class I at some future date. Of the nearby National Park Service lands, Death Valley National Monument carries a Class II designation; both Sequoia and Kings Canyon National Parks are Class I. The closest Class I area to the study area is Domeland Wilderness Area in Sequoia National Forest, approximately 25 miles west-southwest of Coso Basin. Domeland will be considered in more detail in the visibility section.

Table 4.3.1

AMBIENT AIR QUALITY STANDARDS

Pollutant	Averaging Time	California Standards[1]		National Standards[2]		
		Concentration[3]	Method.[4]	Primary[3,5]	Secondary[3,6]	Method[7]
Oxidant (Ozone)	1 hour	0.10 ppm (200 ug/m^3)	Ultraviolet Photometry	160 ug/m^3 (0.08 ppm)	Same as Primary Std.	Chemiluminescent Method
Carbon Monoxide	12 hour	10 ppm (11 mg/m^3)	Non-Dispersive Infrared Spectroscopy	—	Same as Primary Standards	Non-Dispersive Infrared Spectroscopy
	8 hour	—		10 mg/m^3 (9 ppm)		
	1 hour	40 ppm (46 mg/m^3)		40 mg/m^3 (35 ppm)		
Nitrogen Dioxide	Annual Average	—	Saltzman Method	100 ug/m^3 (0.05 ppm)	Same as Primary Standards	Proposed: Modified J-H Saltzman (O_3 corr.) Chemiluminescent
	1 hour	0.25 ppm (470 ug/m^3)		—		
Sulfur Dioxide	Annual Average	—	Conductimetric Method	80 ug/m^3 (0.03 ppm)	—	Pararosaniline Method
	24 hour	0.05 ppm (131 ug/m^3)[9]		365 ug/m^3 (0.14 ppm)	—	
	3 hour	—		—	1300 ug/m^3 (0.5 ppm)	
	1 hour	0.5 ppm (1310 ug/m^3)		—	—	
Suspended Particulate Matter	Annual Geometric Mean	60 ug/m^3	High Volume Sampling	75 ug/m^3	60 ug/m^3	High Volume Sampling
	24 hour	100 ug/m^3		260 ug/m^3	150 ug/m^3	
Sulfates	24 hour	25 ug/m^3	AIHL Method No. 61	—	—	—
Lead	30 Day Average	1.5 ug/m^3	AIHL Method No. 54	—	—	—
Hydrogen Sulfide	1 hour	0.03 ppm (42 ug/m^3)	Cadmium Hydroxide Stractan Method	—	—	—
Hydrocarbons (Corrected for Methane)	3 hour (6-9 a.m.)	—	—	160 ug/m^3 (0.24 ppm)	Same as Primary Standards	Flame Ionization Detection Using Gas Chromatography
Ethylene	8 hour	0.1 ppm	—	—	—	—
	1 hour	0.5 ppm				
Visibility Reducing Particles	1 observation	In sufficient amount to reduce the prevailing visibility to less than 10 miles when the relative humidity is less than 70%	(8)	—	—	—
APPLICABLE ONLY IN THE LAKE TAHOE AIR BASIN:						
Carbon Monoxide	8 hour	6 ppm (7 mg/m^3)	NDIR	—	—	—
Visibility Reducing Particles	1 observation	In sufficient amount to reduce the prevailing visibility to less than 30 miles when the relative humidity is less than 70%	(8)	—	—	—

Table 4.3.1 (continued)

NOTES:

1. California standards are values that are not to be equaled or exceeded.

2. National standards, other than those based on annual averages or annual geometric means, are not to be exceeded more than once per year.

3. Concentration expressed first in units in which it was promulgated. Equivalent units given in parentheses are based upon a reference temperature of 25°C and a reference pressure of 760 mm of mercury. All measurements of air quality are to be corrected to a reference temperature of 25°C and a reference pressure of 760 mm of Hg (1,013.2 millibar); ppm in this table refers to ppm by volume, or micromoles of pollutant per mole of gas.

4. Any equivalent procedure which can be shown to the satisfaction of the Air Resources Board to give equivalent results at or near the level of the air quality standard may be used.

5. National Primary Standards: The levels of air quality necessary, with an adequate margin of safety, to protect the public health. Each state must attain the primary standards no later than three years after that state's implementation plan is approved by the Environmental Protection Agency (EPA).

6. National Secondary Standards: The levels of air quality necessary to protect the public welfare from any known or anticipated adverse effects of a pollutant. Each state must attain the secondary standards within a "reasonable time" after implementation plan is approved by the EPA.

7. Reference method as described by the EPA. An "equivalent method" of measurement may be used but must have a "consistent relationship to the reference method" and must be approved by the EPA.

8. Prevailing visibility is defined as the greatest visibility which is attained or surpassed around at least half of the horizon circle, but not necessarily in continuous sectors.

9. At locations where the state standards for oxidant and/or suspended particulate matter are violated. Federal standards apply elsewhere.

Table 4.3.2
PSD Regulations

Pollutant	Maximum Allowable Increase ($\mu g/m^3$) Class I	Class II	Class III
Particulate Matter:			
Annual geometric mean	5	19	37
24-hour maximum	10	37	75
Sulfur Dioxide:			
Annual arithmetic mean	2	20	40
24-hour maximum	5	91	182
3-hour maximum	25	512	700

4.4 FUGITIVE DUST

Fugitive dust can affect both visibility and public health, and there is a potential for particulate standard exceedance in most arid regions. Lack of abundant rainfall means that the soil will be dry a great portion of time, so dust can be resuspended either by wind erosion or by mechanical turbulence such as automobile traffic. The wind speed threshold for wind erosion of exposed areas is 4.5 m/sec (12 miles/hr) (Bohn, Cuscino, and Cowherd, 1978), which is higher than the average wind speed for both Coso and China Lake. Thus, automobile traffic and other mechanical processes such as road grading are the major contributors to the fugitive dust problem much of the time. Fugitive dust emission factors will be dealt with quantitatively in Section 5.1.3.

The most recent (1977) annual geometric mean TSP value of 51.3 $\mu g/m^3$ for China Lake can be considered to be a reasonable upper limit to the mean fugitive dust concentration. Even though they do not normally constitute a major fraction of the number of atmospheric particles, the relatively large dust particles contribute greatly to the total particulate weight. The 1977 geometric mean falls below both the Federal and State standards listed in Table 4.3.1, so fugitive dust is not a severe problem in Indian Wells Valley. It can be assumed that it is even less of a problem in the Coso area since there are fewer roads and traffic is much lighter.

A drastic divergence from the normally occurring fugitive dust levels at China Lake is the case of the Owens Lake Dust Storm, which might occur up to a dozen times a year. Strong winds of 50 miles per hour or more flow in from the north, carrying with them tremendous quantities of dust from the dry bed of Owens Lake. During such episodes, TSP concentrations have been estimated to be well over 1000 $\mu g/m^3$ (Reinking, Mathews, and St.-Amand, 1975), and visibility can decrease to less than one mile. The dust can extend over an area as large as 3500 square miles (NWC, 1978), encompassing both the Coso and Indian Wells Valley areas.

5.0 IMPACTS OF THE PROPOSED ACTION

This chapter will address the projected air quality impacts if geothermal power production is developed at Coso. Estimates of the probable emissions will be presented, followed by a description of the atmospheric dispersion model used to determine the impacts of these emissions. Next, the numerical results of the model will be tabulated and discussed, with particular emphasis on visibility and on the air quality sensitivity of the Coso area. Finally, recommendation for an air quality monitoring plan will be outlined.

5.1 EMISSIONS OF THE PROPOSED ACTION

Due to the complexity of the geothermal development scenario (as will soon become apparent) only one set of emission rates will be presented here. These will be the most probable projections, and will be based upon the development model of the Proposed Action section (Chapter One of the EIS). It should be cautioned, however, that these predictions are speculative at best, since each geothermal area is unique, and past experience can provide little more than a rough guideline of what to expect in an undeveloped area.

The emission rates presented here are intended to be used as inputs to the atmospheric dispersion model, RAMR. Thus, most probable emission source locations have also been projected, again based upon the development plan of Chapter One of the EIS. In addition, other required model inputs such as stack height and stack gas temperature have been tabulated where applicable.

5.1.1 Major Gaseous Emissions

The principal gaseous emissions associated with geothermal development are the major noncondensible gases (hydrogen sulfide and carbon dioxide), water vapor from flow testing and from the cooling tower, and vehicle exhaust from associated personnel travel and from construction and operation equipment. The contribution of each of these will be discussed here at each of the five stages of field development described in the Proposed Action.

Stage 1 - Preliminary Exploration, which involves the acquisition of geotechnical data. The methods used require non-intensive uses of the land.

The measurements involved in preliminary exploration require only small groups of workers with light-duty vehicles. The level of activity should not be significantly different from that currently existing due to NWC operations in the area,and the only gaseous emissions should be exhaust from a very limited number of vehicles. Thus, modeling is not necessary at this stage of development, and it can be estimated that the air quality impacts will be minimal.

Stage 2 - Exploratory drilling, the drilling of the first wells to evaluate the extent and physical characteristics of the geothermal resource.

Based upon similar development at the Geysers (Rudisill, 1979), it can be assumed that these wells will be drilled one at a time, so each phase of construction can be considered to be occurring independent of the others. Throughout Stage 2, approximately 60 single personal automobile trips (a round trip being two single trips) can be estimated each day to transport workers to and from the testing site. These trips should occur primarily during shift change periods, so this represents 20 single trips (10 in and 10 out) during each of three separate hours each day, based upon a 24-hour, 3-shift work period. In addition, approximately one large truck round trip per day can be assumed; for a conservative analysis this trip can be considered to occur during the shift change period so that the car and truck emissions are additive. The section locations of the road and the projected hourly average exhaust emission rate per vehicle for each section during shift change periods are listed in Table 5.1.1.1. In this and in all the following discussions, vehicle emission factors were obtained from EPA Publication AP-42 (EPA, 1977).

Table 5.1.1.1

Hourly Average Vehicle Emissions and Locations

Source Locations

R37E, T22S, Section 2
R37E, T22S, Section 1
R38E, T21S, Section 31
R38E, T21S, Section 32
R38E, T21S, Section 33
R38E, T21S, Section 34
R38E, T22S, Section 2
R38E, T22S, Section 1
R39E, T22S, Section 6
R39E, T22S, Section 8

Species	Automobile Emission Rate per Section per Vehicle (g/sec)	Truck Emission Rate per Section per Vehicle (g/sec)
CO	0.065	0.008
Hydrocarbons	0.006	0.001
NO_x	0.001	0.006
Particulate	0.00015	0.00036
SO_x	0.00004	0.001

Exploratory drilling and flow testing will occur at various locations throughout the KGRA. For illustration, however, consider an exploratory well at R38E, T22S, Section 8, an area of high geothermal potential. Grading of the drilling pad will be done by approximately six heavy-duty diesel vehicles, resulting in the exhaust emissions per vehicle of Table 5.1.1.2. Once grading is complete, well drilling will begin. Exhaust emissions from the drilling rig are also listed in Table 5.1.1.2.

Flow testing of exploratory wells should be the first source of non-condensible gases and water vapor. The most probable emission rates, based upon the Proposed Action estimates, are shown in Table 5.1.1.3. Estimated flow testing physical parameters are also shown in this table.

Table 5.1.1.2

Exhaust Emissions During
Exploratory Well Development

Species	Pad Grading Emission Rate per Vehicle (g/sec)	Well Drilling Emission Rate (g/sec)
CO	0.14	0.05
Hydrocarbons	0.02	0.02
NO_x	0.11	0.25
Particulates	0.01	0.02
SO_x	0.01	0.02
Aldehydes	0.002	0.004

Table 5.1.1.3

Exploratory Well
Flow Testing Parameters

Species	Emission Rate (g/sec)
H_2S	3.2
CO_2	3.2×10^2
H_2O	3.2×10^4
Stack Parameters	
Physical Stack Height	15.0 m
Stack Gas Temperature	475 K
Stack Inside Top Diameter	1.0 m
Stack Gas Exit Velocity	20.0 m/sec

Stage 3 - Field development, during which sufficient wells to supply the required energy are drilled and power generation facilities are constructed.

Many activities overlap during this period, including well drilling and flow testing, road and transmission line construction, and excavation and construction of power plants. It will be assumed that power plants will be constructed one at a time, and that two drill rigs will be in operation. It is unlikely, however, that both drilling teams would be flow testing at the same time. Toward the end of Stage 3 several power plants will be in operation. To avoid an excessively complicated scenario, however, the emissions from these plants will not be considered here, but in Stage 4.

The labor force should be greatly increased during Stage 3, so approximately 600 single personal vehicles trips will be required each day. About 200 of these will occur during each of several shift-change hours. In addition, about 200 truck trips will be required each day, with approximately 20 per hour during peak hours. The emission locations and the emission rates per vehicle will be the same as those listed in Table 5.1.1.1.

The emission rates for well pad grading and well drilling will be twice those listed in Table 5.1.1.2, since two crews will be working simultaneously. Since only one well will most likely be flow tested at one time, the flow testing parameters will be identical to those in Table 5.1.1.3.

Grading and building activities associated with power plant construction should require about 16 heavy-duty diesel vehicles, the exhaust emissions from which are found in Table 5.1.1.2. Another potential source is a small trailer village of approximately 500 people which might be constructed in Rose Valley to house construction workers. A likely location is R37E, T22S, Section 2. Emissions from this village due to activities such as heating and cooking are estimated in Table 5.1.1.4.

Stage 4 - Resources utilization, during which the resource is utilized to generate electric power. New wells may be drilled as old ones are depleted.

Table 5.1.1.4

Exhaust Emissions
from Worker Village

Species	Worker Village Emission Rate (g/sec)
CO	0.005
Hydrocarbons	0.003
NO_x	0.03
Particulates	0.005
SO_x	0.0002

The major activity here will be power plant operation, as well as drilling of replacement wells. Although some power plants will be in operation while others are still under construction, it will be assumed here that all 12 plants are in full operation. It can be estimated that approximately 400 single personal vehicle trips will be required each day, with approximately 125 occurring in each of several shift-change hours. Also, approximately 50 truck trips will be required each day, with about five per hour during peak hours. The emission locations and the emission rates per vehicle will be the same as those listed in Table 5.1.1.1.

It can be assumed that a replacement well crew will be working in the geothermal field at all times. The pad grading, well drilling, and flow testing emissions should be the same as those listed in Table 5.1.1.2 and 5.1.1.3 for exploratory wells.

The major emissions from the power plant consist of the non-condensible gases from the off-gas ejector and water vapor from the cooling tower. Cooling tower water is scrubbed of particulate matter before entering the plant cycle, so the cooling tower emissions can be assumed to be essentially pure water vapor, with the exception of trace amounts of inorganic impurities which will be discussed in the next section. Total H_2S production per plant is projected to be 10 g/sec, but it is treated with 95% efficiency by hydrogen peroxide (Castrantas, et al., 1978), resulting in an actual emission rate of only 0.50 g/sec. Probable power plant locations with their stack parameters and emission rates per plant are shown in Table 5.1.1.5. These locations are also shown on maps that will be presented in Section 5.3. It is important to recognize that the sites listed in Table 5.1.1.5 are merely probable estimates. Other sites throughout the KGRA (e.g., Rose Valley, Volcano Peak) are also available for leasing under the Proposed Action. Because RAMR (the EPA-required dispersion model) does not consider terrain, the results presented later in this section can be applied to any part of the KGRA without significant loss of accuracy.

Table 5.1.1.5

Power Plant Locations,
Emissions, and Stack Parameters

Plant Locations
R38E, T22S, Section 11
R38E, T22S, Section 13
R39E, T21S, Section 33
R39E, T22S, Section 5
R39E, T22S, Section 6
R39E, T22S, Section 7
R39E, T22S, Section 8
R39E, T22S, Section 9
R39E, T22S, Section 17
R39E, T22S, Section 18
R39E, T22S, Section 19
R39E, T22S, Section 20

Stack Parameter	Off-Gas Ejector	Cooling Tower
Physical Stack Height (m)	15.0	25.0
Stack Gas Temperature (K)	310	310
Stack Inside Top Diameter (m)	1.0	6.0
Stack Gas Exit Velocity (m/sec)	20.0	10.0

Species	Emission Rate per Plant (g/sec)
H_2S (ejector)	0.50
CO_2 (ejector)	1.0×10^3
H_2O (cooling tower)	1.1×10^5

Stage 5 - Close out, which occurs when a given area does not provide sufficient energy to maintain economic electric generation. This phase includes abandonment of wells and restoration of the area.

The emissions from this stage will be essentially the same as those from Stage 4, except no well drilling will occur. The number of power plants will decrease as plants close down and the area is restored.

The emission rates discussed in this section up to this point have been short-term rates during specific stages of geothermal development. It is also instructive to consider the total yearly emissions during a representative year for each of Stages 2, 3, and 4 (Stage 1 has only minor impacts, and Stage 5 can be extrapolated from Stage 4). These are presented in Table 5.1.1.6, and should be compared with the current emission rates discussed in Section 4.2 (particularly Table 4.2.5). The values in Table 5.1.1.6 include emissions from all sources related to geothermal activity (e.g., car and truck travel, drilling, power plant operation, etc.), and have been corrected for such factors as vehicle speed and percent cold operation, average ambient temperature, and duration of the various operations.

Table 5.1.1.6

Total Average Yearly Emissions

Species	Yearly Emissions (Tons/year)		
	Stage 2	Stage 3	Stage 4
CO	30.1	300	194
Hydrocarbons	3.64	33.5	20.4
NO_x	9.28	43.0	17.3
Particulates	0.80	3.62	1.62
SO_x	0.72	3.79	1.32
H_2S	3.04	6.09	212
CO_2	304	609	4.17×10^5
H_2O	3.04×10^4	6.09×10^4	4.59×10^7

5.1.2 Minor Emissions and Trace Elements

In addition to its major constituents of H_2O, CO_2, and H_2S, the geothermal fluid may also contain small fractions of a percent of methane, ammonia, hydrogen, and carbon monoxide, all of which can be volatilized and emitted with the ejector off-gas. All typically occur in such small quantities, however, that they should be of no air quality consequence. Thus, they will not be considered in any further modeling.

Trace quantities of a number of inorganic substances have been found in other geothermal areas (Robertson, et al., 1978). These include Hg, As, Cu, Zn, Se, Pb, Ag, Sb, B, and Cd. Of these, the most likely to be found in gaseous emissions in any appreciable amount is mercury. Mercury is released primarily in the cooling tower air (Crecelius, et al., 1976), and mercury emission rates are typically about 10^{-8} by weight of H_2O emission rates. Thus, in the modeling results presented later in this report, ambient mercury concentrations can be considered to be 10^{-8} times the calculated H_2O concentrations. As a basis for comparison, ambient background mercury concentrations tend to be on the order of 1 ng/m^3 in most parts of the world. It should be reemphasized that each geothermal system is unique, and that trace element concentrations in particular can vary widely from one field to the next and also from point to point within a single field. Nevertheless, natural mercury deposits have for years been known to exist in the Coso area, so it is not unreasonable to assume that gaseous mercury will be present if geothermal development occurs.

5.1.3 Fugitive Dust

Fugitive dust due to geothermal development can result from two general sources -- mechanical disturbance such as automobile traffic or grading activity, and wind erosion of disturbed area. In this section, emission factor equations for each source will be discussed, followed by calculations of projected fugitive dust emission rates at each stage of geothermal development.

The EPA has published an emission factor for fugitive dust from vehicle traffic (EPA, 1978):

$$E = (0.81T)\left(\frac{S}{30}\right)\left(\frac{365-W}{365}\right) . \qquad (5.1.3.1)$$

Here, E is the emission rate in lb/vehicle mile, T is the silt content of the soil (the percentage of particles smaller than 75 μm in diameter), S is the vehicle speed in miles per hour, and W is the mean annual number of days with 0.01 inch or more of rainfall. The equation is valid for vehicle speeds in the range of 30-50 miles per hour. The EPA-recommended value of T for gravel roads is 12%; for dirt roads in the Coso area, an average value of T of 30% has been measured by the Coso EIS geology field crew. The average vehicle speed can be estimated at 30 miles/hour, and W can be set to zero. This gives a conservative view of the typical dry desert conditions, even through there are a few days each year with appreciable rainfall.

Equation (5.1.3.1) estimates the total amount of fugitive dust which is resuspended by vehicle traffic. Only the fraction smaller than 30 μm in diameter, however, is likely to be transported more than a few feet from the roadway, and it is this fraction that we are concerned with here. To account for this, the result of equation (5.1.3.1) must be multiplied by 0.62 for gravel roads, and by 0.32 for dirt roads. All major roads in the KGRA will be gravel following preliminary exploration. Also, equation (5.1.3.1) was developed for vehicles with four wheels. It should be adapted linearly if applied to vehicles with more than four wheels, so all values discussed in this section will be in terms of equivalent four-wheeled vehicles, thereby implicitly including trucks. It should be noted that this emission factor is conservative, and may over-estimate fugitive dust emissions. Other studies (e.g., McCaldin and Heidel, 1978) predict smaller emissions under similar circumstances, but use fewer parameters than does equation (5.1.3.1).

Fugitive dust due to grading and construction activities can be estimated using an emission factor developed in Arizona, New Mexico, and

Nevada (Jutze and Axetell, 1974). The emission factor is 1.4 tons per acre per month (acreage being the area under active construction). This can be expressed as 17 lb/acre hour if it is assumed that all activity occurs during a 40-hour week. This factor includes grading, blasting, etc., as well as equipment traffic over temporary roads at the construction site. It applies only to particles smaller than 30 μm in diameter.

The emission factor for wind erosion from exposed areas is (Bohn, et al., 1978):

$$E = 3400 \, \frac{\left(\frac{e}{50}\right)\left(\frac{S}{15}\right)\left(\frac{f}{25}\right)}{\left(\frac{P\text{-}E}{50}\right)^2} \, , \qquad (5.1.3.2)$$

where E is the emission factor in lb/acre-year for particles smaller than 30 μm in diameter, e is the surface erodibility (12 tons/acre-year in the Coso area, as measured by the Coso EIS geology field crew), S is the silt content (30% for Coso), f is the percentage of the time wind speed exceeds 12 miles/hour, and P-E is the Thornthwaite precipitation-evaporation index (Thornthwaite, 1931). Twelve miles/hour is the threshold wind velocity for dust production; below this value no wind erosion can be expected. For this study, f will be set to 100%, so that dividing the resulting emission rate by 365 x 24 will yield an hourly emission rate for a constant $>$ 12 miles/hour wind. Equation (5.1.3.2) assumes an average wind speed of 15 miles/hour. It should be multiplied by $(u/15)^3$ if used with any other wind speed, u.

A problem with equation (5.1.3.2) is the use of the Thornthwaite P-E index as a measure of the soil moisture. The P-E index is very small in desert regions, thereby resulting in unrealistically large fugitive dust emission predictions. In reality, however, the soil reaches a critical dryness for dust emission at a P-E index of about 25. Thus, the effective P-E index for desert areas can be approximated to be a constant at 25, regardless of local climatic conditions.

As with the gas emissions presented in Section 5.1.1, fugitive dust emissions can be calculated at each stage of geothermal development to be used as inputs to the atmospheric dispersion model. The emission factors discussed in the preceding paragraphs will be used to make these estimates.

Stage 1 - Preliminary Exploration

The level of activity during this stage should not be significantly different from that currently existing due to NWC operations in the area, so it can be estimated that the fugitive dust impacts due to geothermal development will be minimal.

Stage 2 - Exploratory Drilling

Using equation (5.1.3.1), the emission factor for travel on gravel roads is 6.0 lb/vehicle mile. For the hourly maximum of 20 trips required during Stage 2, this yields 120 lb/mile, or 120 lb/hr (15.2 g/sec) for each section traversed if it is assumed that the road extends one mile through each section. This factor of 15.2 g/sec should be applied to each of the sections listed in Table 5.1.1.1.

For grading activities, it can be estimated that the total construction area (including well pad, mud sump, reserve pit, and maintenance roads) will be 5.8 acres. This results in a fugitive dust emission rate of 100 lb/hour, or 12.4 g/sec. For illustration, this emission rate should be applied to R39E, T22S, Section 8.

Stage 3 - Field Development

Dust will probably be the major air quality problem during this construction period, which could last two years for each 50 MW power plant. Toward the end of Stage 3 several power plants will be in operation, and disturbed area will reach a maximum for dust generation by wind erosion. For simplicity of discussion, however, the emphasis here will be on construction activity; wind erosion will be treated separately in Stage 4. Nevertheless, it should be kept in mind that wind erosion and construction can occur simultaneously.

Since approximately 260 equivalent four-wheeled vehicle trips will be required during peak traffic hours, the hourly maximum dust emission rate per section will be about 200 g/sec. These emissions can be assumed to occur in the same sections as those calculated in Stage 2.

Dust emissions from well pad grading will be twice that calculated for Stage 2 since two drilling crews will be operating simultaneously. These emissions, as well as emissions from power plant construction, will be assumed, for purposes of illustration, to occur in R39E, T22S, Section 8, although they will eventually occur in each section which will contain a power plant.

Assuming that only one power plant at a time will be built, it can be estimated that the total acreage under active construction at any given time will be about 20 acres. This results in a total plant construction fugitive dust emission rate of 340 lb/hour, or 43 g/sec.

Stage 4 - Resources Utilization

The fugitive dust emission rate for vehicle traffic will be approximately one-half of that calculated for Stage 3; the rate for replacement well drilling will be identical to that for Stage 2. In both cases, the assumed locations of emissions will be the same as those in the previous stages.

Equation (5.1.3.2) can be used to calculate a fugitive dust emission rate due to wind erosion for a given hour in which the wind speed exceeds 12 miles/hour. The rate for each specified meteorological condition will have to be calculated separately to account for the dependence of emission rate upon wind speed. According to the Proposed Action, the disturbed area for each 50 MW power plant will be approximately 68 acres. Using this value will yield a total wind erosion emission rate for each power plant; this emission rate should be assumed in each of the sections listed in Table 5.1.1.5.

Stage 5 - Closeout

The emissions during the early part of closeout will be essentially the same as those from Stage 4, except no well drilling will occur. As power plants close down, gaseous emissions will decrease. Fugitive dust emissions from the related exposed areas will persist for a number of years, however, until the soil surface is stablized by vegetative restoration.

5.2 ATMOSPHERIC DISPERSION MODEL DESCRIPTION

EPA regulations require that one of the UNAMAP series of guideline dispersion models be used to evaluate the air quality effects of new emission sources. For this project, RAMR (the rural version of RAM) was chosen. Of all the UNAMAP models, RAMR is best suited to handle a combination of multiple point and area sources such as is found at Coso. Its short-term calculation capabilities using multiple receptors make it possible to directly address the one-hour average H_2S standard which is of major interest in geothermal development.

RAMR uses a Gaussian formulation to calculate dispersion of pollutants from the plume centerline downwind of point and area sources. The dispersion parameter values representative of rural areas are taken from the Pasquill-Gifford curves (Turner, 1970). Although RAMR is not considered to be a chemically reactive model, transformation of a pollutant resulting in loss of that pollutant throughout the depth of each plume can, nevertheless, be approximated. This is accomplished by an exponential decrease with travel time from the source, the input parameter being the expected half-life of the emitted pollutant. RAMR does not have the capability to change this parameter value during a given run. Further description of the theoretical basis for RAMR can be found elsewhere (Turner and Novak, 1978).

In examining the results of RAMR, it is very important to recognize the major limitations of the model. First of all, the algorithm is strictly applicable only to locations with level or gently rolling terrain; no terrain correction is included in the model. The Coso study area contains regions of quite rough terrain, so the effects of local topography and meteorology should be kept in mind when interpreting the results. Next, a single set of meteorological inputs is assumed to be representative of the entire area being modeled. Variations in topography, particularly in elevation, can partially invalidate this assumption. Finally, RAMR computations are performed as if the atmosphere had achieved a steady-state condition. Therefore, errors will occur where there is a gradual buildup (or decrease) in concentrations during the shortest averaging period, such as under light wind conditions. Similarly, the transitional phenomenon of fumigation (the lifting of an inversion layer containing a stabilized plume causing mixing of pollutants downard) is not included in calculations made by RAMR.

The version of RAMR used in this study was purchased from the National Technical Information Service, and is the latest version available to the general public; its Julian date is 78124. A FORTRAN listing of RAMR and its related subroutines and preprocessing program is included in Appendix A. All statements which were left in their original form, or were changed in ways which did not change the algorithm (usually to accommodate the idiosyncrasies of the local operating system of the PDP-11/40 computer) are shown with line numbers. All statements which were added to the original version or in which substantive changes were made are shown without line numbers. Most of the additions and substantive changes fell into two categories. First, much of the input-output formalism was altered to be compatible with a terminal-interactive system rather than with a batch operating system as used by NTIS (i.e. EPA). Second, to reduce the root size of the program, most of the large arrays were removed from Common and were placed in Virtual memory. This is necessary in order to run the program on a small computer such as the PDP-11/40; it has no effect upon the calculated results.

5.3 AIR QUALITY IMPACT OF THE EMISSIONS

This section will present the results of the modeling effort using RAMR, and will include a general discussion of these results. Most of the meteorological and emission inputs (source strengths and physical stack parameters) have been discussed in previous sections. There are, however, a few model inputs which have not yet been mentioned; these will be discussed briefly here. The area source height in all cases is assumed to be 2 meters, while the receptor height is set to zero (ground level receptors). All runs use a one-hour averaging period, and specify the area source side length to be one mile, with sources thereby corresponding approximately to the sections on USGS topographical maps. Receptor locations are specified in two ways -- first, at locations of estimated maximum ambient concentrations downwind of major point and area sources, and second, by constructing a "honeycomb" grid of receptors designed to cover an entire area. The area covered is approximately 150 square miles (square or rectangular), and the honeycomb receptors are placed one mile apart. Since the major species of interest (H_2S and fugitive dust) can be considered essentially non-reactive over a one-hour span (Perry, Atkinson, and Pitts, 1976), the reactant half-life is set to 30000 seconds (8.33 hours).

The modeling results are summarized in the following tables. Each table includes three entries for each of the classes of meteorological parameters presented in Table 4.1.3. The first of these entries is the maximum ambient pollutant concentration calculated within the KGRA. The second and third entries are example concentrations at other locations; these examples were chosen to be typical of the study area, and were used in place of complete receptor tables because of the voluminous amount of data that would have been involved. Dashed entries in the tables represent calculated zero concentrations through the study area. The location of each reported concentration is coded by three numbers found immediately below the concentration. The first number is the east coordinate (e.g., 38 represents R38E), the second number is the south coordinate (e.g., 22 represents T22S), and the third number is the section number. It is important to recognize

Table 5.3.1

Stage 2
CO from Vehicles

Met. Class	Maximum Concentration (μg/m^3 & Location)	Example Outlying Concentrations (μg/m^3 & Location) 1	2
A	76 38, 22, 11	14 38, 22, 29	4.2 38, 22, 33
B	76 38, 22, 11	16 38, 22, 21	6.0 37, 22, 24
C	10.2 38, 22, 12	2.0 39, 22, 20	0.6 38, 22, 20
D	13 39, 22, 17	5.8 39, 22, 32	2.0 38, 22, 20
E	20 39, 22, 17	13 39, 22, 31	6.2 38, 22, 20
F	8.4 38, 22, 12	2.0 38, 22, 18	0.6 38, 22, 23
G	7.8 38, 21, 27	2.4 38, 21, 23	1.6 39, 21, 32
H	4.6 38, 21, 27	0.4 38, 21, 21	0.2 38, 21, 10
I	10 38, 22, 2	0.4 39, 22, 21	0.2 38, 22, 20
J	8.2 39, 21, 31	1.8 38, 21, 21	1.0 38, 21, 10
K	2.0 38, 22, 3	0.6 38, 22, 10	0.4 38, 22, 20
L	3.6 39, 22, 5	2.8 38, 22, 6	2.0 39, 22, 9
M	40 39, 22, 17	10 38, 22, 9	4.2 39, 22, 32

Figure 5.3.1. CO from Vehicles - Met Class H

▲ = Emission Sources

Concentration in (μg/m³)

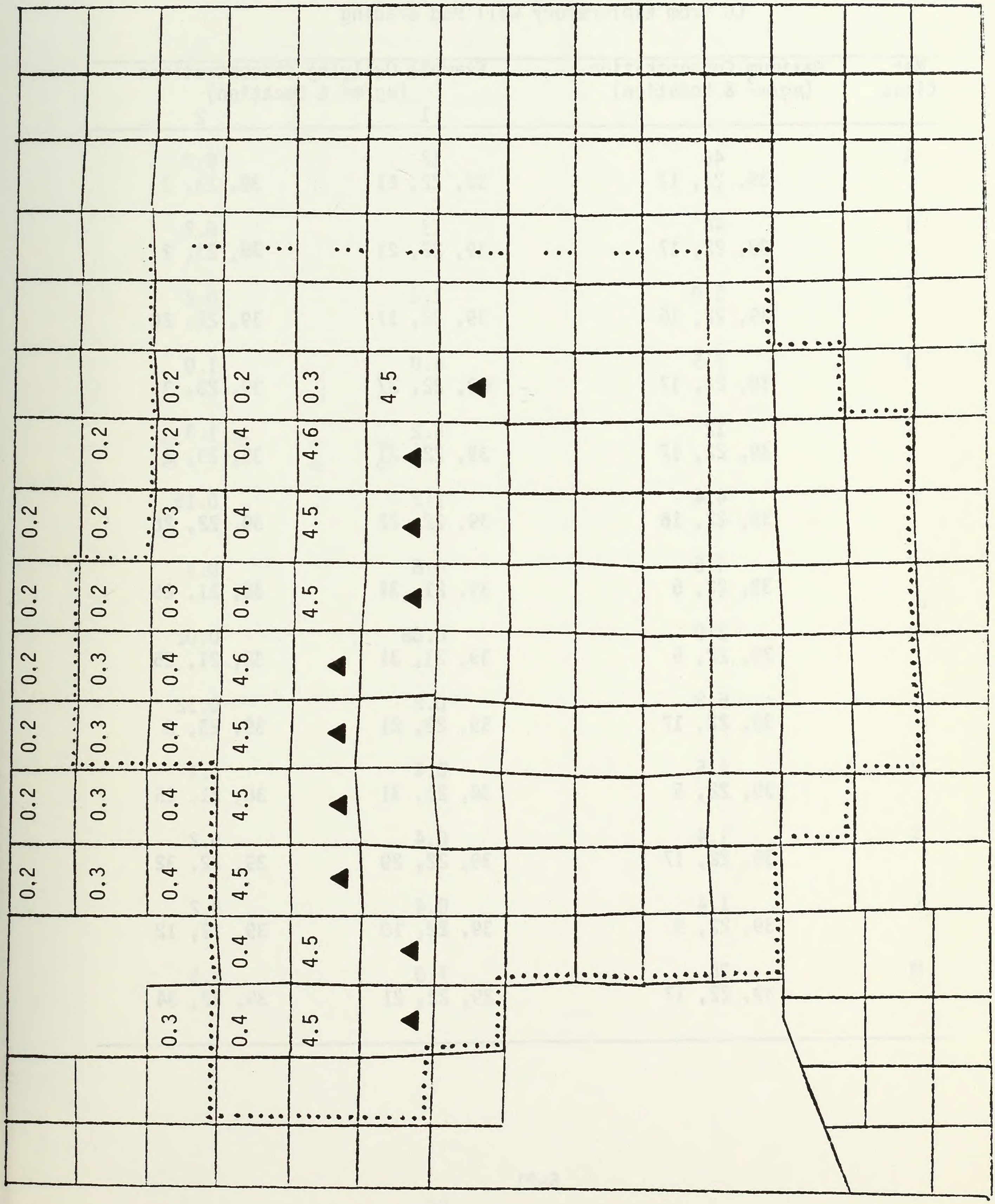

Table 5.3.2

Stage 2
CO from Exploratory Well Pad Grading

Met. Class	Maximum Concentration ($\mu g/m^3$ & Location)	Example Outlying Concentrations ($\mu g/m^3$ & Location) 1	2
A	46 39, 22, 17	17 39, 22, 21	6.2 39, 23, 2
B	46 39, 22, 17	13 39, 22, 21	6.2 39, 23, 2
C	5.0 39, 22, 16	1.0 39, 22, 17	0.2 39, 22, 26
D	7.5 39, 22, 17	4.0 39, 22, 27	1.0 39, 23, 3
E	12 39, 22, 17	5.2 39, 22, 21	1.3 39, 23, 3
F	4.4 39, 22, 16	1.2 39, 22, 22	0.15 39, 22, 26
G	4.6 39, 22, 5	0.6 39, 21, 31	0.1 38, 21, 25
H	3.0 39, 22, 5	0.08 39, 21, 31	0.02 38, 21, 25
I	6.8 39, 22, 17	0.2 39, 22, 21	0.12 39, 23, 2
J	4.5 39, 22, 5	0.4 39, 21, 31	0.1 38, 21, 25
K	1.4 39, 22, 17	0.4 39, 22, 20	0.2 39, 22, 32
L	1.4 39, 22, 9	0.4 39, 22, 10	0.2 39, 22, 12
M	25 39, 22, 17	7.0 39, 22, 21	3.5 39, 22, 34

Figure 5.3.2. Stage 2 - CO from Exploratory Well Pad Grading - Met Class J

▲ = Emission Source

Concentration in ($\mu g/m^3$)

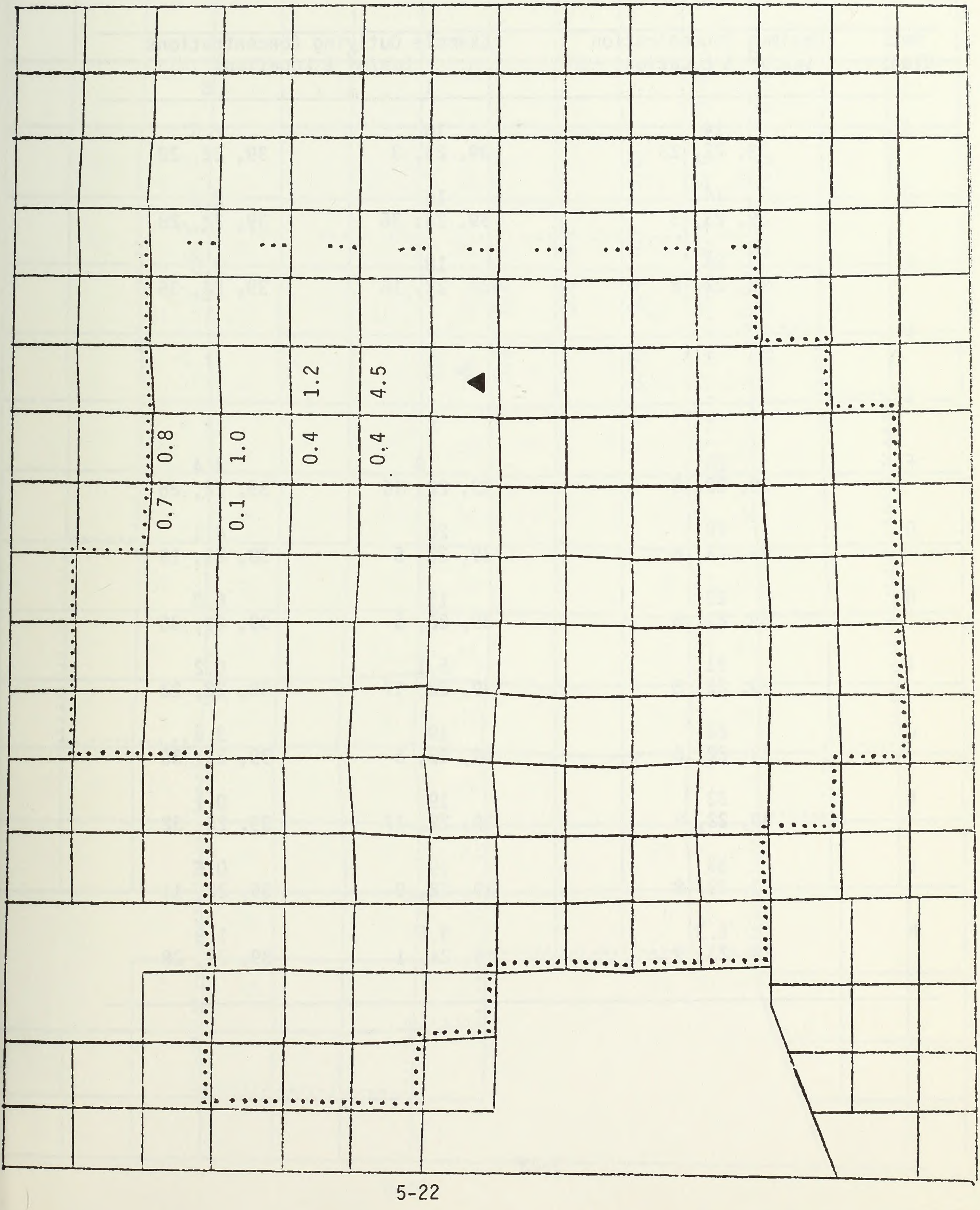

Table 5.3.3

Stage 2
H_2S from Exploratory Well Flow Testing

Met. Class	Maximum Concentration (μg/m^2 & Location)	Example Outlying Concentrations (μg/m^3 & Location)	
		1	8
A	14 39, 22, 28	10 39, 23, 3	2.5 39, 22, 28
B	14 39, 23, 3	10 39, 23, 36	2.2 39, 22, 28
C	26 39, 22, 8	18 39, 22, 16	2.0 39, 22, 36
D	- -	- -	- -
E	- -	- -	- -
F	28 39, 22, 8	18 39, 22, 16	2.4 39, 22, 26
G	28 39, 22, 8	20 39, 22, 5	4.1 38, 21, 13
H	29 39, 22, 8	15 39, 22, 5	6.0 39, 21, 30
I	21 39, 22, 8	5.1 39, 22, 17	0.2 39, 22, 22
J	28 39, 22, 8	19 39, 22, 5	3.5 39, 21, 30
K	33 39, 22, 8	19 39, 22, 17	0.1 39, 22, 32
L	33 39, 22, 8	19 39, 22, 9	0.6 39, 22, 11
M	5.3 39, 23, 3	3.5 39, 24, 1	1.9 39, 22, 28

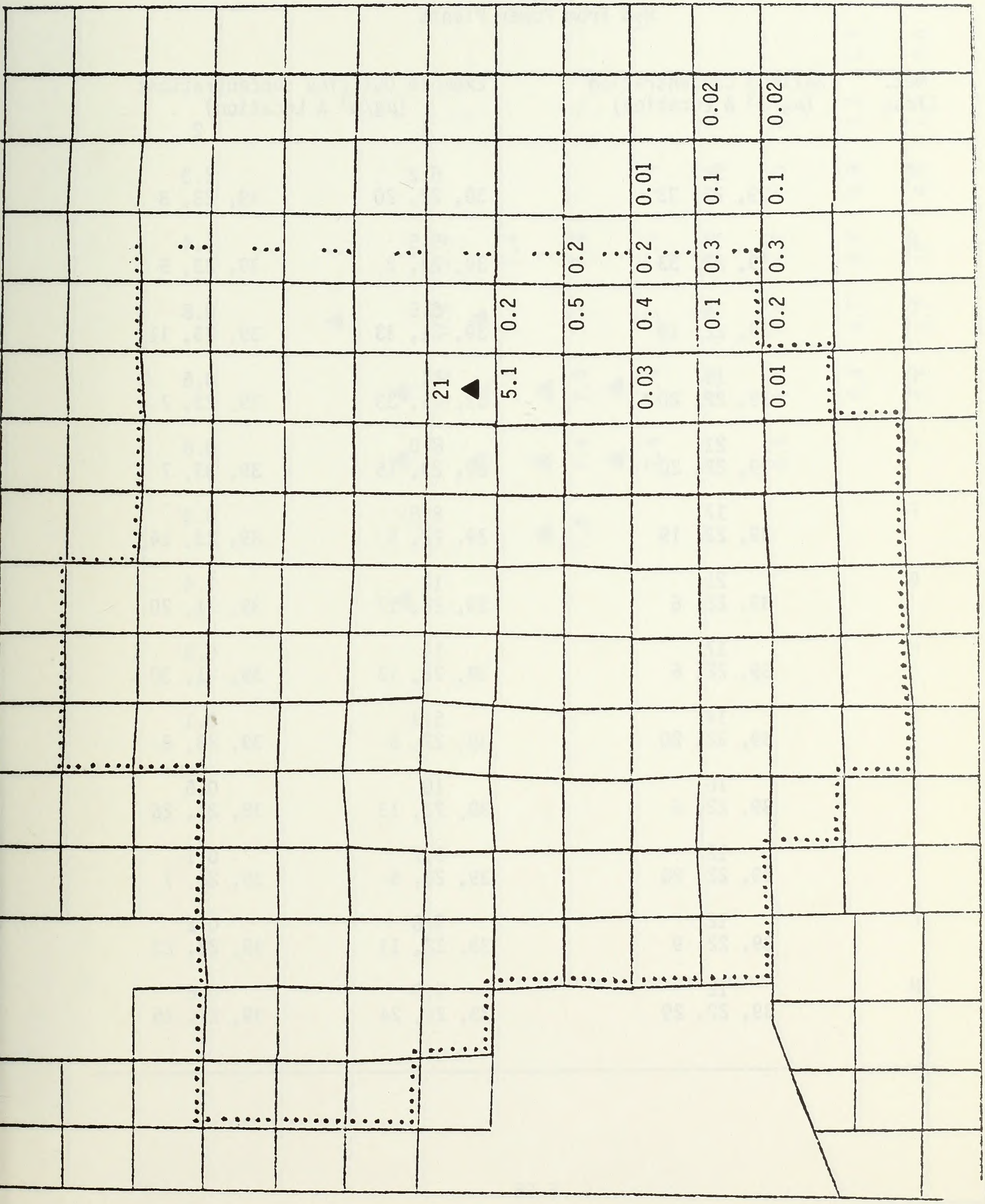

Figure 5.3.3. H_2S from Exploratory Well Flow Testing - Met Class I

▲ = Emission Source

Concentration in ($\mu g/m^3$)

Table 5.3.4

Stage 4
H_2S from Power Plants

Met. Class	Maximum Concentration ($\mu g/m^3$ & Location)	Example Outlying Concentrations ($\mu g/m^3$ & Location) 1	2
A	9.0 39, 22, 33	6.2 39, 22, 20	2.3 39, 23, 8
B	12 39, 22, 33	5.5 39, 23, 2	1.4 39, 23, 5
C	16 39, 22, 19	8.5 39, 21, 33	0.8 39, 23, 11
D	19 39, 22, 20	11 39, 21, 33	0.6 39, 23, 7
E	21 39, 22, 20	8.0 39, 23, 15	0.8 39, 33, 7
F	17 39, 22, 19	8.8 39, 22, 5	0.3 39, 23, 14
G	21 39, 22, 6	12 39, 22, 17	1.4 39, 21, 20
H	17 39, 22, 6	14 38, 22, 13	0.3 39, 21, 30
I	14 39, 22, 20	5.3 39, 22, 5	0.1 39, 23, 8
J	16 39, 22, 6	10 38, 22, 13	0.5 38, 21, 26
K	12 39, 22, 20	5.7 39, 22, 5	0.1 39, 23, 7
L	12 39, 22, 9	5.8 38, 22, 11	0.2 39, 22, 23
M	12 39, 22, 29	5.0 38, 22, 24	0.6 39, 22, 15

Figure 5.3.4. H_2S from Power Plants - Met Class B

▲= Emission Source

Concentration in (µg/m³)

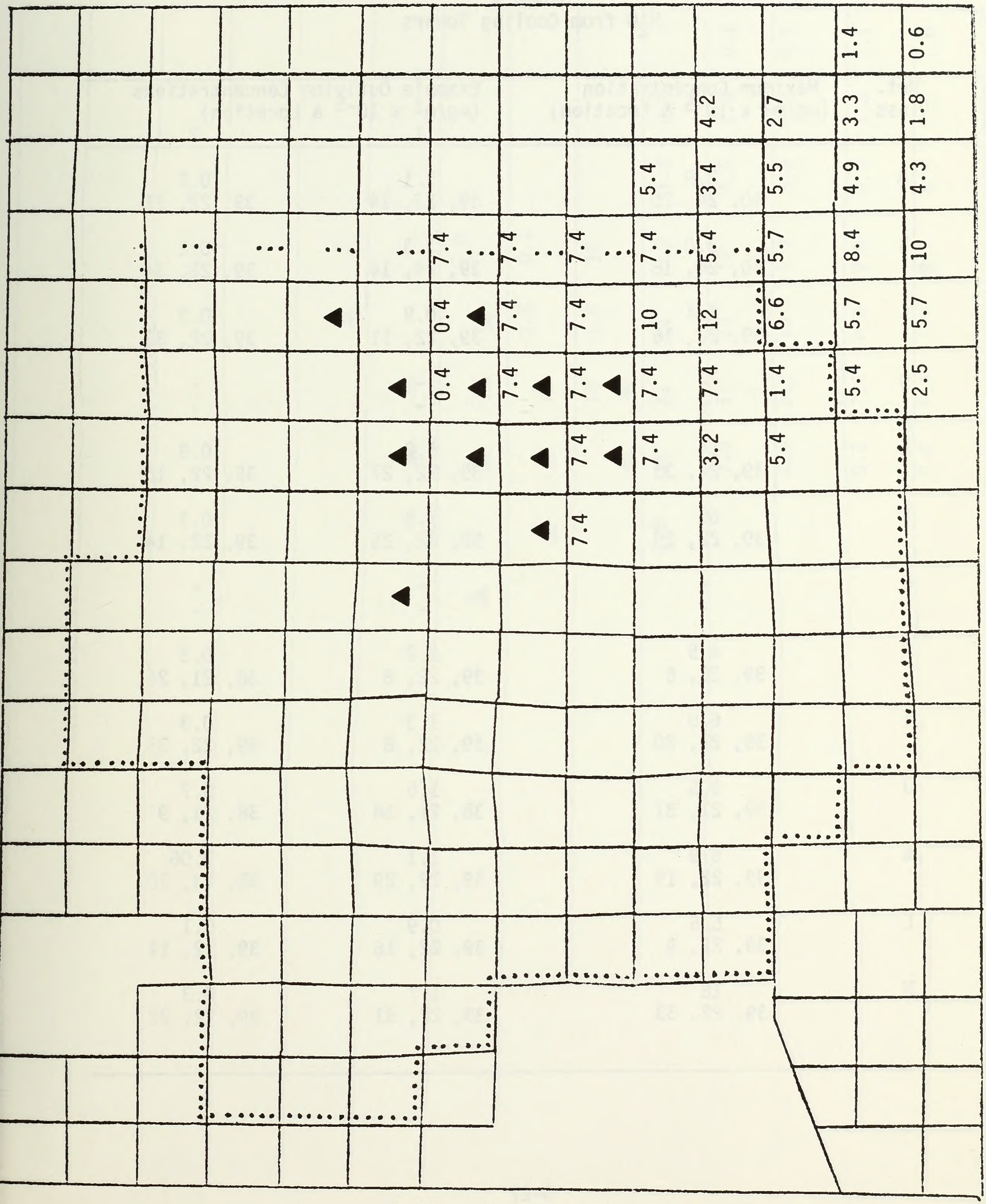

Table 5.3.5

Stage 4
H_2O from Cooling Towers

Met. Class	Maximum Concentration (μg/m^3 x 10^{-5} & Location)	Example Outlying Concentrations (μg/m^3 x 10^{-5} & Location)	
		1	2
A	2.9 40, 24, 20	1.1 39, 23, 14	0.2 39, 22, 21
B	3.0 40, 24, 18	1.3 39, 24, 14	0.2 39, 22, 34
C	2.4 39, 22, 16	0.9 39, 22, 11	0.3 39, 22, 33
D	- -	- -	- -
E	14 39, 22, 33	5.2 39, 22, 27	0.8 39, 22, 10
F	65 39, 22, 29	7.3 39, 22, 25	0.3 39, 22, 14
G	- -	- -	- -
H	4.5 39, 22, 6	2.2 39, 22, 8	0.3 38, 21, 26
I	6.0 39, 22, 20	1.3 39, 22, 8	0.3 39, 22, 35
J	3.5 39, 21, 31	1.5 38, 21, 34	0.7 38, 21, 9
K	6.9 39, 22, 19	1.1 39, 22, 29	0.06 38, 23, 10
L	6.6 39, 22, 9	0.9 39, 22, 16	0.1 39, 22, 14
M	18 39, 22, 33	1.7 39, 22, 31	0.3 39, 22, 22

Figure 5.3.5. Stage 4 - H_2O from Cooling Towers - Met Class E

▲ = Emission Sources

Concentration in ($\mu g/m^3 \times 10^{-5}$)

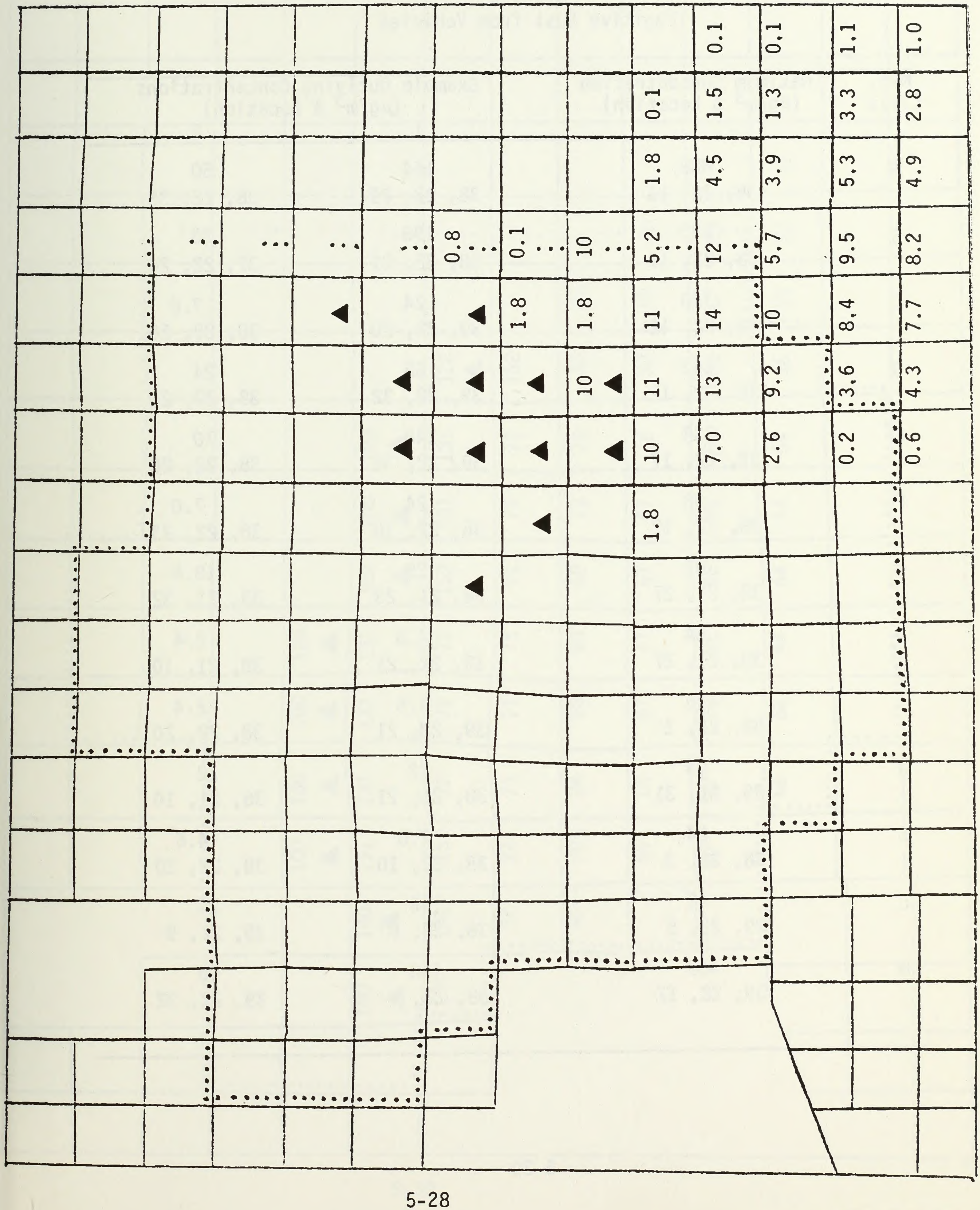

Table 5.3.6

Stage 2

Fugitive Dust from Vehicles

Met. Class	Maximum Concentration ($\mu g/m^3$ & Location)	Example Outlying Concentrations ($\mu g/m^3$ & Location) 1	2
A	888 38, 22, 11	164 38, 22, 29	50 38, 22, 33
B	888 38, 22, 11	190 38, 22, 21	70 37, 22, 24
C	120 38, 22, 12	24 39, 22, 20	7.0 38, 22, 20
D	152 39, 22, 17	68 39, 22, 32	24 38, 22, 20
E	234 39, 22, 17	148 39, 22, 31	70 38, 22, 20
F	98 38, 22, 12	24 38, 22, 18	7.0 38, 22, 23
G	92 38, 21, 27	28 38, 21, 23	18.8 39, 21, 32
H	54 38, 21, 27	4.6 38, 21, 21	2.4 38, 21, 10
I	116 38, 22, 2	4.6 39, 22, 21	2.4 38, 22, 20
J	94 39, 21, 31	22 38, 21, 21	12 38, 21, 10
K	24 38, 22, 3	7.0 38, 22, 10	4.6 38, 22, 20
L	42 39, 22, 5	32 38, 22, 6	24 39, 22, 9
M	468 39, 22, 17	118 38, 22, 9	50 39, 22, 32

Figure 5.3.6. Stage 2 - Fugitive Dust from Vehicles - Met Class D

▲ = Emission Sources

Concentration in (μg/m³)

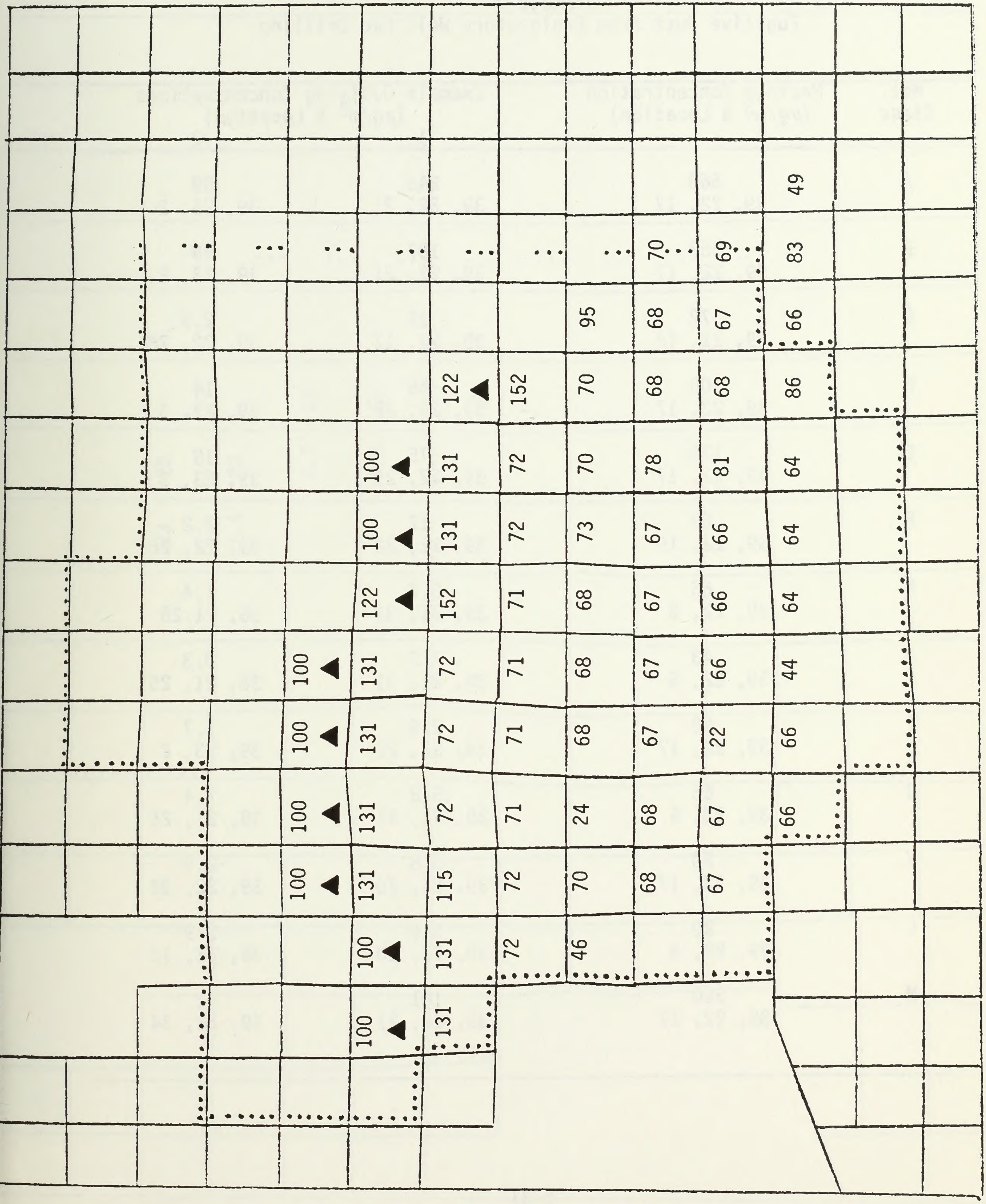

Table 5.3.7

Stage 2
Fugitive Dust from Exploratory Well Pad Drilling

Met. Class	Maximum Concentration ($\mu g/m^3$ & Location)	Example Outlying Concentrations ($\mu g/m^3$ & Location) 1	2
A	663 39, 22, 17	245 39, 22, 21	89 39, 23, 2
B	663 39, 22, 17	187 39, 22, 21	89 39, 23, 2
C	72 39, 22, 16	14 39, 22, 17	2.9 39, 22, 26
D	108 39, 22, 17	58 39, 22, 27	14 39, 23, 3
E	173 39, 22, 17	75 39, 22, 21	19 39, 23, 3
F	63 39, 22, 16	17 39, 22, 22	2.2 39, 22, 26
G	66 39, 22, 5	8.7 39, 21, 31	1.4 38, 21.25
H	43 39, 22, 5	1.2 39, 21, 31	0.3 38, 21, 25
I	98 39, 22, 17	2.9 39, 22, 21	1.7 39, 23, 2
J	65 39, 22, 5	5,8 39, 21, 31	1,4 38, 21, 25
K	20 39, 22, 17	5.8 39, 22, 20	2.9 39, 22, 32
L	20 39, 22, 9	5.8 39, 22, 10	2.9 39, 22, 12
M	360 39, 22, 17	101 39, 22, 21	51 39, 22, 34

Figure 5.3.7. Stage 2 - Fugitive Dust from Exploratory Well Pad Drilling - Met Class G

▲ = Emission Source

Concentration in ($\mu g/m^3$)

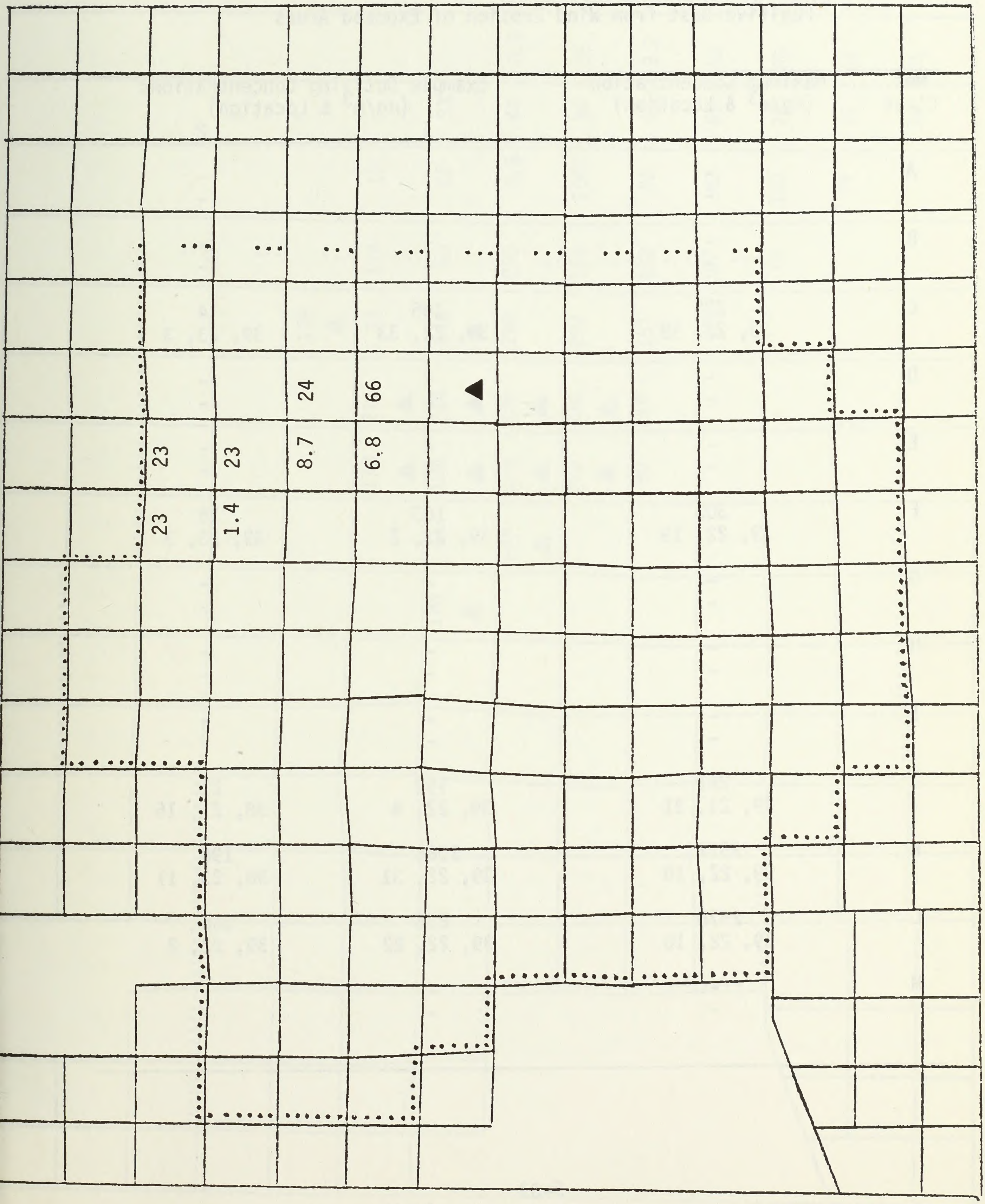

Table 5.3.8

Stage 4
Fugitive Dust from Wind Erosion of Exposed Areas

Met. Class	Maximum Concentration ($\mu g/m^3$ & Location)	Example Outlying Concentrations ($\mu g/m^3$ & Location) 1	2
A	- -	- -	- -
B	- -	- -	- -
C	225 39, 22, 19	105 39, 22, 33	14 39, 23, 3
D	- -	- -	- -
E	- -	- -	- -
F	303 39, 22, 19	103 39, 23, 2	18 39, 23, 3
G	- -	- -	- -
H	- -	- -	- -
I	- -	- -	- -
J	261 39, 21, 31	152 39, 22, 4	21 38, 21, 16
K	2522 39, 22, 19	1084 39, 22, 31	196 38, 23, 11
L	2578 39, 22, 10	826 39, 22, 22	566 39, 22, 2
M	- -	- -	- -

Figure 5.3.8. Stage 4 - Fugitive Dust from Wind Erosion of Exposed Areas - Met Class F

▲ = Emission Sources

Concentration in ($\mu g/m^3$)

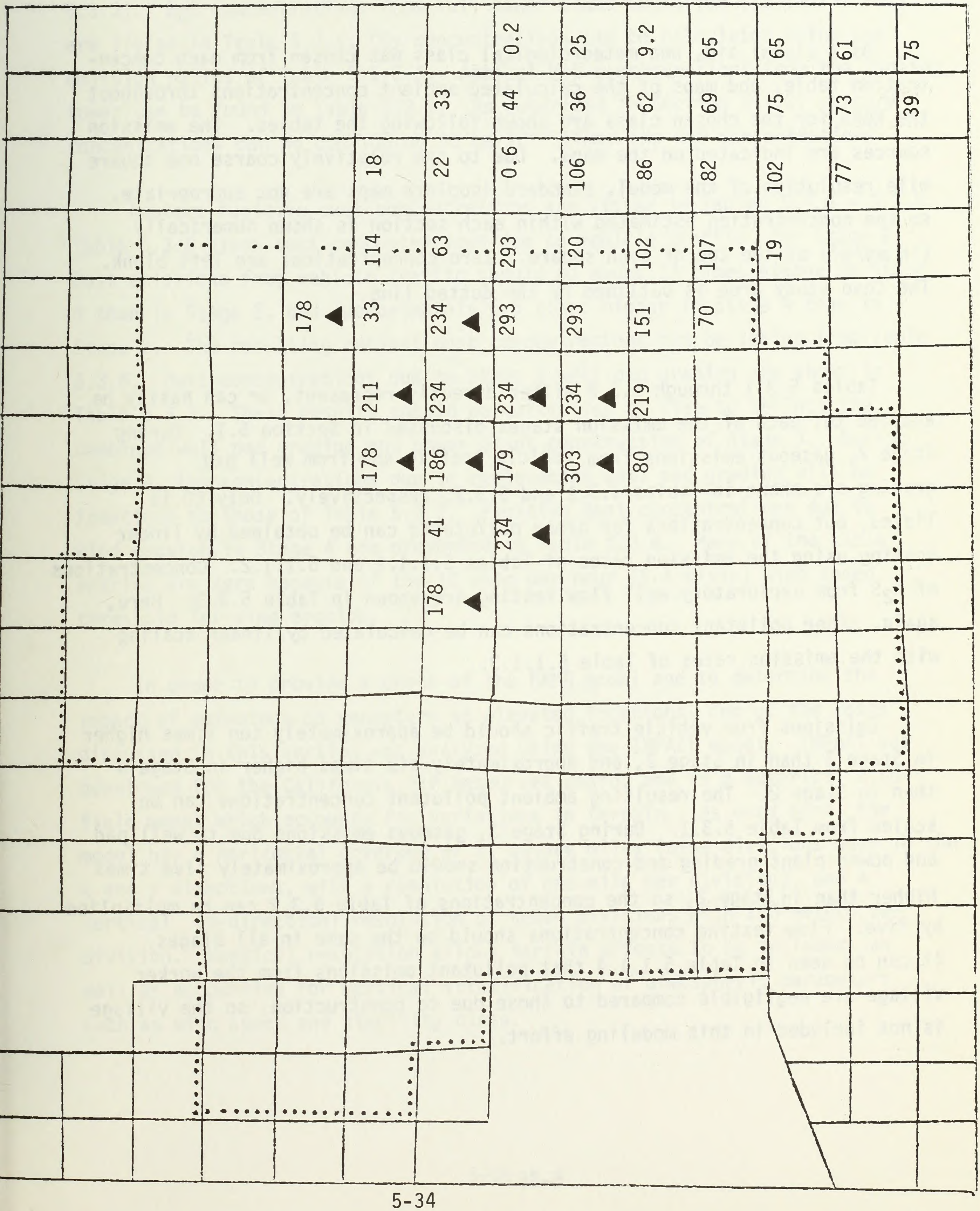

Table 5.3.8

Stage 4
Fugitive Dust from Wind Erosion of Exposed Areas

Met. Class	Maximum Concentration ($\mu g/m^3$ & Location)	Example Outlying Concentrations ($\mu g/m^3$ & Location)	
		1	2
A	- -	- -	- -
B	- -	- -	- -
C	225 39, 22, 19	105 39, 22, 33	14 39, 23, 3
D	- -	- -	- -
E	- -	- -	- -
F	303 39, 22, 19	103 39, 23, 2	18 39, 23, 3
G	- -	- -	- -
H	- -	- -	- -
I	- -	- -	- -
J	261 39, 21, 31	152 39, 22, 4	21 38, 21, 16
K	2522 39, 22, 19	1084 39, 22, 31	196 38, 23, 11
L	2578 39, 22, 10	826 39, 22, 22	566 39, 22, 2
M	- -	- -	- -

Figure 5.3.8. Stage 4 - Fugitive Dust from Wind Erosion of Exposed Areas - Met Class F

▲ = Emission Sources

Concentration in ($\mu g/m^3$)

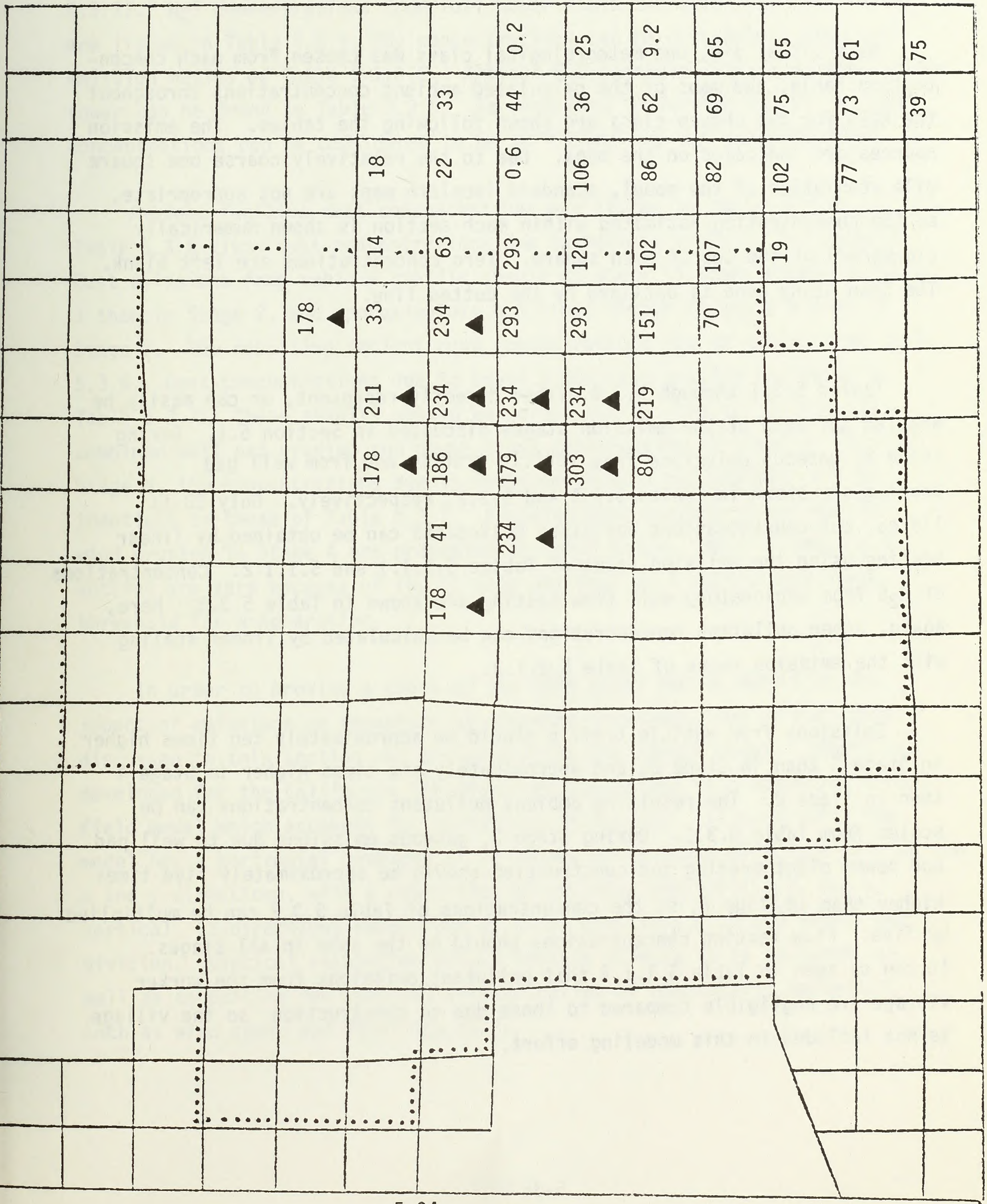

that all concentrations tabulated here are in addition to any background concentration that might already exist, i.e., these concentrations represent incremental increases due to geothermal development.

As a visual aid, one meteorological class was chosen from each concentration table, and maps of the calculated ambient concentrations throughout the KGRA for the chosen class are shown following the tables. The emission sources are indicated on the maps. Due to the relatively coarse one square mile resolution of the model, standard isopleth maps are not appropriate, so the concentration estimated within each section is shown numerically (in $\mu g/m^3$) at the top of each square. Zero concentrations are left blank. The Coso study area is outlined by the dotted line.

Tables 5.3.1 through 5.3.8 either directly represent, or can easily be adapted to, each of the emission stages discussed in Section 5.1. During Stage 2, gaseous emissions from vehicle traffic and from well pad grading are shown in Tables 5.3.1 and 5.3.2, respectively. Only CO is listed, but concentrations for other pollutants can be obtained by linear scaling using the emission rates of Tables 5.1.1.1 and 5.1.1.2. Concentrations of H_2S from exploratory well flow testing are shown in Table 5.3.3. Here, again, other pollutant concentrations can be calculated by linear scaling with the emission rates of Table 5.1.1.3.

Emissions from vehicle traffic should be approximately ten times higher in Stage 3 than in Stage 2, and approximately six times higher in Stage 4 than in Stage 2. The resulting ambient pollutant concentrations can be scaled from Table 5.3.1. During Stage 3, gaseous emissions due to well pad and power plant grading and construction should be approximately five times higher than in Stage 2, so the concentrations of Table 5.3.2 can be multiplied by five. Flow testing concentrations should be the same in all stages. It can be seen in Table 5.1.1.4 that pollutant emissions from the worker village are negligible compared to those due to construction, so the village is not included in this modeling effort.

For Stage 4, the pollutant concentrations due to drilling and flow testing of new wells should be the same as those for Stage 2 (Tables 5.3.2 and 5.3.3). H_2S concentrations from full power plant operation (12 facilities) are listed in Table 5.3.4; CO_2 concentrations can be calculated using the emission ratios of Table 5.1.1.5. Ambient H_2O concentrations from the cooling tower can be found in Table 5.3.5. As described in Section 5.1.2, mercury concentrations can be considered to be 10^{-8} times the H_2O concentrations.

Ambient fugitive dust concentrations are listed in Tables 5.3.6 - 5.3.8. Table 5.3.6 gives dust concentrations due to vehicle traffic for Stage 2. Dust emissions from vehicle traffic should be about 13 times higher in Stage 3 than in Stage 2, and approximately 6.5 times higher in Stage 4 than in Stage 2. The resulting ambient dust concentrations can be scaled from Table 5.3.6. Dust concentrations due to Stage 2 well pad grading are shown in Table 5.3.7. These results should be multiplied by five to reflect the combined well pad grading and power plant construction of Stage 3. During Stage 4, the concentrations due to replacement well pad grading will be identical to those of Table 5.3.7. Fugitive dust concentrations due to wind erosion in Stage 4 are presented in Table 5.3.8. Many of the table entries are zero because of the 12 mile per hour (5.4 m/sec) wind speed threshold for wind erosion.

In order to provide a check of the RAMR model and to determine the impact of emissions on receptors at elevated locations, one of the cases discussed in this section was analyzed using the IMPACT model. IMPACT was developed for the California Air Resources Board, and is a numerical wind-field model which accounts for variations in terrain. As used here, the model has a horizontal coverage of 81 square miles (nine divisions each in the x and y directions, with a resolution of one mile per division), and a vertical (z-direction) resolution of seven divisions with 200 meters per division. Vertical resolution allows terrain effects to be included, as well as accounting for vertical stratification of atmospheric parameters such as wind speed and stability class.

The particular case chosen for analysis was emission of hydrogen sulfide from power plants under meteorological class B (F stability, 1 m/sec wind speed). This highly stable condition should be a good approximation of worst-case terrain effects because pollutants can collect in basins and canyons with very little dispersion. The locations and physical parameters of the emission sources are the same as those listed in Table 5.1.1.5.

The results of the IMPACT model run are shown in Figure 5.3.9 as surface-level concentrations for each square. Terrain effects are included implicitly in these values due to the variation in elevation from square to square. Figure 5.3.9 should be compared to the RAMR results shown in Figure 5.3.4 and in line two of Table 5.3.4. Such a comparison shows that the ambient levels predicted by IMPACT are uniformly lower than those predicted by RAMR, presumably because IMPACT allows for more vertical dispersion than does RAMR. The fact that IMPACT predicted lower concentrations even at elevated receptor locations is a good indication that RAMR is a conservative model in rugged terrain as well as in flat or gently rolling areas.

In order to understand the air quality impacts of geothermal development, it is useful to point out the maximum concentration of each pollutant as calculated by RAMR and to relate these concentrations to government air quality standards, keeping in mind that all values reported here are one-hour averages. The maximum concentrations of gaseous pollutants due to construction and vehicular traffic (as derived from Tables 5.3.1 and 5.3.2) are shown in Table 5.3.9. None of these concentrations exceed the government standards of Table 4.3.1.

From Table 5.3.4, the maximum ambient H_2S concentration to be expected from full power plant operation is 21 $\mu g/m^3$, exactly one-half of the state one-hour standard of 42 $\mu g/m^3$. The H_2S maximum from well flow testing is 33 $\mu g/m^3$, occurring during strong-wind conditions. Although this is, by itself, well below the state standard, it is possible that power plant operation and flow testing during Stage 4 could combine to cause an exceedance of the standard in a localized area. Examination of Tables 5.3.3 and 5.3.4

Figure 5.3.9. IMPACT Results, Stage 4 - H_2S from Power Plants
Met Class B

▲ = Emission Sources

Concentration in ($\mu g/m^3$)

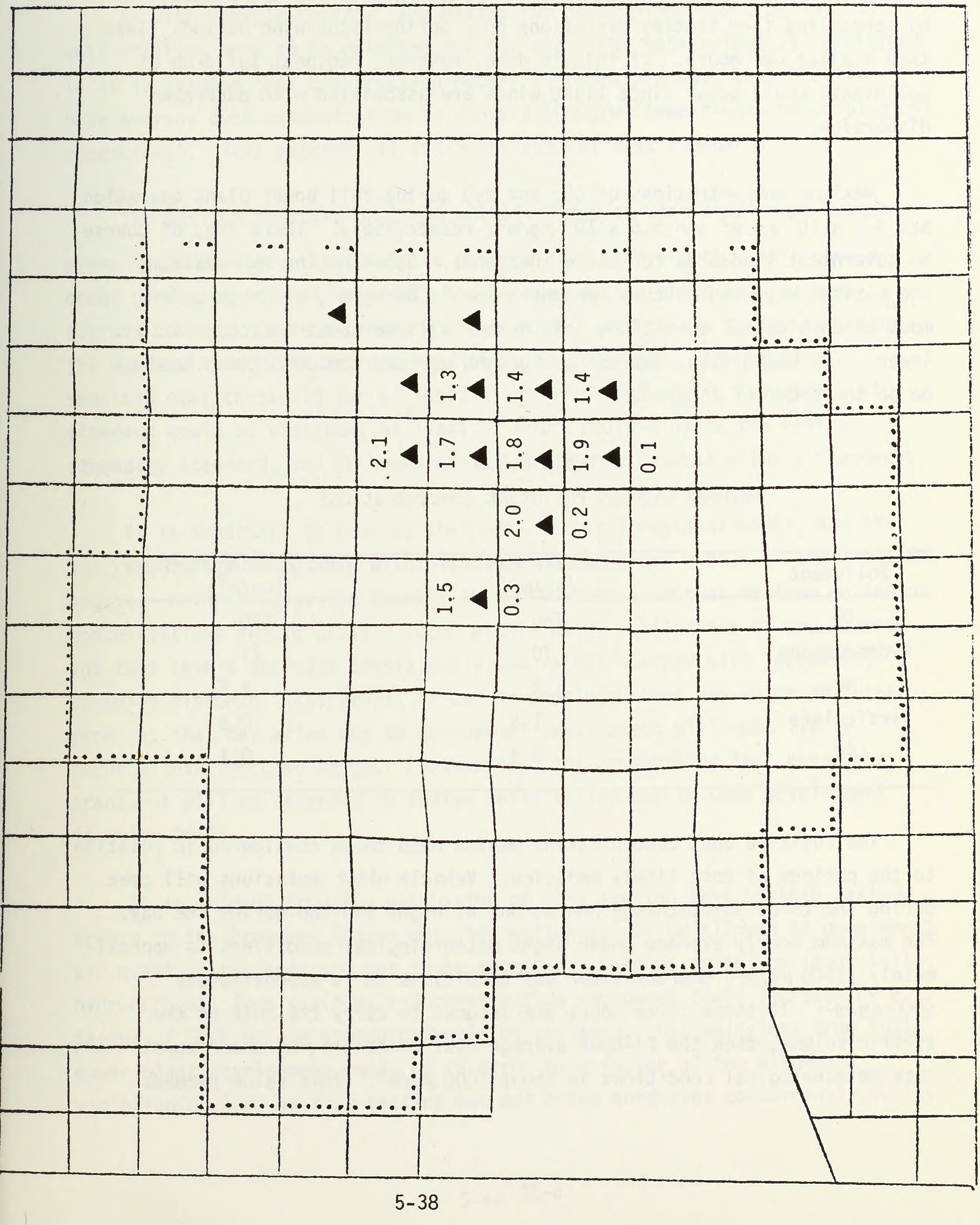

reveals that such an exceedance is most likely to occur during periods of strong winds. It should be possible to remain within the H_2S standard by scheduling flow testing operations only during light wind periods (less than 5 miles per hour). If this is done, however, regional build-up of pollutants could occur since light winds are associated with decreased dispersion.

Maximum concentrations of CO_2 and H_2O during full power plant operation are 4.2×10^4 $\mu g/m^3$ and 6.5×10^6 $\mu g/m^3$, respectively. There are, of course, no government standards for these compounds. Based on the H_2O maximum, the maximum expected mercury concentration is 65 ng/m^3, although under most meteorological conditions this number will be about a factor of 10 lower. For comparison, ambient background mercury concentrations tend to be on the order of 1 ng/m^3.

Table 5.3.9

Maximum Gaseous Pollutant Concentrations

Pollutant	Vehicle Maximum ($\mu g/m^3$)	Construction Maximum ($\mu g/m^3$)
CO	760	230
Hydrocarbons	70	21
NO_x	12	3.5
Particulate	1.8	0.5
SO_x	0.4	0.1

The fugitive dust concentration maxima need to be considered in relation to the periods of most likely emission. Vehicle dust emissions will peak during the three shift-change hours, one at night and two during the day. The maximum hourly average under night meteorological conditions is approximately 11500 $\mu g/m^3$, whereas under day conditions it is approximately 6000 $\mu g/m^3$. If these three hours are assumed to carry the bulk of the traffic volume, then the 24-hour average dust concentration under worst case meteorological conditions is about 1000 $\mu g/m^3$. This value exceeds all state and Federal dust standards.

As with vehicle traffic, the maxima for power plant construction and well drilling need to be weighted for day and night meteorological conditions. If it is assumed that construction occurs 24 hours per day, then the 24-hour average dust concentration is about 2300 $\mu g/m^3$ (worst-case meteorological conditions). This exceeds all state and Federal dust standards.

The maximum fugitive dust concentration due to wind erosion of exposed areas is 2578 $\mu g/m^3$. It should be pointed out, however, that this should occur during periods of extremely high winds, during which natural dust sources commonly cause exceedance of suspended particulate matter standards. The maximum under less extreme conditions is 303 $\mu g/m^3$. If the wind remained over threshold for at least eight hours out of 24, then the state standard would be violated; at least 12 hours would violate the Federal secondary standard, and 20 hours would violate the Federal primary standards.

It is important to realize that RAMR is not a regional model, and that its results are valid only within about a 20 kilometer radius of the emission source. Nevertheless, the results presented here show that maximum pollutant concentrations should usually occur within about a kilometer of the source, and that levels decrease consistently and rather quickly with increasing downwind distance. Therefore, it can be concluded that any major pollutant problems that may arise due to geothermal development will most likely occur within the Coso Range. Furthermore, the probability that government standards will be exceeded in Indian Wells Valley due to Coso development is quite small.

It is evident from the discussion of this section that certain maximum errors in the Proposed Action emission estimates can be allowed if government air quality standards are not to be exceeded. Gaseous emissions (especially hydrocarbons) from vehicles and construction equipment could increase by a factor of 2.5 before standards would be violated. H_2S emissions from full power plant development could be in error by a factor of two without a violation as long as flow testing was not being conducted concurrently during high winds (this case has already been discussed). The H_2S emissions from flow testing by itself could be increased by a factor of 1.25 without exceeding standards. The standards for suspended particulate matter would be exceeded under the current estimates for total road mileage and disturbed area in the Proposed Action. However, certain mitigation measures to be discussed in a later section could bring fugitive dust concentrations within standard.

Several points should be considered in analyzing the results presented in this section. First of all, RAMR is a rather conservative model, i.e. it tends to over-predict pollutant concentrations. Thus, the resulting values should be looked upon as upper limits to the actual case. Furthermore, any dispersion model can provide only an estimate, and an uncertainty in the results of $\pm$20% is considered to be quite good; $\pm$50% or more is more reasonable in many cases. Next, the equations used to calculate fugitive dust emissions are also conservative. They assume all emitted dust particles greater than 30 μm in diameter to be indefinitely suspended, while the larger of these might actually travel no more than a few kilometers. Although the matter is unresolved, recent studies in Arizona (McCaldin and Heidel, 1978) have measured vehicle dust emission factors more than a factor of two lower than those predicted by the EPA equations used here. Thus, the present fugitive dust concentrations should be accepted with this in mind. Finally, treatment of H_2S by H_2O_2 is probably greater than 95% efficient, so actual H_2S emission rates may be lower than those quoted here. Ninety-five percent control efficieny can be achieved with a high degree of certainty.

5.4 AIR QUALITY MONITORING PLAN

The predicted ambient pollutant concentrations discussed in the preceding sections are all based upon the emissions estimates of the Proposed Action. If these estimates are incorrect, however, the actual concentrations could be either larger or smaller than those predicted. As geothermal development proceeds, it will be necessary to maintain a constant check on ambient pollutant levels in order to determine whether or not further mitigation will be required to meet government standards.

There are a number of species for which an air monitoring system could be designed. For maximum cost-effectiveness, however, measurement of fugitive dust and H_2S levels should give a reasonable indication of both suspended particulate matter and gaseous pollutant concentrations. H_2S seems to be the most likely of any gaseous pollutants to exceed current standards, and the predicted ratios of other emission rates to H_2S rates should also provide an estimate of the ambient levels of other species without actually going to the expense of monitoring those species directly.

It is critical that monitoring devices be placed in the areas of most probable maximum ambient concentration. Considering the predominant wind directions in the Coso area, one monitoring device should be placed to the north-northwest, and one to the south-southeast, of each major emission source. For H_2S emitted from power plants under most meteorological conditions, the monitors should be approximately 0.5 km from each plant. For fugitive dust from both grading activities and wind erosion, the monitors should be placed approximately 1.0 km from the center of the disturbed area.

The costs of such a monitoring system can be based upon current prices, although inflation during the several-decade productive lifetime of the geothermal resource could rapidly invalidate these numbers. The price of an H_2S monitor with a strip chart recorder falls within the range of $1500 to $2000. A high-volume sampler for suspended particulates cost approximately $500; collection filters for the sampler would be about one dollar each.

Labor costs for field maintenance of the instruments and for laboratory analysis of the filters would be in addition to the above prices, and are usually found to exceed the costs of the instruments themselves over an extended period.

Monitoring of trace elements may also be advisable, but this should be decided on a case-by-case basis due to the wide variability of concentrations both within a given field and among separate fields. Tests of the well fluid should reveal the predominant trace elements present, and monitoring plans can be developed accordingly if necessary. Based on the history of mining in the area, mercury is a likely candidate for a monitoring program. As with other monitoring devices, trace element monitors should be placed about one-half kilometer downwind of an off-gas ejector, or about 2 kilometers downwind of a cooling tower, depending upon the emission source.

5.5 VISIBILITY IMPACT

One of the major air quality concerns is the impact of geothermal development upon visibility. The California desert has traditionally enjoyed very good visibility, and preservation of this visibility is considered to be important both to the public for its aesthetic value, and to the NWC for its value in allowing weapons testing to be observed from long range. The Navy is concerned with visbility not only in the "visible" range (i.e. as perceived by the human eye), but also in the infrared due to their weapons system requirements. Both spectral regions will be addressed in this section.

5.5.1 Visible Spectrum

Considering the emission levels projected for geothermal development at Coso, the pollutant most likely to lead to visibility degradation is hydrogen sulfide. Hydrogen sulfide in itself, however, should not pose a problem. Rather, H_2S can react to form SO_2, which can then undergo further chemical conversion to sulfate aerosol which, along with nitrate aerosol, is one of the most common visibility-reducing species (see, for example, Cass, 1976). The initial reaction in the sulfate-formation process, and the principal atmospheric reaction of H_2S (Thiemens and Schwartz, 1978), is believed to be:

$$\bullet OH + H_2S \longrightarrow H_2O + HS\bullet \, . \qquad (5.5.1.1)$$

The rate constant for this reaction at 298 K is 5.25×10^{-12} cm^3 molec^{-1} sec^{-1} (Perry, Atkinson, and Pitts, 1976), so, at a typical OH radical concentration of 3×10^6 molecule cm^{-3}, the half-life of H_2S in the lower troposphere due to reaction (5.5.1.1) is approximately 12 hours. The half-life of the SO_2-to-sulfate process is about 24 hours (Levine and Schwartz, 1978), so it can be concluded that H_2S emitted at Coso on a given day will not have formed appreciable quantities of sulfate aerosol until the next day.

Due to the time scale involved, the dispersion of sulfate aerosol is a regional problem, not confined to the Coso study area. Considering the prevailing wind directions at Coso, the adjacent areas of most interest are Owens Valley and Indian Wells Valley. As mentioned, however, RAMR is not a regional model, so concentrations in these areas cannot be calculated directly. The most reasonable approximation method is to calculate concentrations at the fringes of the study area, where RAMR is still valid, and assume these concentrations to be upper limits to the levels that would be found further downwind after more dispersion had occurred. Doing so, the upper limit sulfate concentration due to H_2S emitted from full power plant development is calculated to be approximately 1 $\mu g/m^3$. This should make a contribution to B_{scat} of about 0.04 ($x10^{-4}$ m^{-1}) (Trijonis, 1978). Applying the Koschmieder visibility formula, and using the China Lake average B_{scat} of 0.4 ($x\ 10^{-4}$ m^{-1}), the calculated effect would be to decrease visibility from about 61 miles to about 55 miles. This represents approximately a 10% decrease in visibility.

It must be stressed again that this projected visibility degradation represents an upper limit. Although it cannot be quantitated by RAMR, dispersion throughout Indian Wells Valley over a 24 hour period should result in considerably lower sulfate concentrations and, consequently, less visibility degradation. Furthermore, sulfur species can be lost from the atmosphere through precipitation and through dry deposition (Judiekis and Wren, 1977; Judeikis and Stewart, 1977), thereby further decreasing the visibility degradation.

Visibility degradation due to fugitive dust from wind erosion will occur only when the wind velocity is above the erosion threshold. Commonly under these circumstances, however, natural dust sources have already markedly decreased the visibility, so disturbed area erosion should have little further effect. A more important concern in terms of geothermal development is that of dust from construction activity during light to moderate winds, when wind erosion will not be a factor. This is likely to be a local rather than a regional problem, since most dust particles commonly settle out within a few kilometers of their source. Thus, RAMR results can be used to estimate concentrations. The maximum ambient dust level that one would expect from construction, averaged over the entire study area, is approximately 20 $\mu g/m^3$. According to Trijonis (1978), this should contribute about 0.08 to B_{scat}, assuming a typical desert dust particle size distribution. Again using Koschmieder's formula, this would predict a visibility of 51 miles, compared to the annual mean of 61 miles, a decrease of 16%. This is, however, an upper limit, since Koschmieder's formual assumes a constant B_{scat} throughout the visual range, whereas high ambient dust concentrations would be a local phenomenon, most likely not extending over a 51 mile range. Also, 20 $\mu g/m^3$ is the average dust concentration only under certain meteorological conditions. In many cases, this values would be a factor of ten or more lower, resulting in only minimally decreased visibility.

A specific problem in terms of air quality, and visibility in particular, is that of Class I areas. The Class I areas in the Coso region are Sequoia and Kings Canyon National Parks, and Domeland Wilderness Area in Sequoia National Forest. Due to the meteorology and topography of the area, it is unlikely that more than trace amounts of pollutants from the Coso geothermal development would find their way to these areas. Thus, it can be estimated that there will be no measurable effect upon the PSD increments allowed for Class I areas. Nevertheless, there could be visibility effects in terms of vistas from mountain peaks in these Class I areas, looking across Owens Valley or Indian Wells Valley. The upper limit to visibility degradation discussed in this section would apply here. Domeland is the closest Class I area to Coso; however, it has few areas over 8000 feet in elevations, and thus offers few sweeping views to the east because of the intervening Sierra Nevada ridge. Sequoia and Kings Canyon, on the other hand, have a number of peaks at over 12,000 feet along their eastern boundaries, including Mt. Whitney at 14,494 feet, so visibility is of more interest in these parks.

5.5.2 Infrared Spectrum

The main infrared-absorbing species which can be expected from geothermal development are CO_2 and H_2O. As with H_2S, RAMR is unable to calculate regional average concentrations of these species, so average concentrations in the fringe areas of the KGRA will be used as upper limits. Doing so, the upper limits to CO_2 and H_2O ambient level increases due to full power plant development are calculated to be 1 mg/m^3 (0.6 ppm) and 100 mg/m^3 (135 ppm), respectively. These can be compared to typical ambient concentrations of 345 ppm for CO_2 and 5 g/m^3 for H_2O. Thus, geothermal development should result in an upper limit increase of 0.2% and 2.0% for CO_2 and H_2O, respectively.

These increases should be insignificant in terms of infrared attenuation since natural levels of CO_2 and H_2O can fluctuate more than this quite readily and quite often (consider a foggy or overcast day, for example). Nevertheless, a series of calculations was performed to quantitate the specific effects of geothermal development. The computer program LOWTRAN 4 was used to calculate infrared attenuation as a function of wavelength (Selby, et al., 1978). By utilizing the absorption spectra and relative amounts of the major infrared absorbing gases in the atmosphere, as well as a haze model to account for the attenuating effects of aerosol particles, this program can calculate transmittance along a given path length throughout the infrared. The program was used in a mode such that the concentration of either CO_2 or H_2O could be altered without changing the concentrations of other atmospheric gases.

CO_2 absorbs infrared radiation primarily in three bands located around 2.7 μ, 4.2 μ, and 15 μ. Therefore, these regions were selected for careful study. The results of the calculations were straightforward. Obviously, there were no effects at wavelengths where neither gas absorbs. Also, no additional attenuation was observed near the centers of the major absorption bands; ambient concentrations of both H_2O and CO_2 are high enough that there is already essentially zero transmittance at these wavelengths. The only observable effects were on the fringes of the major bands. A 2% increase in H_2O concentration resulted in up to a 5% increase in absorption at several of these fringe wavelengths, whereas the absorption effect a 0.2% CO_2 increase was never more than 1%.

6.0 MITIGATION MEASURES

All emissions and ambient concentrations discussed up to this point have been based upon the assumptions of the Proposed Action. As was pointed out in Section 5.0, however, several of these assumptions could lead to violations of government air quality standards. A number of mitigation measures are presented here which could assist in bringing these emissions within regulations.

First of all, it is possible that the State one-hour H_2S standard could be exceeded by a combination of full power plant development and flow testing of a new well. This would be likely to occur only if the wind speed were greater than five miles per hour. Thus, the potential H_2S air quality problem could be mitigated by scheduling flow testing only during periods of light wind. This measure is not fail-safe, however, since it is dependent upon weather predictions, and once the flow test begins it continues until it is completed regardless of how the weather might change. Also, regional build-up of pollutants could occur since light winds are associated with decreased dispersion.

Fugitive dust could be a potential air quality problem at all stages of geothermal development. To reduce dust emission from vehicle traffic, it might be advisable to bring employees into the construction area by bus from U.S. 395. Equation (5.1.3.1), the vehicle dust emission factor, is an approximately linear function of the number of wheels traversing an area. Busing could markedly reduce the total number of wheel-miles required, probably decreasing vehicle dust emissions by a factor of ten or more.

Graveling exposed areas would serve to reduce the fugitive dust emissions due to wind erosion. Equation (5.1.3.2), the wind erosion emission factor, is a function of both silt content, which would be decreased by more than a factor of two by graveling, and soil erodibility, which would decrease by a factor of six (USDA, 1968). Thus, the total dust emission factor would be expected to decrease by more than a factor of ten.

Finally, any fugitive dust problem can be mitigated by watering. Examination of equation (5.3.1.1) reveals that dust emissions are assumed to be negligible on days during which 0.01 inch or more of rain falls. Thus, efficient watering can effectively eliminate fugitive dust emissions. It is assumed that a watering truck might operate on access roads immediately preceding the morning and afternoon rush hours, and at grading and construction sites throughout the workday.

It should be recognized that hydrogen sulfide pollution control devices in the power plant are considered to be a part of the Proposed Action, and not a mitigation measure. Treatment of hydrogen sulfide by hydrogen peroxide has been found to be greater than 95% efficient in field operation, so 95% abatement has been assumed throughout this impact analysis.

7.0 CONCLUSIONS

The major conclusions of this report can be summarized by the following statements:

1. The State standard for hydrogen sulfide could be exceeded under certain conditions. Ambient levels of other gaseous pollutants are expected to fall within both Federal and State standards.

2. The hydrogen sulfide standards should not be exceeded under most conditions. The only calculated exception to this would arise from concurrent full power plant development and new well flow testing with wind speeds greater than five miles per hour.

3. Fugitive dust standards could be exceeded under a number of circumstances. Several mitigation measures are suggested which could effectively control these exceedances.

4. Maximum ground-level ambient pollutant concentrations are, in most cases, expected to occur within about a kilometer of their emission source. This means that any potential pollution problems are likely to occur within the KGRA, and not in surrounding areas such as Indian Wells Valley.

5. Uppper limits are predicted for regional visibility degradation due to both hydrogen sulfide conversion to sulfate (10%) and fugitive dust (16%).

6. Regional increases in H_2O and CO_2 concentrations should fall within natural fluctuation limits. The effects of any such increases upon attentuation of infrared radiation should be insignificant.

8.0 REFERENCES

Russel Bohn, Thomas Cuscino, Jr., and Chatten Cowherd, Jr., "Fugitive Emissions from Integrated Iron and Steel Plants," EPA Report 600/2-78-050 (1978).

California Air Resources Board (CARB), "California Air Quality Data: Summary of 1977 Air Quality Data, Gaseous and Particulate Pollutants," CARB Technical Services Division (1977a).

California Air Resources Board (CARB), "Plans Development Program for Air Conservation Program for California," September 1976, revised February 1977 (1977b).

Glen R. Cass, "The Relationship Between Sulfate Air Quality and Visibility at Los Angeles," Caltech EQL Memorandum No. 18 (1976).

Harry M. Castrantas, Larry R. Hampshire, and Byron B. Woertz, "Hydrogen Sulfide Abatement During Geothermal Steam Drilling," Lake County Geothermal Environmental Seminar (1978).

China Lake NWC, "Draft Environmental Statement for the Navy Coso Geothermal Development Program," NWC Public Works Department (1978).

E. A. Crecelius, D. E. Robertson, J. S. Fruchter, and J. D. Ludwick, "Chemical Forms of Mercury and Arsenic Emitted by a Geothermal Power Plant," Trace Substances in Environmental Health, 10, 287 (1976).

Environmental Protection Agency, "Compilation of Air Pollutant Emission Factors," Publication AP-42 (1977).

Environmental Protection Agency, "Supplement No. 8 for Compilation of Air Pollutant Emission Factors," Publication AP-42, Supplement 8 (1978).

George Jutze and Kenneth Axetell, "Investigation of Fugitive Dust, Volume I - Sources, Emissions, and Controls," EPA Report 450/3-74-036a (1974).

Peter F. Lester and Richard L. Simon, "Fluxes of Air Pollutants into the California Desert from the Los Angeles Basin," Global Weather Consultants (1978).

Stuart Z. Levine and Stephen E. Schwartz, "Construction of Surrogate Chemical Mechanisms for Atmospheric Photochemical Systems," IX Intl. Conf. on Photochemistry (1978).

Roy O. McCaldin and Karen J. Heidel, "Particulate Emissions from Vehicle Traffic Over Unpaved Roads," Air Pollution Control Association Annual Meeting, Paper 78-14.2 (1978).

W.E.K. Middleton, "Vision Through the Atmosphere," University of Toronto Press (1952).

James R. Ouimette, "Survey and Evaluation of the Environmental Impact of Naval Weapons Center Activities," China Lake NWC Technical Memorandum 2426 (1974).

R. A. Perry, R. Atkinson, and J. N. Pitts, Jr., J. Chem. Phys. 64, 3237 (1976).

Roger F. Reinking, Larry A. Mathews, and Pierre St. Amand, "Dust Storms Due to the Dessication of Owens Lake," Intl. Conf. on Environmental Sensing and Assessment, Las Vegas, Nevada (1975).

David E. Robertson, Jonathan S. Fruchter, J. Donald Ludwick, Connie L. Wilkerson, Eric A. Crecelius, and John C. Evans, "Chemical Characterization of Gases and Volatile Heavy Metals in Geothermal Effluents," Transactions of the Geothermal Resources Council 2, 579 (1978).

J. Rudisill, Natomas Co., personal communication (1979).

J.E.A. Selby, F. X. Kniezys, J. H. Chetwynd, Jr., and R. A. McClatchey, "Atmospheric Transmittance/Radiance: Computer Code LOWTRAN 4," U.S. Air Force Report AFGL-TR-78-0053 (1978).

Mark W. Thiemens and Stephen E. Schwartz, "The Fate of HS Radical Under Atmospheric Conditions," 13th Informal Photochemistry Conference (1978).

C. W. Thornthwaite, "Climates of North America According to a New Classification," Geograph. Rev. 21, 633 (1931).

John Trijonis, "Written Testimony before the California Energy Commission in the matter of Notice of Intention of Southern California Edison Company, Re: Application for Certification of Combined Cycle Generating Station," (1978).

D. Bruce Turner, "Workbook of Atmospheric Dispersion Estimates," EPA Report AP-26 (1970).

D. Bruce Turner and Joan Hrenko Novak, "User's Guide for RAM," EPA Publication 600/8-78-016 (1978).

APPENDIX A

RAMR

This is a computer printout which was not easily possible to reproduce. It is available for review in the Bakersfield District Office, Bureau of Land Management, 800 Truxtun Avenue, Rm. 311, Bakersfield, California 93301. Telephone (805) 861-4191.

9.0 COSO GEOTHERMAL RESOURCE AREA CLIMATOLOGY

9.1 GEOGRAPHICAL DESCRIPTION

The Coso Geothermal Resource Area (CGRA) is located in the southern California high desert region. Two-thirds of the CGRA are within the United States China Lake Naval Weapons Center, between the towns of Haiwee and China Lake. Meteorological data from numerous southern California stations, as well as several stations within the CGRA were used to develop a climatological description of the CGRA and the surrounding high desert region. (See Figure 1, Table 1 and Figure 2).

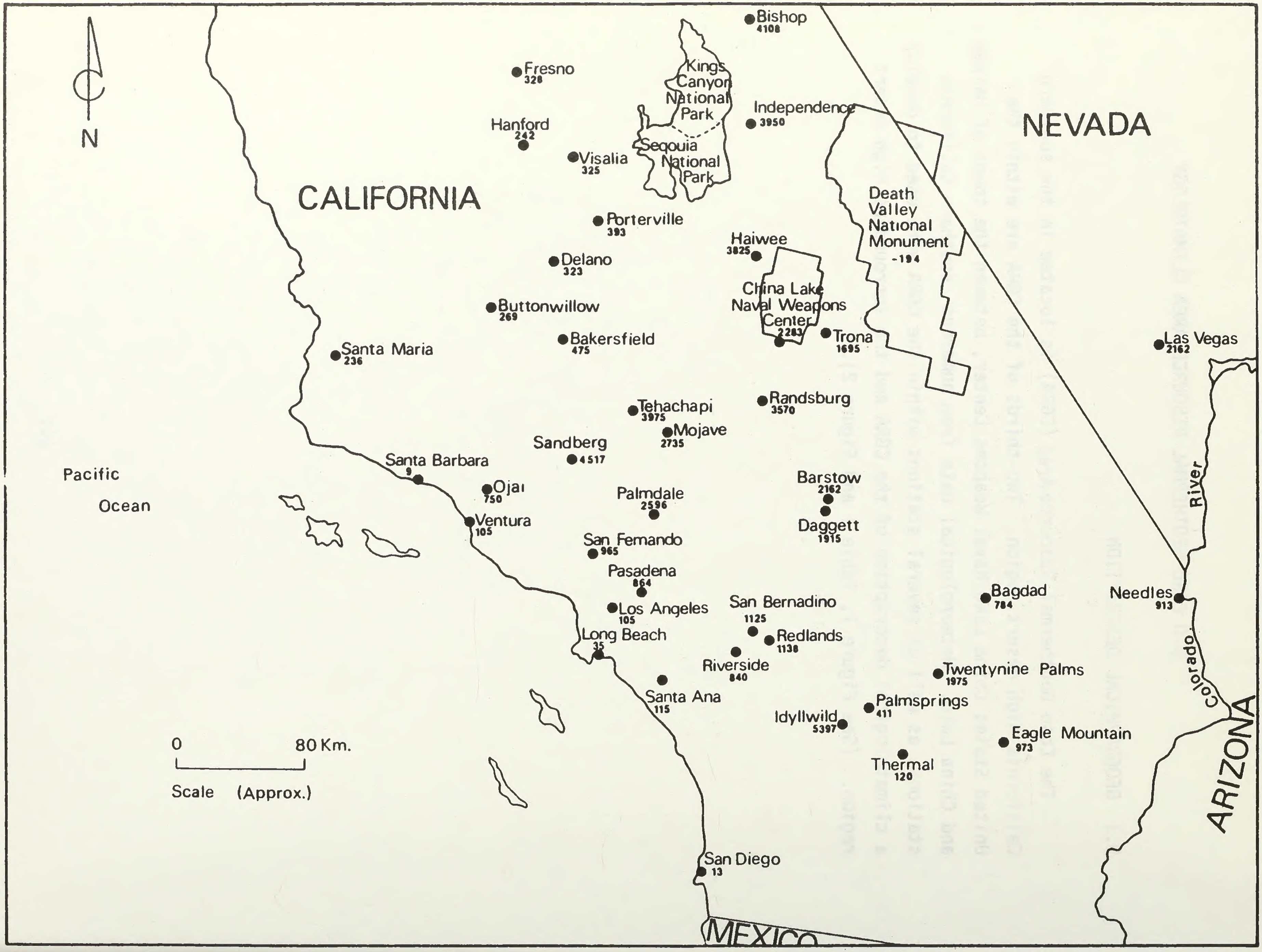
N
Bishop
4108
Fresno
328
Kings Canyon National Park
Independence
3950
NEVADA
Hanford
242
Visalia
325
Sequoia National Park
CALIFORNIA
Porterville
393
Death Valley National Monument
-194
Haiwee
3825
Delano
323
China Lake Naval Weapons Center
2283
Buttonwillow
269
Trona
1695
Bakersfield
475
Santa Maria
236
Las Vegas
2162
Randsburg
3570
Tehachapi
3975
Mojave
2735
Sandberg
4517
Santa Barbara
9
Pacific
Ocean
Ojai
750
Barstow
2162
Palmdale
2596
River
Ventura
105
Daggett
1915
San Femando
965
Pasadena
864
Bagdad
784
Needles
913
Los Angeles
105
San Bernadino
1125
Long Beach
35
Redlands
1138
Riverside
840
Colorado
Twentynine Palms
1975
Santa Ana
115
Palmsprings
411
Idyllwild
5397
Eagle Mountain
973
0
80 Km.
Scale (Approx.)
Thermal
120
ARIZONA
San Diego
13
MEXICO

Table 1 - Coso Geothermal Resource Area

1 - High Probability Geothermal Resource Area.
2 - Moderate Probability Geothermal Resource Area.
3 - Low Probability Geothermal Resource Area.
And outlined in pencil is Uncertain Geothermal Resource Area.

COSO Area Stations	Elevation (feet)
Airport Lake	2,300 ft.
Little Lake	3,180 ft.
Rose Valley Ranch	3,435 ft.
Coso Basin	3,560 ft.
Red Hill	3,600 ft.
Haiwee	3,825 ft.
Cactus Flats	5,000 ft.

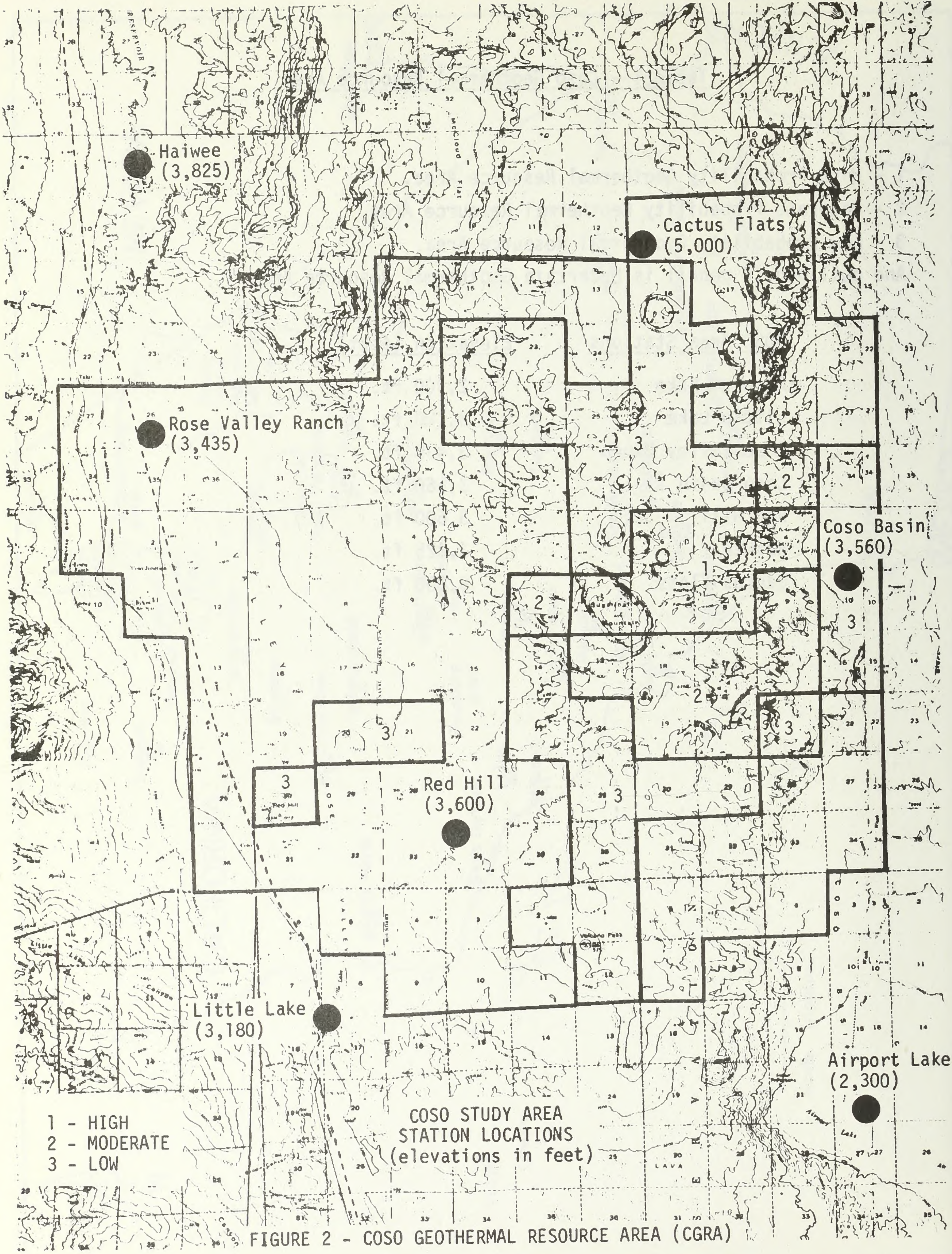

FIGURE 2 - COSO GEOTHERMAL RESOURCE AREA (CGRA)

9.2 CLIMATOLOGICAL DESCRIPTION

The climate of the CGRA, typical of the southern California high desert region, is characterized by hot summers, cool to cold winters, large diurnal temperature ranges, low humidity, and little cloudiness or visibility restriction. The CGRA's latitudinal and continental positions are under the direct influence of the semi-permanent high pressure cell located over the eastern Pacific Ocean. This high pressure cell annually migrates north during summer, blocking the passage of cyclonic storms into the CGRA. During the winter season, the high pressure cell migrates southward permitting the cyclonic storms to move through the area (although anticyclonic circulation is prevalent year round).

Local topography in the CGRA is an important climatic factor. The Sierra Nevada Mountains to the west form a barrier to passing storms and frontal systems, and create a rainshadow effect over the CGRA. As the air descends down the leeside of these mountains, it warms at the adiabatic lapse rate, the air stability is increased, and the potential of condensation decreased. As a result, precipitation varies from 55 to 20 inches on the windward side of the Sierras to less than 10 inches annually in the CGRA. Temperatures in the higher elevations of the CGRA average 5^{o}F to 15^{o}F cooler than those at China Lake (elevation 2,283 feet) whose mean annual temperature is 64.0^{o}F. The north-south orientation of the mountains and valleys in the CGRA exert influence on the regional air flow pattern, creating south to southeasterly or north to northwesterly winds most of the year.

9.3 TEMPERATURE

Temperature within the CGRA may vary up to 15°F as a direct result of differences in elevation. Assuming an atmospheric lapse rate of 5.4°F/1,000 feet (dry adiabatic) the temperature at Cactus Flats (5,000 feet) would be almost 15°F cooler than the temperature at China Lake (2,283 feet) (See Table 2).

The mean annual temperature at China Lake is 64.0°F. Monthly normals range from 43.1°F in January to 86.2°F in July. The daily temperature extremes show a normal daily minimum in January of 28.7°F while the normal daily maximum is 102.3°F in July. Temperature normals and extremes for China Lake are presented in Table 3.

Table 4 shows the monthly temperature extremes, °F, for the CGRA and surrounding high desert region (including Las Vegas, NV) for the period August 1977 through September 1978. It is difficult to discern patterns from the data due to its incompleteness, but the table does reveal the large temperature ranges between the monthly maximum and minimum temperatures, with some differences of 60°F to 70°F.

Daily temperature comparisons of CGRA station data are presented in Table 5. Daily maximum, minimum, and hourly average temperatures from seven stations are depicted for nine days of August 1978. Noticeable are the consistently high maximum temperature at Airport Lake due to its low elevation; the cooler minimum temperatures found at Rose Valley Ranch as a result of night-time cool air drainage into the Rose Valley; and the cooler daily hourly average temperatures at Cactus Flats due to its high elevation. Figure 3 is an example of one daily temperature plot derived from Table 5.

Mean annual and monthly temperatures for selected stations of southern California are presented in Figures 4a through 4m. Observable from the

Table 2. Temperature Differences Assuming an Adiabatic Lapse Rate

Station	Elevation (ft)	Base Elevation (ft)	Temperature Change with Elevation Assuming a Lapse Rate of 5.4°F/1000 ft
China Lake	2283	0	0°F
Airport Lake	2300	17	-0.09°F
Little Lake	3180	897	-4.84°F
Rose Valley Ranch	3435	1152	-6.22°F
Coso Basin	3560	1277	-6.90°F
Red Hill	3600	1317	-7.11°F
Haiwee	3825	1542	-8.33°F
Cactus Flats	5000	2717	-14.67°F

Table 3

Monthly Temperature Normals and Extremes, ^{o}F,
China Lake, California (1946-1976)

Month	Record High	Maximum	Normal Average	Minimum	Record Low
January	77	57.8	43.1	28.7	0
February	83	63.8	49.0	34.2	14
March	92	69.0	54.4	39.7	17
April	98	76.8	61.9	46.6	28
May	107	86.2	70.7	55.2	34
June	114	95.5	79.4	63.1	42
July	116	102.3	86.2	70.0	52
August	112	100.5	84.1	67.7	50
September	110	94.0	77.2	60.3	39
October	102	81.9	65.4	48.8	21
November	88	68.0	52.4	37.0	18
December	86	58.6	43.7	29.1	2
Annual	116	79.5	64.0	48.4	0

Table 4 Monthly Temperature Extremes, °F
High Desert Stations (including Las Vegas
August 1977 through September 1978

	Maximum and Minimum Monthly Temperatures									
Month	2162 ft Las Vegas NV	2283 ft China Lake	2300 ft Airport Lake	3180 ft Little Lake	3435 ft Rose Valley Ranch	3560 ft Coso Basin	3600 ft Red Hill	3825 ft Haiwee	4150 ft Bishop	5000 ft Cactus Flats
8-77	115 68	113 59	107* 55	N/A N/A	97 * 53	95 * 48	N/A N/A	97* 59	107 51	93 * 48
9-77	109 57	105 49	110* 47	N/A N/A	98 * 37	99 * 37	88 * 46	102* 54	98 36	96 * 41
10-77	96 48	93 36	98* 33	N/A N/A	88 29	65 * 23	94 * 37	91 40	97 29	86 * 38
11-77	84 31	83 23	86* 29	74* 23	74 15	72 11	73 * 39	76 24	78 17	74 * 49
12-77	75 31	77 24	73* 50	71* 27	68 * 16	65 * 16	72 * 27	74* 28	73 20	70 * 59
1-78	66 31	66 26	65* 34	62* 22	58 * 16	58 * 16	62 23	59* 28	61 19	44 * 33
2-78	74 33	74 30	N/A N/A	69 22	64 15	61 * 16	69 20	64* 24	67 20	60 * 20
3-78	85 41	88 37	N/A N/A	66* 33	75 22	81 20	**103 30	80* 30	77 25	67 * 22
4-78	88 40	89 35	N/A N/A	80* 34	76 19	78 25	**104 * 50	81 31	82 25	73 20
5-78	102 46	100 40	N/A N/A	92* 38	94 25	92 * 25	**107 33	97 36	92 28	86 22
6-78	110 62	N/A N/A	N/A N/A	100* 48	100 40	103 * 37	108 * 51	105 53	99 44	95 * 35
7-78	115 66	N/A N/A	111* 54	100* 52	105 40	106 35	108 * 50	106* 51	104 44	99 * 34
8-78	114 61	N/A N/A	117 41	101* 47	109 38	112* 40	109 * 52	109 53	106 41	104 * 32
9-78	106 49	N/A N/A	101* 45	97* 54	N/A N/A	N/A N/A	96 * 52	N/A N/A	94 32	** 8 42

*Only partial data available for the month.

**Maximum temperature questionable

N/A No monthly data available

Table 5

CGSA Daily Temperature Comparisons
1. Daily Maximum Temperature
2. Daily Minimum Temperature
3. Daily Hourly Average Temperature

Date		Airport Lake (2300)	Little Lake (3180)	Rose Valley Ranch(3435)	Coso Basin (3560)	Red Hill (3600)	Haiwee (3820)	Cactus Flats (5000)
8-11-78	1.	104	98	97	98	99	96	92
	2.	72	72	63	72	70	73	66
	3.	87.0	84.3	78.5	84.3	82.3	82.9	78.8
8-12-78	1.	104	98	92	99	100	96	86
	2.	62	62	53	60	68	67	54
	3	83.9	82.1	76.9	79.8	82.7	80.9	71.7
8-13-78	1.	97	93	90	92	92	91	84
	2.	59	68	54	57	68	62	48
	3.	78.6	81.9	76.5	75.3	80.4	79.2	68.1
8-14-78	1.	95	91	90	91	92	89	84
	2.	51	62	49	53	67	63	53
	3.	75.3	76.7	69.5	76.5	77.2	74.9	69.2
8-25-78	1.	94	88	87	89	90	86	81
	2.	41	46	39	40	53	53	34
	3.	70.5	70.5	64.2	66.9	72.3	71.0	60.5
8-26-78	1.	96	90	89	91	93	90	83
	2.	44	52	46	44	52	54	39
	3.	72.2	72.2	68.6	68.9	74.0	74.1	63.7
8-27-78	1.	99	94	94	94	95	95	89
	2.	47	58	52	51	57	62	49
	3.	74.5	77.4	72.2	73.2	77.4	76.4	70.7
8-30-78	1.	103	96	96	96	97	96	89
	2.	50	64	53	54	66	68	49
	3.	78.9	81.8	77.4	76.4	82.1	81.3	69.1
8-31-78	1.	99	94	92	92	93	93	84
	2.	52	57	47	51	54	58	42
	3.	75.9	76.5	70.0	72.5	75.9	76.8	64.4

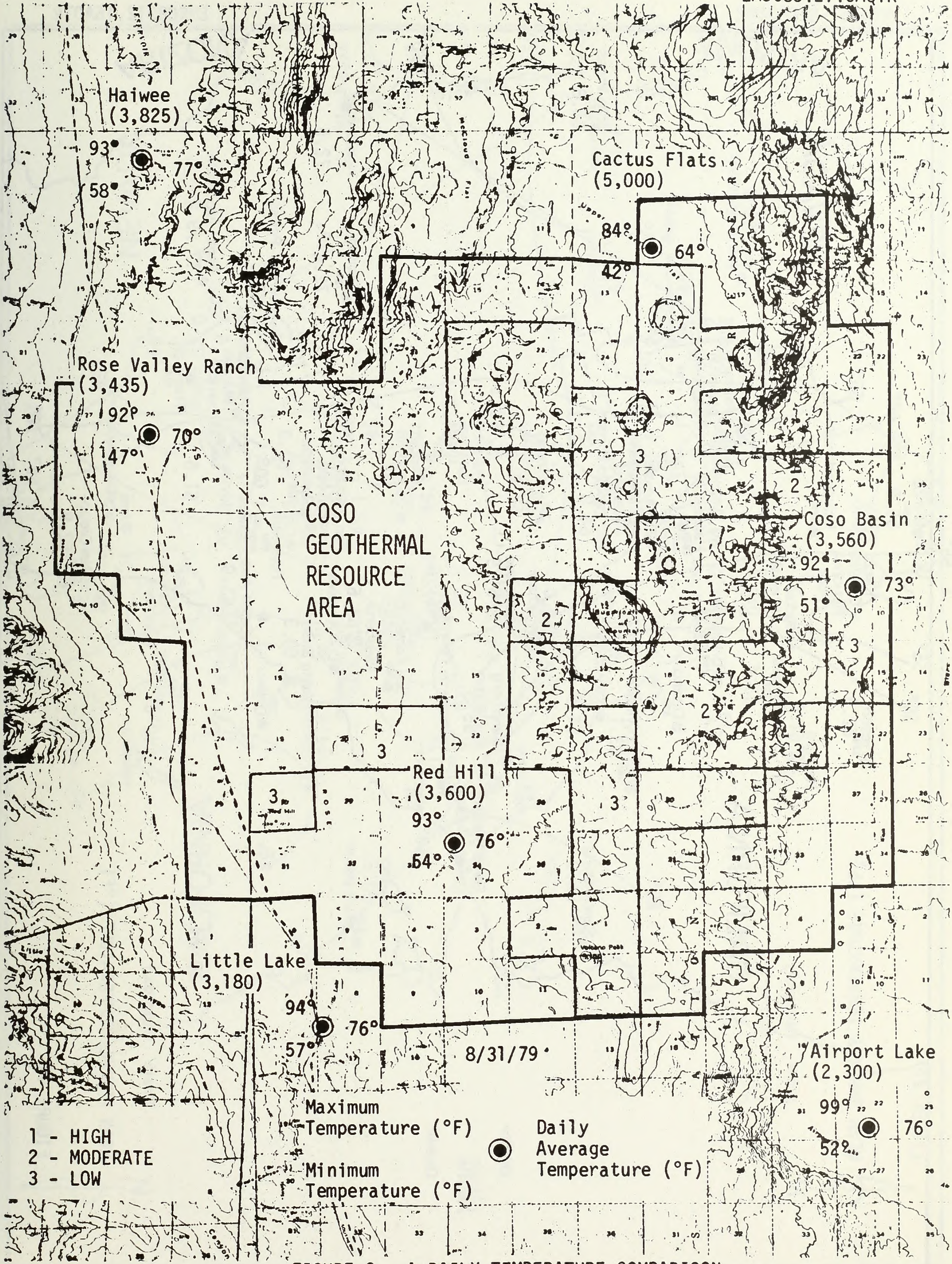

FIGURE 3 - A DAILY TEMPERATURE COMPARISON

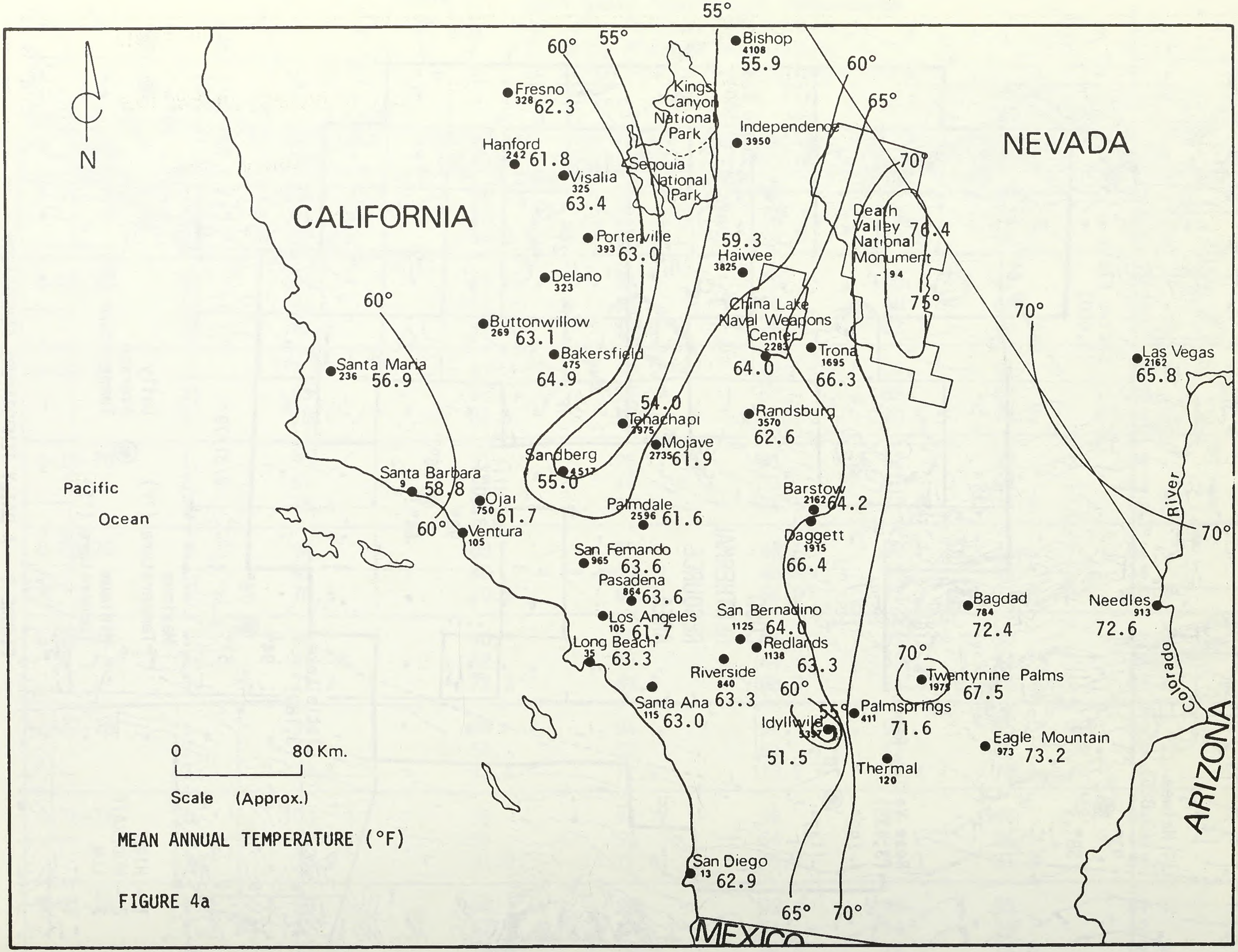

MEAN ANNUAL TEMPERATURE (°F)

FIGURE 4a

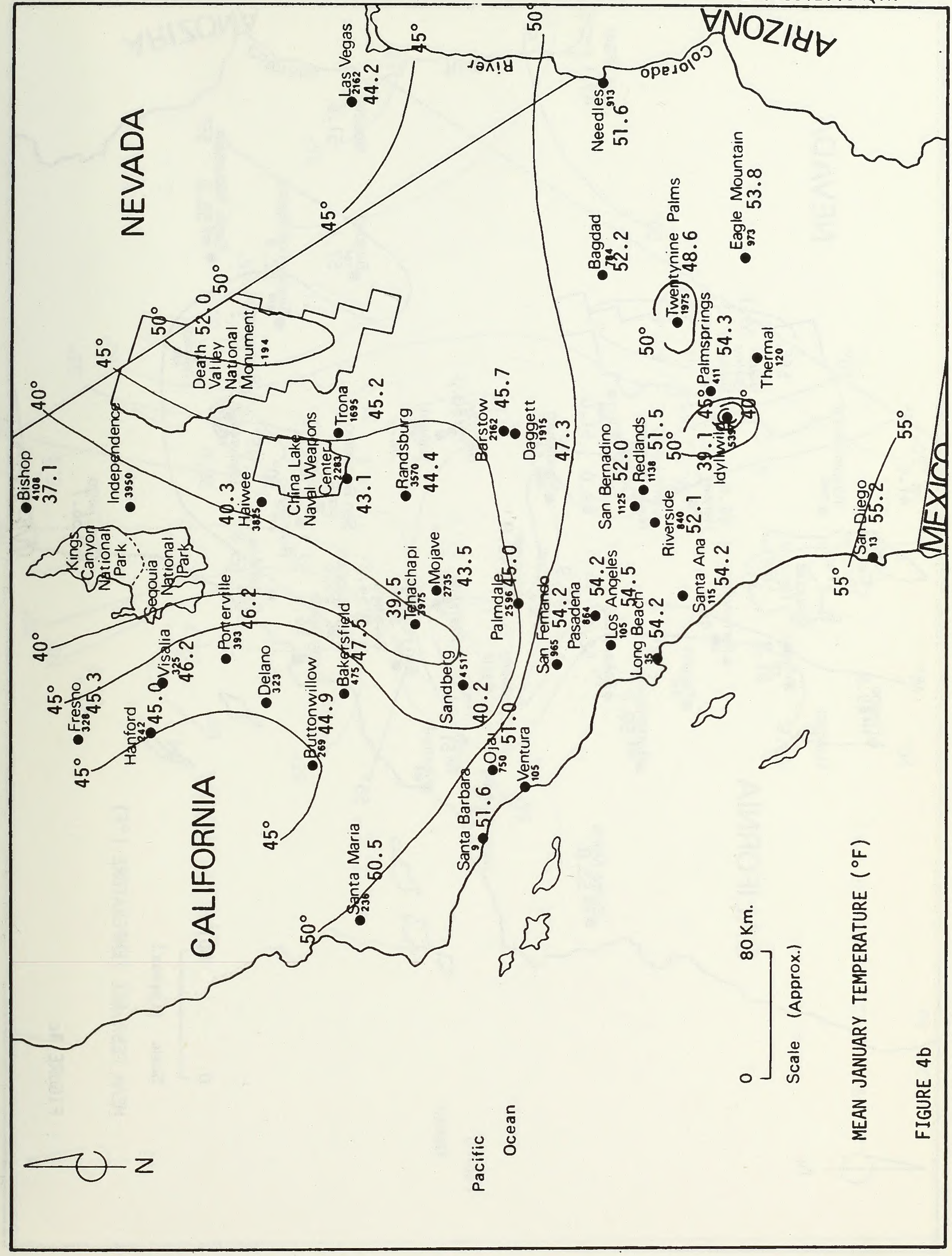

MEAN JANUARY TEMPERATURE (°F)

FIGURE 4b

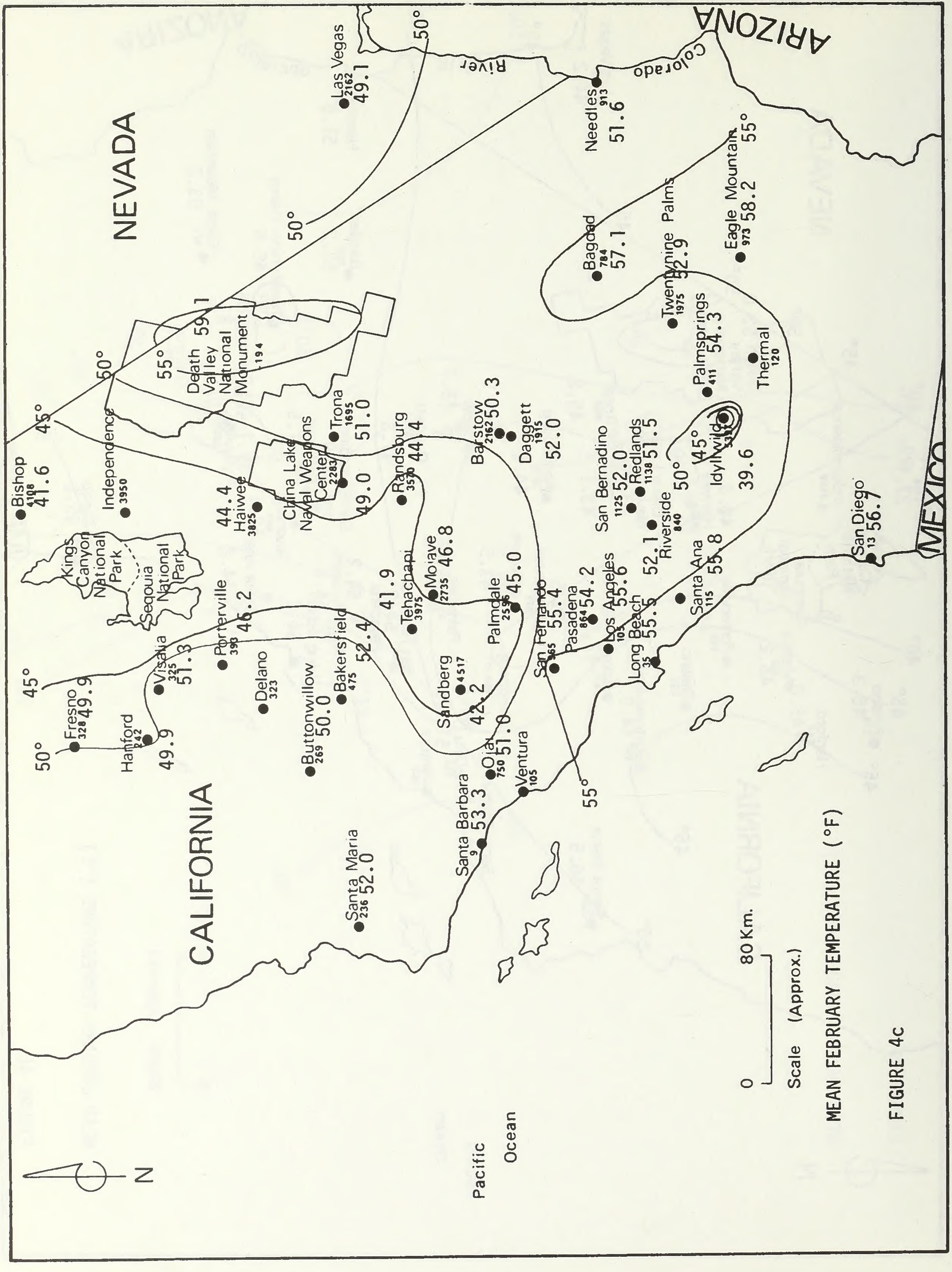

MEAN FEBRUARY TEMPERATURE (°F)

FIGURE 4c

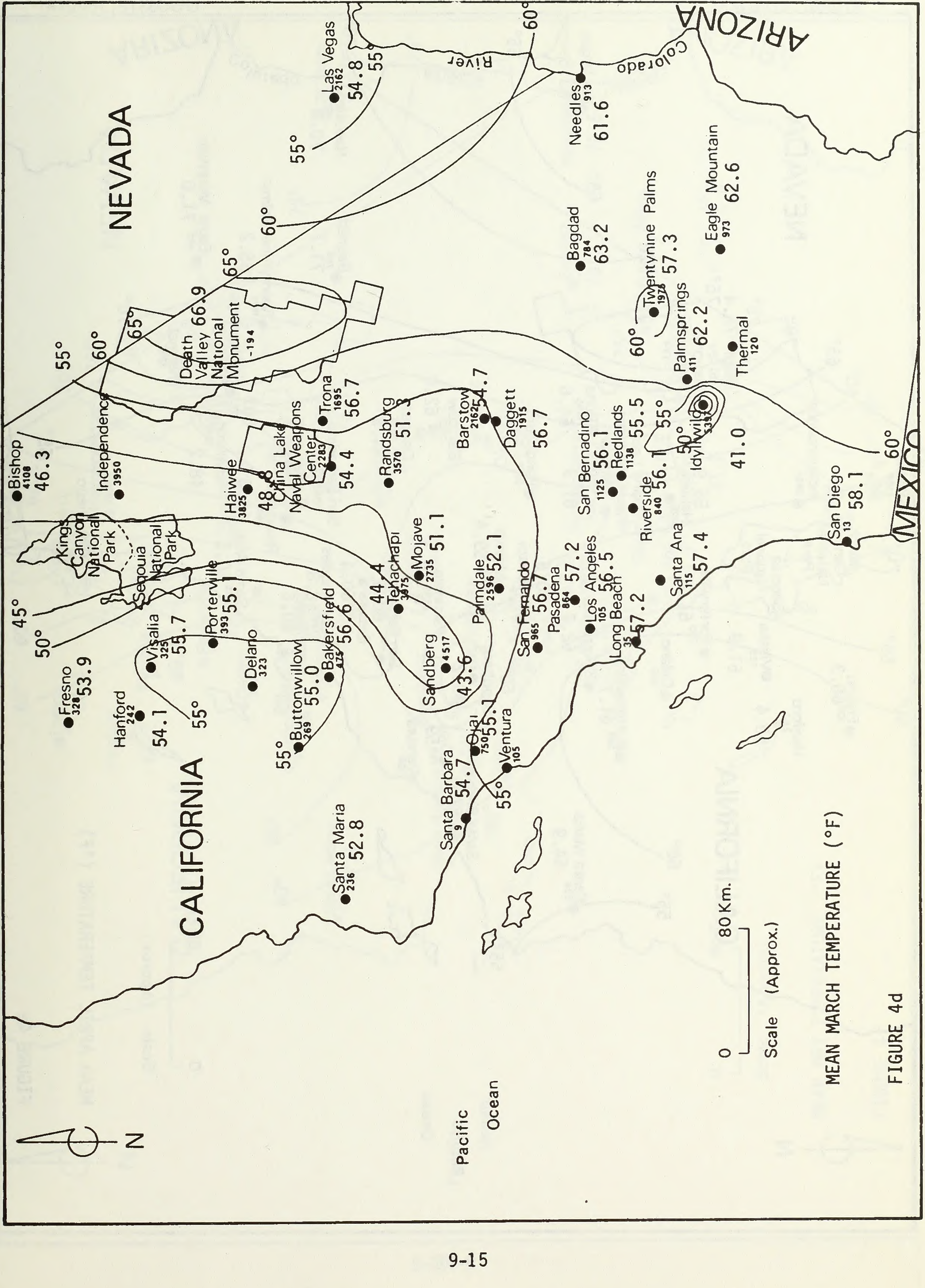

MEAN MARCH TEMPERATURE (°F)

FIGURE 4d

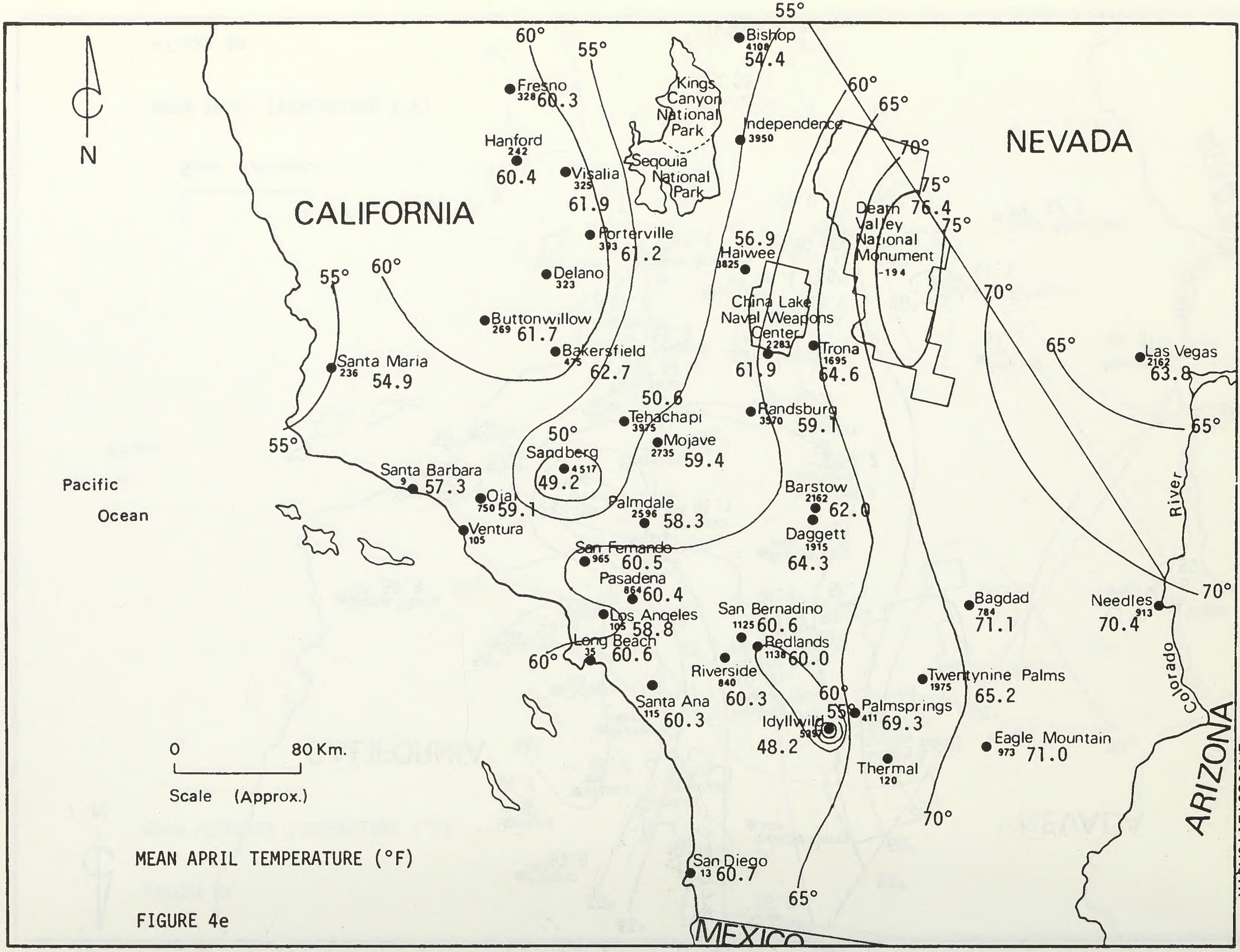

MEAN APRIL TEMPERATURE (°F)

FIGURE 4e

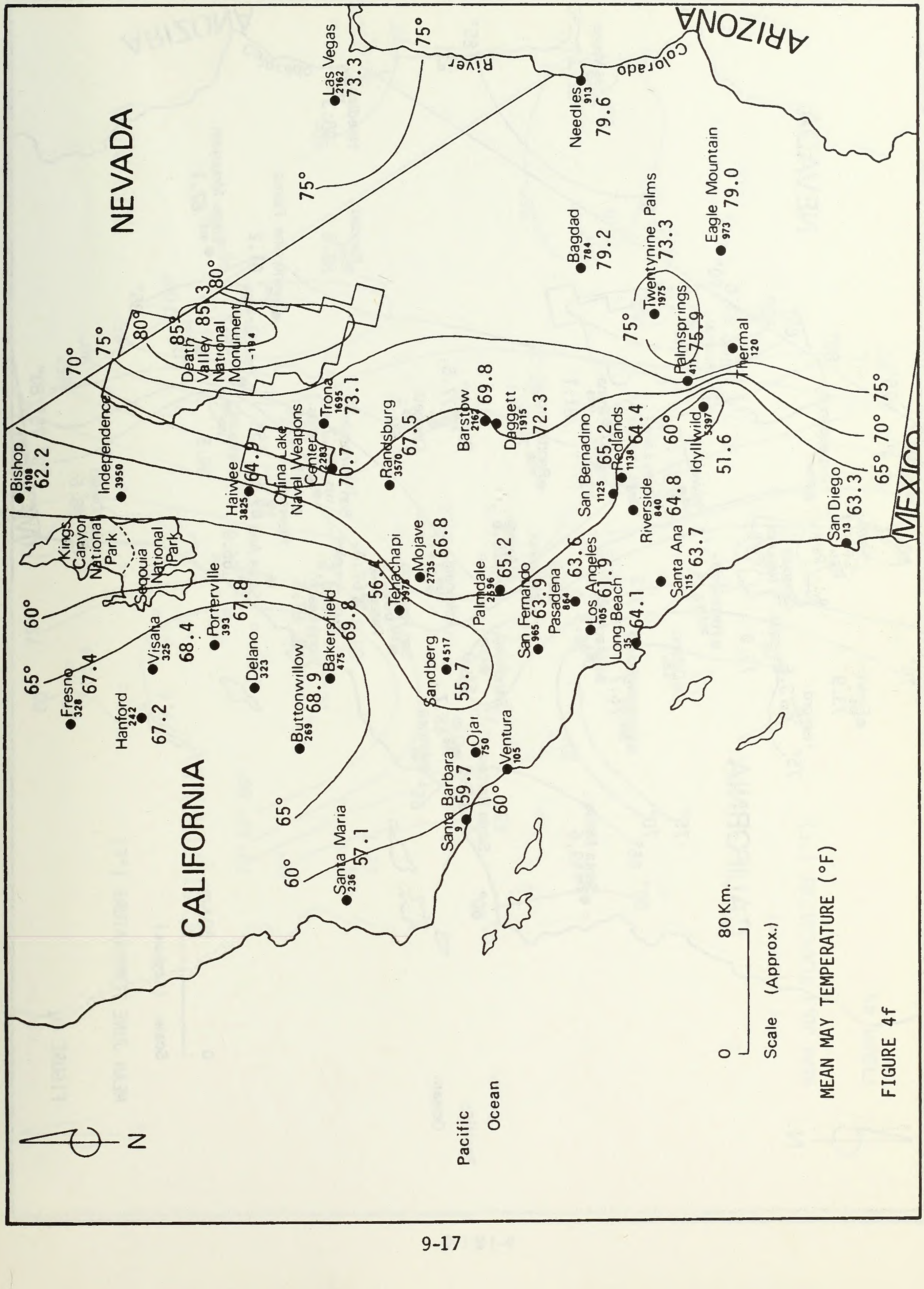

MEAN MAY TEMPERATURE (°F)

FIGURE 4f

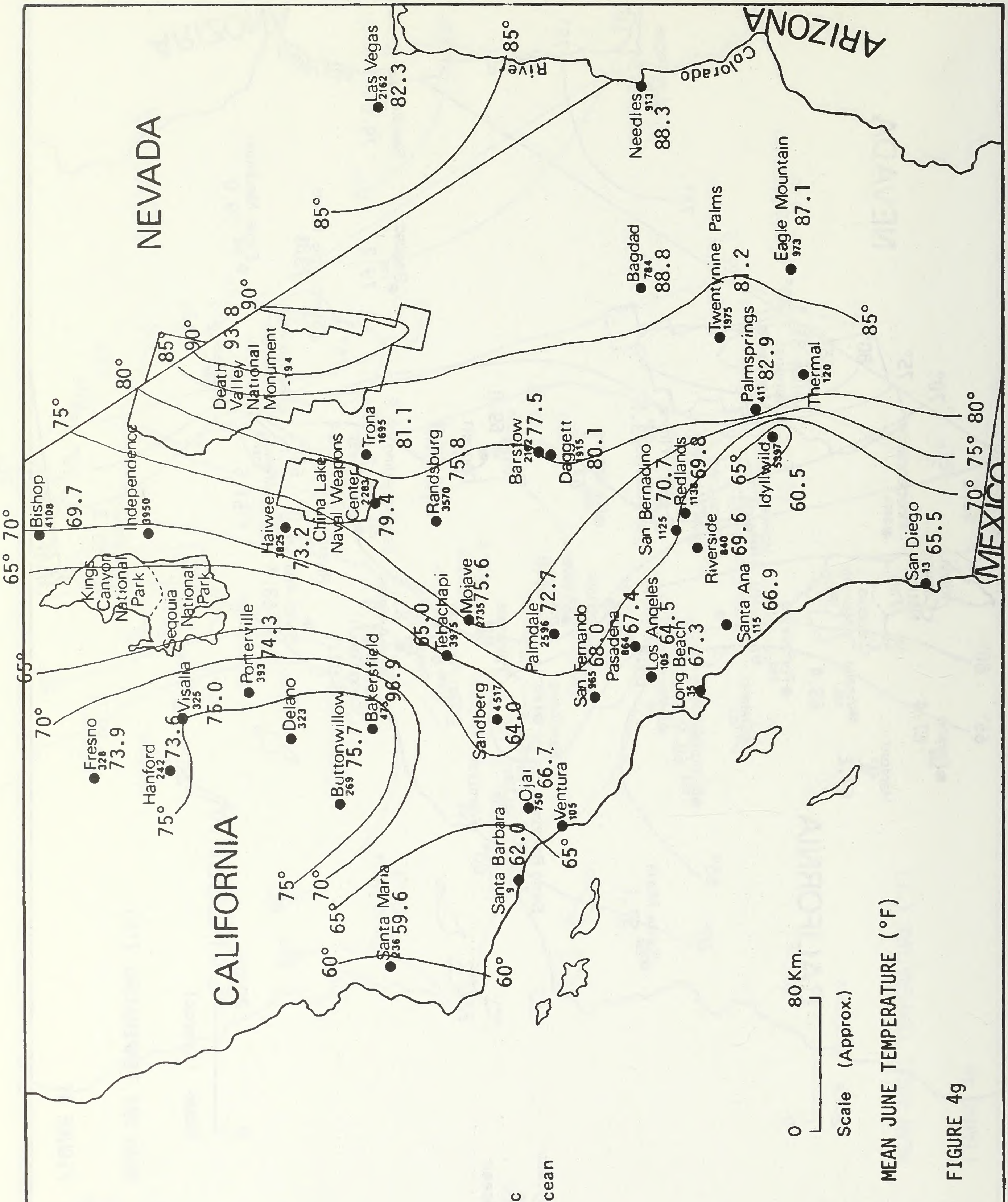

MEAN JUNE TEMPERATURE (°F)

FIGURE 4g

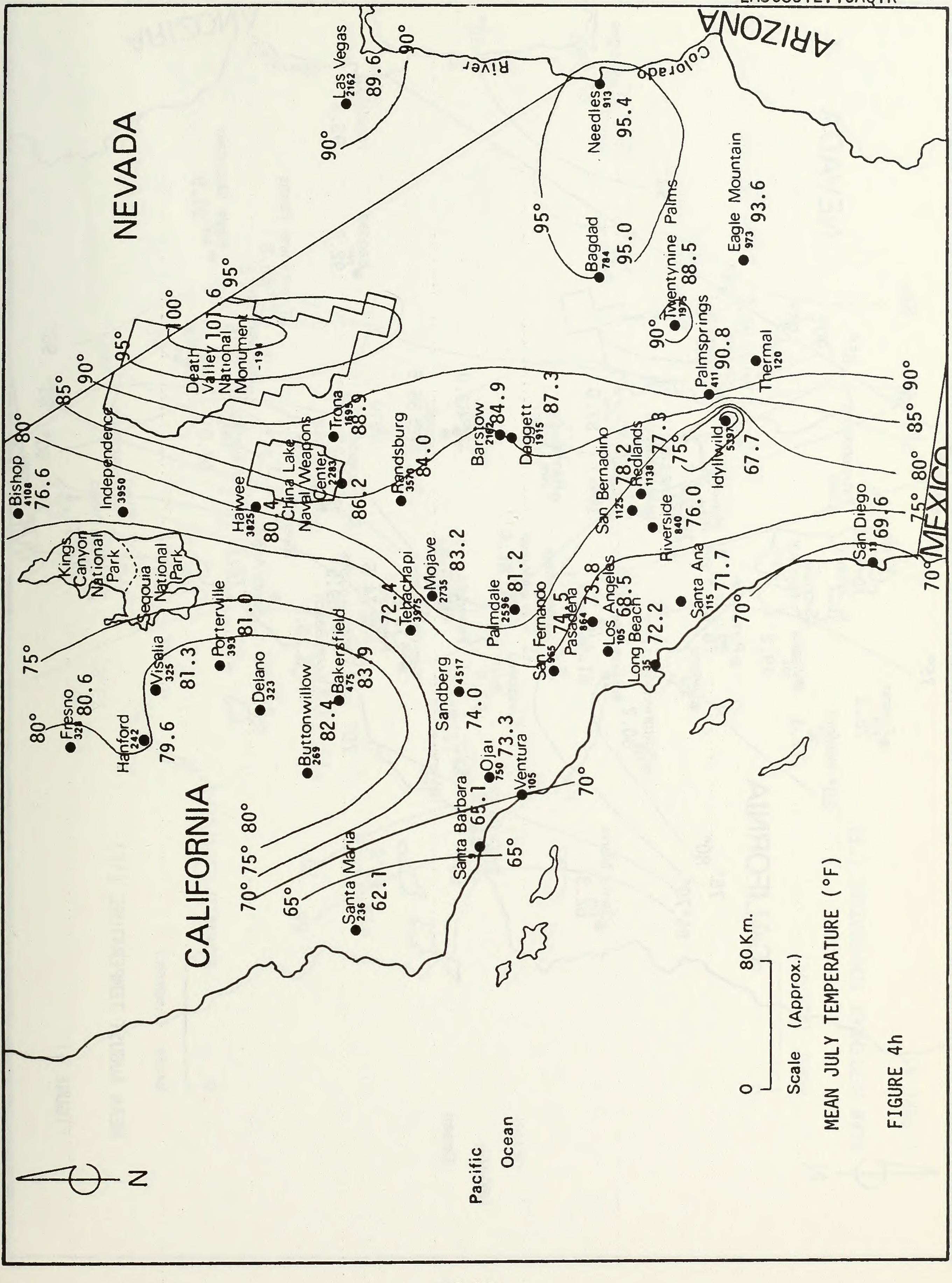

MEAN JULY TEMPERATURE (°F)

FIGURE 4h

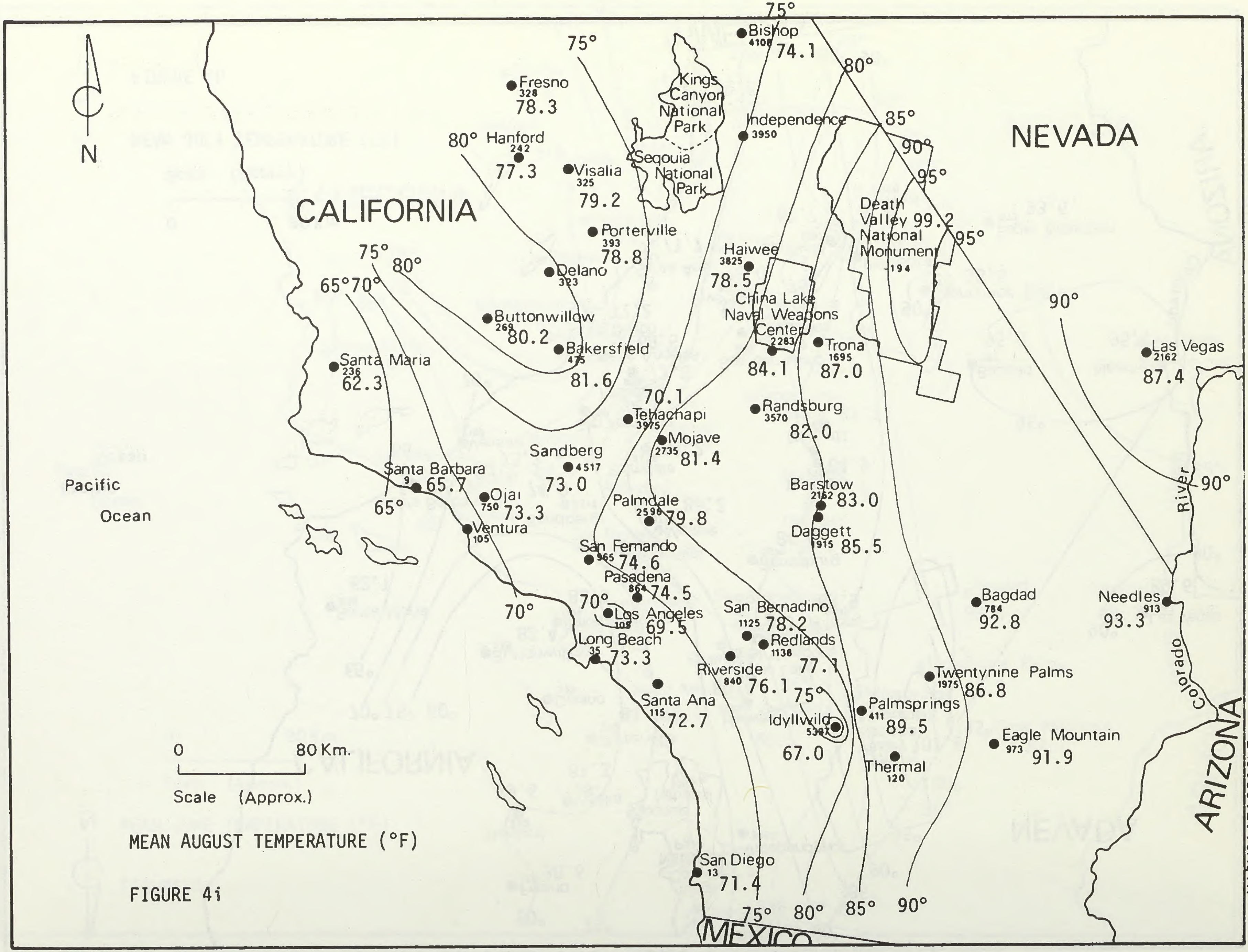

MEAN AUGUST TEMPERATURE (°F)

FIGURE 4i

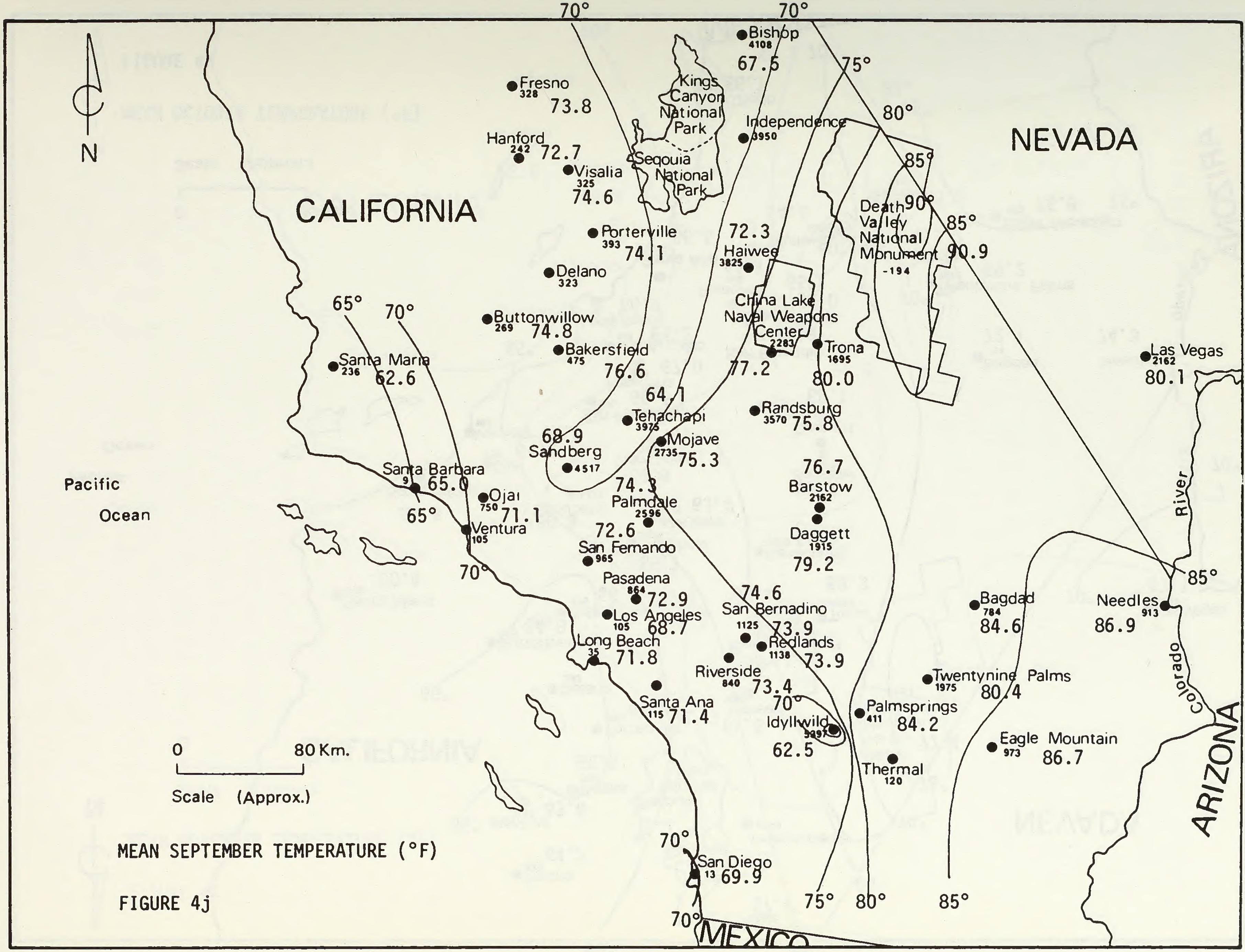

MEAN SEPTEMBER TEMPERATURE (°F)

FIGURE 4j

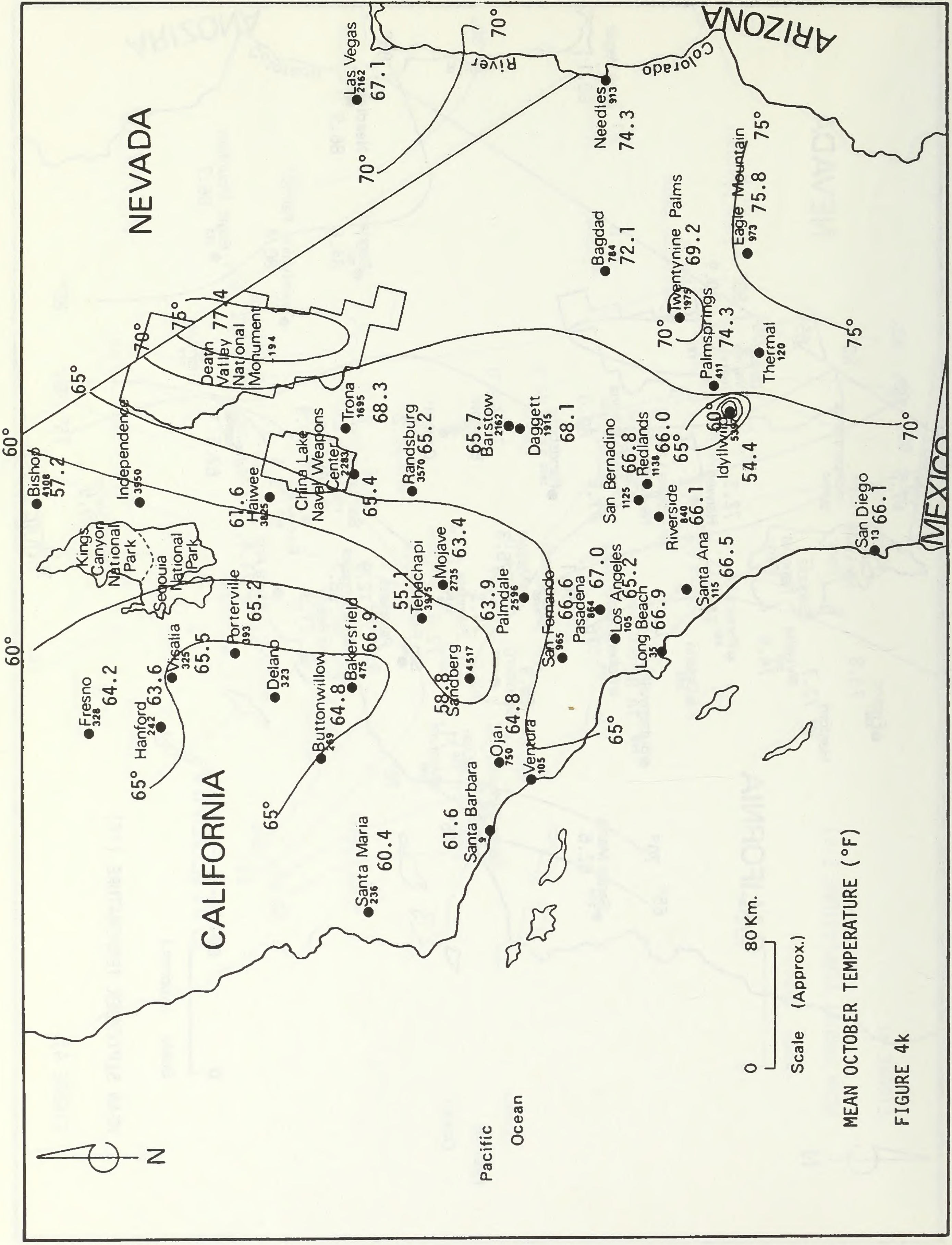

MEAN OCTOBER TEMPERATURE (°F)

FIGURE 4k

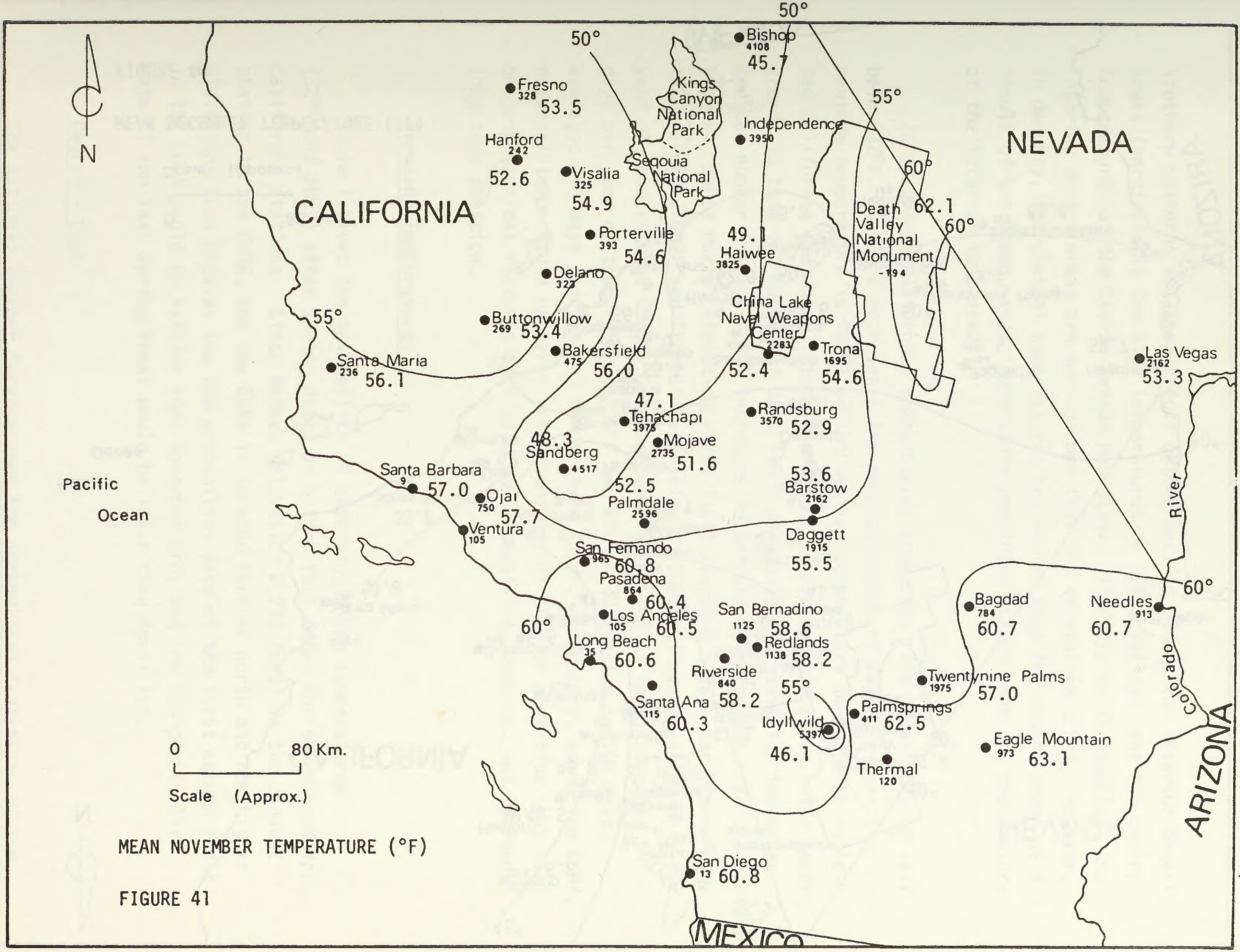

MEAN NOVEMBER TEMPERATURE (°F)

FIGURE 41

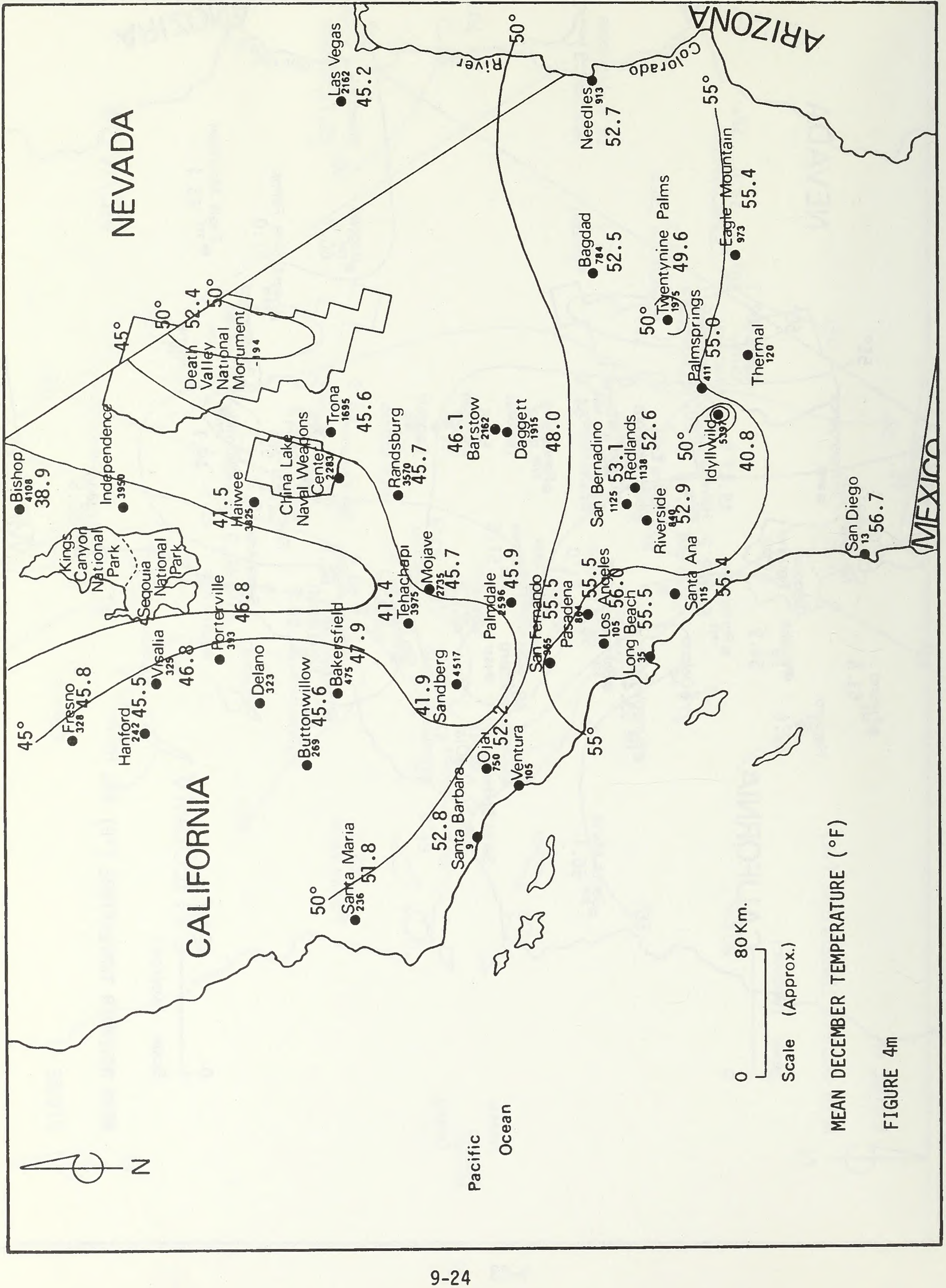

MEAN DECEMBER TEMPERATURE (°F)

FIGURE 4m

isotherm patterns are the effects of the Pacific Ocean, the interior desert areas (particularly the high temperatures of Death Valley), and the cooler temperatures of the Sierra Nevada Mountains. In July, as is expected, the interior desert areas are much warmer than the coastal sections. However, in January, the coastal temperatures are warmer than the desert areas as a result of the ocean water temperature remaining warmer than the temperature of the interior land areas.

In southern California, temperatures sometimes rise above 90°F or fall below 32°F. Table 6 represents the average number of days per year the maximum temperature is ≥90°F or the minimum temperature is ≤32°F at selected California stations listed in order of increasing elevation. The general trend is that the number of days ≥90°F descreases as elevation increases and the number of days ≤32°F increases in increasing elevation. In contrast however, Santa Maria (elevation = 236 feet) averages 5 days per year of temperatures ≥90°F and Thermal (elevation - 120 feet) averages 180 days per year of temperatures ≥90°F; Sandberg (elevation - 4517 feet) averages 59 days per year of temperatures ≤32°F and Bishop (elevation = 4108 feet) averages 143 days per year of temperature ≤32°F. Therefore, as in the CGRA, regional temperature patterns are dependent not only on elevation, but also on geopgraphical features such as oceans, mountains, deserts, and latitude/longitude position.

Freezing Temperatures

Table 7 gives the probability of observing given temperatures (32°F and 28°F) after spring dates or before fall dates for seven southern California stations. Since Mojave (elevation 2,735 feet) is the closest station to the CGRA, and the CGRA is located farther north and has higher elevations than Mojave; the 50% probability date of the first autumn frost in the CGRA would be earlier than November 3rd, and the 50% probability date of the last spring frost would be later than April 1st.

Degree - Days

The National Weather Service uses the accumulated deviations of air

Table 6

Number of Days per Year the Maximum Temperature ⩾ 90°F or the Minimum Temperature ⩽ 32°F

Station	Elevation (ft)	Days ⩾ 90°F	Days ⩽ 32°F
San Diego	13	3	< 0.5
Long Beach	35	22	1
Los Angeles	105	5	< 0.5
Thermal	120	180	12
Santa Maria	236	5	24
Fresno	328	107	28
Porterville	393	112	26
Palm Springs	411	181	10
Bakersfield	475	110	11
Needles	913	165	6
Eagle Mountain	973	154	1
Trona	1695	148	47
Daggett	1915	135	31
Twentynine Palms	1975	151	33
Barstow	2162	136	57
Las Vegas, NV	2162	132	39
China Lake	2283	60*	70
Palmdale	2596	102	59
Mojave	2735	107	68
Randsburg	3570	105	33
Haiwee	3825	77	73
Tehachapi	3975	36	104
Bishop	4108	95	143
Sandberg	4517	20	59

*Days Maximum Temperature > 100°F.

Table 7. Probability of Observing Given Temperatures After Spring Dates or Before Dates (Month/Day)

Station/Elevation (ft)	Season/Temp °F	Probability (%)								
		10	20	30	40	50	60	70	80	90
Porterville/393	Spring 32	4/5	3/23	3/14	3/5	3/26	2/18	2/10	2/1	1/18
	Spring 28	2/24	2/14	2/7	2/1	1/27	1/21	1/15	1/7	12/26
	Fall 32	11/10	11/16	11/20	11/24	11/27	11/30	12/4	12/8	12/14
	Fall 28	11/25	12/3	12/9	12/13	12/18	12/22	12/27	1/3	1/12
Palm Springs/411 *earlier than Jan. 1. **later than Dec. 31.	Spring 32	3/3	2/24	2/18	2/13	2/8	2/3	1/28	1/19	*
	Spring 28	2/13	2/5	1/29	2/11	1/13	*	*	*	*
	Fall 32	11/12	11/20	11/26	12/1	12/6	12/12	12/20	**	**
	Fall 28	12/11	12/23	**	**	**	**	**	**	**
Daggett/1915	Spring 32	3/23	3/15	3/8	3/3	2/26	2/21	2/16	2/9	2/1
	Spring 28	3/10	2/28	2/21	2/15	2/9	2/4	1/29	1/21	1/12
	Fall 32	11/4	11/11	11/16	11/20	11/24	11/28	12/2	12/7	12/14
	Fall 28	11/16	11/24	11/30	12/5	12/9	12/14	12/19	12/24	1/1
Twentynine Palms/1975	Spring 32	4/8	3/31	3/25	3/20	3/16	3/11	3/6	2/28	2/20
	Spring 28	3/28	3/16	3/8	3/1	2/22	2/15	2/7	1/29	1/14
	Fall 32	11/3	11/8	11/13	11/16	11/20	11/23	11/27	12/1	12/7
	Fall 28	11/12	11/20	11/27	12/2	12/7	12/13	12/18	12/25	1/6
Palmdale/2596	Spring 32	4/22	4/13	4/7	4/2	3/28	3/23	3/18	3/11	3/3
	Spring 28	3/17	3/18	3/12	3/7	3/3	2/26	2/20	2/14	2/6
	Fall 32	10/26	11/1	11/3	11/6	11/9	11/11	11/14	11/16	11/21
	Fall 28	11/10	11/14	11/18	11/22	11/25	11/29	12/2	12/6	12/12
Mojave/2735	Spring 32	4/26	4/17	4/11	4/6	4/1	3/27	3/22	3/16	3/7
	Spring 28	4/7	3/29	3/25	3/20	3/17	3/13	3/9	3/5	2/26
	Fall 32	10/18	10/23	10/27	10/31	11/3	11/5	11/8	11/12	11/17
	Fall 28	11/4	11/8	11/11	11/13	11/16	11/19	11/21	11/24	11/28
Tehachapi/3975	Spring 32	5/24	5/17	5/12	5/8	5/5	5/1	4/27	4/23	4/17
	Spring 28	4/29	4/20	4/15	4/10	4/5	3/31	3/26	3/19	3/9
	Fall 32	9/23	9/27	10/2	10/5	10/8	10/11	10/14	10/17	10/22
	Fall 28	9/27	10/8	10/14	10/18	10/23	10/27	11/1	11/5	11/14

temperatures from an index temperature of 65^{o}F to estimate winter heating fuel requirements and summer air conditioning loads. Agricultural interests apply index temperatures depending on the crop in question for determining growing degree-days. Degree-days are calculated by taking the difference between the mean daily temperature and the established index temperature for heating degree-days and cooling degree-days. These values are then accumulated over a desired period.

For numerous southern California stations, the relative distribution of heating and cooling degree-days annually and by months is shown in Figures 5a-m and 6a-m. Note that for the CGRA, heating requirements are needed from September through June and cooling requirements are needed from April through October.

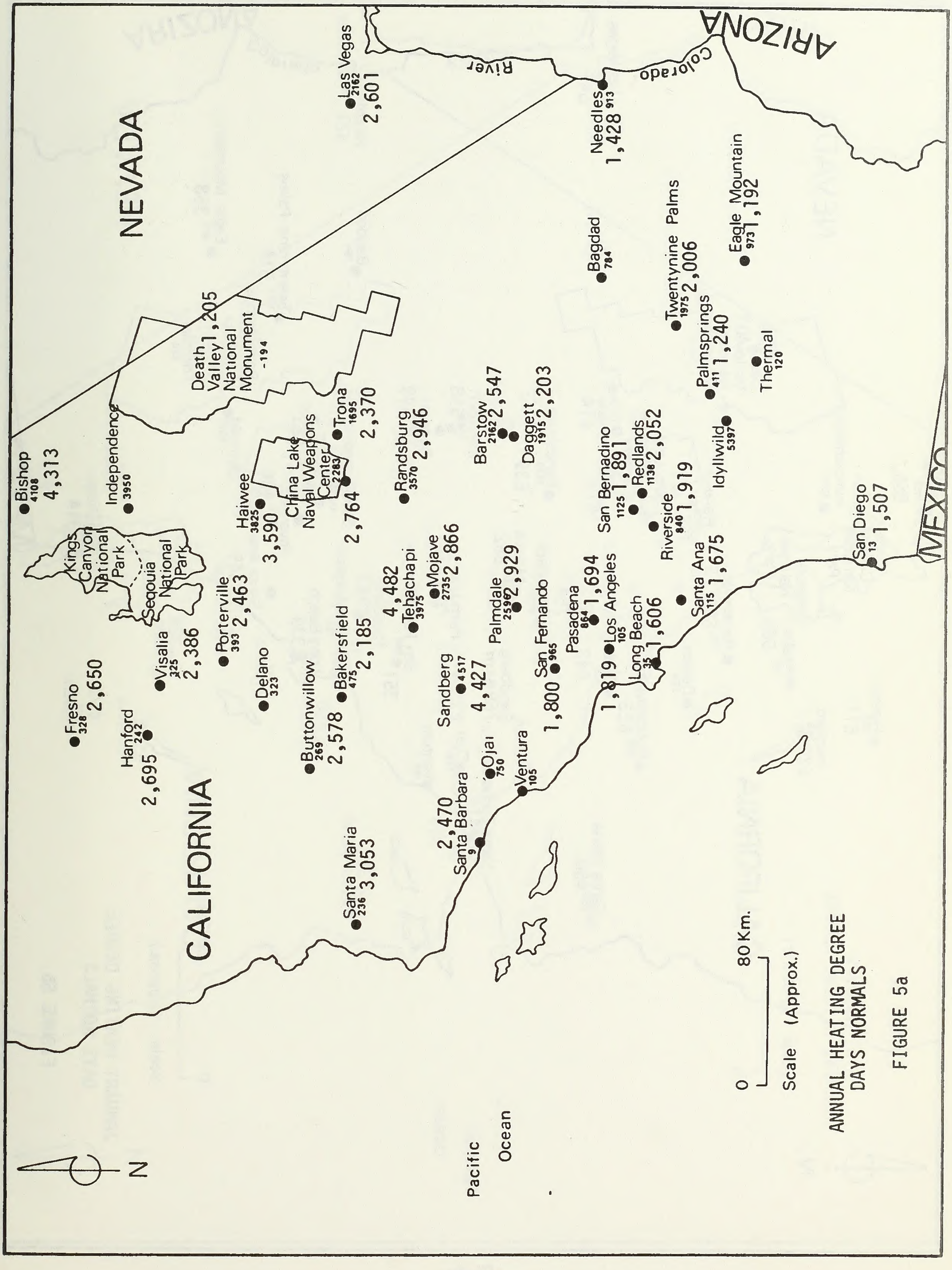

ANNUAL HEATING DEGREE DAYS NORMALS

FIGURE 5a

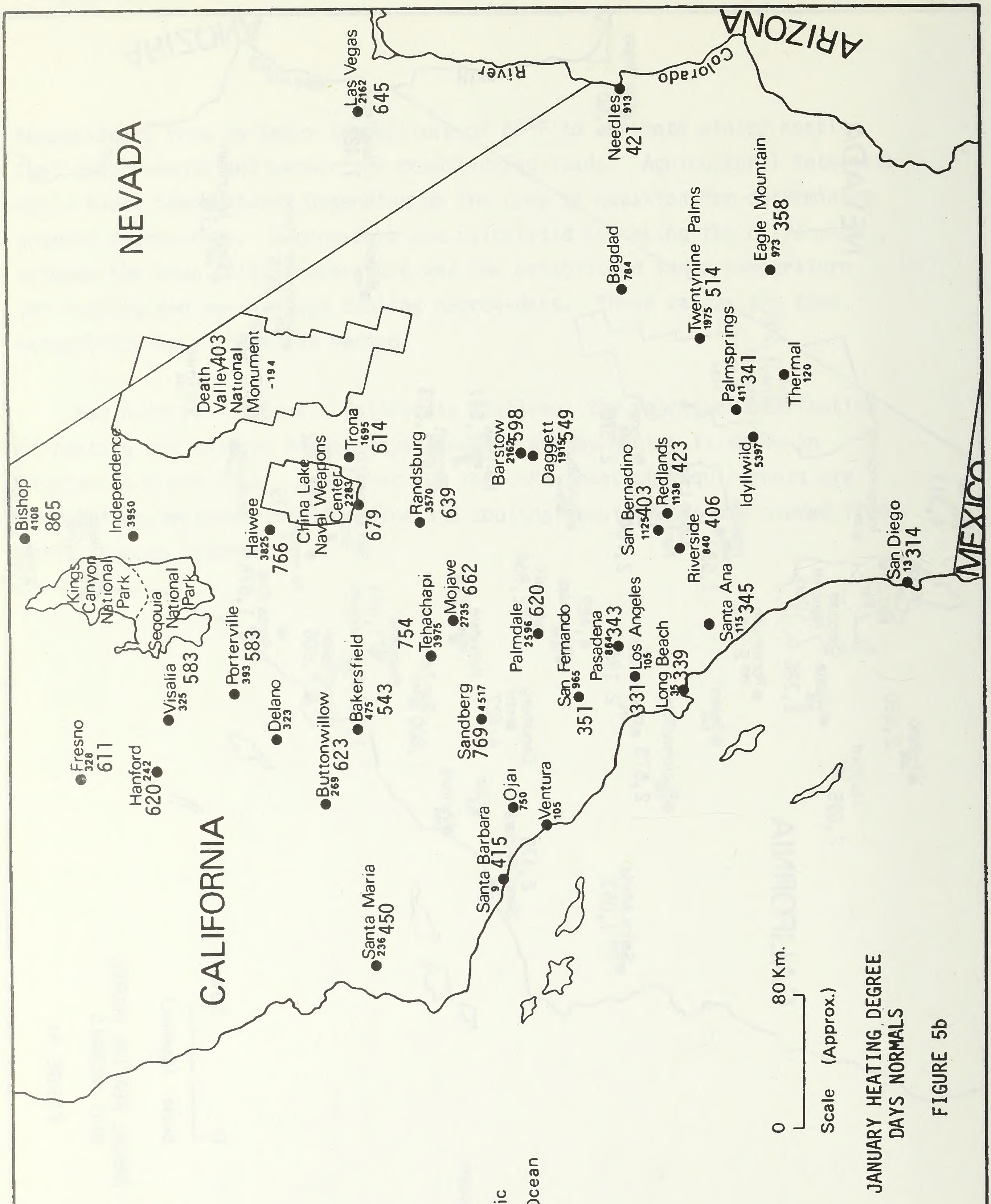

JANUARY HEATING DEGREE DAYS NORMALS

FIGURE 5b

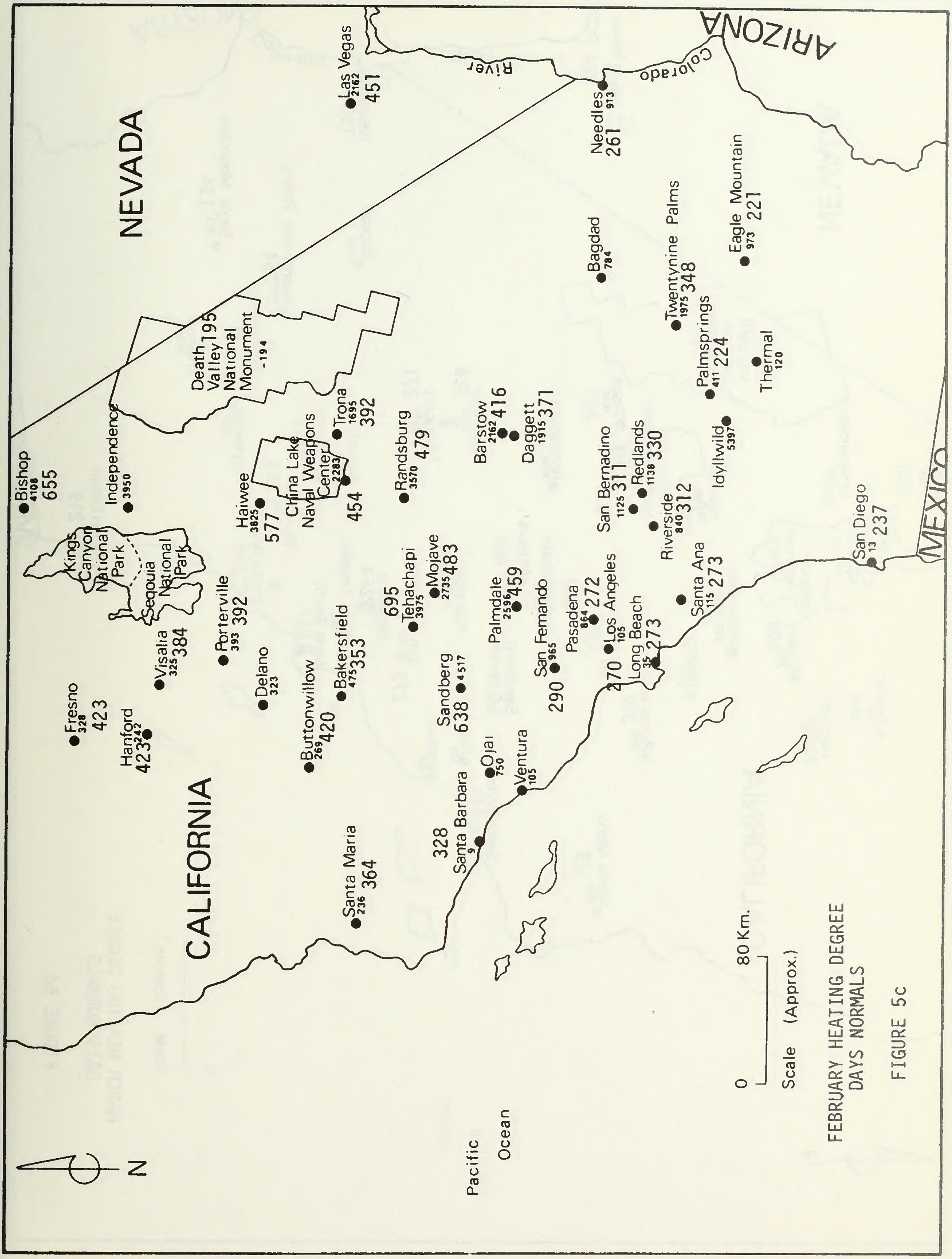

FEBRUARY HEATING DEGREE DAYS NORMALS

FIGURE 5c

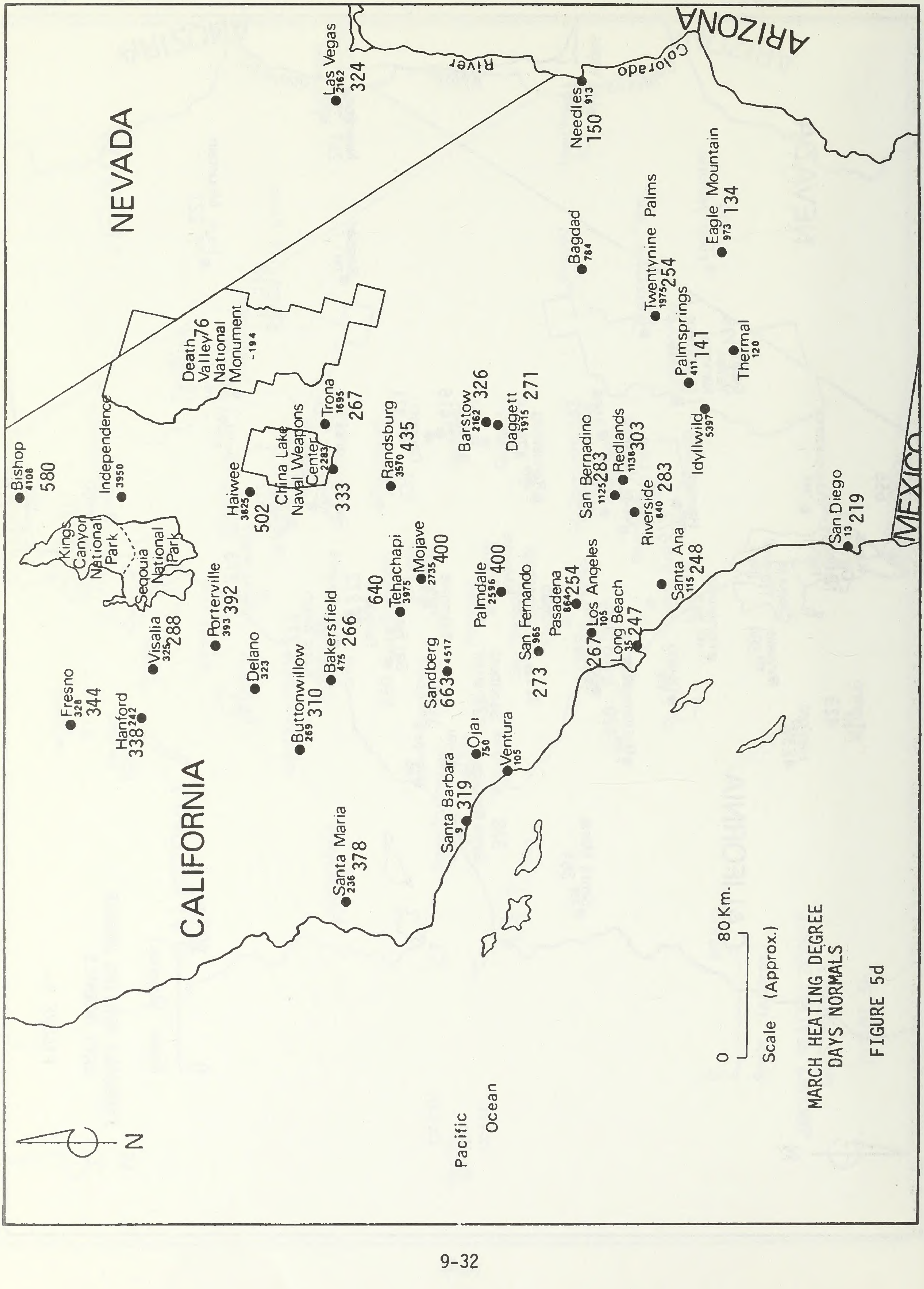

MARCH HEATING DEGREE DAYS NORMALS

FIGURE 5d

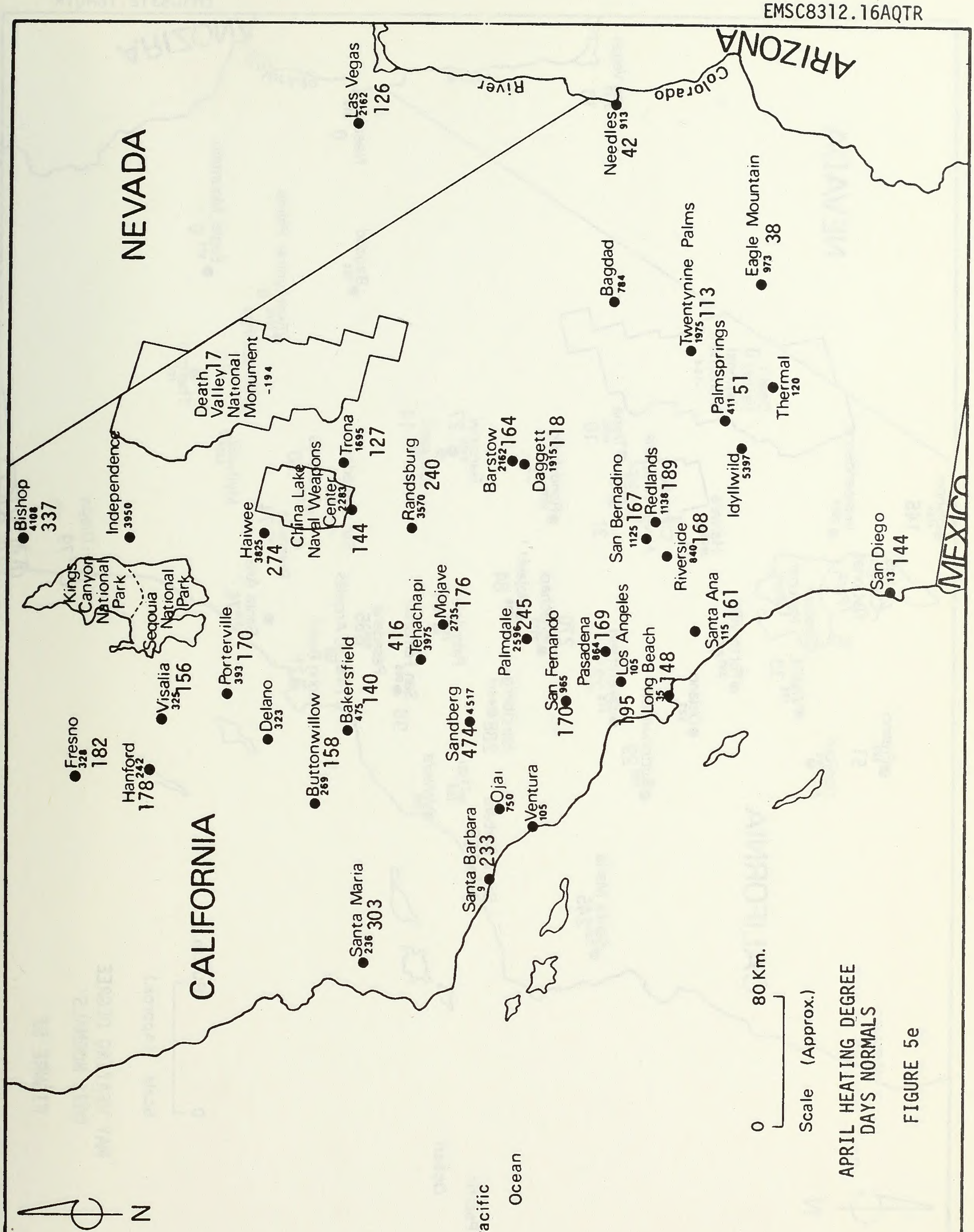

APRIL HEATING DEGREE DAYS NORMALS

FIGURE 5e

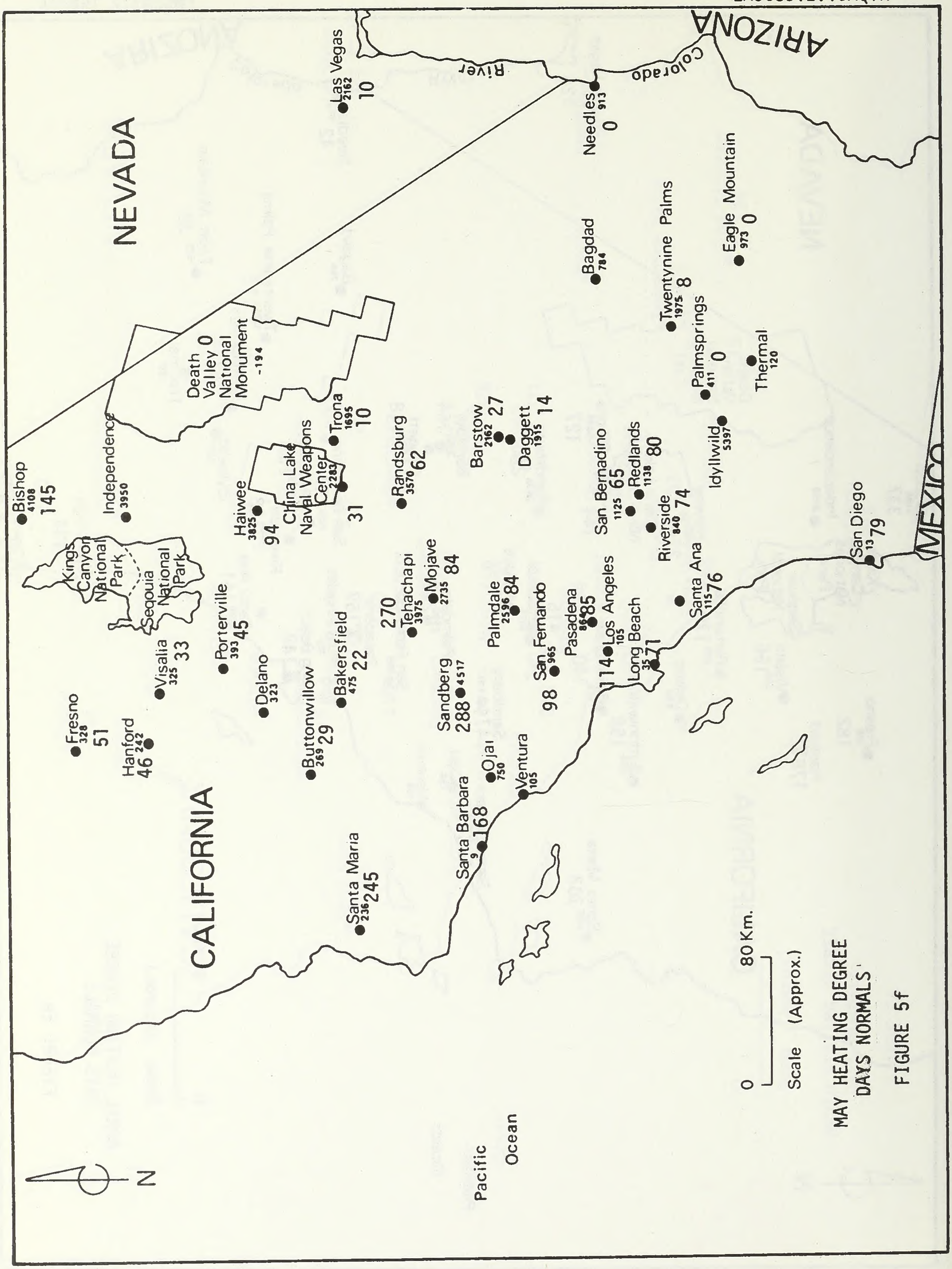

MAY HEATING DEGREE DAYS NORMALS

FIGURE 5f

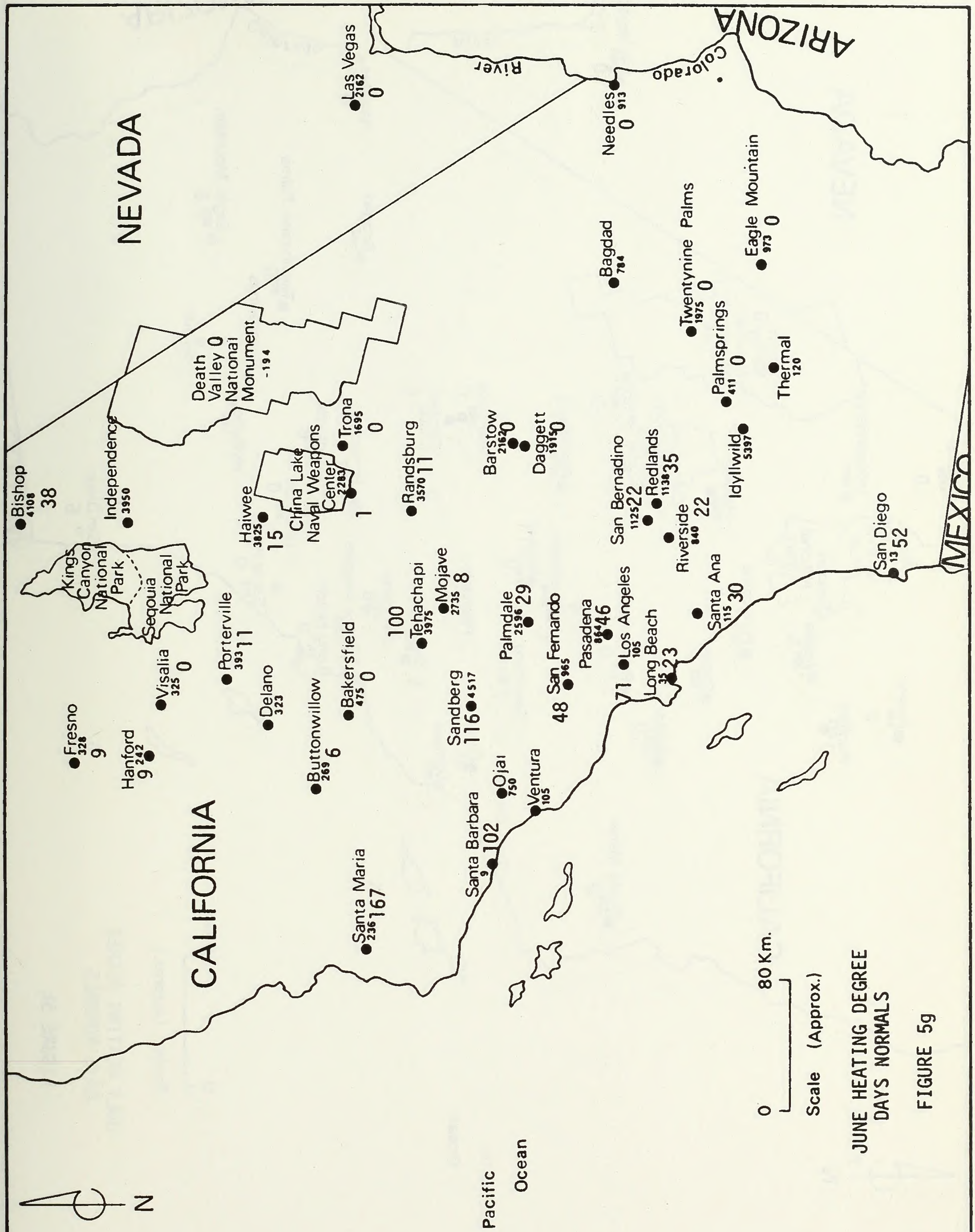

JUNE HEATING DEGREE DAYS NORMALS

FIGURE 5g

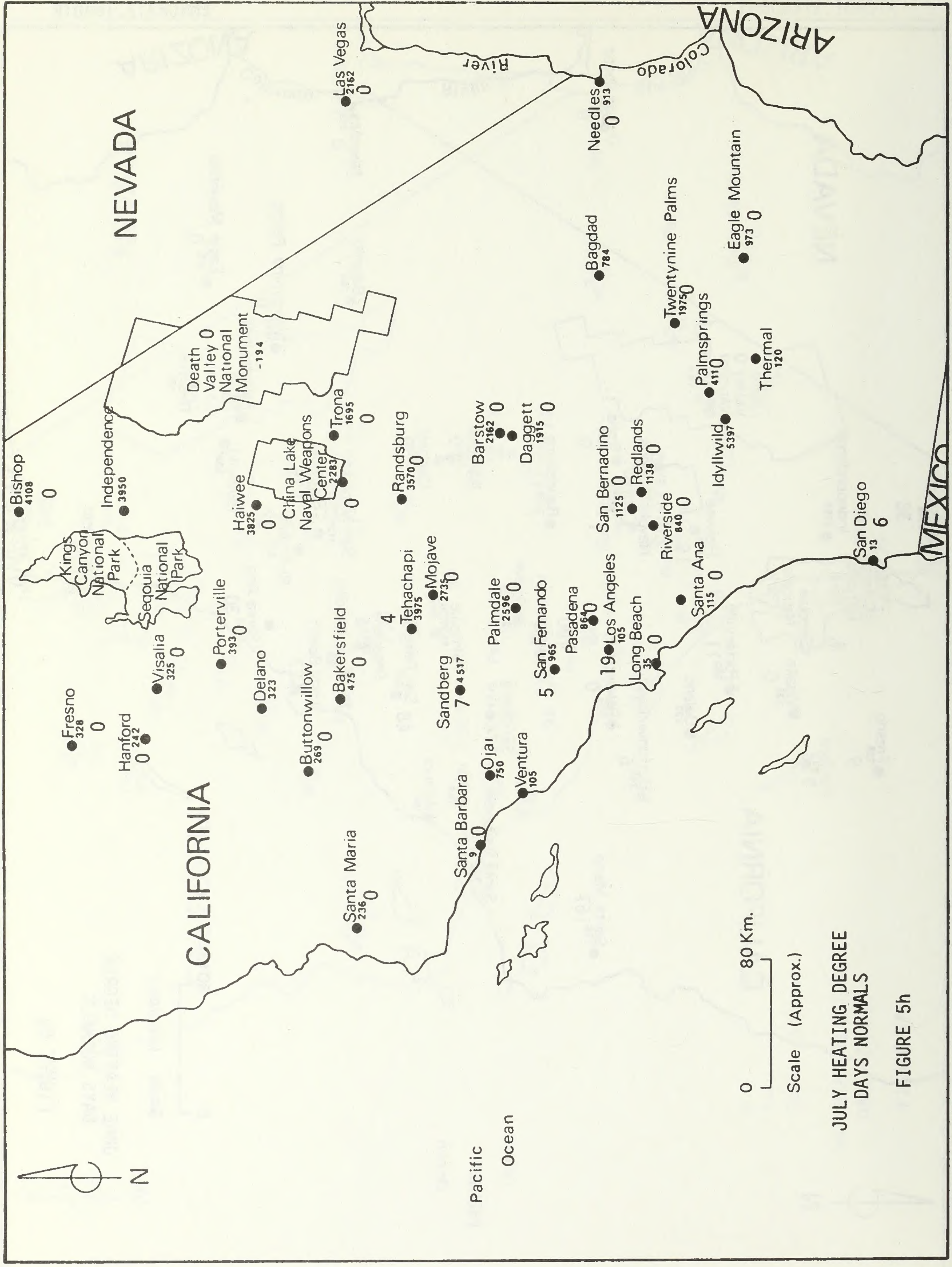

JULY HEATING DEGREE DAYS NORMALS

FIGURE 5h

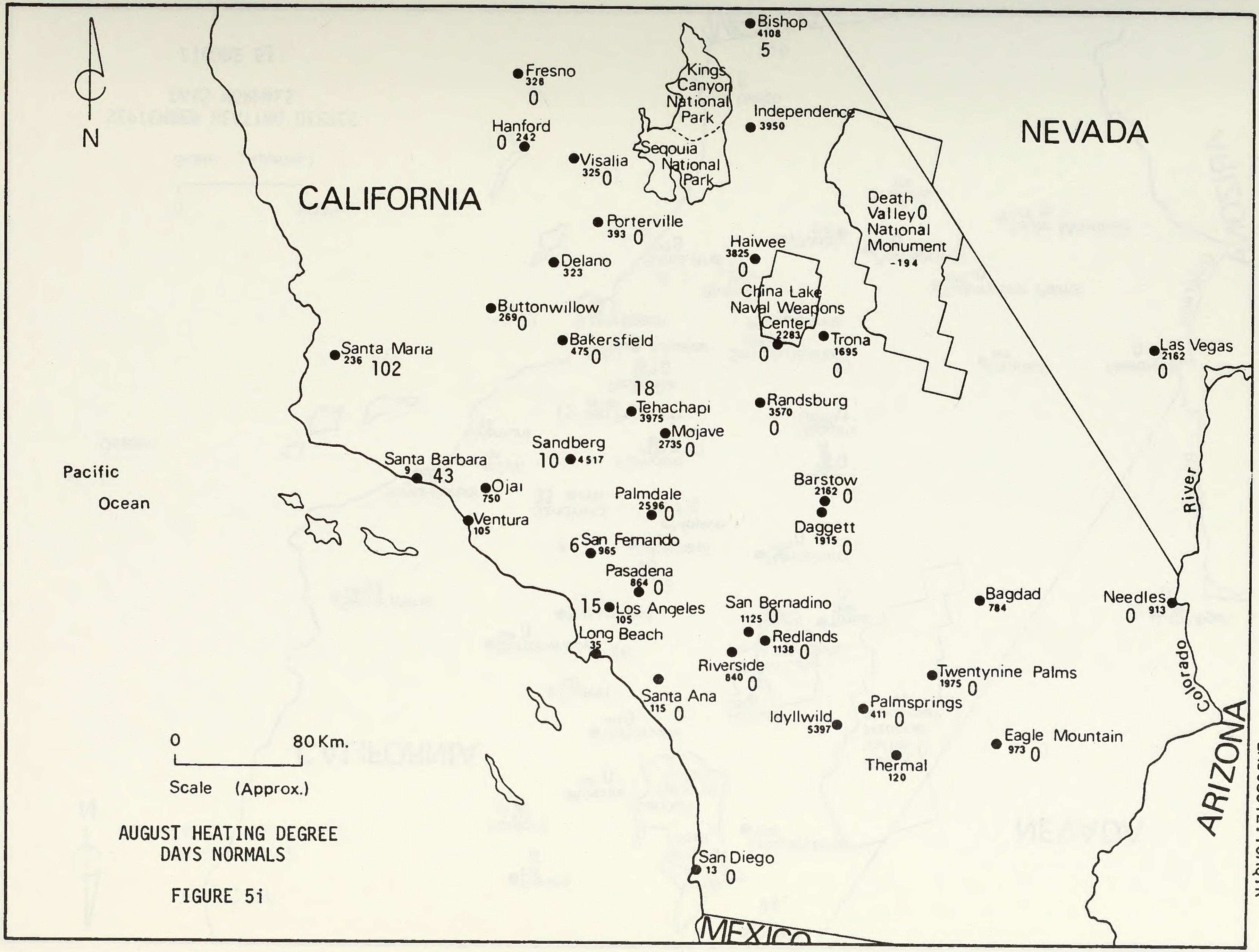

AUGUST HEATING DEGREE DAYS NORMALS

FIGURE 5i

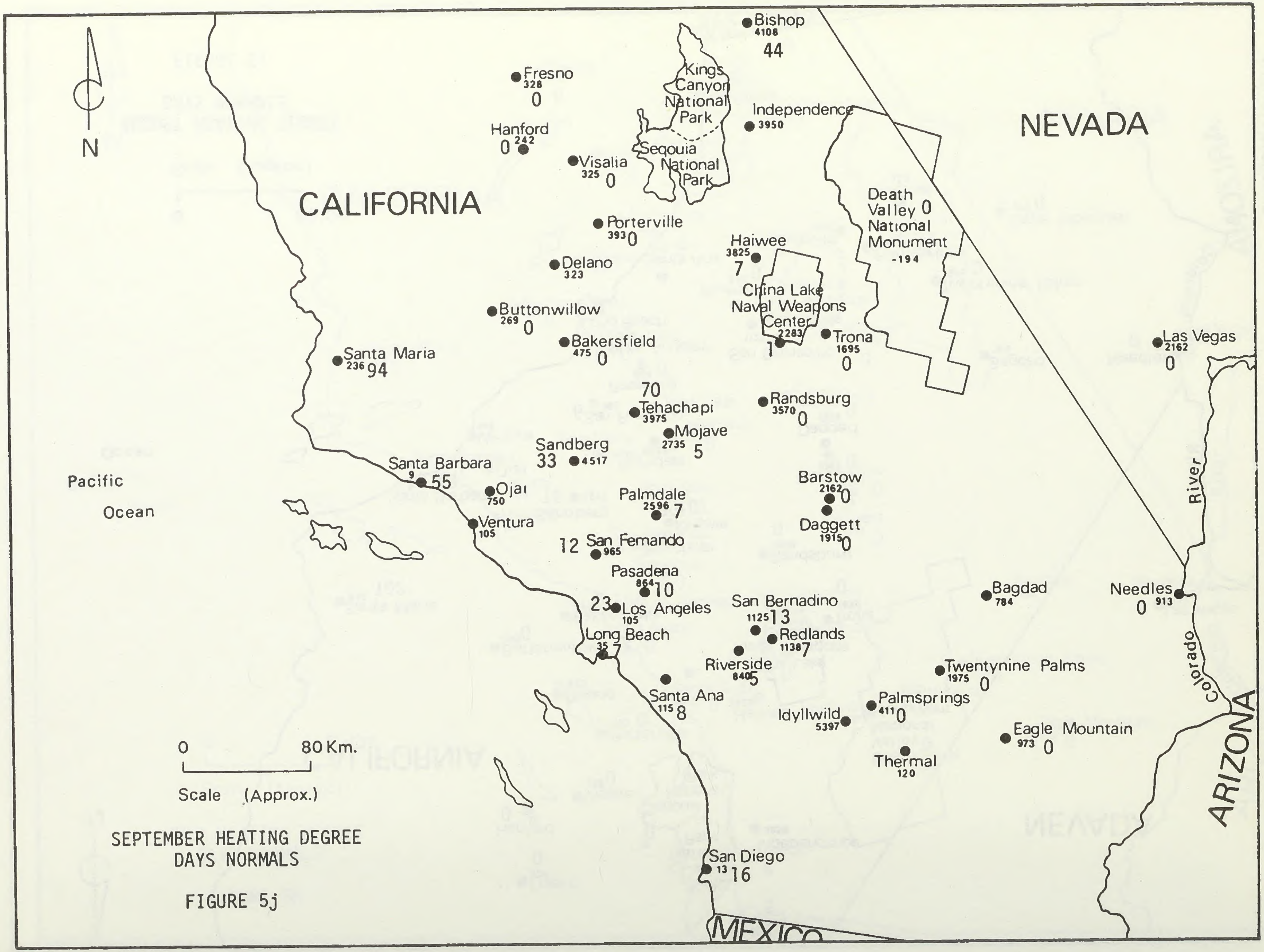

SEPTEMBER HEATING DEGREE
DAYS NORMALS

FIGURE 5j

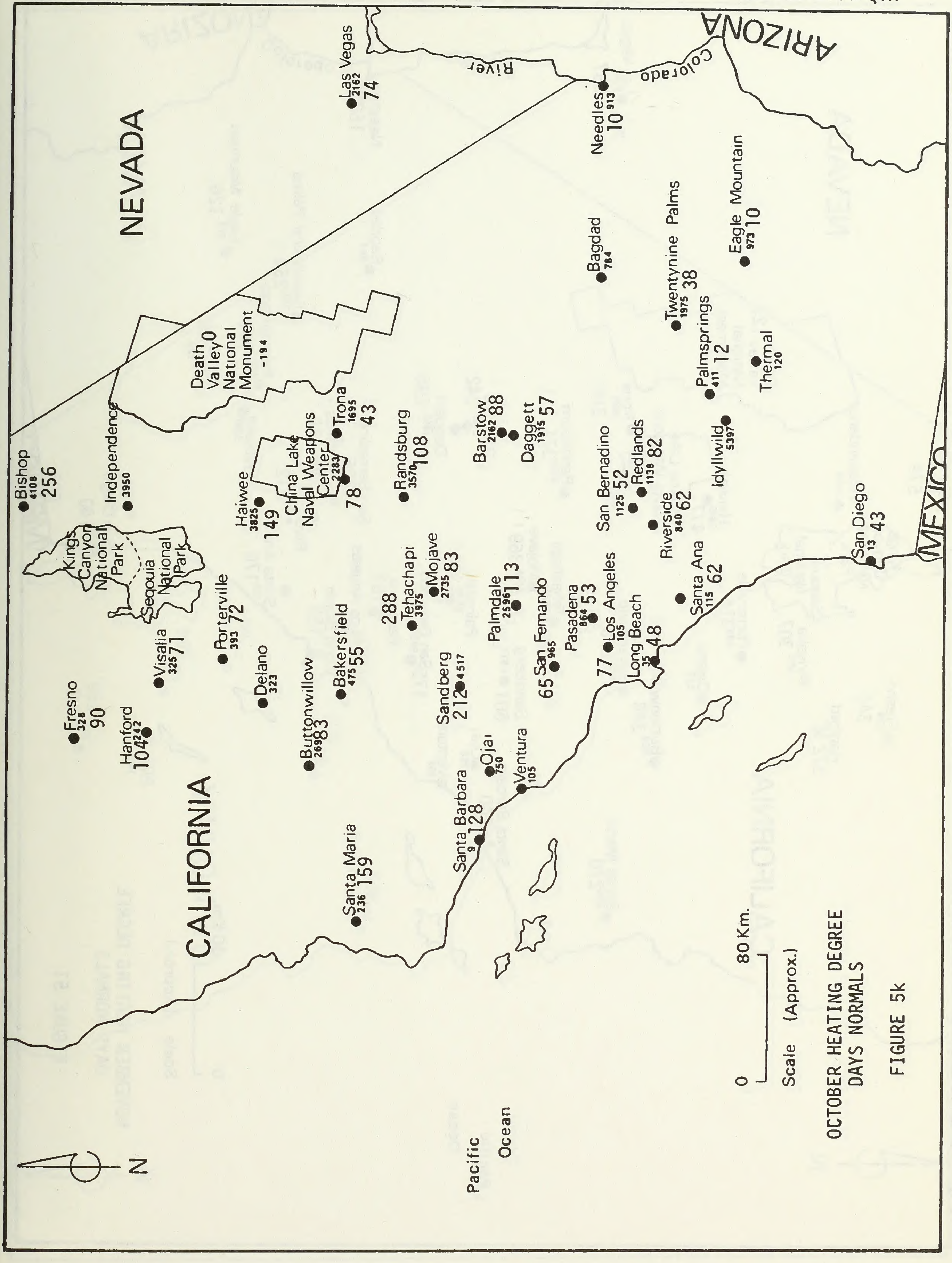

OCTOBER HEATING DEGREE DAYS NORMALS

FIGURE 5k

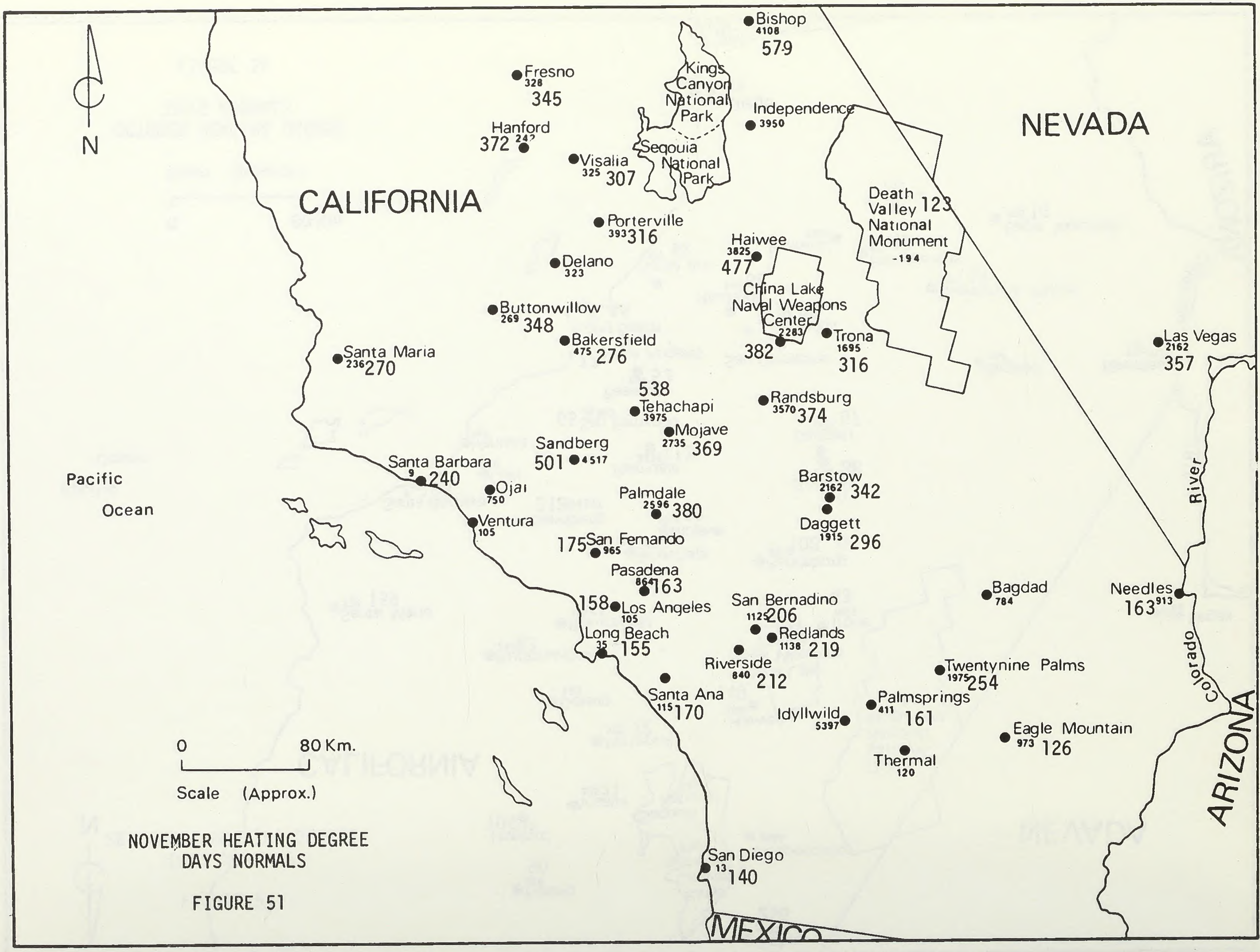

NOVEMBER HEATING DEGREE DAYS NORMALS

FIGURE 51

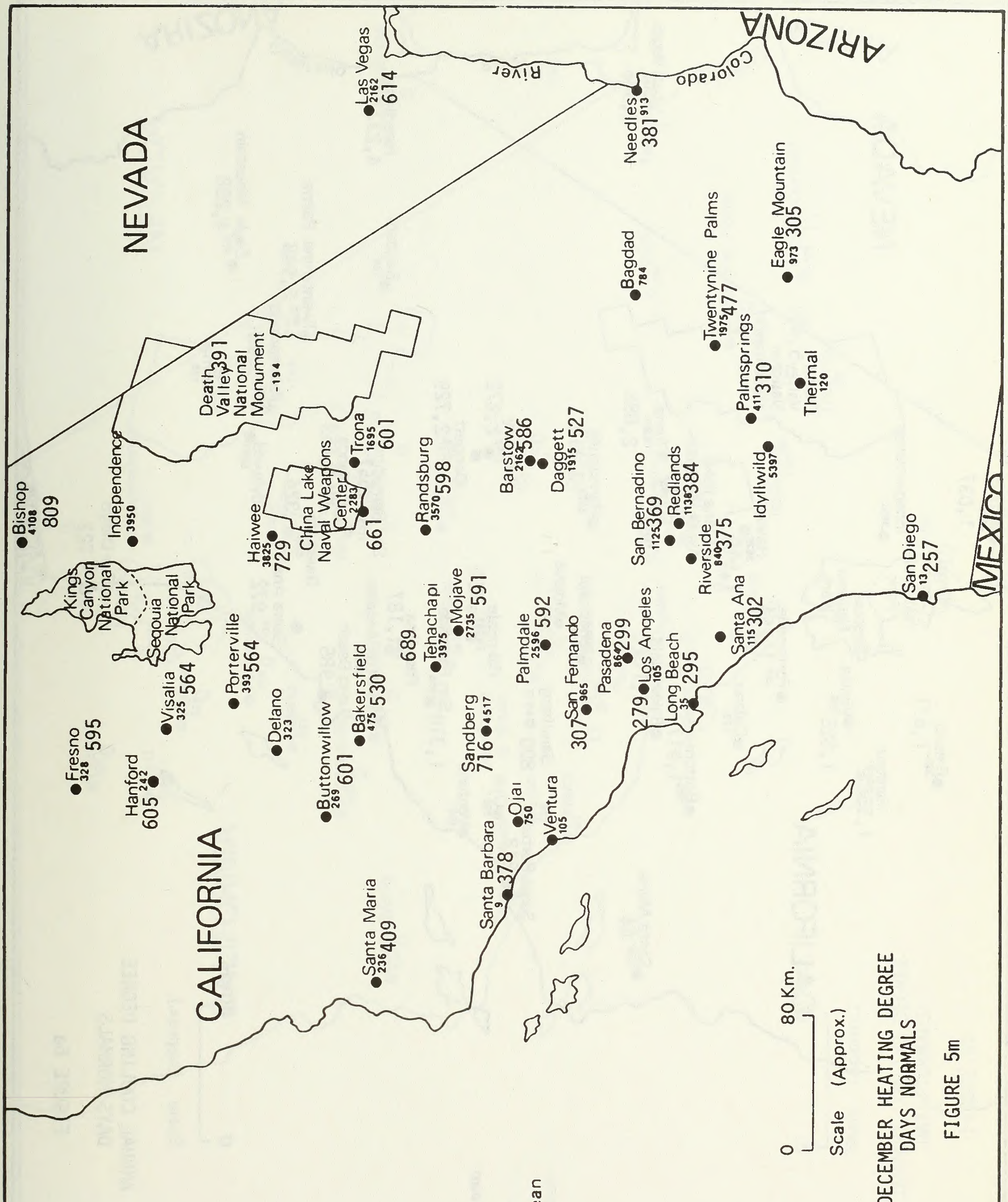

DECEMBER HEATING DEGREE DAYS NORMALS

FIGURE 5m

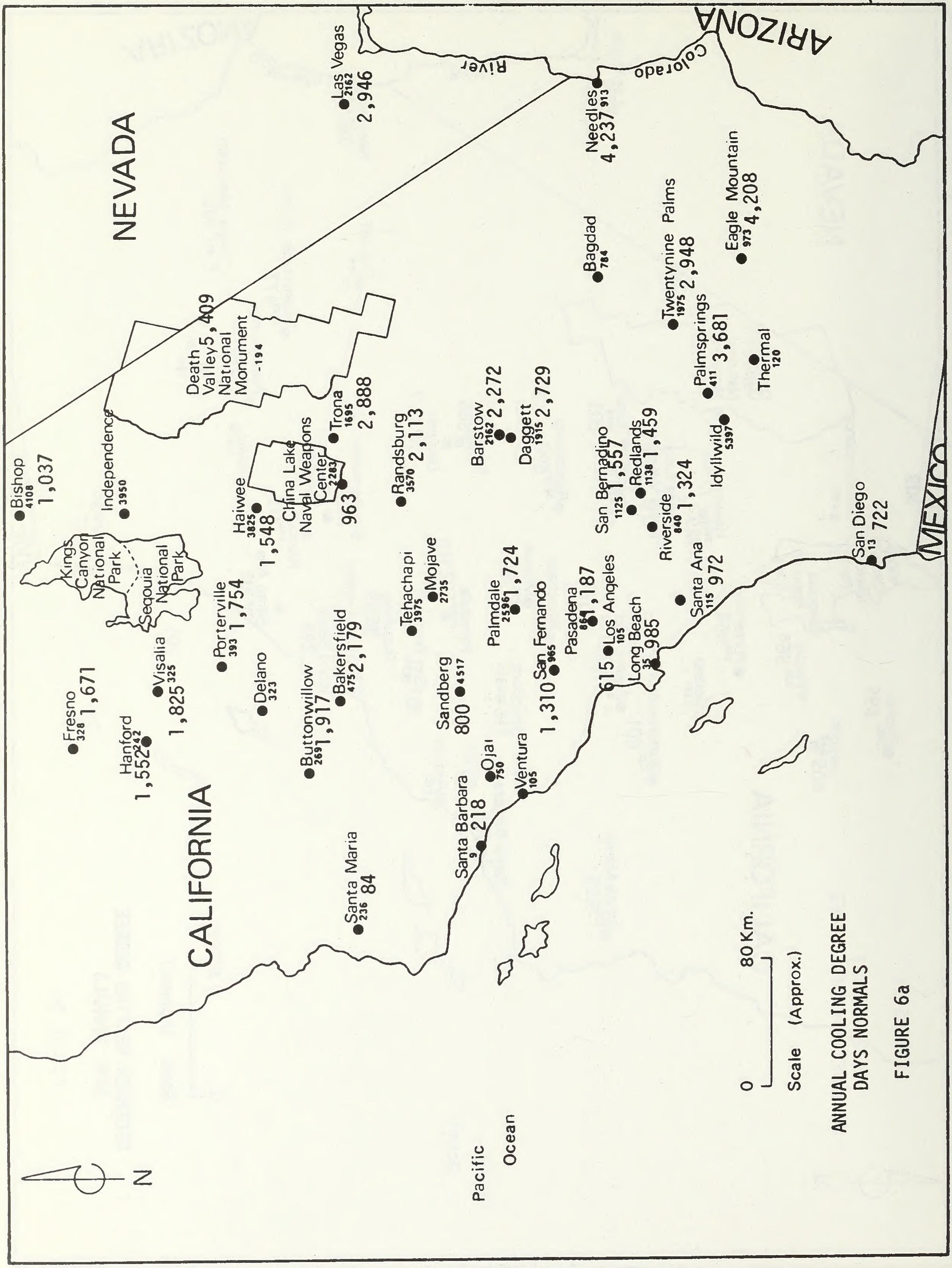

ANNUAL COOLING DEGREE DAYS NORMALS

FIGURE 6a

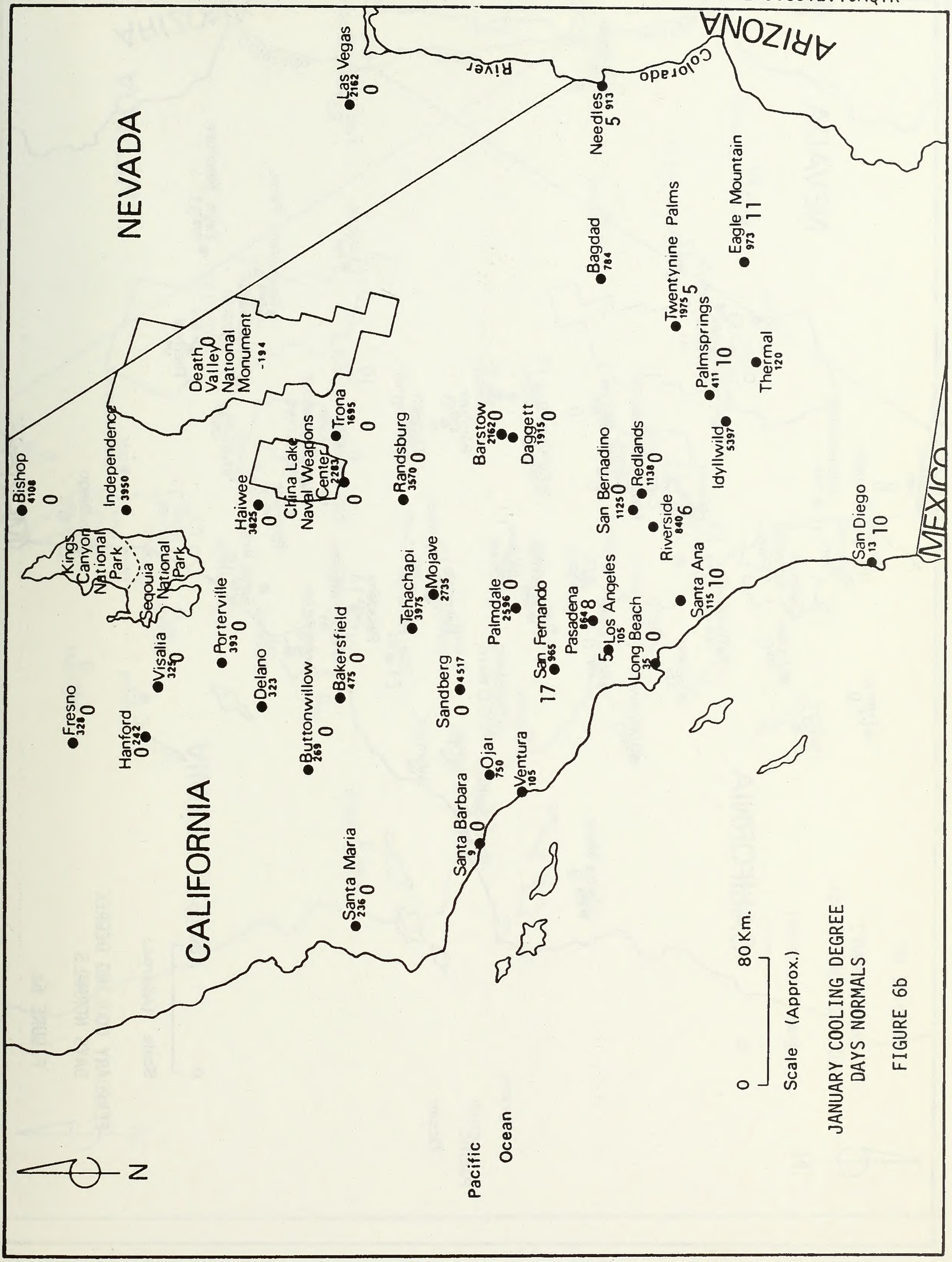

JANUARY COOLING DEGREE DAYS NORMALS

FIGURE 6b

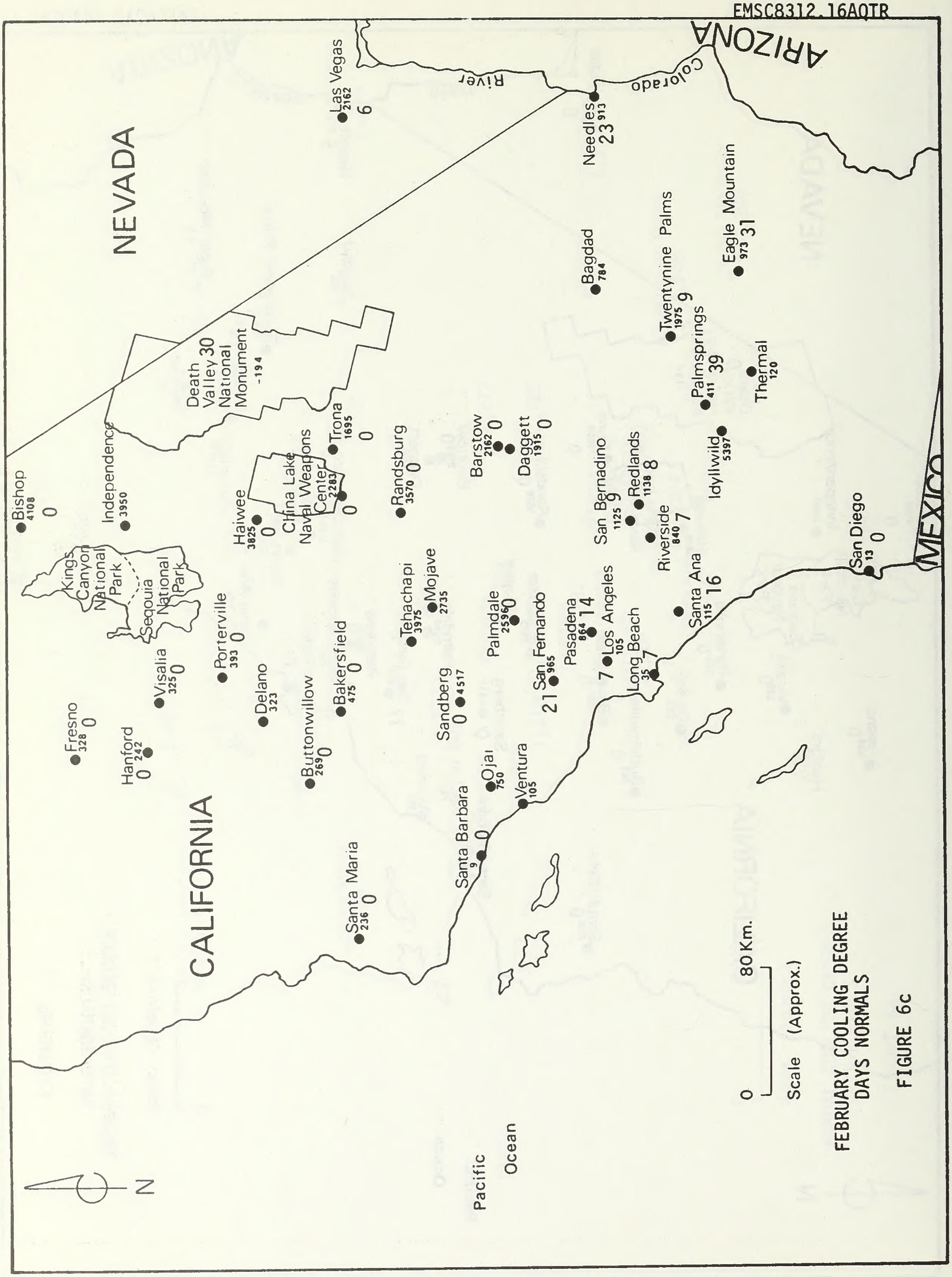

FEBRUARY COOLING DEGREE DAYS NORMALS

FIGURE 6c

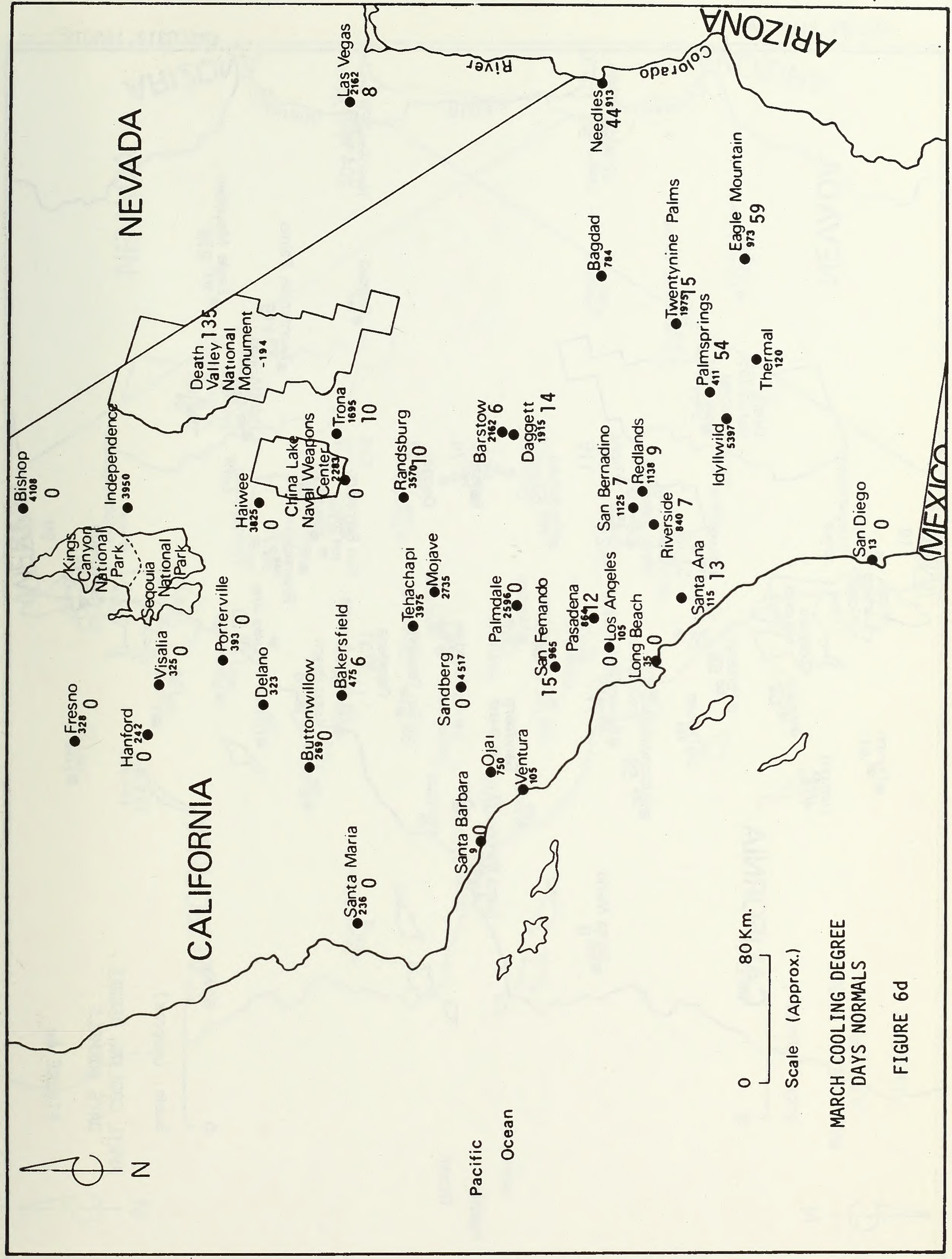

MARCH COOLING DEGREE DAYS NORMALS

FIGURE 6d

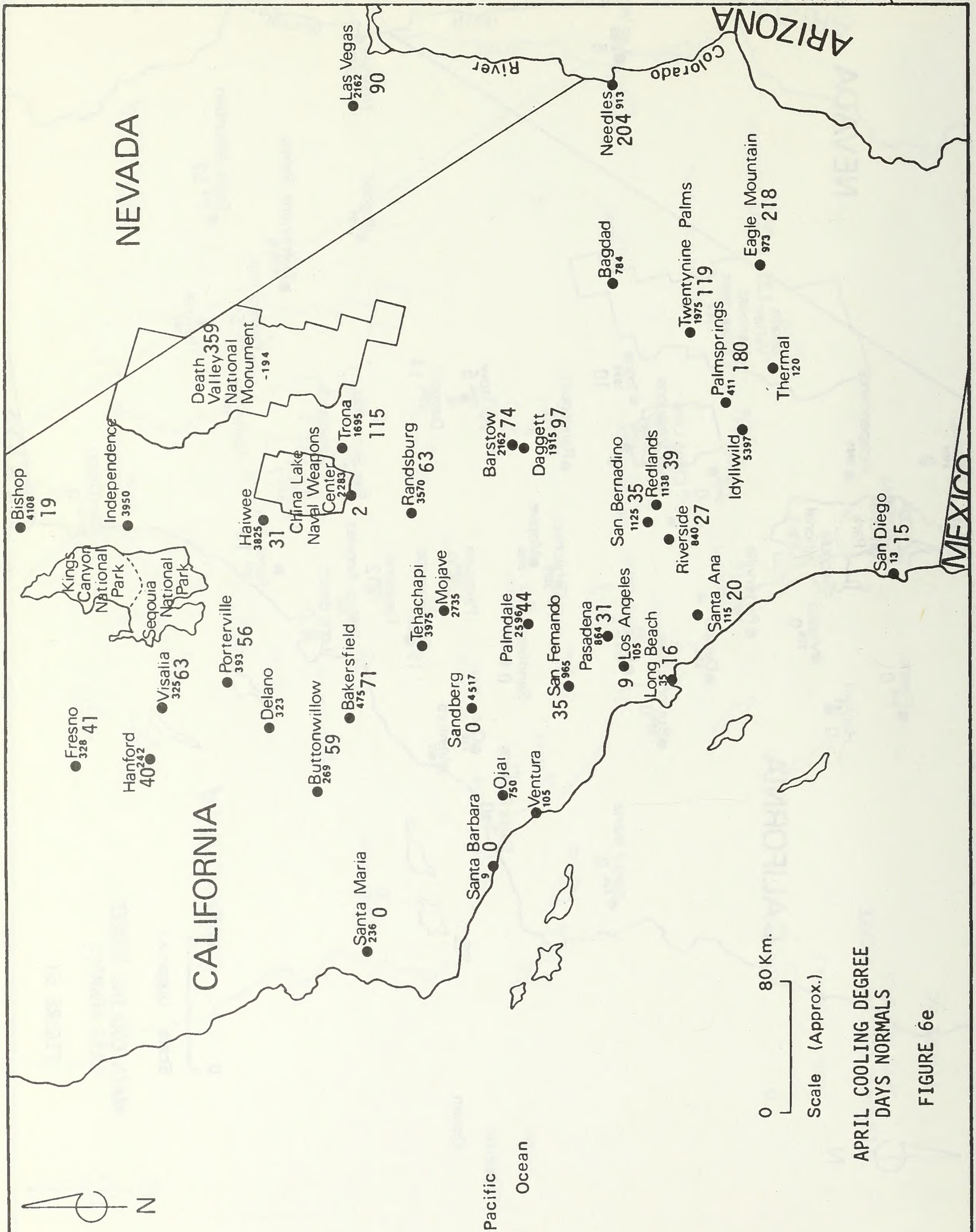

APRIL COOLING DEGREE DAYS NORMALS

FIGURE 6e

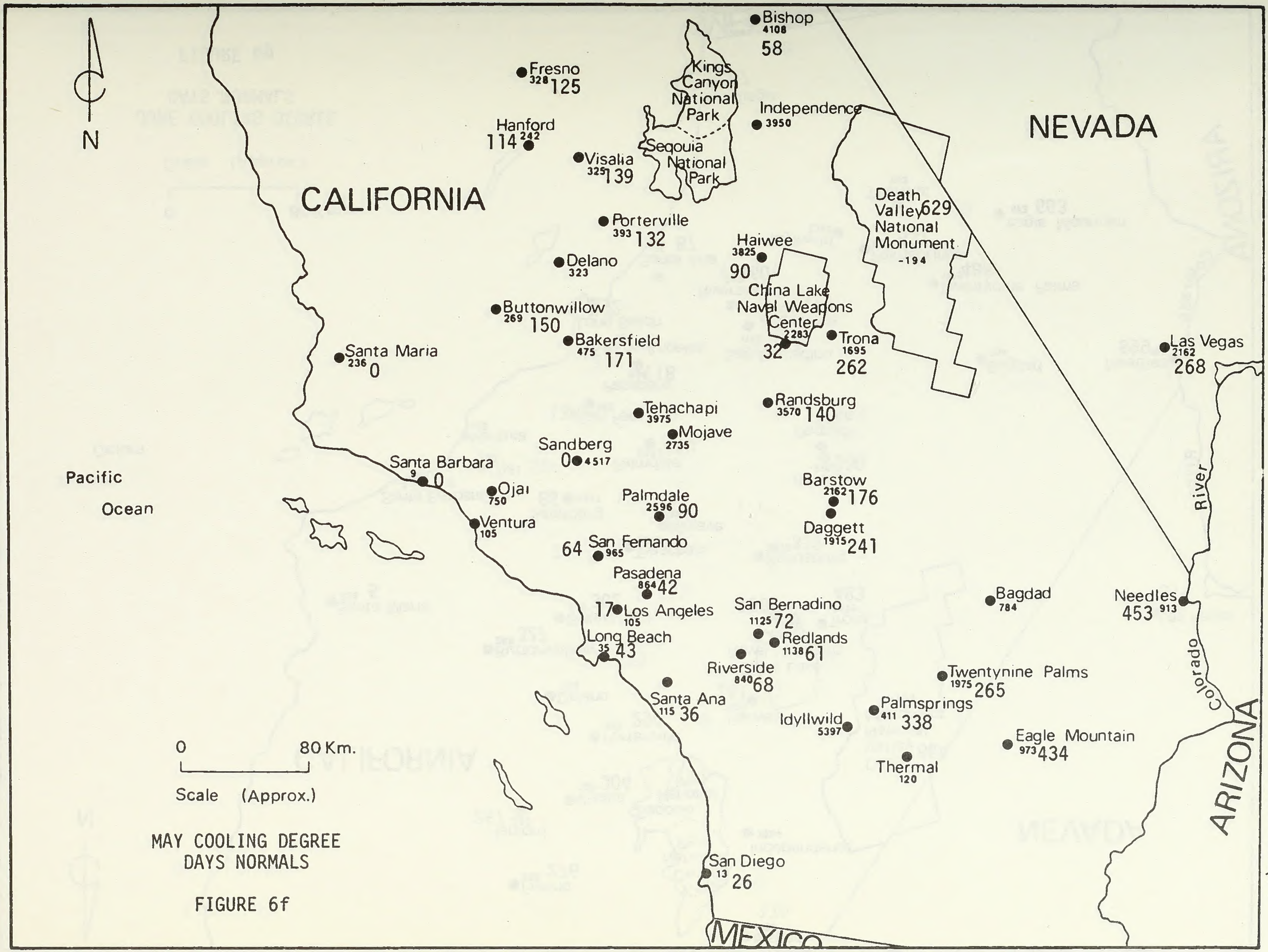

MAY COOLING DEGREE DAYS NORMALS

FIGURE 6f

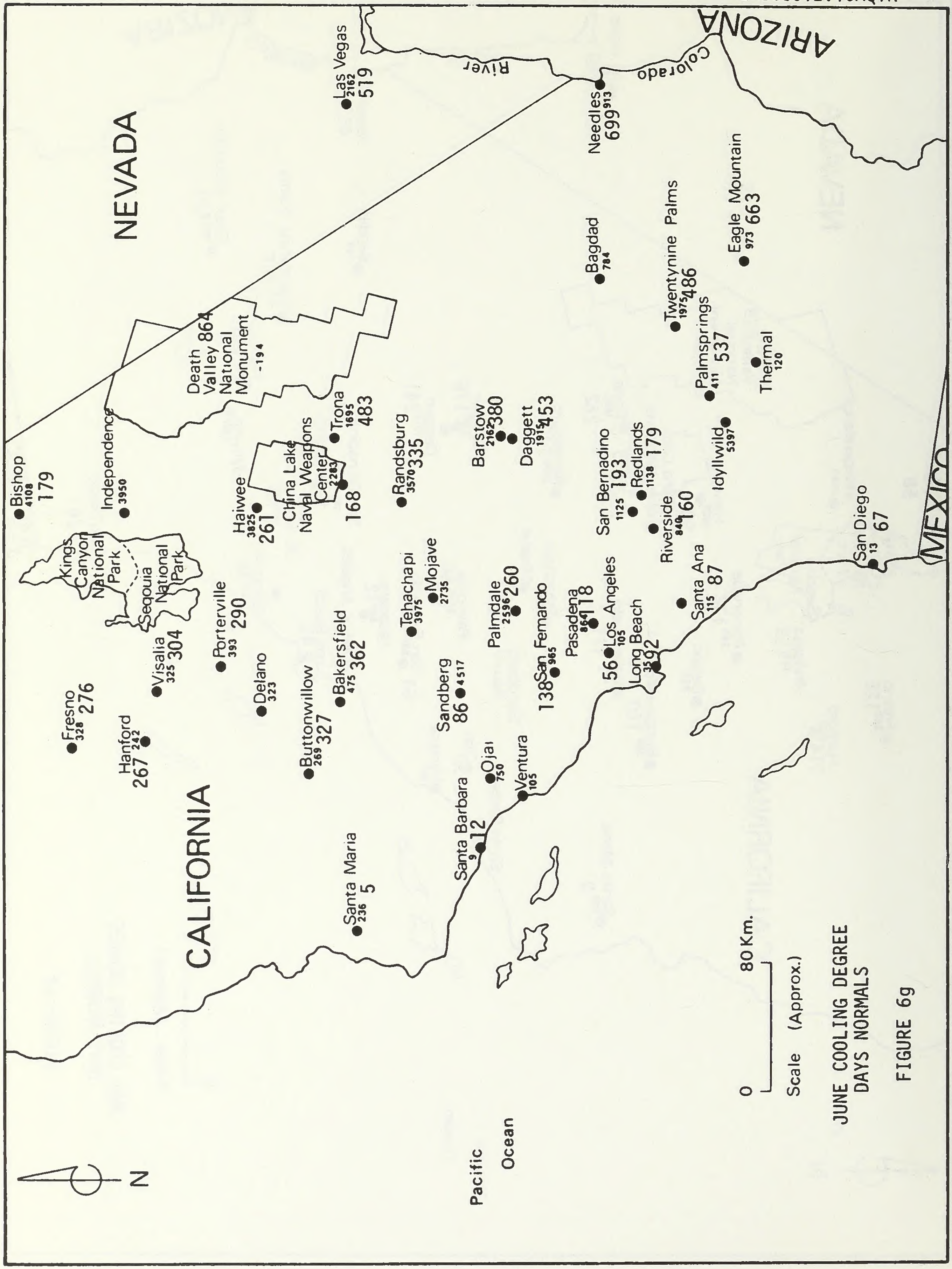

JUNE COOLING DEGREE
DAYS NORMALS

FIGURE 6g

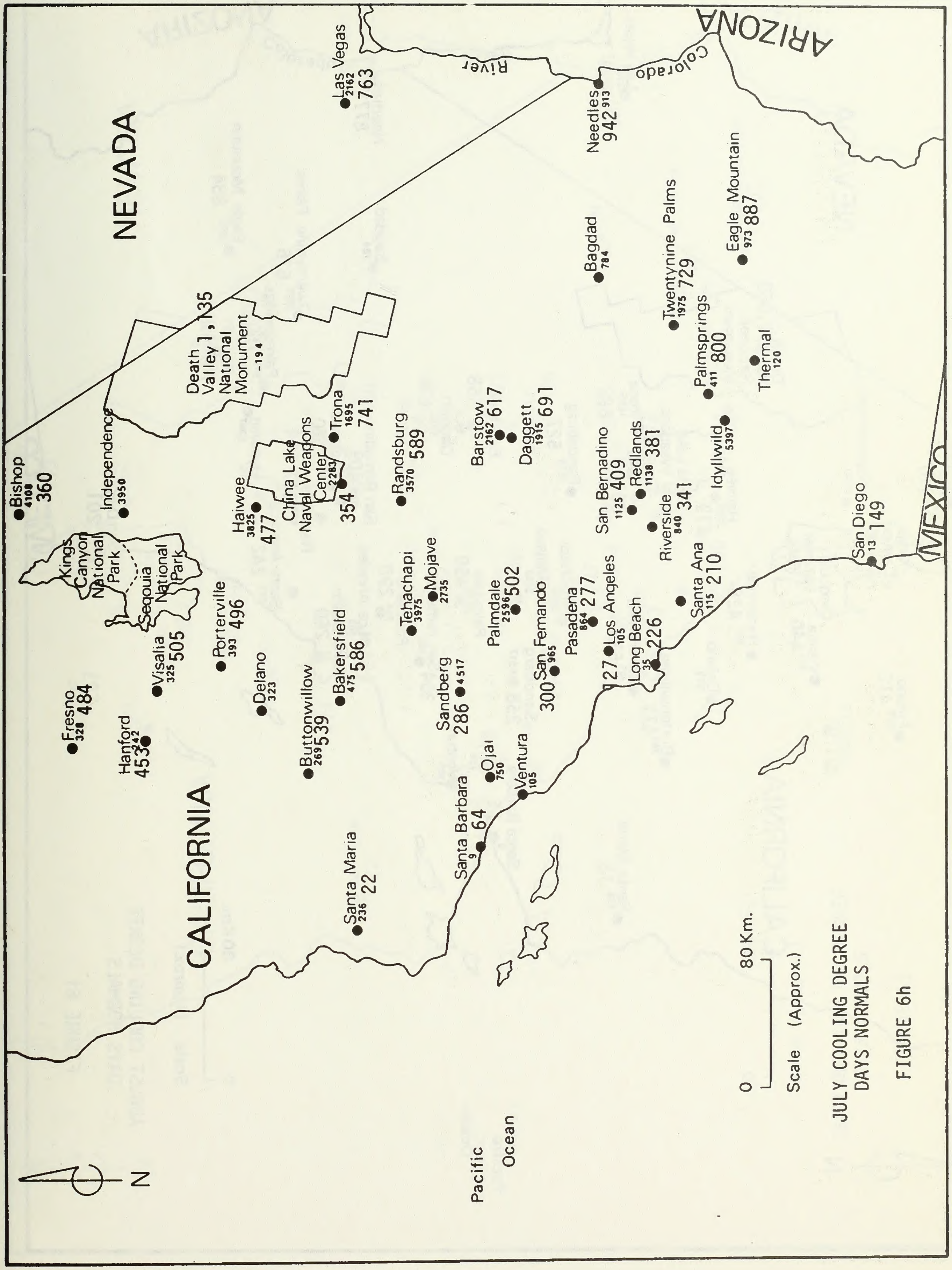

JULY COOLING DEGREE DAYS NORMALS

FIGURE 6h

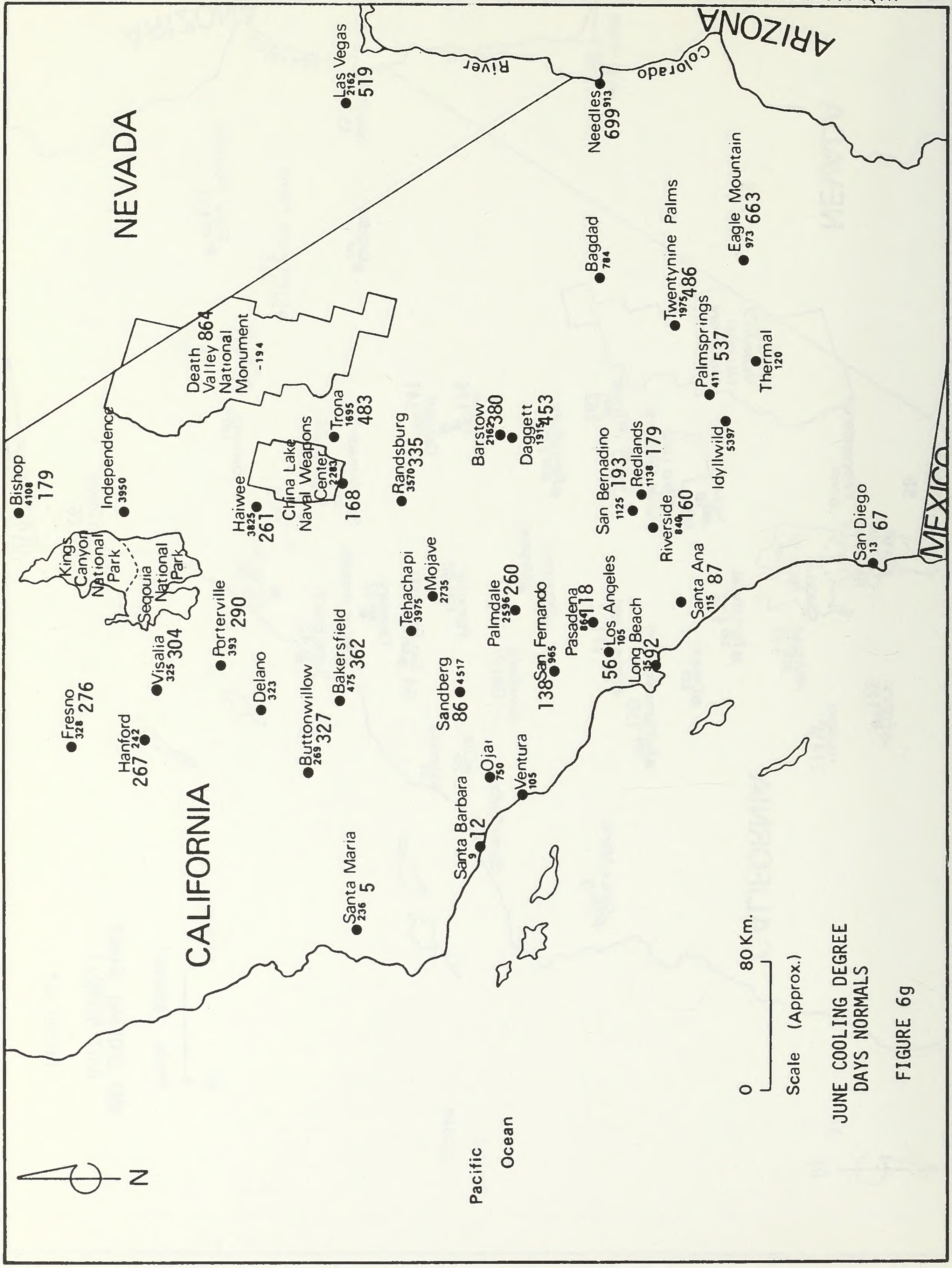

JUNE COOLING DEGREE DAYS NORMALS

FIGURE 6g

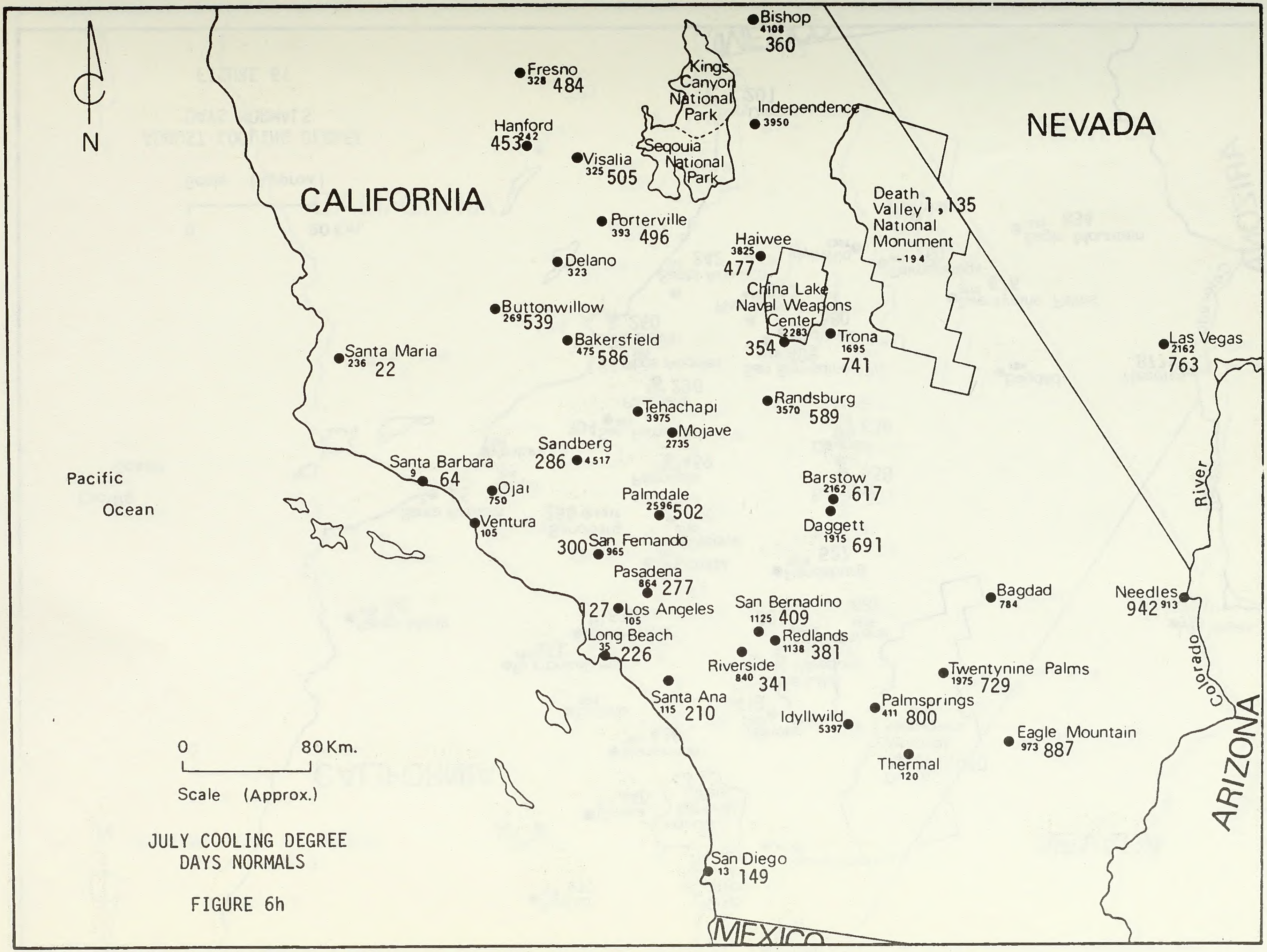

JULY COOLING DEGREE DAYS NORMALS

FIGURE 6h

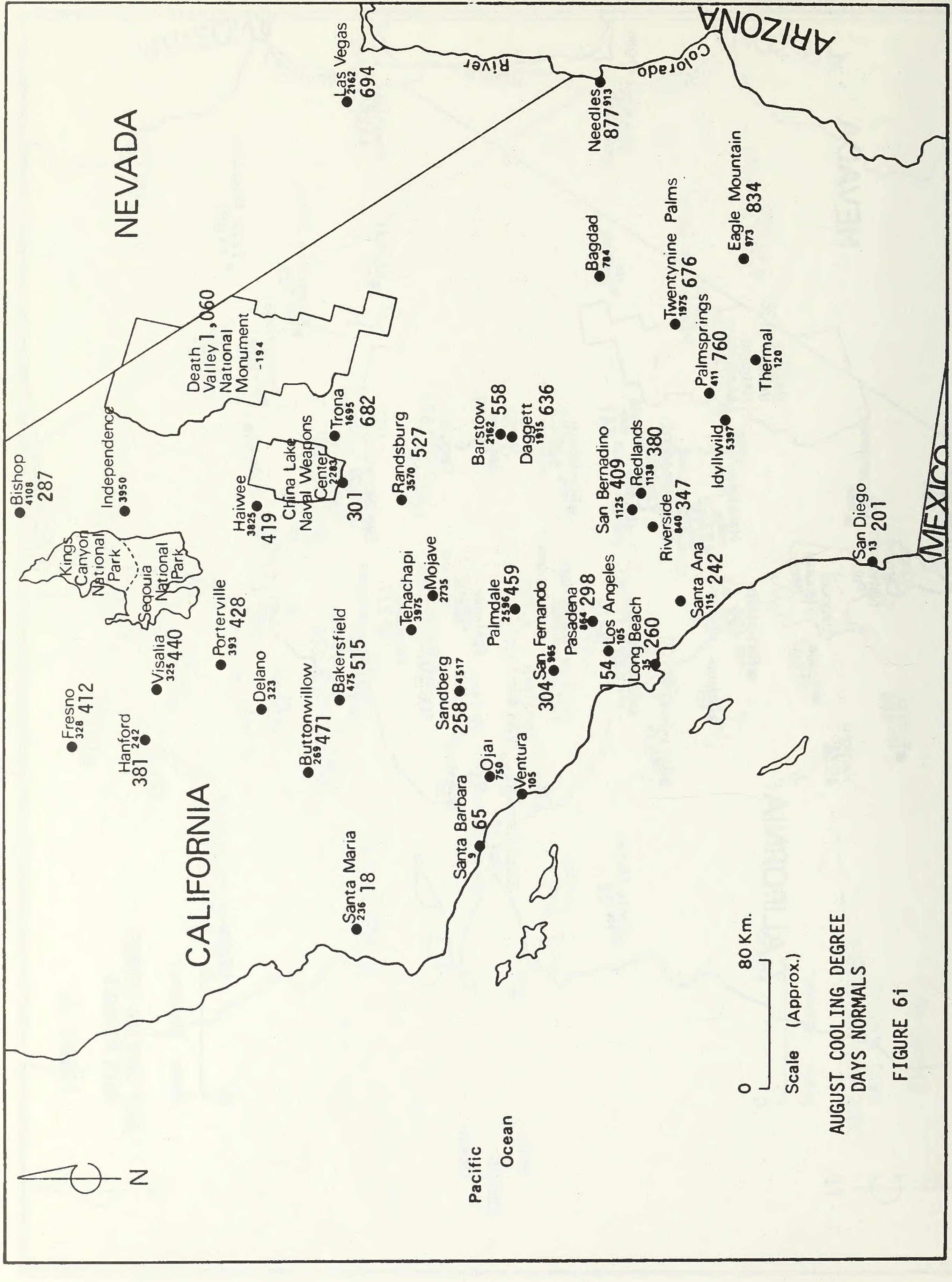

AUGUST COOLING DEGREE DAYS NORMALS

FIGURE 61

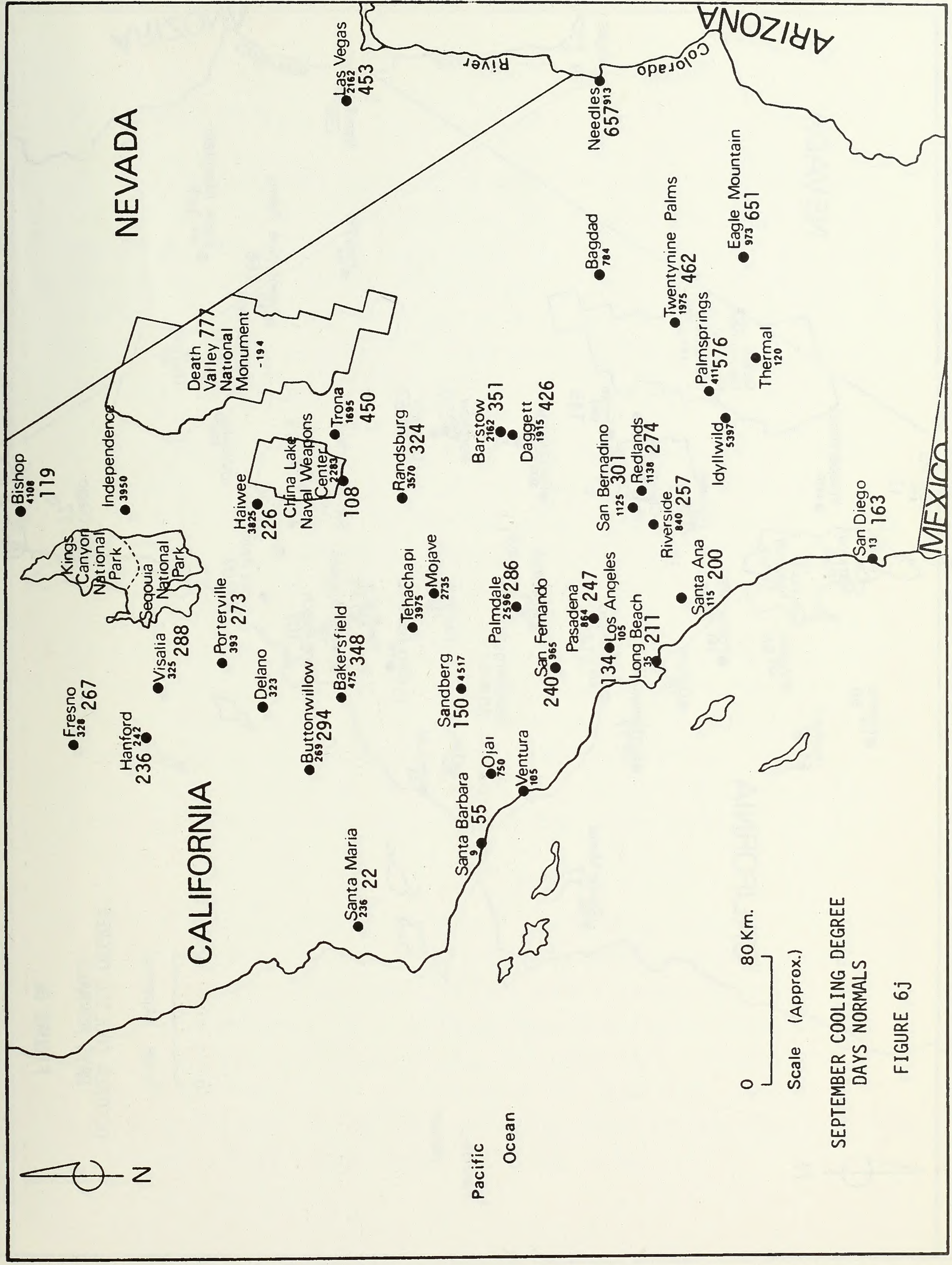

SEPTEMBER COOLING DEGREE DAYS NORMALS

FIGURE 6j

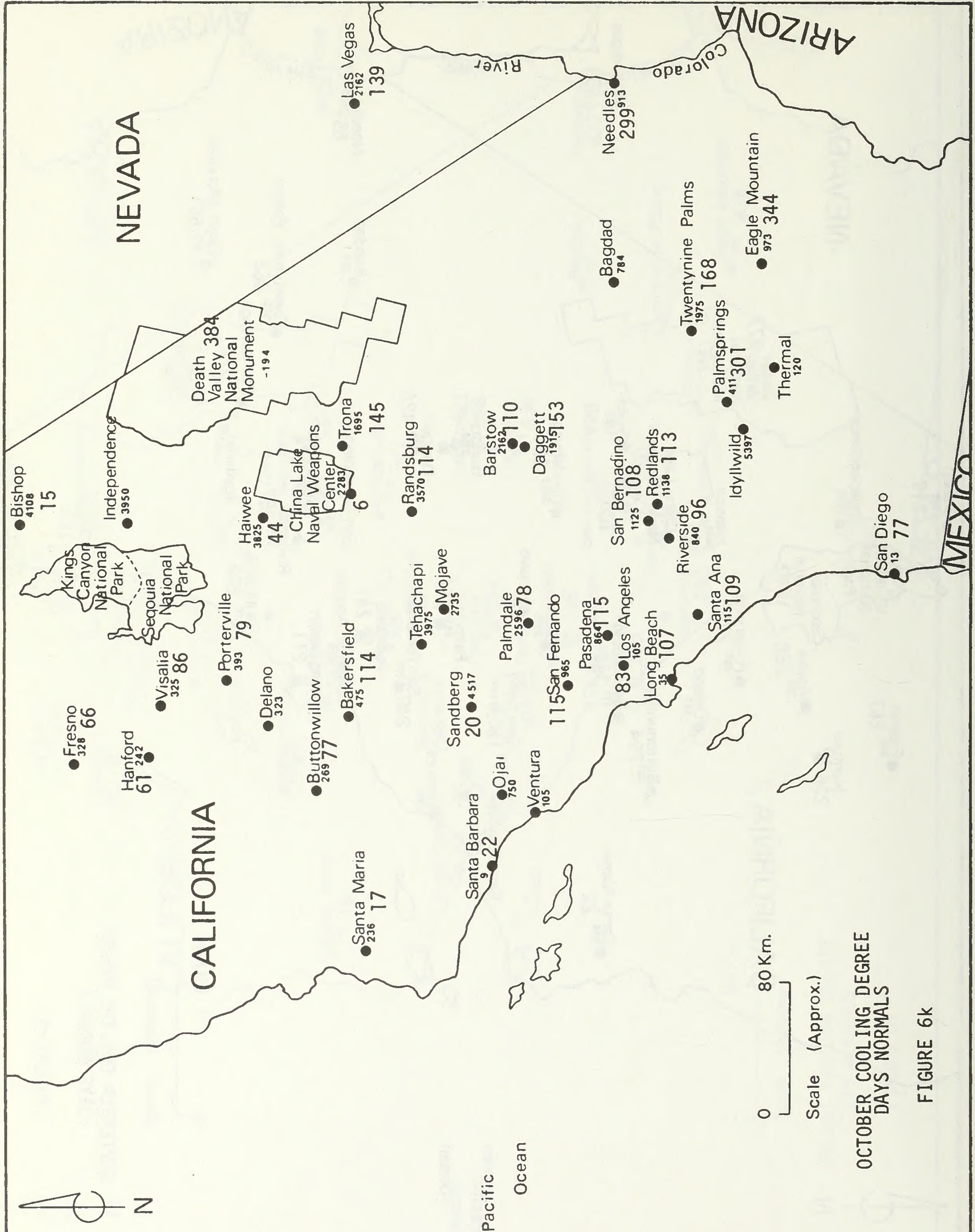

OCTOBER COOLING DEGREE DAYS NORMALS

FIGURE 6k

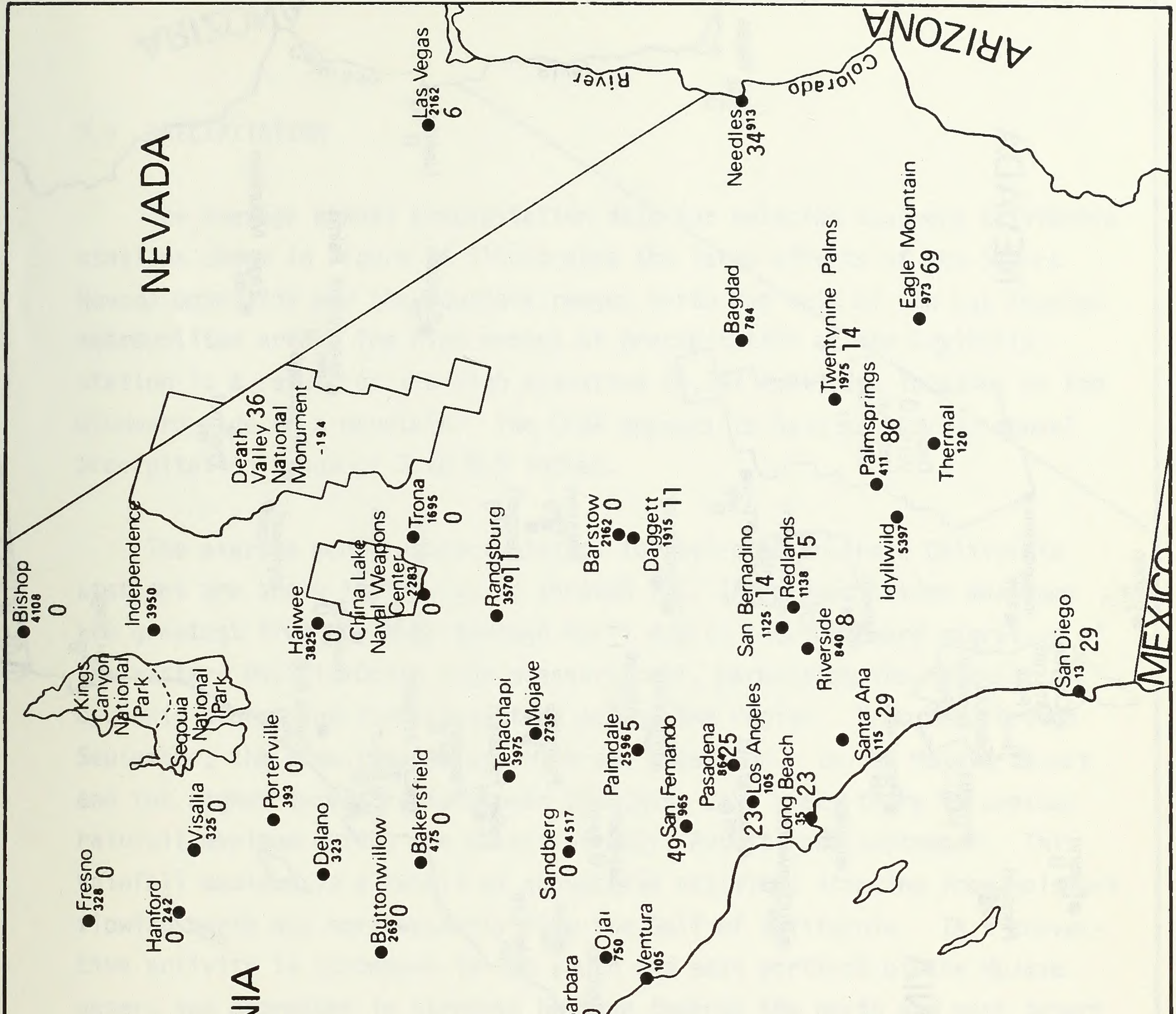

NOVEMBER COOLING DEGREE DAYS NORMALS

FIGURE 61

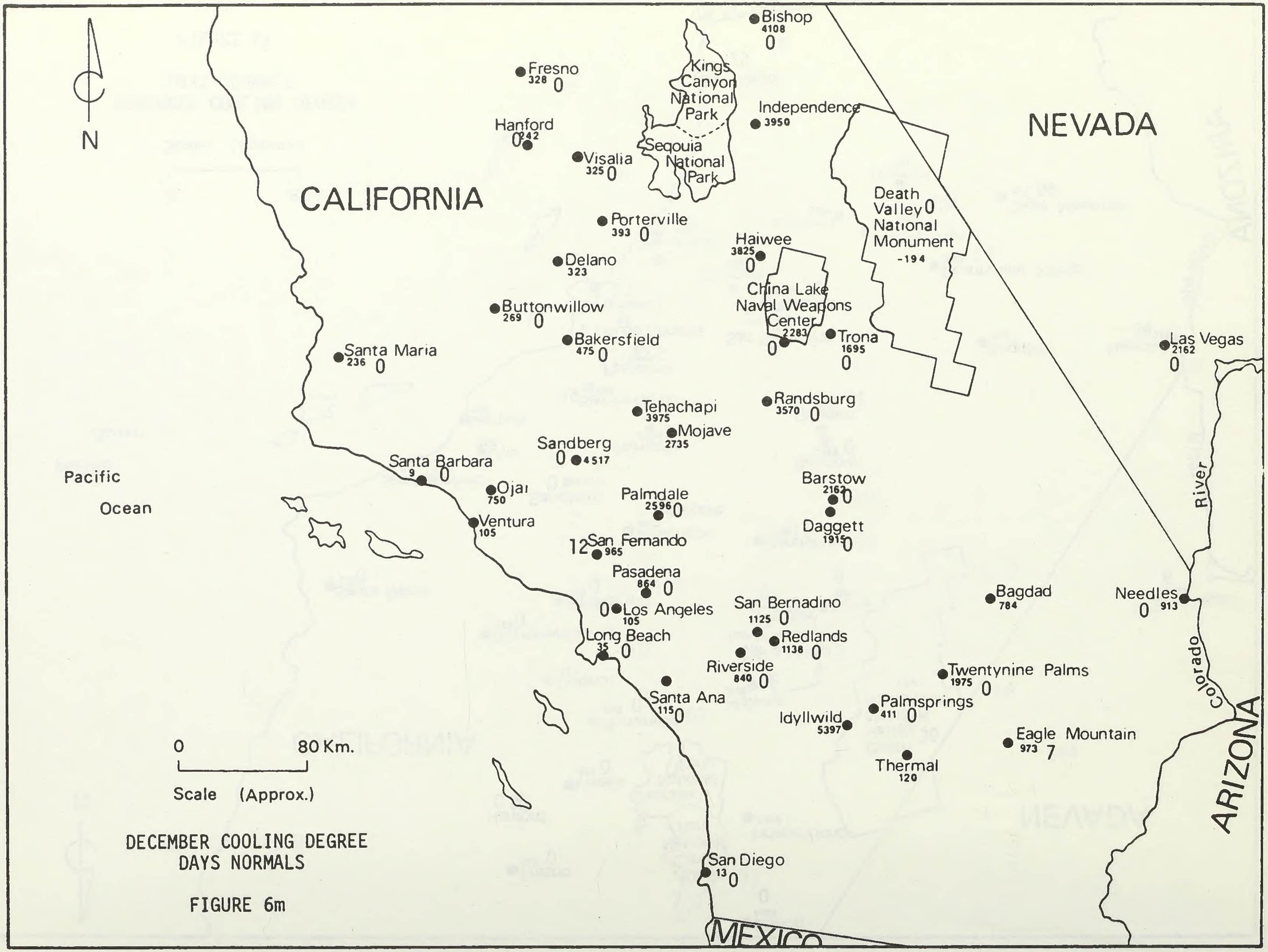

DECEMBER COOLING DEGREE DAYS NORMALS

FIGURE 6m

9.4 PRECIPITATION

The average annual precipitation data for selected southern California stations shown in Figure 7A illustrates the large effects of the Sierra Nevada mountains and the mountain ranges north and east of the Los Angeles metropolitan area. The high amount of precipitation at the Idyllwild station is a result of its high elevation (5,397 feet) and location on the windward side of a mountain. The CGRA appears to have an average annual precipitation range of 3 to 6.5 inches.

The average monthly precipitation for selected southern California stations are shown in Figures 7b through 7m. The precipitation maximums are greatest from November through April due to the southward migration of the eastern Pacific Ocean high pressure cell, permitting the movement of cyclonic storms and frontal systems across the region. From May through September, the area remains dry with one exception. In the Mojave desert and the higher desert regions near the China Lake area, there is another rainfall maximum during the months of July, August, and September. This rainfall maximum is a result of convective activity, stemming from moisture flowing north and northwesterly from the Gulf of California. This convective activity is strongest in the south and east portions of the Mojave desert and decreases in strength heading towards the north and west desert areas.

Table 8 shows the greatest 24-hour precipitation amounts for selected southern California stations. The extreme amounts for most of the stations occur in December through March, but the desert station extremes occur from July through September, as a result of convective precipitation. Tables 9 and 10 show the mean number of days with precipitation ≥0.10 and ≥0.01 inches respectively. From Table 10, note that China Lake, the station closest to the CGRA, has at least one day per month per year (average) with precipitation ≥0.01 inches, except the month of June.

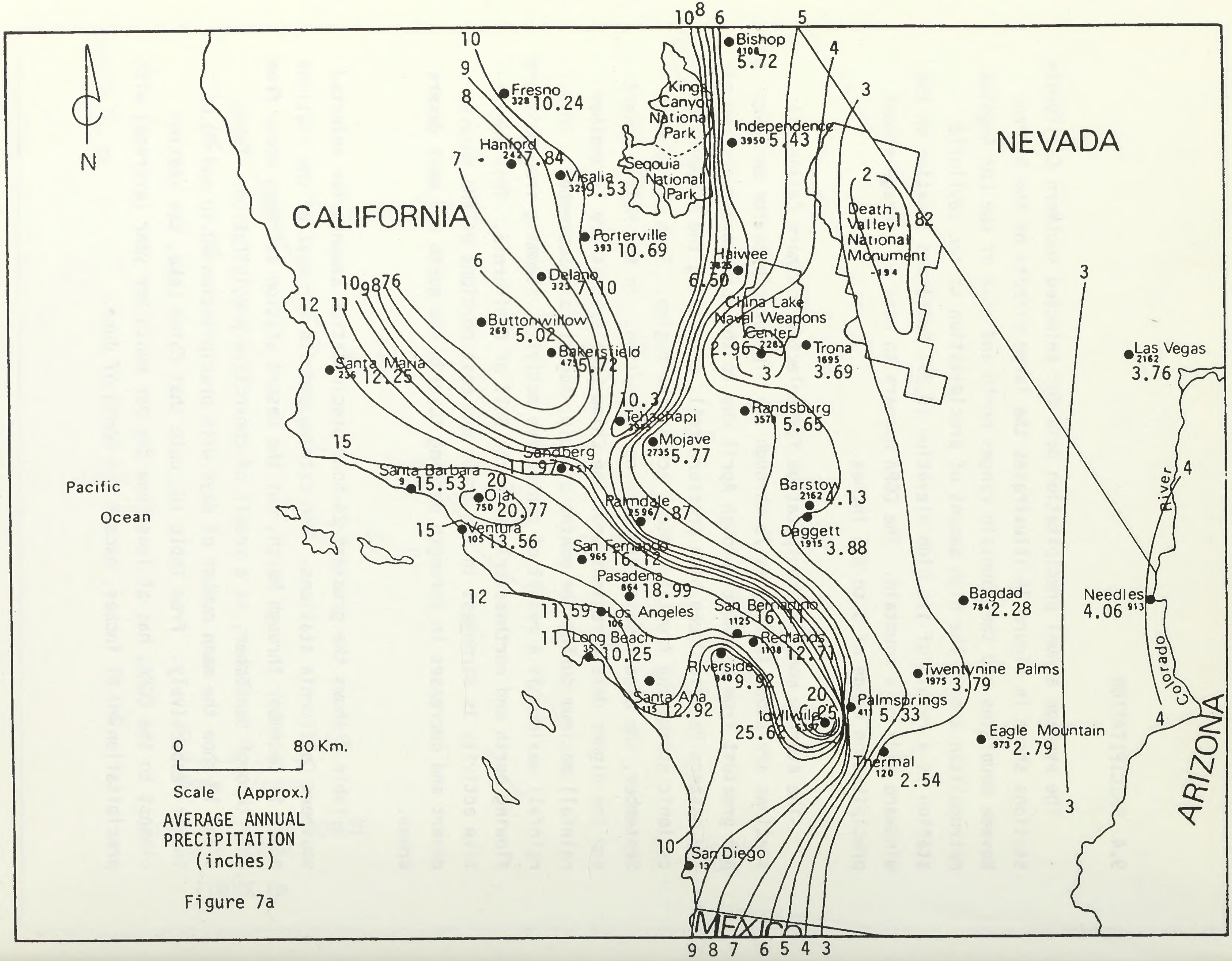

AVERAGE ANNUAL PRECIPITATION (inches)

Figure 7a

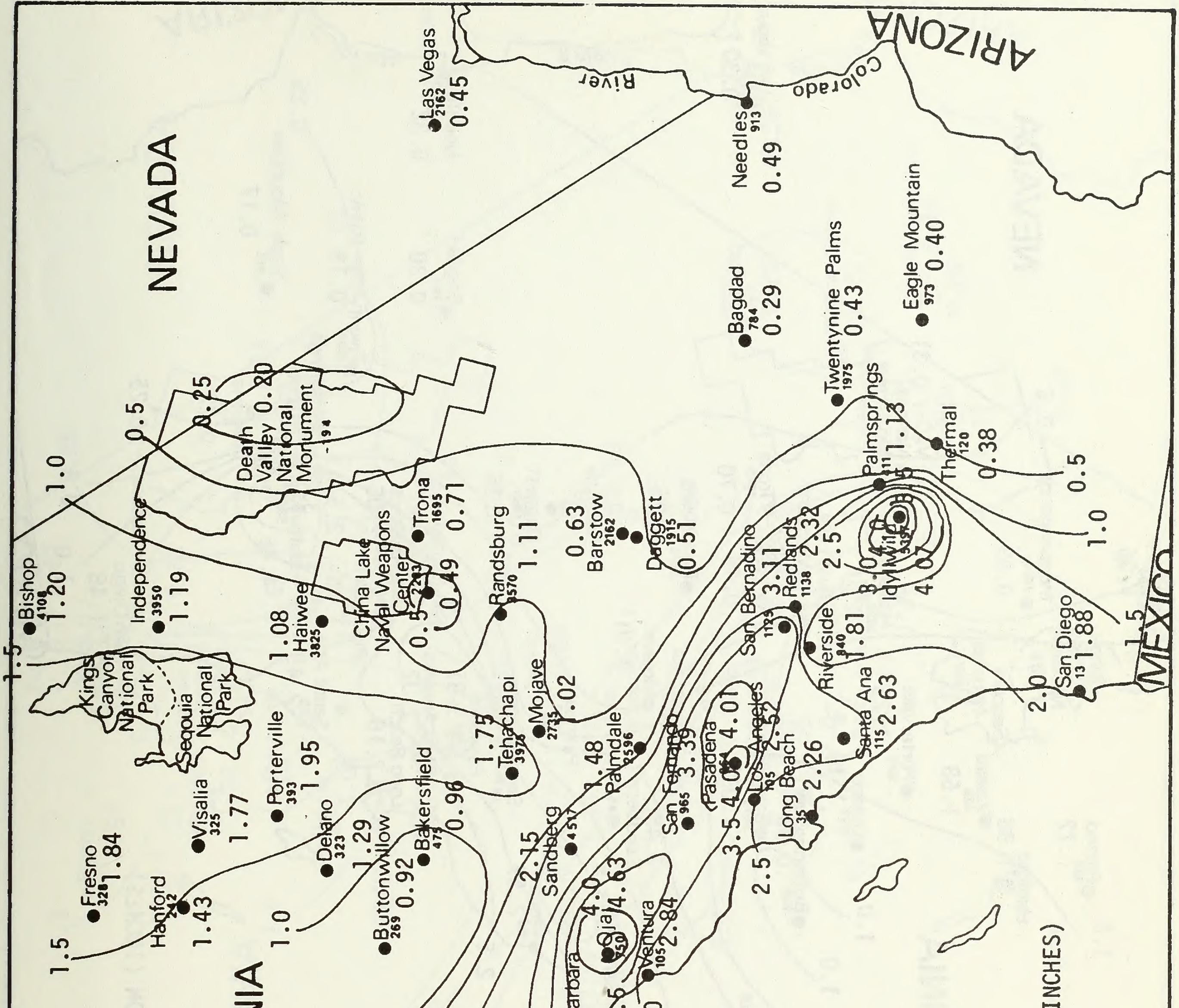

AVERAGE JANUARY PRECIPITATION (INCHES)

FIGURE 7b

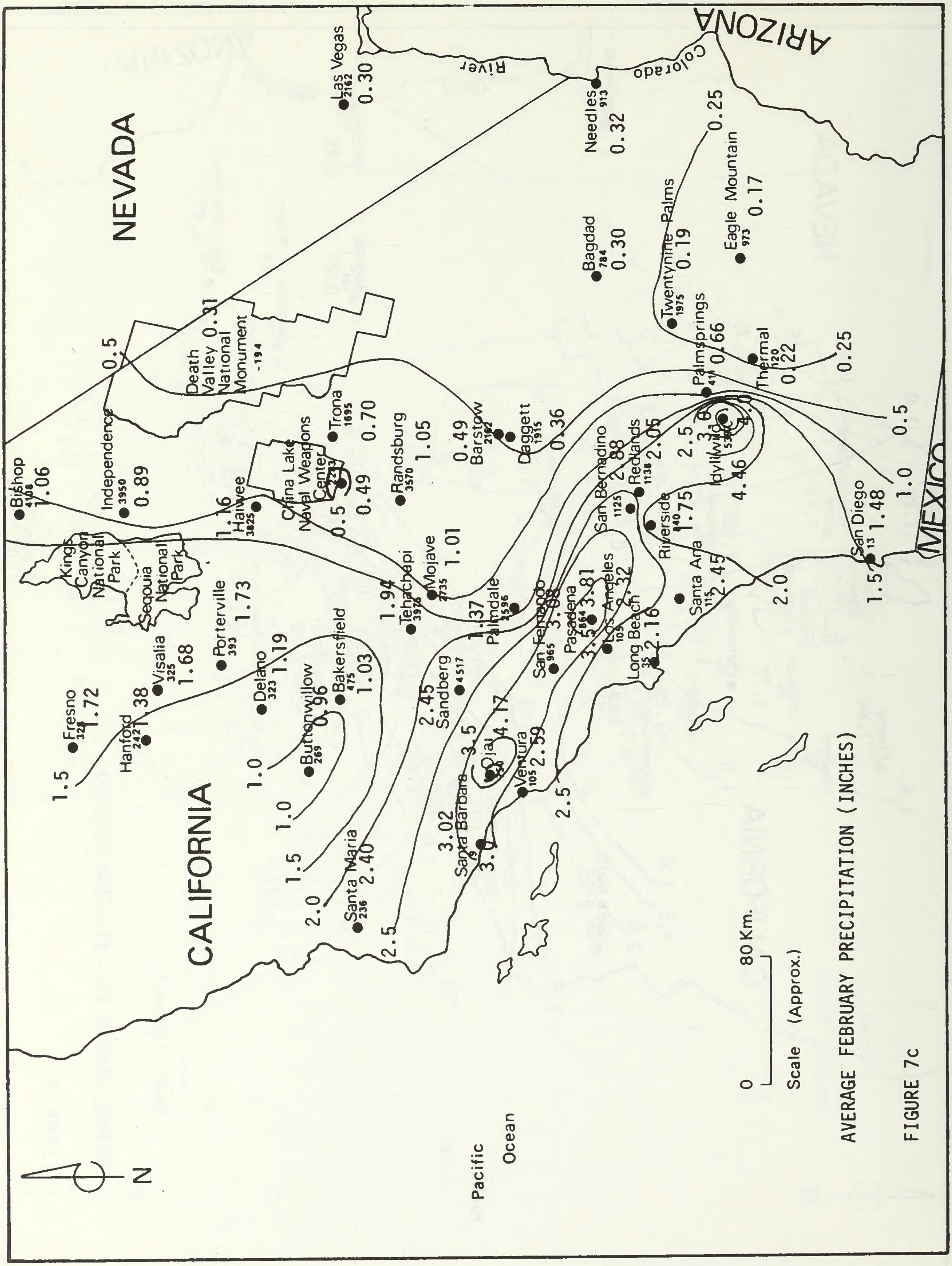

AVERAGE FEBRUARY PRECIPITATION (INCHES)

FIGURE 7c

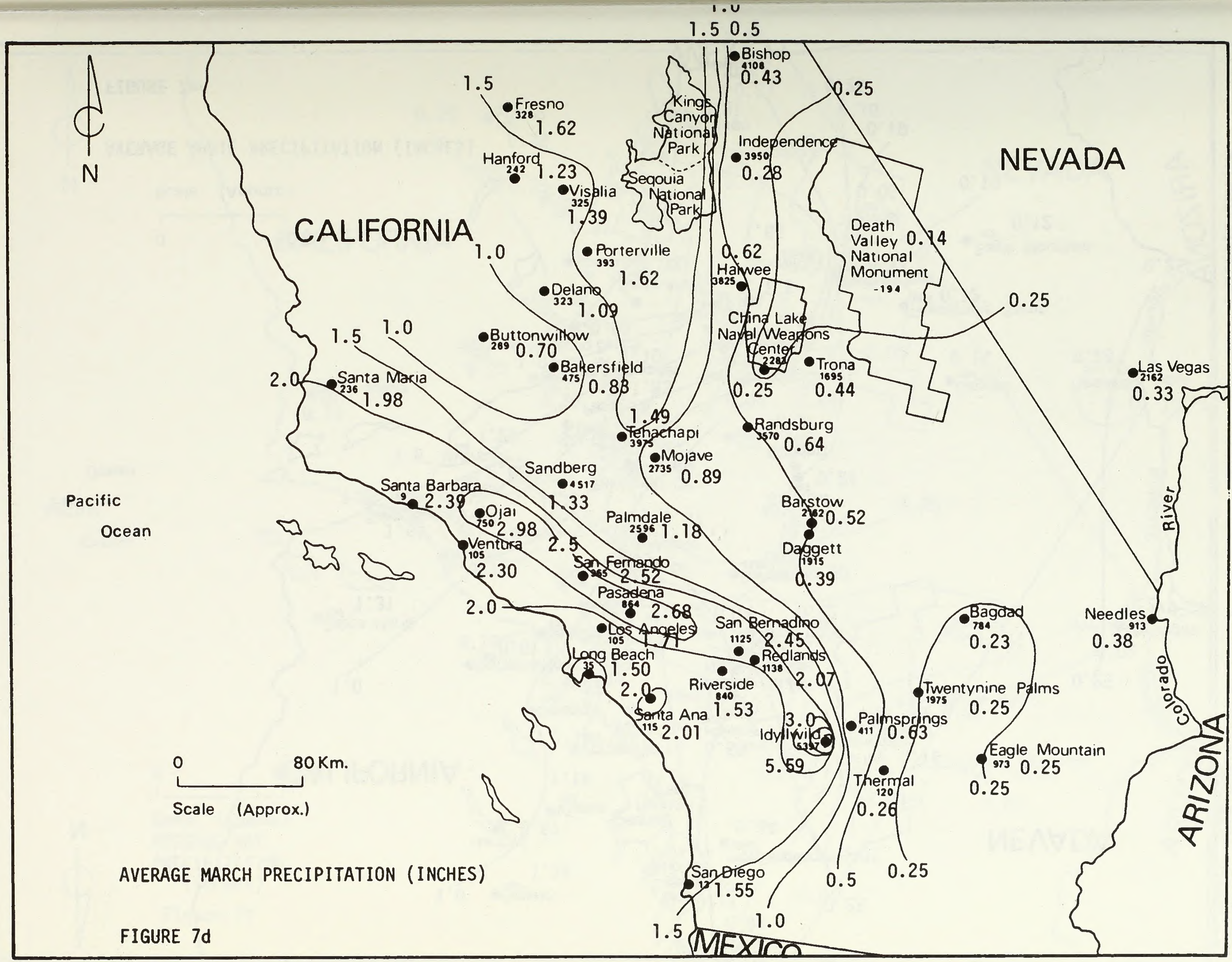

AVERAGE MARCH PRECIPITATION (INCHES)

FIGURE 7d

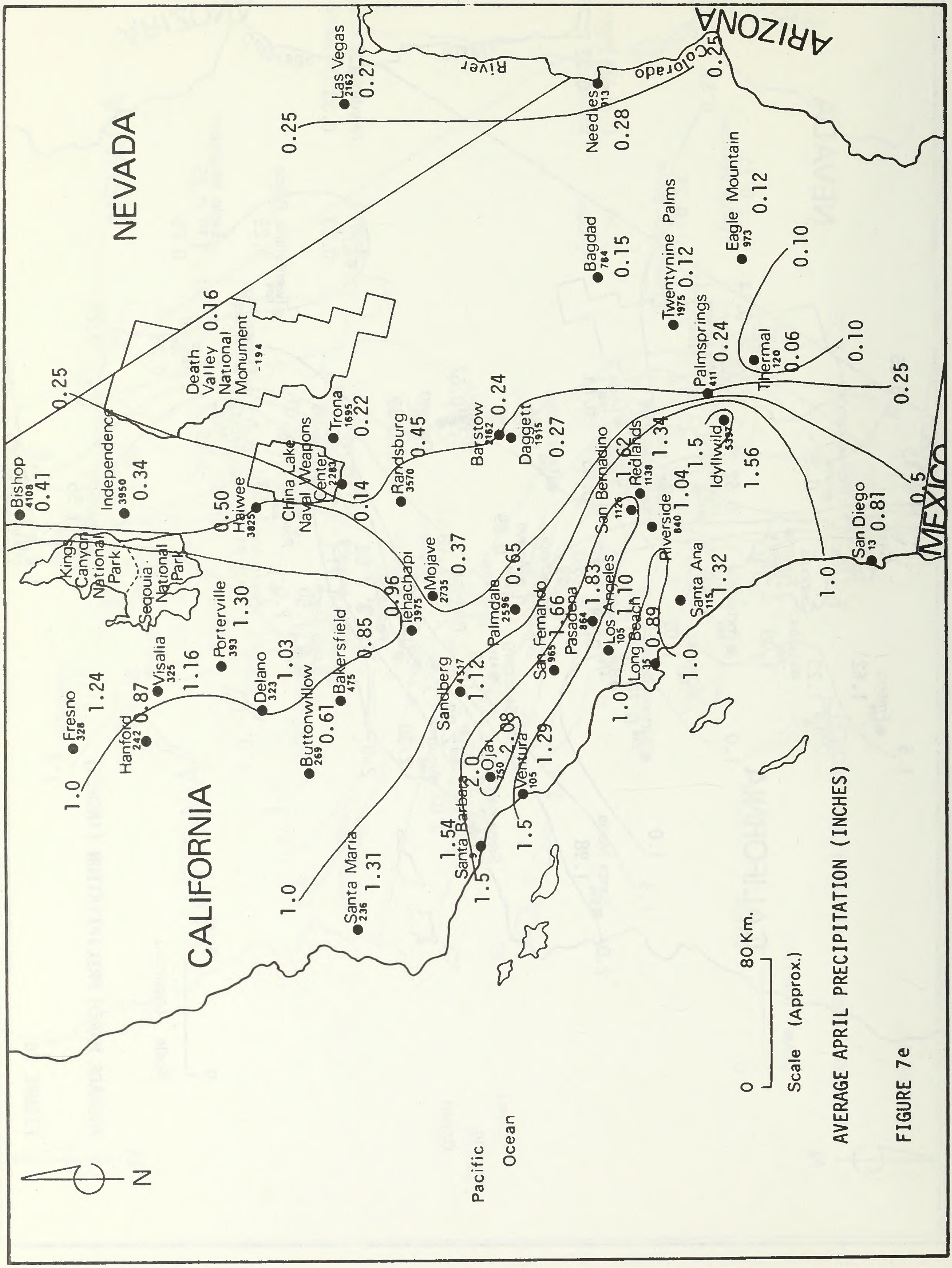

AVERAGE APRIL PRECIPITATION (INCHES)

FIGURE 7e

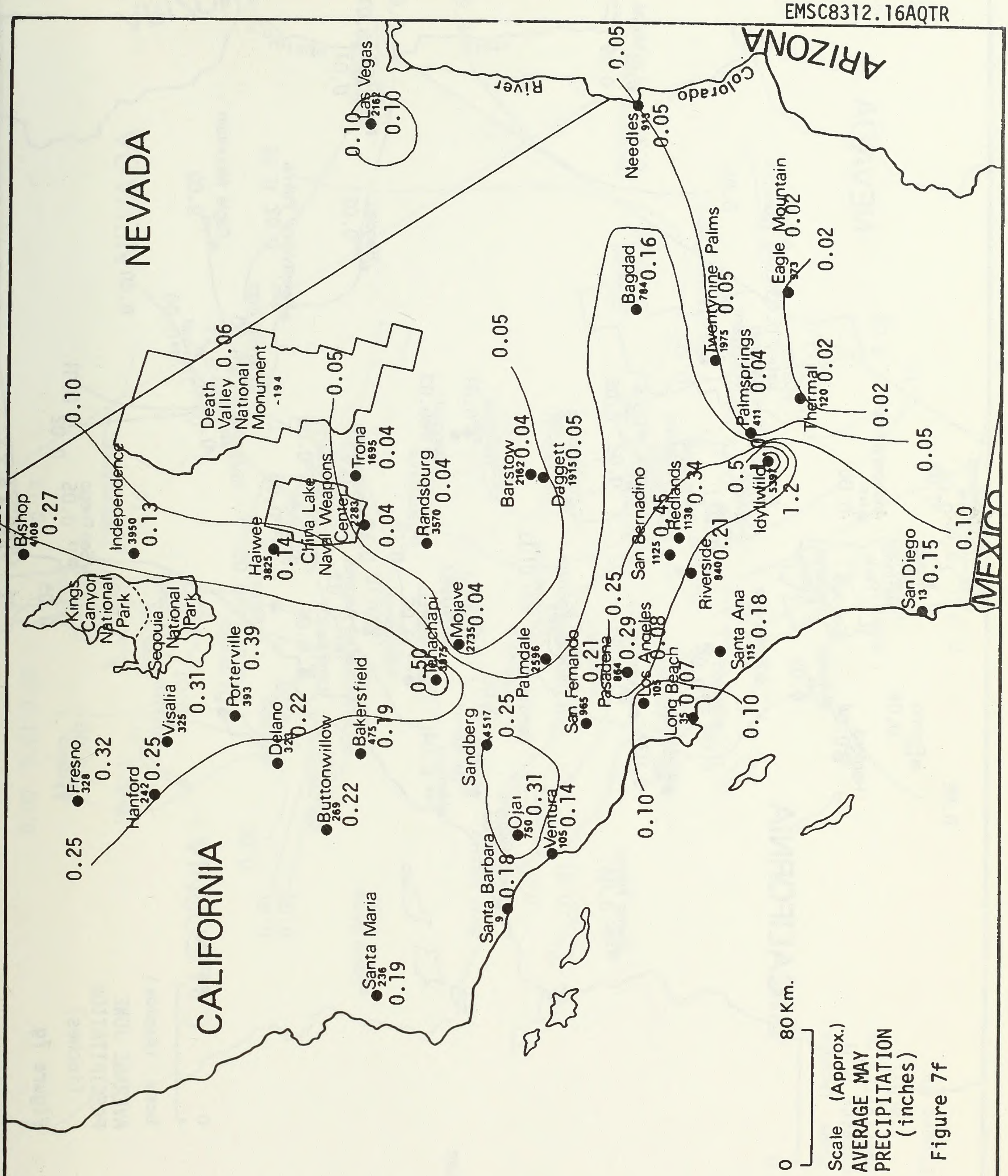

Scale (Approx.)

AVERAGE MAY PRECIPITATION (inches)

Figure 7f

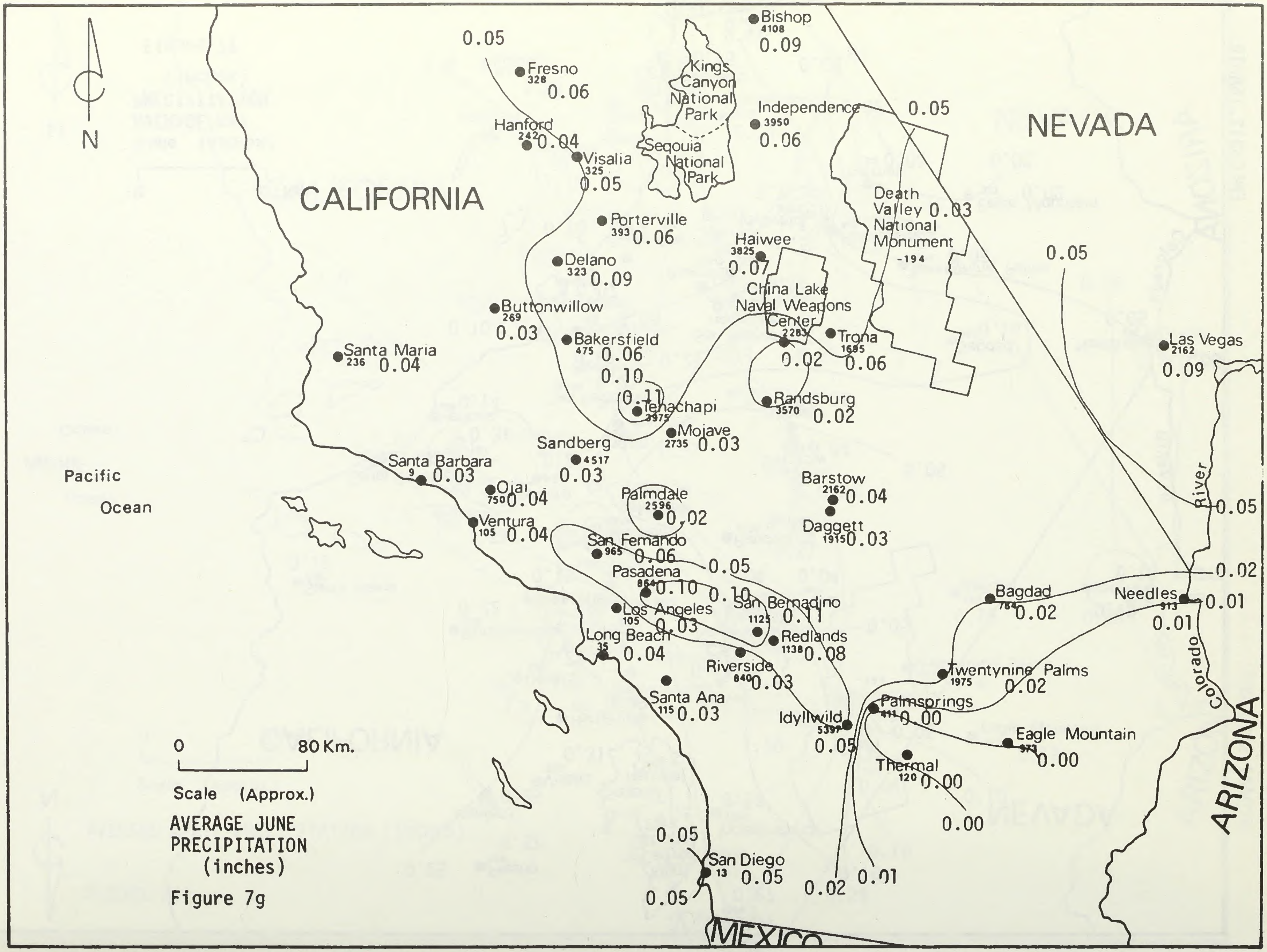

AVERAGE JUNE PRECIPITATION (inches)

Figure 7g

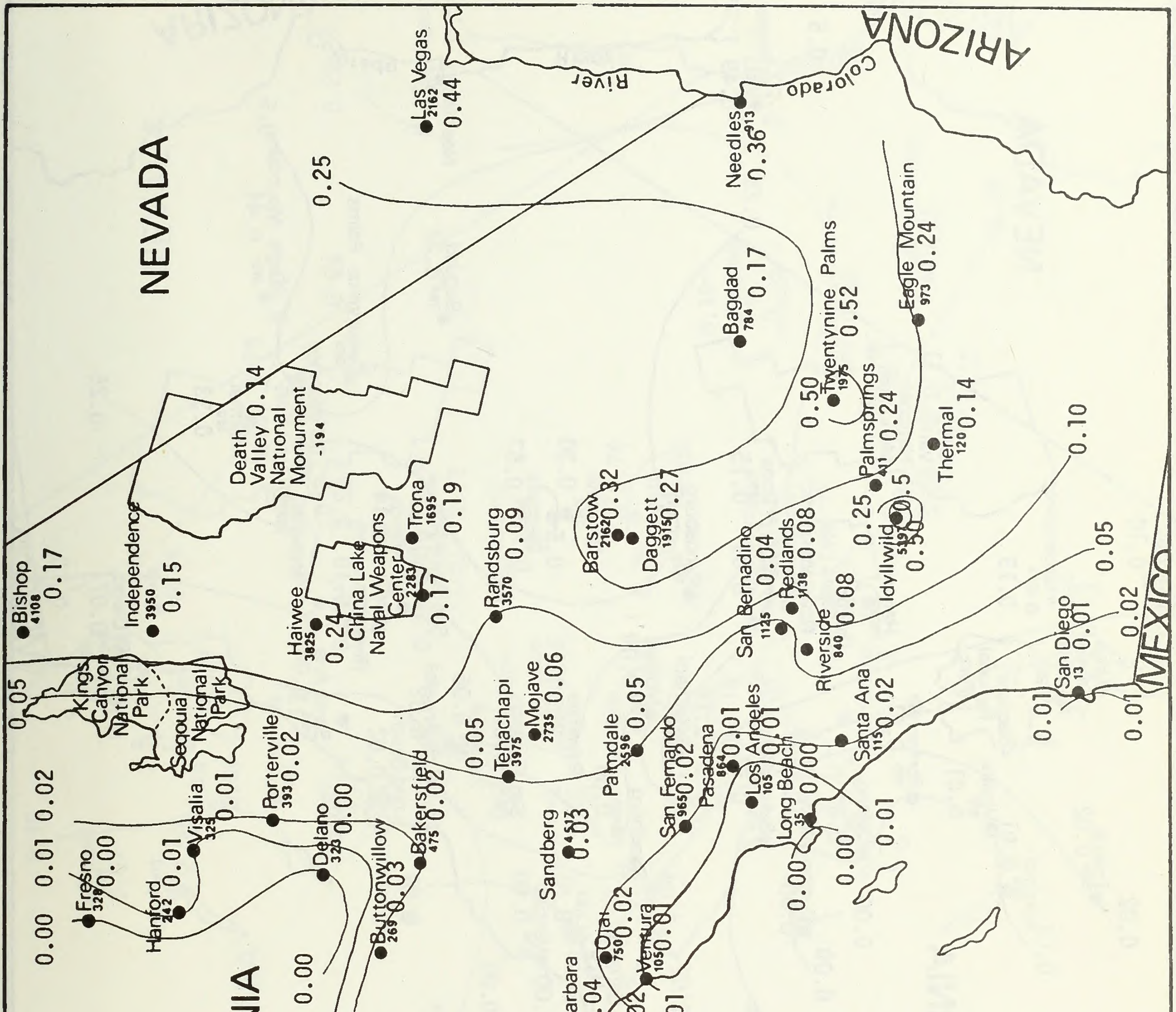

AVERAGE JULY PRECIPITATION (inches)

Figure 7h

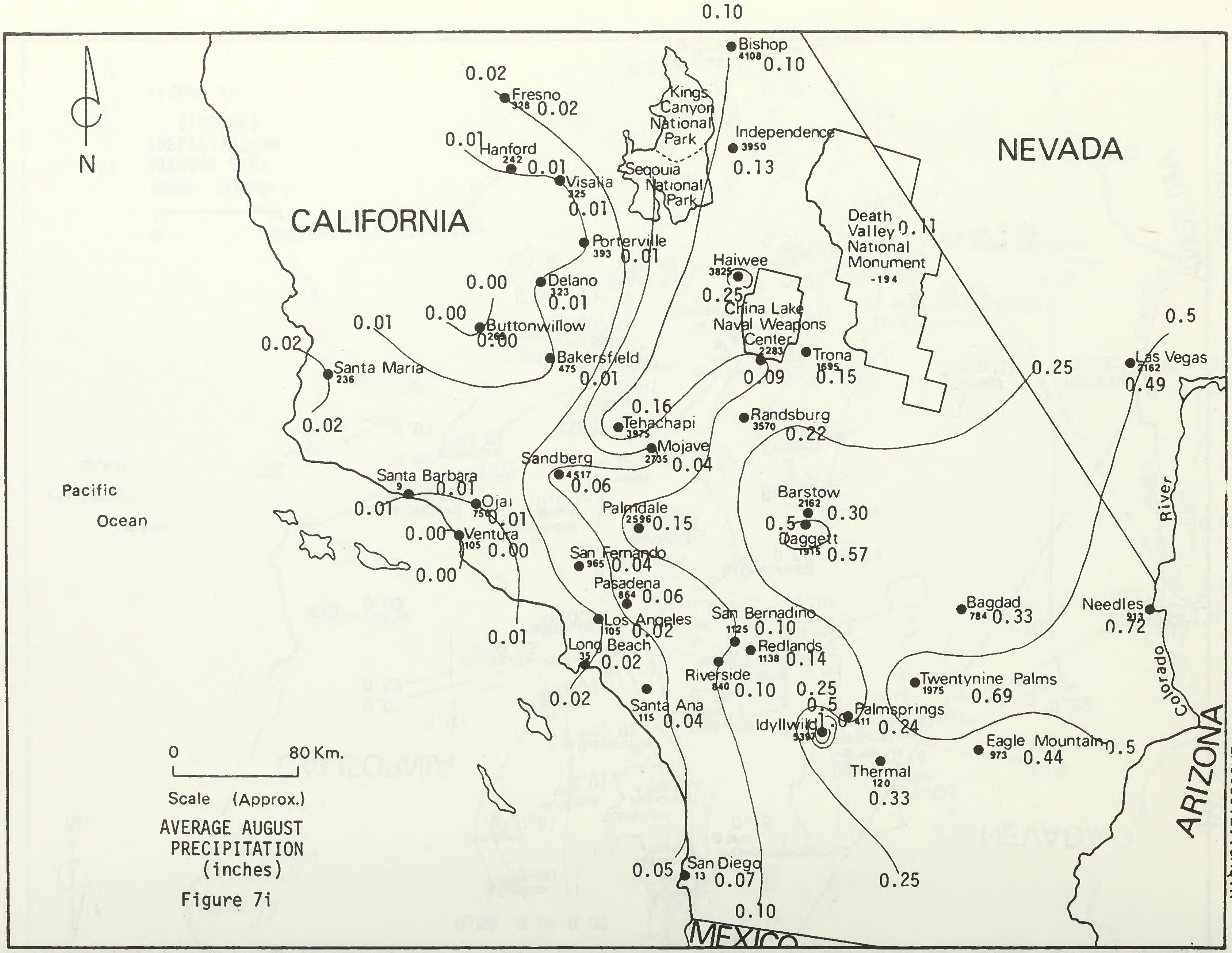

AVERAGE AUGUST PRECIPITATION (inches)

Figure 7i

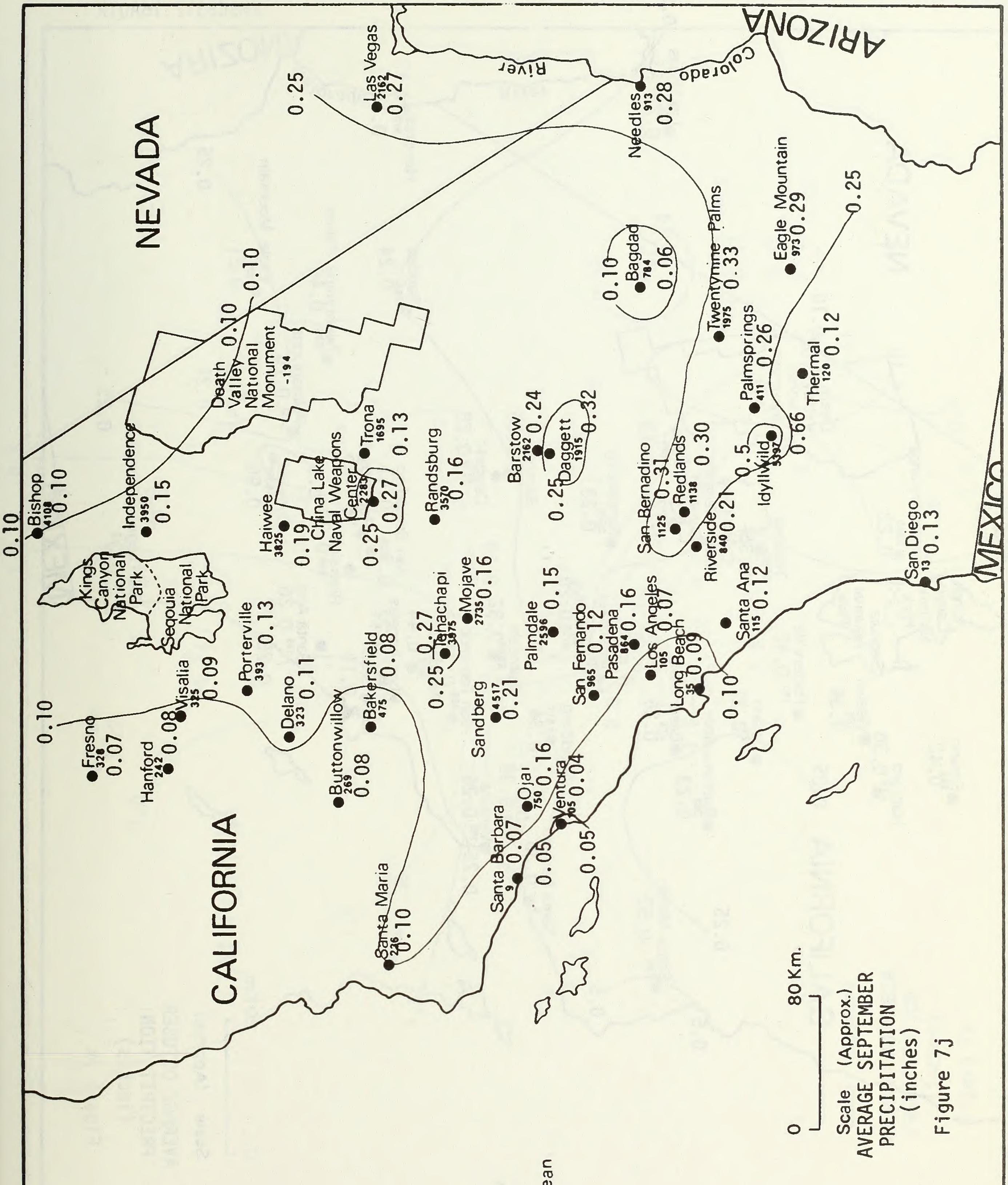

AVERAGE SEPTEMBER PRECIPITATION (inches)

Figure 7j

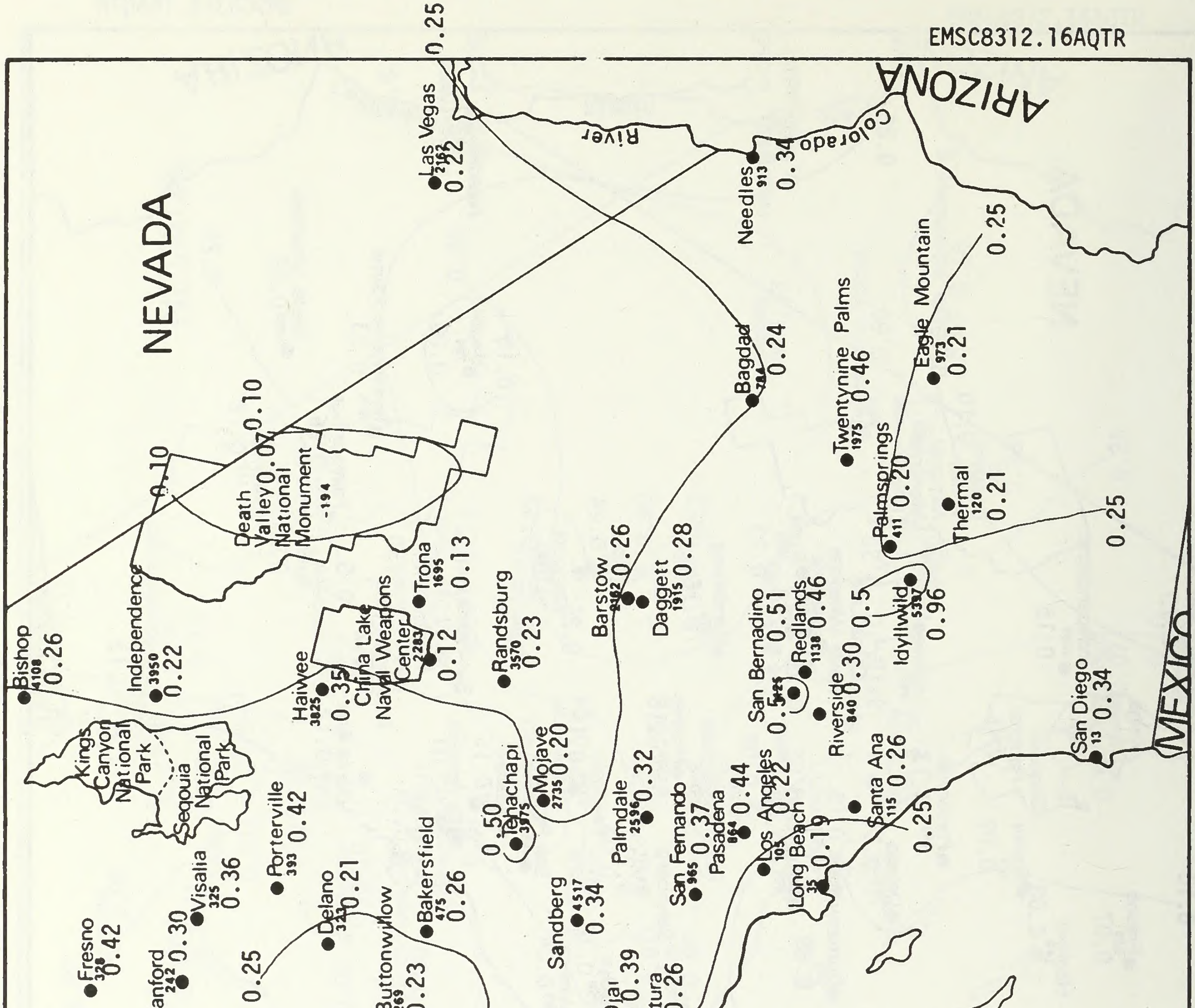

AVERAGE OCTOBER PRECIPITATION (inches)

Figure 7k

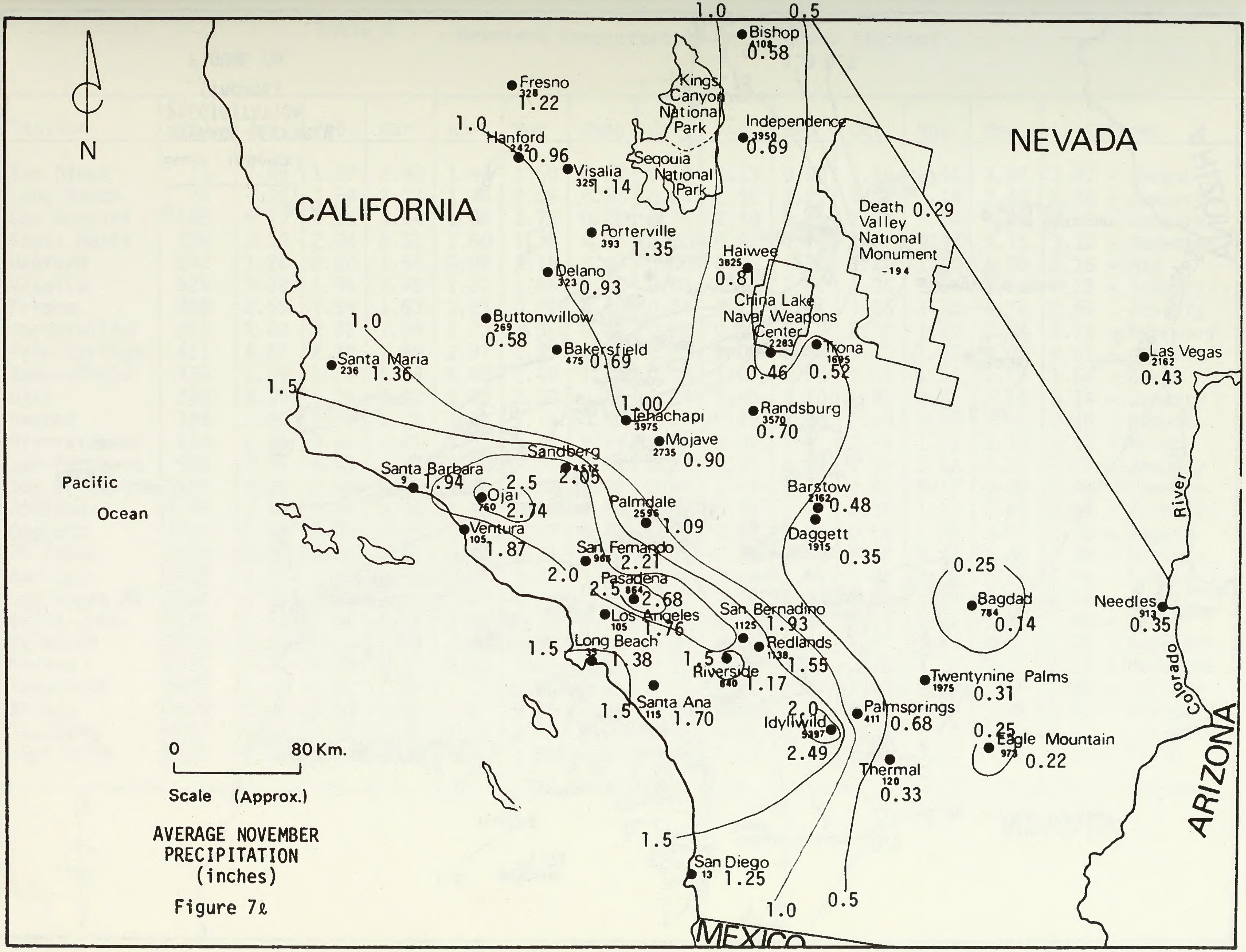

AVERAGE NOVEMBER PRECIPITATION (inches)

Figure 7ℓ

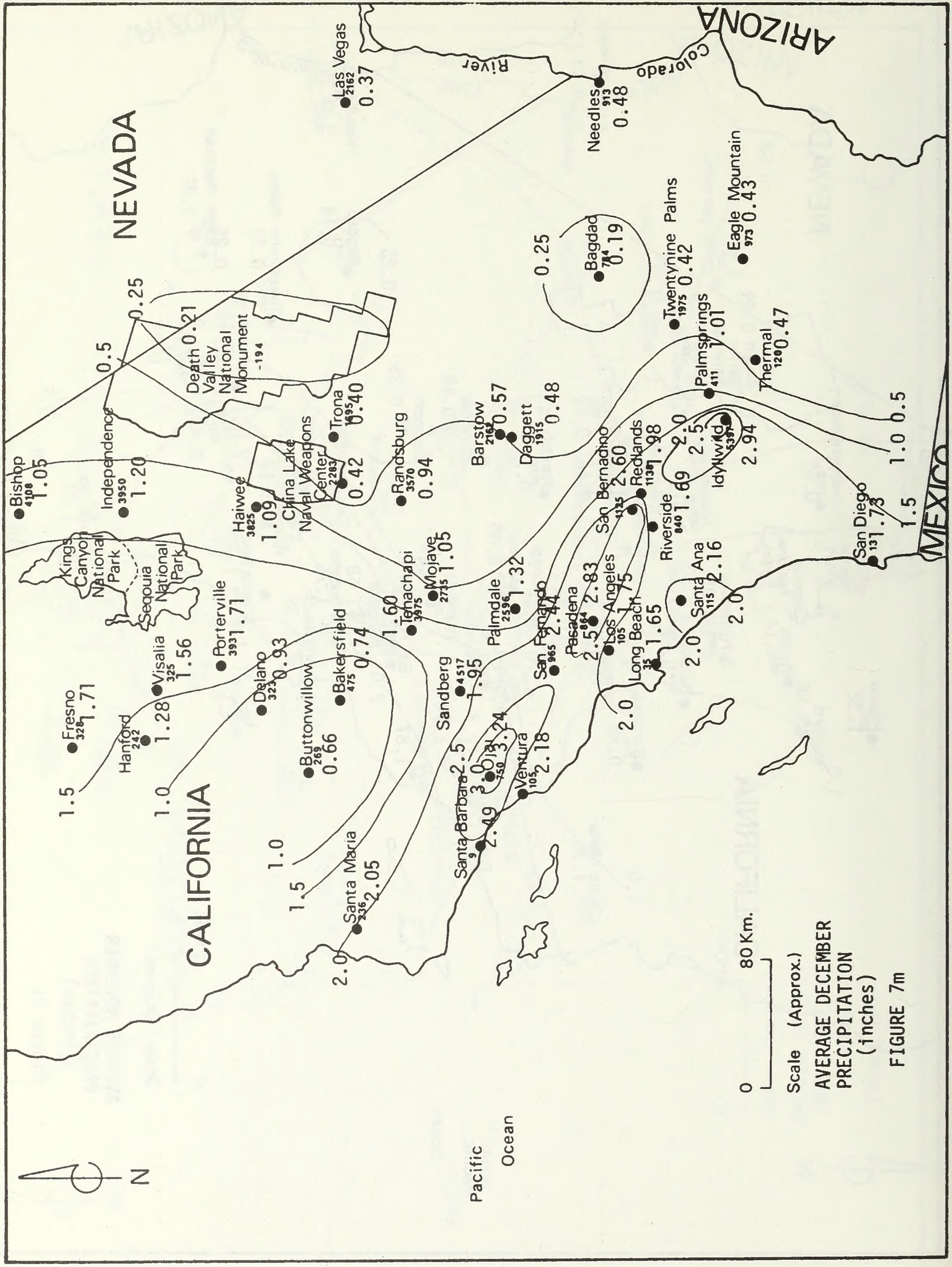

AVERAGE DECEMBER PRECIPITATION (inches)

FIGURE 7m

Table 8 Greatest Precipitation in 24 Hours (inches)

Station	Elev. (ft)	Jan.	Feb.	Mar.	Apr.	May	June	July	Aug.	Sep.	Oct.	Nov.	Dec.	Extreme
San Diego	13	2.65	1.82	2.40	1.40	1.50	0.28	0.10	2.13	0.90	1.20	2.44	3.07	3.07 - December
Long Beach	35	6.86	3.59	2.13	1.49	2.06	0.52	0.04	1.90	1.21	0.70	3.14	3.43	6.86 - January
Los Angeles	105	6.19	4.16	3.54	1.88	1.72	0.29	0.15	2.40	4.20	1.77	5.60	3.01	6.19 - January
Santa Maria	236	2.55	2.34	2.55	1.60	1.35	0.26	0.62	0.85	1.78	2.07	1.93	3.15	3.15 - December
Hanford	242	1.26	2.00	1.55	0.92	2.16	1.00	0.08	0.28	1.22	1.20	1.10	1.10	2.16 - May
Visalia	325	3.22	1.45	2.45	1.37	1.56	0.50	0.03	0.22	1.81	1.30	1.36	1.50	3.22 - January
Fresno	328	2.59	1.99	1.63	1.23	0.96	0.60	0.04	0.25	0.91	1.55	1.35	1.76	2.59 - January
Porterville	393	1.82	2.72	1.04	1.23	1.83	0.24	0.08	0.13	0.69	2.13	1.61	2.34	2.72 - February
Palm Springs	411	4.57	2.30	1.90	1.97	0.55	0.37	2.80	2.03	1.80	2.75	1.62	4.02	4.57 - January
Bakersfield	475	1.09	1.19	1.68	1.00	1.40	1.10	0.30	1.03	0.56	1.51	1.54	1.15	1.68 - March
Ojai	750	8.15	5.70	7.90	3.30	2.00	0.48	0.24	0.60	4.10	1.95	3.85	5.15	8.14 - January
Bagdad	784	1.50	1.20	1.75	1.10	1.75	0.50	1.29	2.20	1.00	2.00	0.80	1.48	2.20 - August
Riverside	840	2.59	3.22	4.41	3.07	1.39	0.24	0.10	2.01	1.71	2.27	1.31	3.28	4.42 - March
San Fernando	965	7.55	4.55	3.03	2.92	2.51	0.68	0.59	0.51	2.29	1.59	3.43	4.31	7.55 - January
San Bernardino	1125	5.29	3.78	4.46	3.85	1.24	1.02	0.42	1.21	1.72	1.68	2.12	3.86	5.28 - January
Redlands	1138	3.44	2.93	3.08	1.98	1.62	0.55	0.57	0.70	1.55	2.78	1.55	2.49	3.44 - January
Daggett	1915	1.03	0.70	0.88	0.65	0.37	0.45	0.96	2.06	1.11	0.66	1.08	1.01	2.06 - August
29 Palms	1975	0.88	0.73	0.80	0.48	0.34	0.11	2.34	2.16	1.43	2.55	0.82	1.08	2.55 - October
Barstow	2162	1.03	1.00	1.50	0.61	0.80	1.93	1.35	2.79	1.50	0.85	2.00	2.07	2.79 - August
Las Vegas,NV	2162	1.01	1.19	1.14	0.97	0.80	0.75	1.32	2.59	1.07	0.70	1.78	0.95	2.59 - August
China Lake	2283	1.26	1.28	1.62	0.88	0.19	0.29	1.35	0.75	1.54	0.58	1.03	1.14	1.62 - March
Palmdale	2596	2.44	2.43	2.39	0.88	0.35	0.15	0.28	1.05	1.02	1.63	1.63	3.43	3.43 - December
Mojave	2735	1.74	2.03	1.74	0.94	0.43	0.54	0.47	0.76	1.31	0.70	1.18	2.81	2.81 - December
Tehachapi	3975	1.78	1.64	1.74	1.77	0.63	0.63	0.30	2.03	2.20	2.84	1.89	1.47	2.84 - October
Bishop	4108	3.32	3.64	1.49	1.47	0.95	0.32	0.86	0.46	0.59	1.05	1.79	3.35	3.64 - February
Sandberg	4517	4.09	4.87	2.97	2.01	2.43	0.49	0.49	1.83	2.68	1.86	6.87	3.74	6.87 - November
Idyllwild	5397	2.94	3.40	4.37	2.35	1.26	0.37	1.12	2.23	1.80	1.40	2.54	3.26	4.37 - March

Table 9. Mean Number of Days with Precipitation ⩾ 0.10 Inches

Station	Elev. (ft)	Annual	Jan.	Feb.	Mar.	Apr.	May	June	July	Aug.	Sep.	Oct.	Nov.	Dec.
Porterville	393	25	4	4	4	3	1	0	0	0	0	1	3	4
Daggett	1915	10	1	1	1	1	0	0	1	1	1	1	1	1
29 Palms	1975	9	1	0	1	0	0	0	1	2	1	1	1	1
Palmdale	2596	17	3	3	3	2	< ½	< ½	< ½	1	< ½	1	1	3
Mojave	2735	12	2	3	2	1	< ½	< ½	< ½	< ½	< ½	1	1	2
Tehachapi	3975	24	5	4	4	2	2	< ½	< ½	< ½	< ½	1	2	4

Table 10. Mean Number of Days with Precipitation ⩾ 0.01 Inches

Station	Elev. (ft)	Annual	Jan.	Feb.	Mar.	Apr.	May	June	July	Aug.	Sep.	Oct.	Nov.	Dec.
San Diego	13	41	6	6	7	5	2	1	< ½	< ½	1	2	5	6
Long Beach	35	30	5	4	4	3	1	< ½	< ½	< ½	1	2	3	5
Los Angeles	105	35	6	6	5	3	1	1	1	< ½	1	2	3	5
Santa Maria	236	45	7	7	7	5	2	1	< ½	< ½	1	2	5	7
Fresno	328	42	8	7	6	5	2	1	< ½	< ½	1	2	5	7
Bakersfield	475	36	5	6	6	4	2	< ½	< ½	< ½	1	2	3	5
Las Vegas	2162	24	3	2	2	2	1	1	3	3	2	2	2	2
China Lake	2283	15	2	2	1	1	1	< 1	1	1	1	1	2	2
Bishop	4108	29	4	3	3	3	3	2	2	2	2	2	2	3
Sandberg	4517	40	6	6	6	4	2	< ½	< ½	1	1	2	4	6

The precipitation data for the CGRA are presented in Table 10a as Daily Comparative Rainfall Data for the Coso Geothermal Resource Area. With only 24 days of data and only 9 days of complete precipitation data, it is difficult to extract conclusions. However, by comparing the number of days the maximum daily rainfall was observed at each station: Cactus Flats - 9 day, Haiwee - 8 days, Coso Basin - 4 days, Airport Lake - 2 days (with one day's maximum equal between Cactus Flats and Haiwee); and by comparing the number of days each station had the maximum daily rainfall, using only the 9 days of complete precipitation data: Cactus Flats - 5 days, Haiwee - 2 days, Coso Basin - 1 day, Airport Lake - 1 day; it appears that a rainfall maximum occurs at Cactus Flats due to its 5,000 foot elevation, and a secondary rainfall maximum occurs at Haiwee due to its 3,825 foot elevation and location near the Sierra Nevada mountains. Also, Coso Basin (3,560 feet) and Airport Lake (2,300 feet) have rainfall minimums because of their low elevations and locations east and south of Cactus Flats and Haiwee. Breaking down rainfall data into monthly statistics (See Table 11) shows the most frequent occurrance of the maximum rainfall days in February, March, and July.

Snowfall

No snowfall data for the CGRA were available for presentation. Therefore, average annual snowfall amounts (inches) were projected for seven station within the CGRA (See Table 13) using an Exponential Curve Fit program. Known average annual snowfall amounts (inches)and elevations(feet) of several southern California desert stations (See Table 12), together with elevations (feet) of the CGRA stations, were used to project snowfall amounts. The projected snowfall amounts for the CGRA are shown in Table 13. The snowfall amounts shown are a function of elevation, with no other factors included.

Relative Humidity

The closest station to the CGRA with relative humidity data was China

Table 10a. Daily Comparative Rainfall Data for the Coso Geothermal Resource Area

Date	Sta.	Amount (inches)	Date	Sta.	Amount (inches)	Date	Sta.	Amount (inches)	Date	Sta.	Amount (inches)	Date	Sta.	Amount (inches)
8/16/77	AL	.09	12/12/77	AL	N/A	2/10/78	AL	.60	3/4/78	AL	.00	4/15/78	AL	.01
	CF	.10		CF	N/A		CF	N/A		CF	1.27		CF	.09
	CB	.00		CB	.09		CB	.00		CB	.03		CB	.13
	H	N/A		H	.41		H	.20		H	.00		H	.08
8/17/77	AL	.88	2/5/78	AL	.07	2/28/278	AL	.75	3/9/78	AL	.01	4/25/78	AL	N/A
	CF	1.69		CF	N/A		CF	.97		CF	.07		CF	.04
	CB	.00		CB	.24		CB	.95		CB	.00		CB	.05
	H	N/A		H	.55		H	.00		H	.00		H	.02
8/18/77	AL	.02	2/7/78	AL	.01	3/1/78	AL	.36	3/21/78	AL	.15	7/24/78	AL	N/A
	CF	.18		CF	N/A		CF	.38		CF	.17		CF	.13
	CB	.00		CB	.00		CB	.00		CB	N/A		CB	.63
	H	N/A		H	.30		H	.00		H	.17		H	N/A
12/22/77	AL	N/A	2/8/78	AL	.51	3/2/78	AL	.05	3/30/78	AL	.21	9/4/78	AL	N/A
	CF	N/A		CF	N/A		CF	.06		CF	.45		CF	.04
	CB	.07		CB	.00		CB	.00		CB	.31		CB	.02
	H	.05		H	.55		H	.00		H	.65		H	.00
2/26/77	AL	N/A	2/9/78	AL	.75	3/3/78	AL	.78	3/31/78	AL	.58			
	CF	N/A		CF	N/A		CF	.06		CF	1.11			
	CB	.28		CB	.00		CB	.02		CB	1.04			
	H	.32		H	.95		H	.00		H	1.24			

AL = Airport Lake
CF = Cactus Flats
CB = Coso Basin
H = Haiwee
N/A = No Data Available

Table 11. Number of Days per Month per Station of Maximum Daily Rainfall

Month	Stations			
	Airport Lake	Cactus Flats	Coso Basin	Haiwee
December			1	2
February	1	1		4
March	1	4		2
April			2	
July			1	
August		3		
September		1		

Table 12. Data Points Used in the Exponential Curve Fit Equation for Projecting Snowfall Amounts in the CGRA

Southern California Desert Stations	Actual Elev. (feet)	Reduced Elev. (x) (feet)	Average Annual (y) Snowfall (inches)
Tehachapi	3975	2060	29.5
Sandberg	4517	2602	28.5
Bishop	4108	2193	8.6
Palmdale	2596	681	2.9
Mojave	2735	820	1.9
Las Vegas	2162	247	1.4
Twentynine Palms	1975	60	1.1
Daggett	1915	0	0.9
China Lake	2283	368	Trace (0.1)

The exponential curve fit program used the equation: $\ln y = \ln a + bx$, where (x) equals the station elevation in feet and (y) equals the average annual snowfall in inches. The station elevations are reduced so that the lowest station elevation equals zero, and the data points better fit the curve. The program computations were as follows:

$$a = 0.57, \ b = 1.51 \times 10^{-3}$$

$$\ln y = \ln(0.57) + 1.51 \times 10^{-3}(x)$$

$$y = 0.57e \ 1.51 \times 10^{-3}(x)$$

Correlation coefficient (r) = 0.84

Table 13. Projected Average Annual Snowfall Amounts for the CGRA

CGRA Station	Actual Elevation (feet)	Reduced (used in program as x) Elevation (feet)*	Projected Average Annual (used in program as y) Snowfall Amounts (inches)
Airport Lake	2300	385	1.02
Little Lake	3180	1265	3.87
Rose Valley Ranch	3435	1520	5.69
Coso Basin	3560	1645	6.88
Red Hill	3600	1685	7.31
Haiwee	3825	1910	10.22
Cactus Flats	5000	3085	60.79**(15.20)

*Used Daggett's elevation of 1915 feet as a base elevation of zero feet.

**Cactus Flats snowfall amount over-projected by approximately 400% because the actual elevation of Cactus Flats is higher than any station elevation used as a data point in the exponential curve fit program.

Table 14. Mean Monthly Relative Humidity-China Lake (1946-1976)

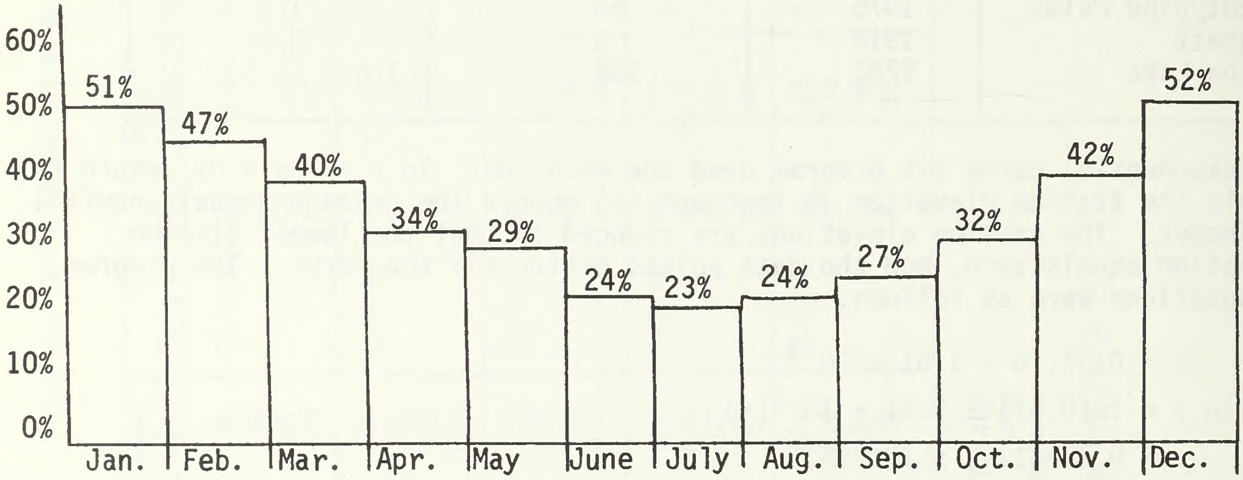

Lake. Table 14 shows the Mean Monthly Relative Humidity for China Lake for the period 1946-1976. Maximum and minimum mean relative humidities occur during the winter and summer months respectively.

Cloudiness

The Mean Number of Days Clear, Partly Cloudy, Cloudy (Sunrise to Sunset) for China Lake, Bishop, and Las Vegas, NV., are presented in Table 15. China Lake, the closest station to the CGRA, has an average of 74 days (20.3%) per year of cloudiness. All three stations have a maximum number of cloudy days per month during the winter season and a maximum number of clear days per month during the summer and early fall season.

Evaporation

The Mean Annual Lake Evaporation (inches) presented in Figure 8 was taken from the U.S. Department of Commerce Climatic Atlas. The CGRA appears to have a mean annual lake evaporation of approximately 54 to 78 inches per year.

Table 15. Mean Number of Days Clear, Partly Cloudy, Cloudy (Sunrise to Sunset)

Month	Las Vegas (2162 ft)			China Lake (2283 ft)			Bishop (4108 ft)		
	Clear	Partly Cloudy	Cloudy	Clear	Partly Cloudy	Cloudy	Clear	Partly Cloudy	Cloudy
January	14	7	10	12	8	11	15	11	5
February	13	7	8	12	7	9	14	10	4
March	14	9	8	13	9	9	15	12	4
April	17	7	6	14	9	7	16	11	3
May	19	7	5	14	11	6	20	9	2
June	22	5	3	20	7	3	25	4	1
July	19	9	3	21	7	3	24	6	1
August	22	7	2	23	6	2	26	4	1
September	23	5	2	24	4	2	25	4	1
October	21	6	4	20	6	5	22	8	1
November	16	7	7	15	8	7	19	9	2
December	15	7	9	14	7	10	16	11	4
Annual	215	83	67	202	89	74	237	99	29
Years of Record	(1949-1977)			(1953-1977)			(1946-1976)		

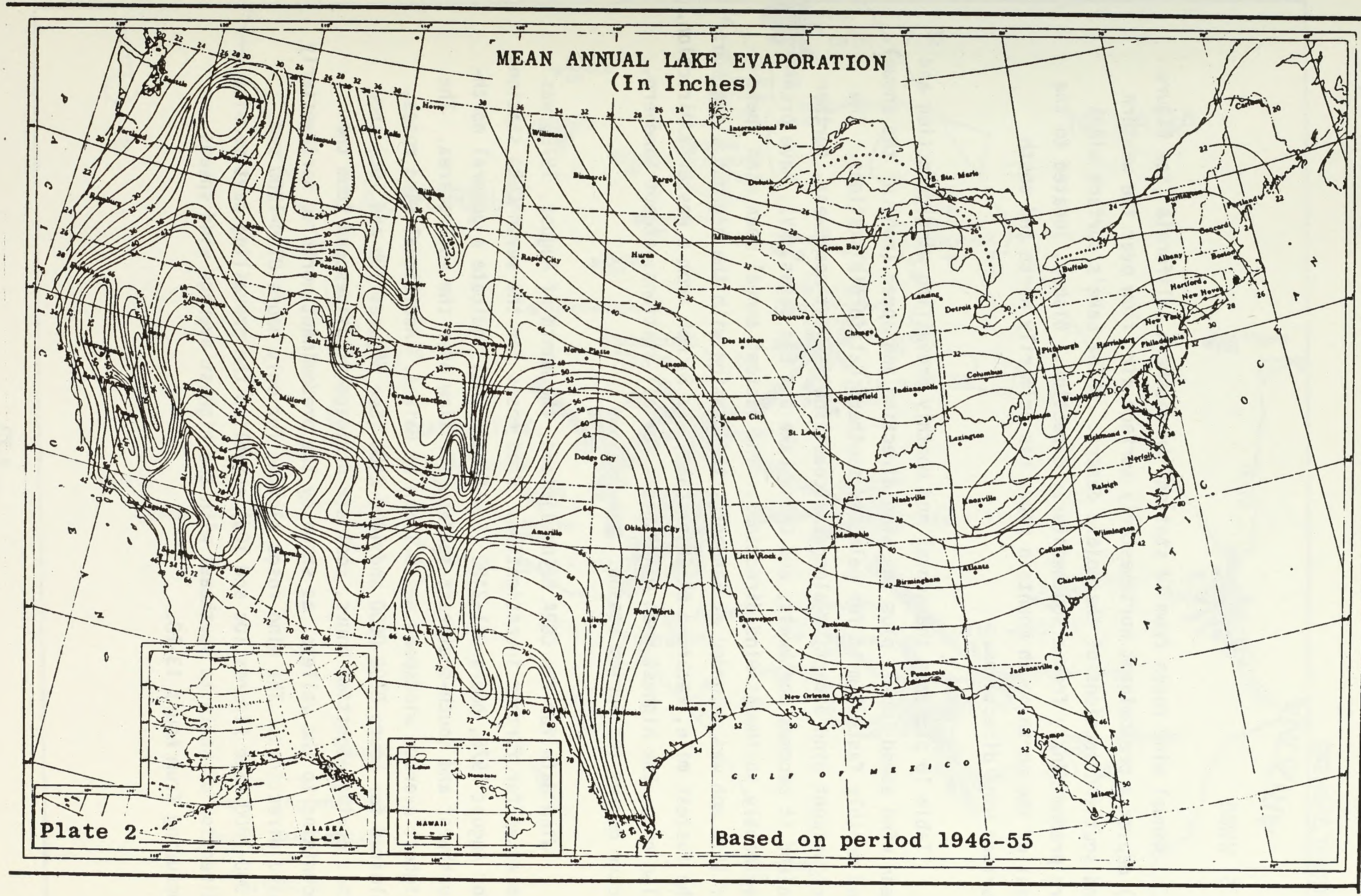

Figure 8. Lake Evaporation

9.5 WINDS

Annual wind roses from 10 stations in southern California (See Figure 9) depict a predominant northwesterly surface air flow over the western and southern sections of the Mojave desert. China Lake's surface winds are predominantly from a southwesterly direction. Bishop, located to the east of the north-south mountain rage, has primarily north and south surface wind directions.

Table 16 presents the annual and monthly prevailing wind direction and mean wind speed (mph), plus the wind direction and speed (mph) of the annual and monthly fastest mile for selected southern California stations. The predominent wind direction along the coastline is west-northwest, further inland it becomes northwest, and China Lake and Las Vegas, NV., have predominantly southwest wind directions. The fastest annual mean wind speed of 15.3 mph was recorded at Sandberg, the station with the highest elevation. The fastest mile, recorded at China Lake, was 81 mph from a westerly direction. Also note, the highest mean wind speeds for all stations, except Sandberg, occur during the Spring season.

Wind data for the CGRA being limited, the month of August, 1978, was selected for further investigation. Wind roses for the seven CGRA stations for August 1978, hours 011-2400 (See Figure 10a) indicate a general north-northwest and south-southeast surface air flow over the entire area. The highest average windspeed was 8.1 mph at Haiwee. Additional wind roses, plotted for hours 0100-0600 and 1900-2400 (See Figures 10b and 10c) show that during nighttime hours, cool air drainage winds descend from the mountains to the valleys, as shown by the predominant north to northwesterly wind directions. The wind roses plotted for only hours 0700-1200 and 1300-1800 (See Figures 10c and 10d) establish the prevailing daytime wind direction of south to southeast with the highest average wind speeds occuring from hours 13-18.

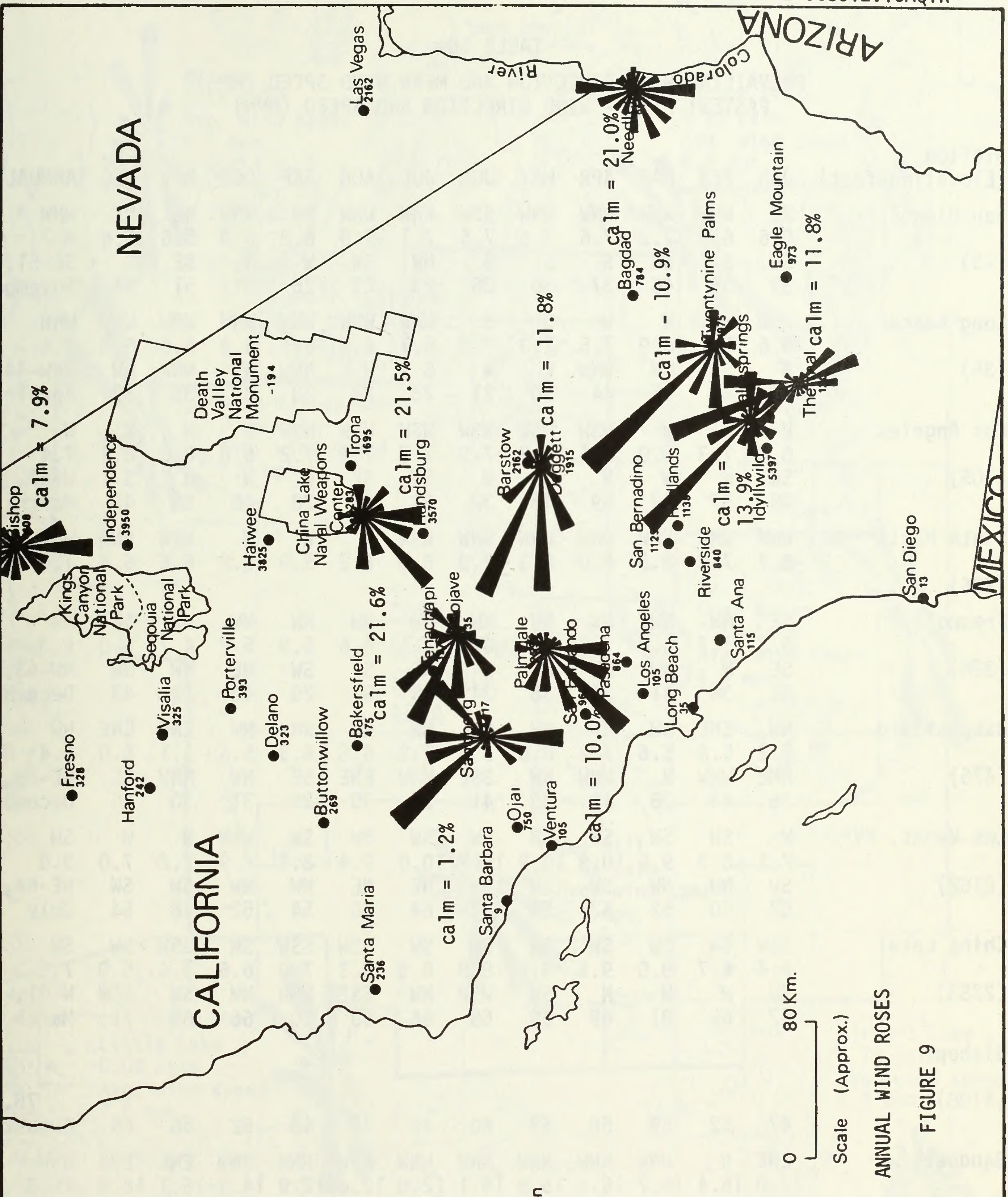

ANNUAL WIND ROSES

FIGURE 9

TABLE 16

PREVAILING WIND DIRECTION AND MEAN WIND SPEED (MPH)
FASTEST MILE - WIND DIRECTION AND SPEED (MPH)

STATION (Elevation-feet)	JAN	FEB	MAR	APR	MAY	JUN	JUL	AUG	SEP	OCT	NOV	DEC	ANNUAL
San Diego	NE	WNW	WNW	WNW	WNW	SSW	WNW	WNW	NW	WNW	NE	NE	WNW
	5.6	6.3	7.2	7.6	7.6	7.5	7.1	7.0	6.8	6.3	5.6	5.4	6.7
(13)	SW	S	SW	S	S	S	NW	SW	W	N	SE	S	SE-51,
	39	35	46	37	30	26	23	23	25	31	51	34	November
Long Beach	WNW	W	W	W	S	S	WNW	WNW	WNW	WNW	WNW	WNW	WNW
	5.6	6.1	6.9	7.5	7.3	7.0	6.7	6.5	6.1	5.8	5.6	5.3	6.4
(35)	S	S	NW	WNW	W	W	S	W	NNW	NW	NNW	NW	WNW-44,
	37	40	35	44	30	21	23	23	23	37	35	39	April
Los Angeles	W	W	W	WSW	WSW	WSW	WSW	WSW	WSW	W	W	W	W
	6.6	7.3	8.0	8.4	8.2	7.9	7.7	7.6	7.2	6.8	6.5	6.4	7.4
(105)	SW	N	W	N	N	W	SW	SE	W	W	N	S	W-62,
	48	57	62	59	45	32	31	33	28	46	55	49	March
Santa Maria**	WNW	WNW	WNW	WNW	WNW	WNW	WNW	W	W	W	WNW	WNW	WNW
	6.7	7.2	8.3	8.0	8.3	7.9	6.5	6.2	5.9	6.2	6.6	6.4	7.0
(236)													
Fresno	SE	NW	NW	NW	NW	NW	NW	NW	NW	NW	NW	SE	NW
	5.3	5.7	6.8	7.2	7.9	8.1	7.1	6.6	5.9	5.2	4.7	5.0	6.3
(328)	SE	W	NW	NW	N	W	NE	S	SW	NE	NW	NW	NW-43,
	32	38	41	36	38	34	25	31	29	40	29	43	December
Bakersfield	NW	ENE	NW	NW	NW	NW	NW	NW	WNW	NW	ENE	ENE	NW
	5.2	5.8	6.6	7.2	8.0	8.0	7.2	6.8	6.3	5.6	5.1	5.0	6.4
(475)	NNE	WNW	N	WNW	NW	SSE	WNW	ENE	SE	NW	NNW	SE	SE-46,
	35	44	38	40	38	41	25	30	35	31	30	46	December
Las Vegas, NV	W	SW	SW	SW	SW	SW	SW	SW	SW	WSW	W	W	SW
	7.1	8.3	9.9	10.9	10.9	10.7	10.0	9.4	8.7	7.9	7.2	7.0	9.0
(2162)	SW	NW	NW	SW	SW	SW	NE	NE	NW	NW	SW	SW	NE-64,
	52	60	52	52	54	52	64	55	54	52	46	54	July
China Lake	SSW	SW	SW	SW	SW	SW	SW	SSW	SSW	SW	SSW	SW	SW
	5.4	6.7	9.0	9.5	9.6	8.8	8.5	8.3	7.0	6.6	5.4	5.0	7.5
(2283)	SW	W	W	N	SW	WSW	NW	ESE	WSW	NW	SW	SSW	W-81,
	77	69	81	69	66	68	66	53	60	66	65	71	March
Bishop*													
(4108)													75,
	47	52	59	58	53	60	46	75	48	52	56	66	August
Sandberg	ENE	N	NNW	NNW	NNW	NNW	NNW	NNW	NNW	NNW	ENE	ENE	NNW
	17.0	16.4	16.7	16.4	15.9	15.1	12.8	12.6	12.9	14.9	16.1	16.4	15.3
(4517)	SSW	NW	NNW	N	NNW	NNW	NNW	NNW	N	NNW	NNW	NNW	NW-77,
	64	77	74	64	59	64	46	40	45	53	62	53	February

* Only fastest wind speed data available.
** Only prevailing wind direction and mean wind speed data available.

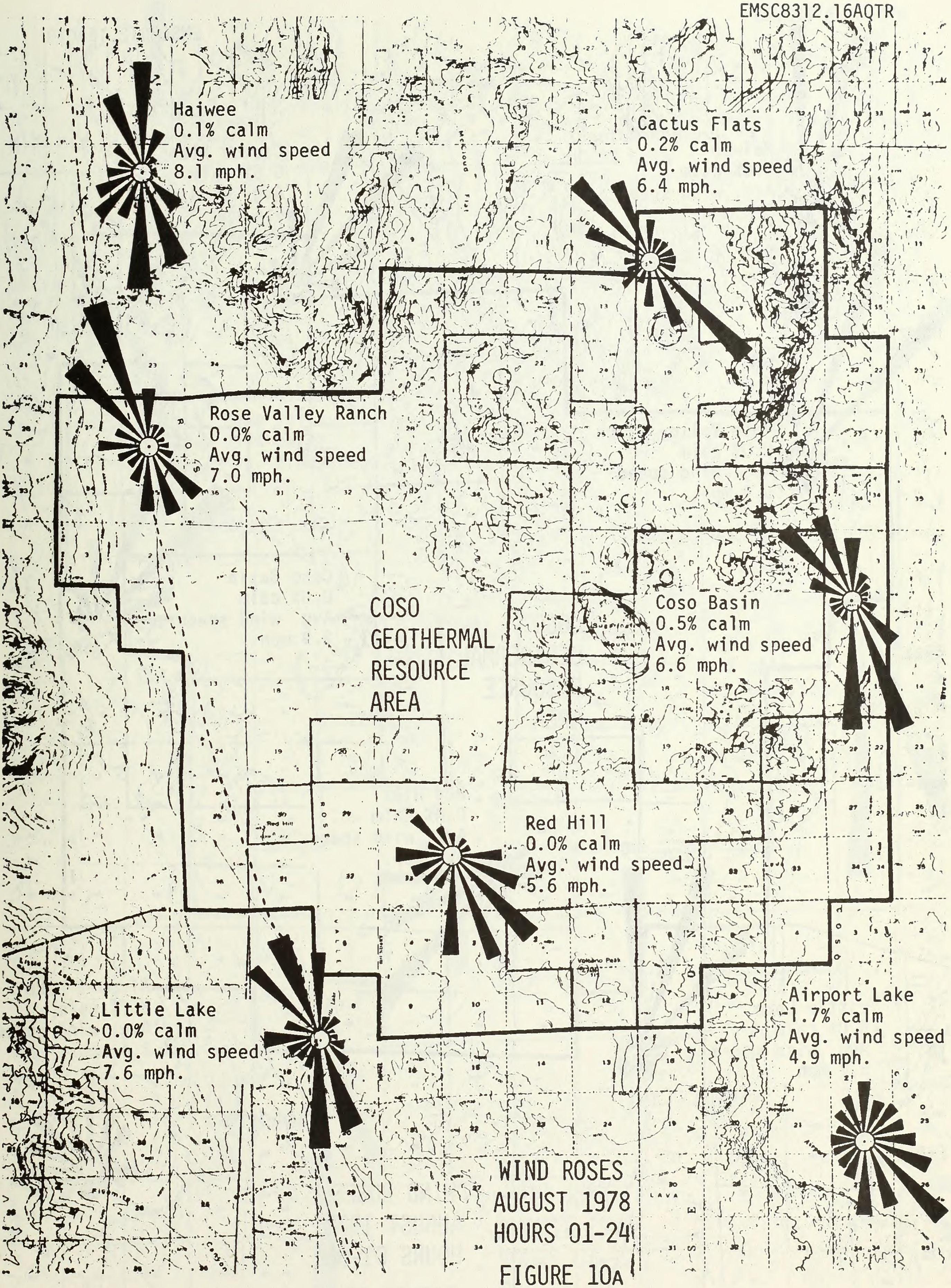

WIND ROSES
AUGUST 1978
HOURS 01-24

FIGURE 10A

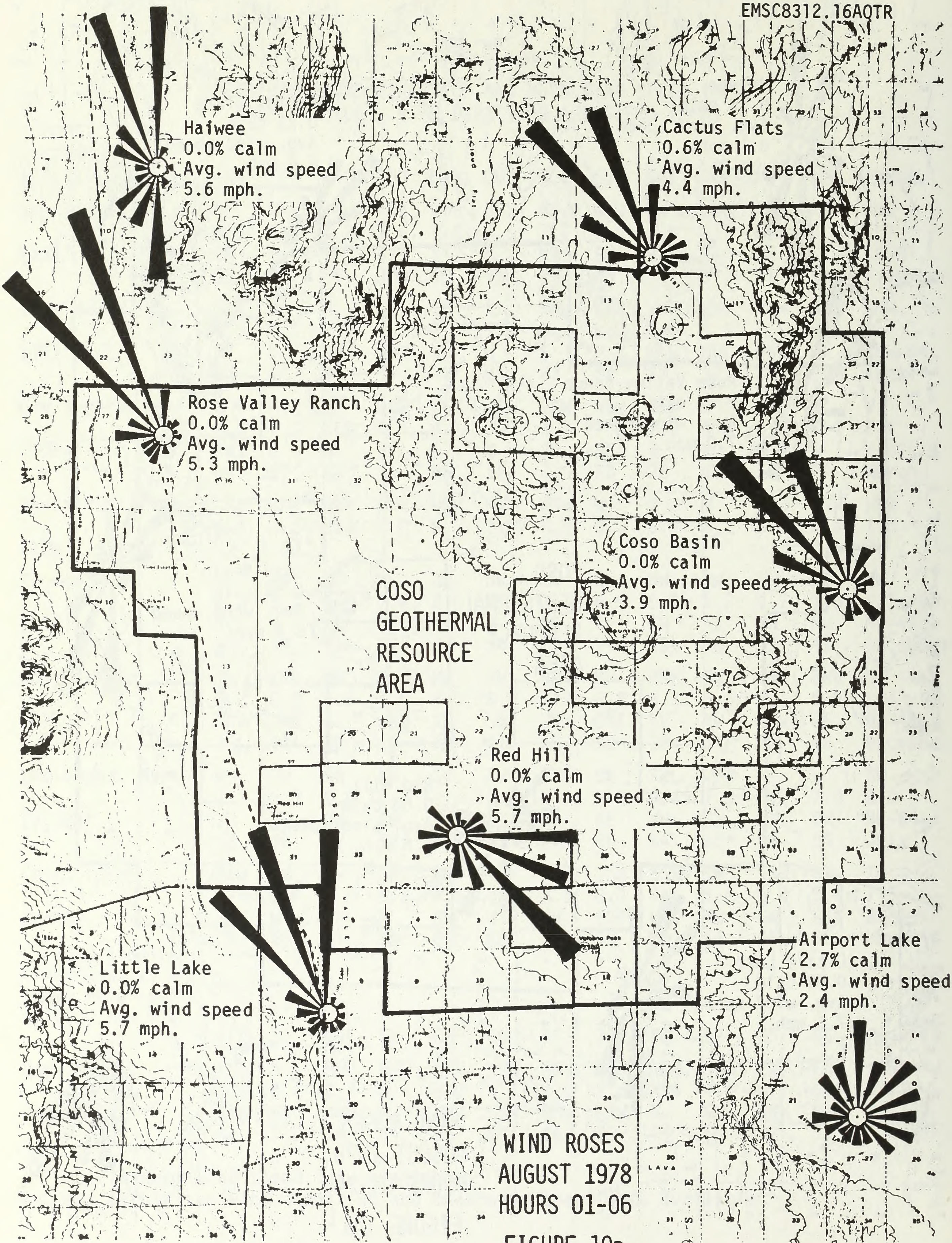

WIND ROSES
AUGUST 1978
HOURS 01-06

FIGURE 10B

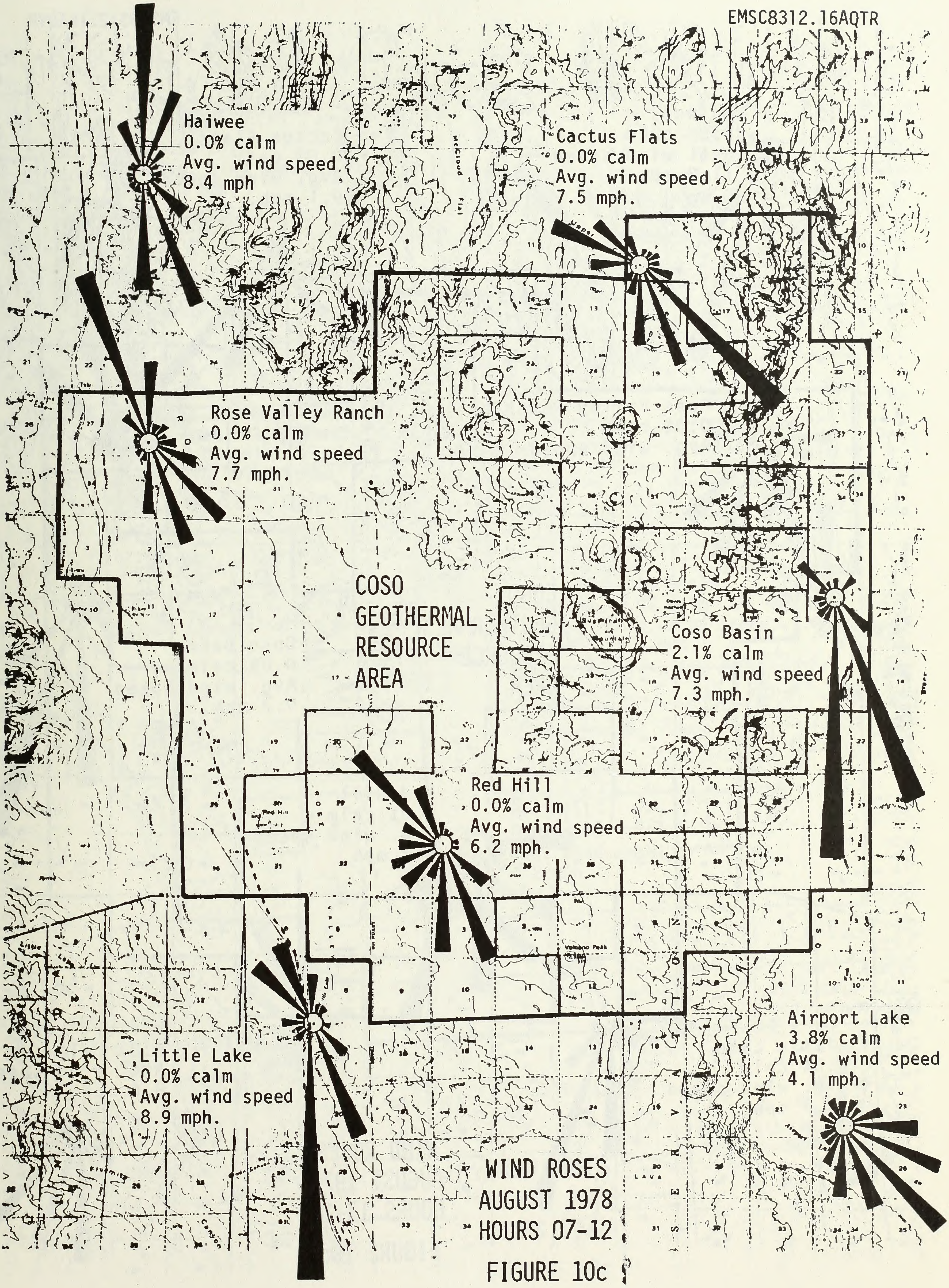

WIND ROSES
AUGUST 1978
HOURS 07-12

FIGURE 10c

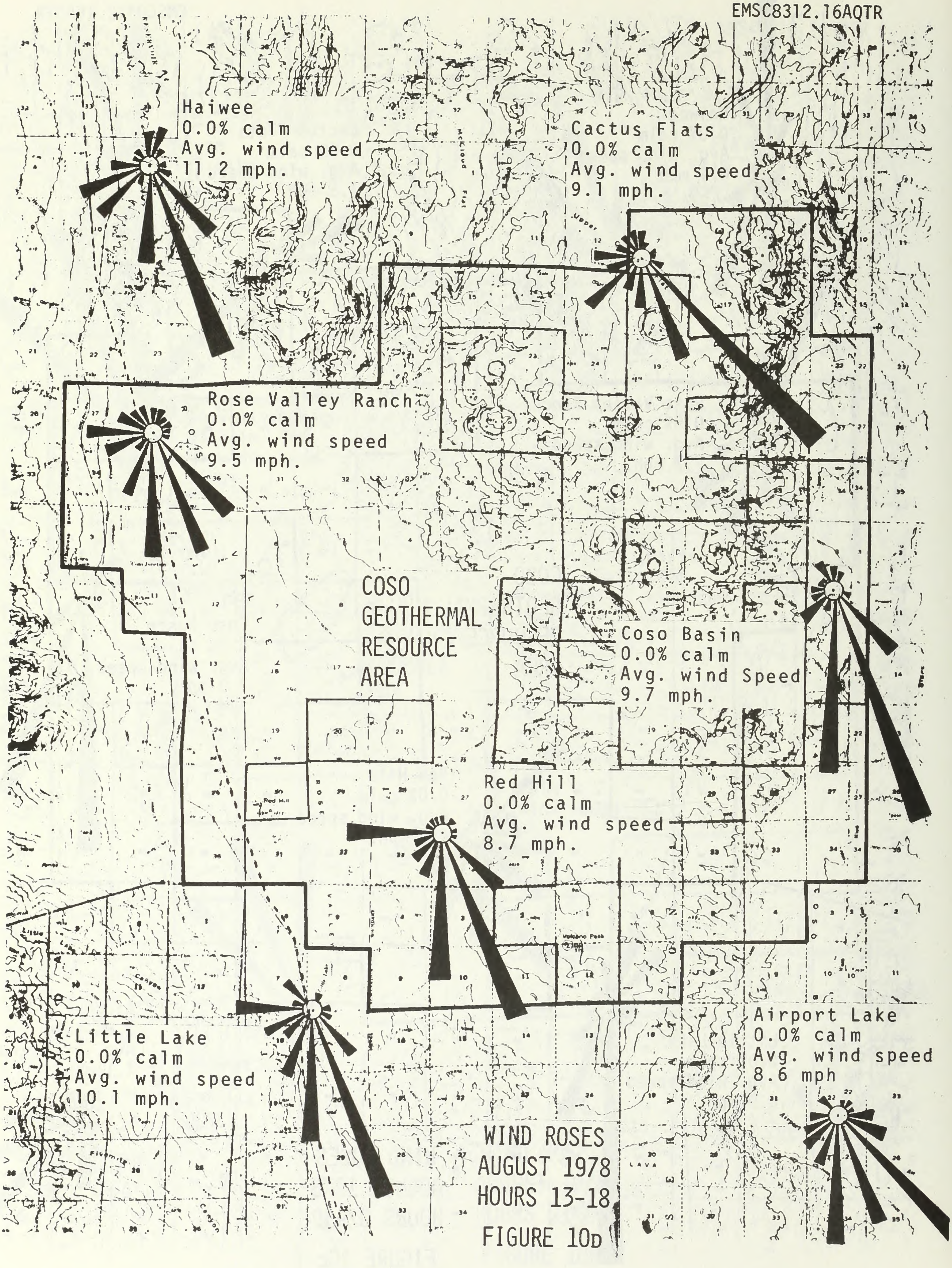

Haiwee
0.0% calm
Avg. wind speed
11.2 mph.

Cactus Flats
0.0% calm
Avg. wind speed
9.1 mph.

Rose Valley Ranch
0.0% calm
Avg. wind speed
9.5 mph.

Coso Basin
0.0% calm
Avg. wind Speed
9.7 mph.

Red Hill
0.0% calm
Avg. wind speed
8.7 mph.

Little Lake
0.0% calm
Avg. wind speed
10.1 mph.

Airport Lake
0.0% calm
Avg. wind speed
8.6 mph

WIND ROSES
AUGUST 1978
HOURS 13-18

FIGURE 10D

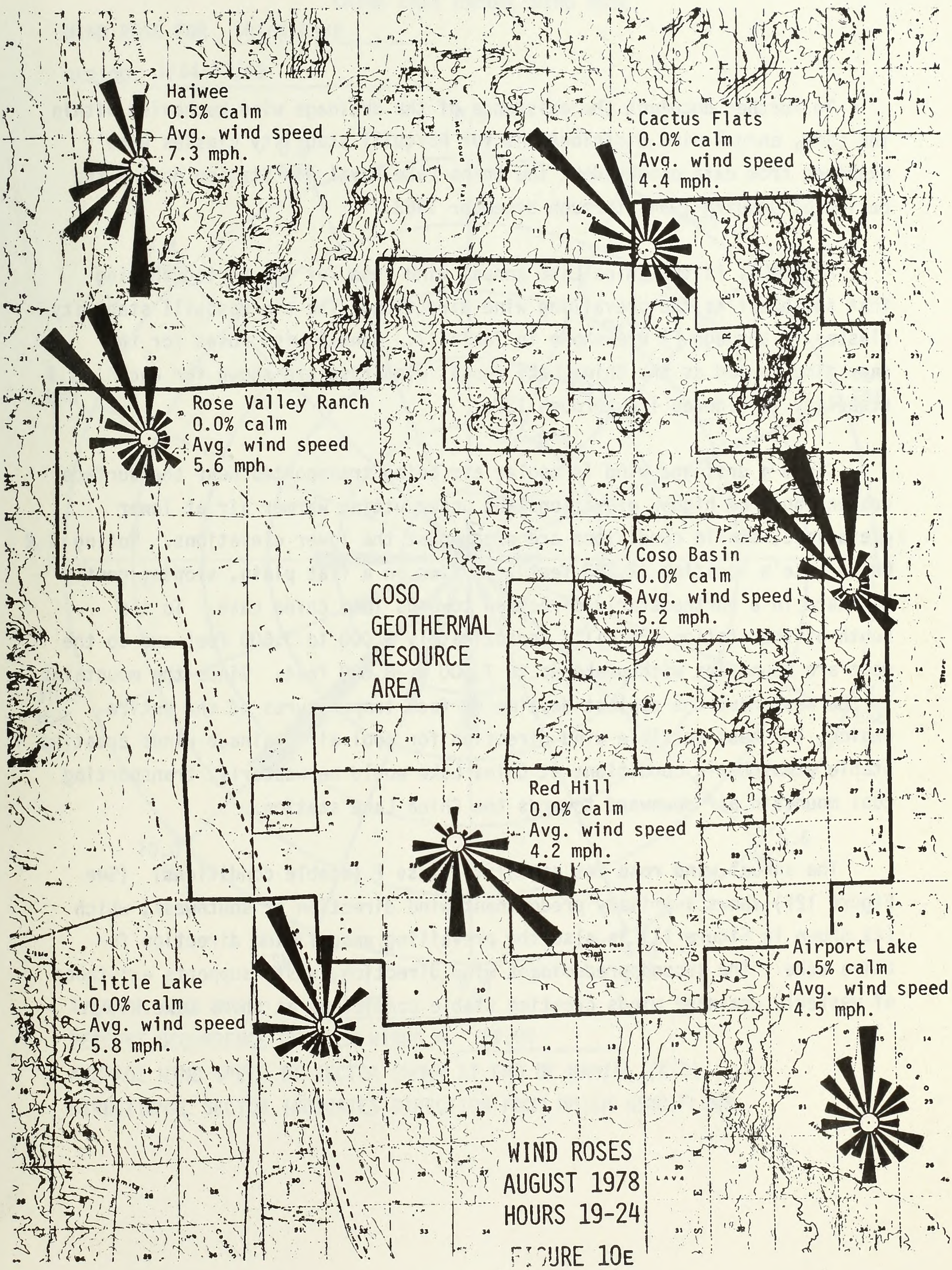

WIND ROSES
AUGUST 1978
HOURS 19-24

FIGURE 10E

To further document the existence of the drainage wind mechanism within the CGRA, annual wind distributions for Pasquill stability classes were examined from data observed at the China Lake Naval Air Station during the period of January 1954, through December 1963.

Figure 11 is the China Lake annual wind rose for the period showing that southwest is the prevailing wind direction. The six Pasquill stability classes (A through F) are shown in Table 17. Annual wind roses for the same time period as the China Lake annual wind rose are shown for each stability in Figures 12a through 12f.

Since a drainage wind is cooler air being transported near the surface descending from higher elevations and undercutting warmer air at lower elevations, stable conditions are created at the lower elevations. Noting China Lake's location (2,283 feet), it lies on a flat plain, sloping gently downward in a northeasterly direction towards lake China Lake. To the south of the station are hills approximately 3,000 to 3,500 feet and to the west are mountains with peaks up to 7,000 or 8,000 feet. Since the mountains to the west have the coolest daytime surface temperatures of the entire region, the best possible wind direction for cool air drainage winds creating stable atmospheric conditions at China Lake would be westerly, transporting cool mountain air downward towards the China Lake station.

The annual wind rose for stability class F (stable conditions) (See Figure 12f) shows a primary predominant wind direction of southwest, which (as shown in Figure 11) is also the prevailing annual wind direction for China Lake. The second predominant wind direction, west, supports existence of westerly drainage winds creating stable conditions at China Lake.

FIGURE 11

CHINA LAKE ANNUAL WIND ROSE

WIND ROSE FOR China Lake

PERIOD 1/54-12/63

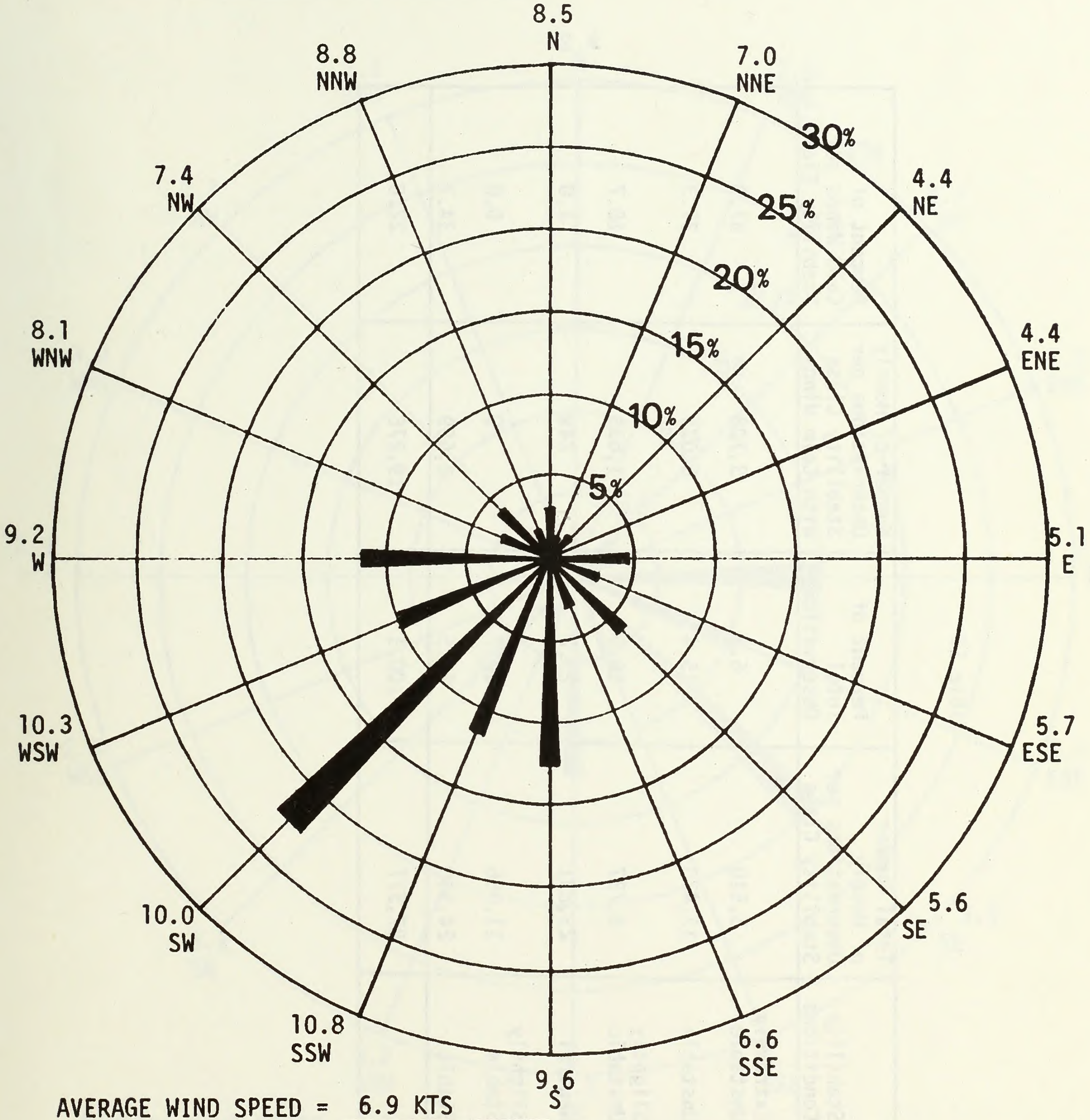

AVERAGE WIND SPEED = 6.9 KTS

PERCENT OCCURRENCE OF CALM WINDS = 22.0%

AVERAGE WIND SPEED BY SECTOR SHOWN AT END OF RADIAL (KTS)

DIRECTIONAL SECTOR INDICATES DIRECTION FROM WHICH WIND FLOWS

Table 17

Pasquill's Stability Classes	Stability Conditions	Total Number of Hourly Observations per Stability Class	Percent of Total Observations	Number of Hourly Observations per Stability Class with Calm Winds	Percent of Calm Winds per Stability Class
A	Extremely Unstable	5,510	6.3	3,708	67.3
B	Unstable	13,473	15.4	5,025	37.3
C	Slightly Unstable	8,737	10.0	1,635	18.7
D	Neutral	23,831	27.2	249	1.0
E	Slightly Stable	11,086	12.7	0	0.0
F	Stable	24,940	28.5	8,659	34.7
TOTALS		87,577	100.1	19,276	22.0

FIGURE 12a
ANNUAL WIND ROSE
STABILITY CLASS A

WIND ROSE FOR China Lake

PERIOD 1/54 - 12/63

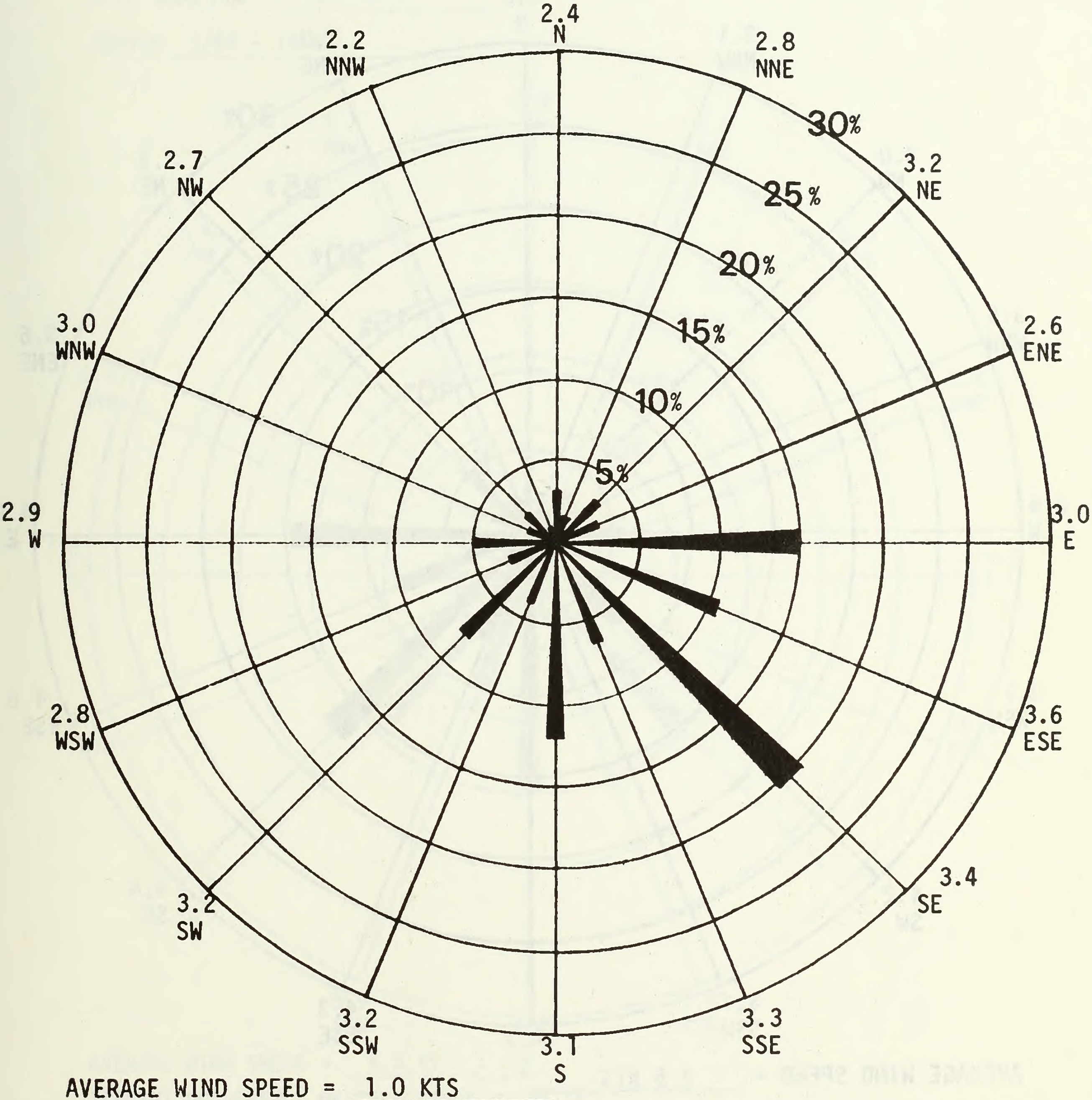

AVERAGE WIND SPEED = 1.0 KTS

PERCENT OCCURRENCE OF CALM WINDS = 67.3%

AVERAGE WIND SPEED BY SECTOR SHOWN AT END OF RADIAL (KTS)

DIRECTIONAL SECTOR INDICATES DIRECTION FROM WHICH WIND FLOWS

FIGURE 12b
ANNUAL WIND ROSE
STABILITY CLASS B

WIND ROSE FOR China Lake

PERIOD 1/54 - 12/63

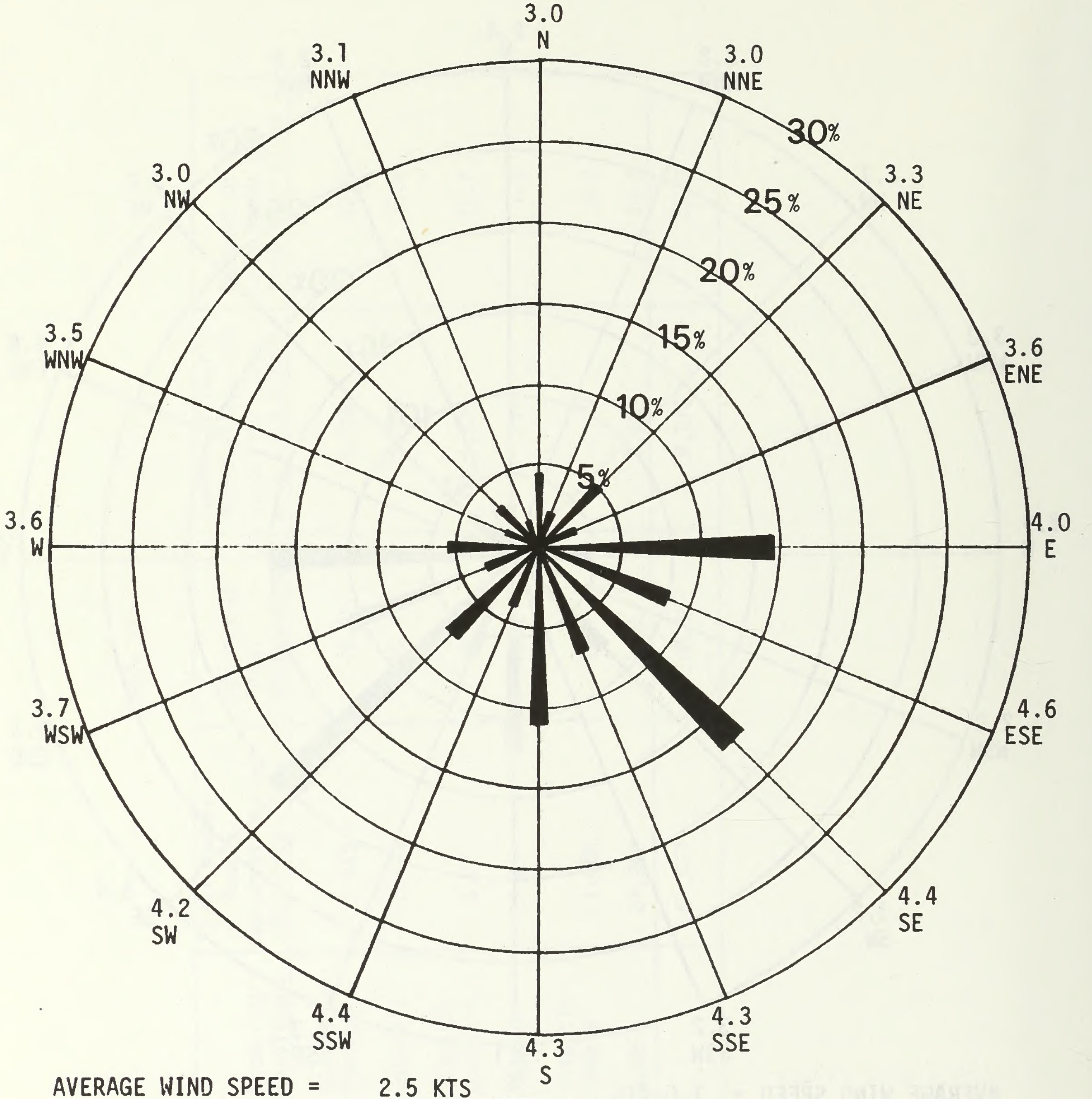

AVERAGE WIND SPEED = 2.5 KTS

PERCENT OCCURRENCE OF CALM WINDS = 37.3%

AVERAGE WIND SPEED BY SECTOR SHOWN AT END OF RADIAL (KTS)

DIRECTIONAL SECTOR INDICATES DIRECTION FROM WHICH WIND FLOWS

FIGURE 12c
ANNUAL WIND ROSE
STABILITY CLASS C

WIND ROSE FOR China Lake

PERIOD 1/54 - 12/63

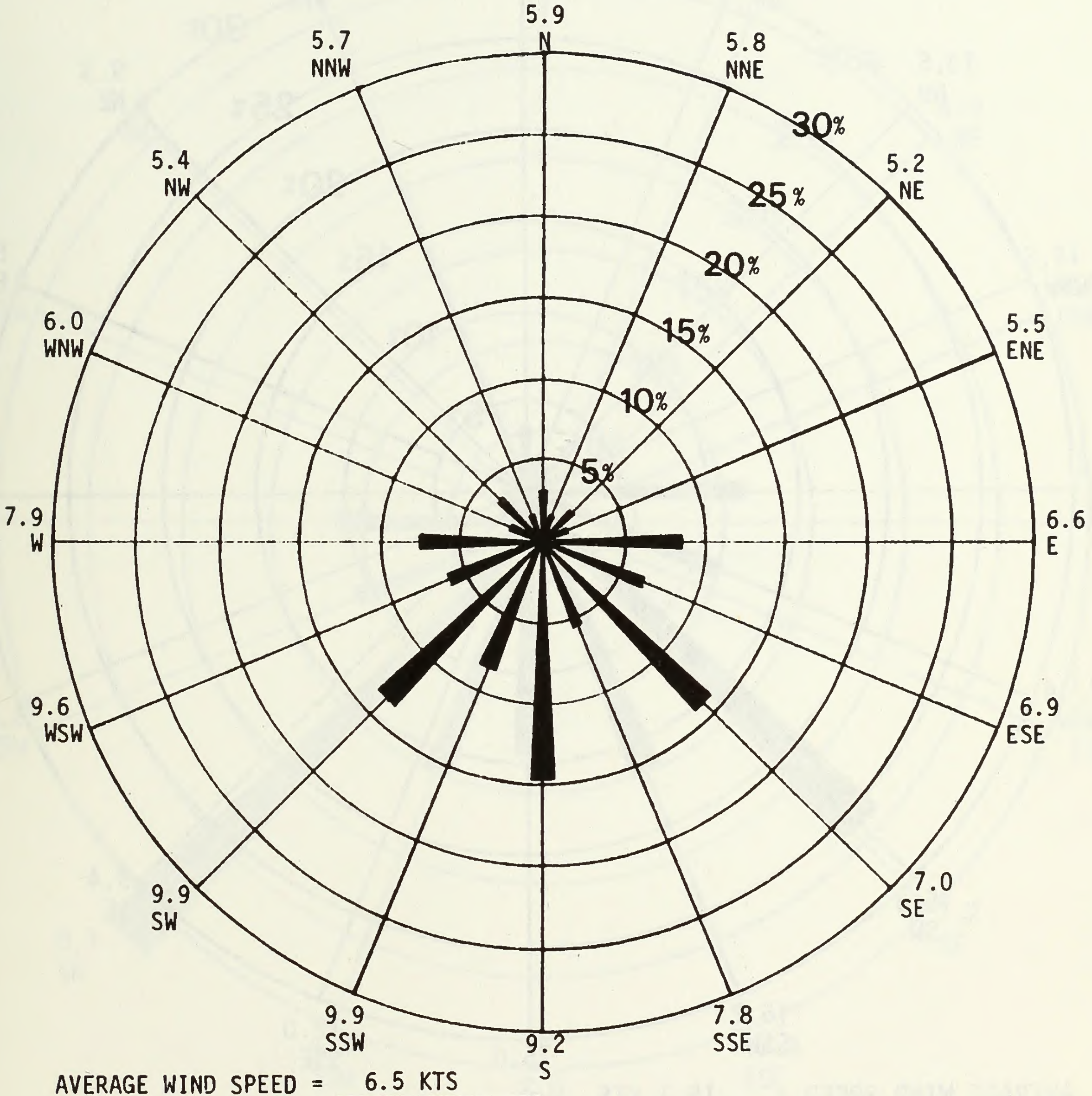

AVERAGE WIND SPEED = 6.5 KTS

PERCENT OCCURRENCE OF CALM WINDS = 18.7%

AVERAGE WIND SPEED BY SECTOR SHOWN AT END OF RADIAL (KTS)

DIRECTIONAL SECTOR INDICATES DIRECTION FROM WHICH WIND FLOWS

FIGURE 12d
ANNUAL WIND ROSE
STABILITY CLASS D

WIND ROSE FOR China Lake

PERIOD 1/54 - 12/63

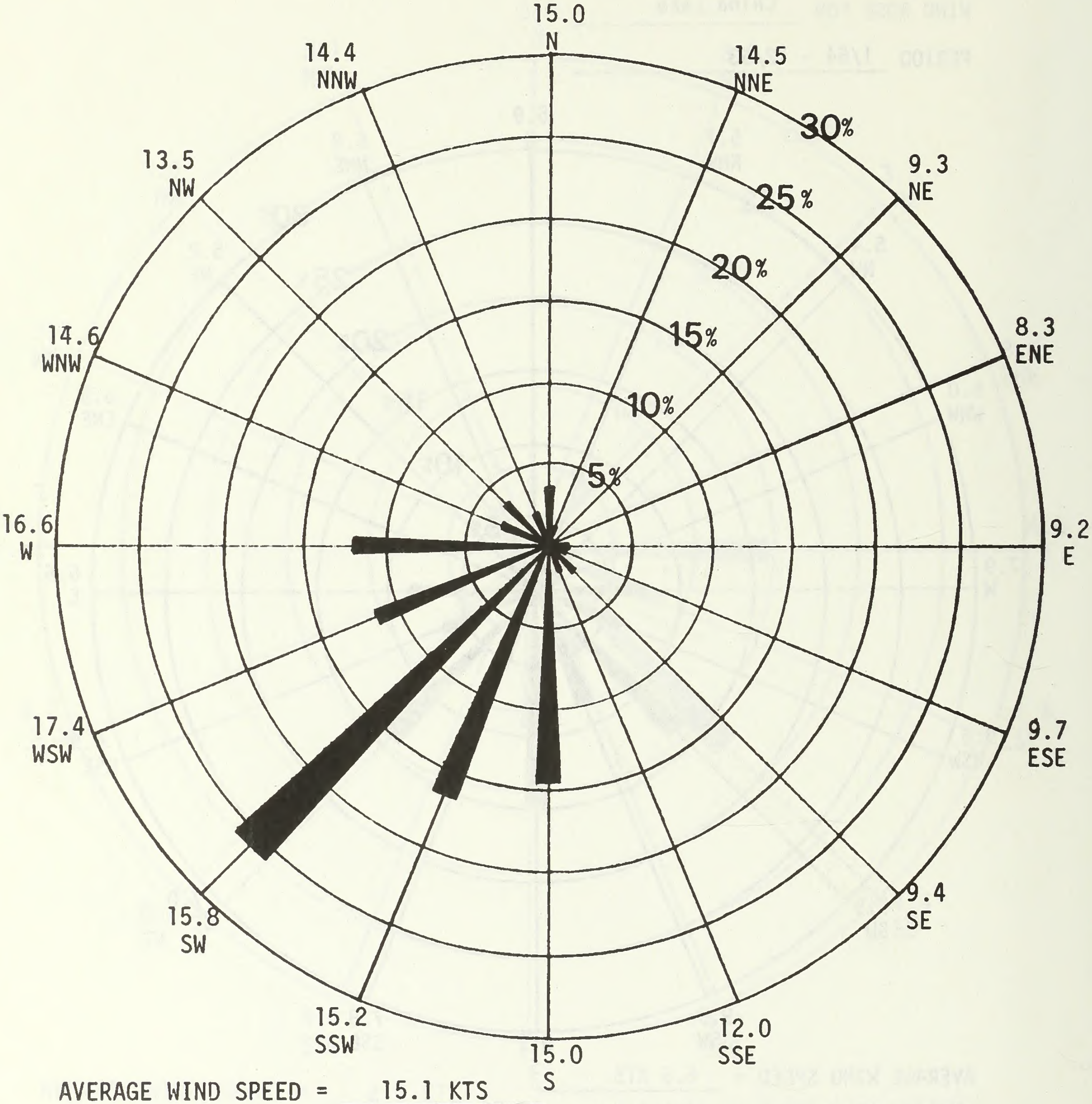

AVERAGE WIND SPEED = 15.1 KTS

PERCENT OCCURRENCE OF CALM WINDS = 1.0%

AVERAGE WIND SPEED BY SECTOR SHOWN AT END OF RADIAL (KTS)

DIRECTIONAL SECTOR INDICATES DIRECTION FROM WHICH WIND FLOWS

FIGURE 12e
ANNUAL WIND ROSE
STABILITY CLASS E

WIND ROSE FOR China Lake

PERIOD 1/54 - 12/63

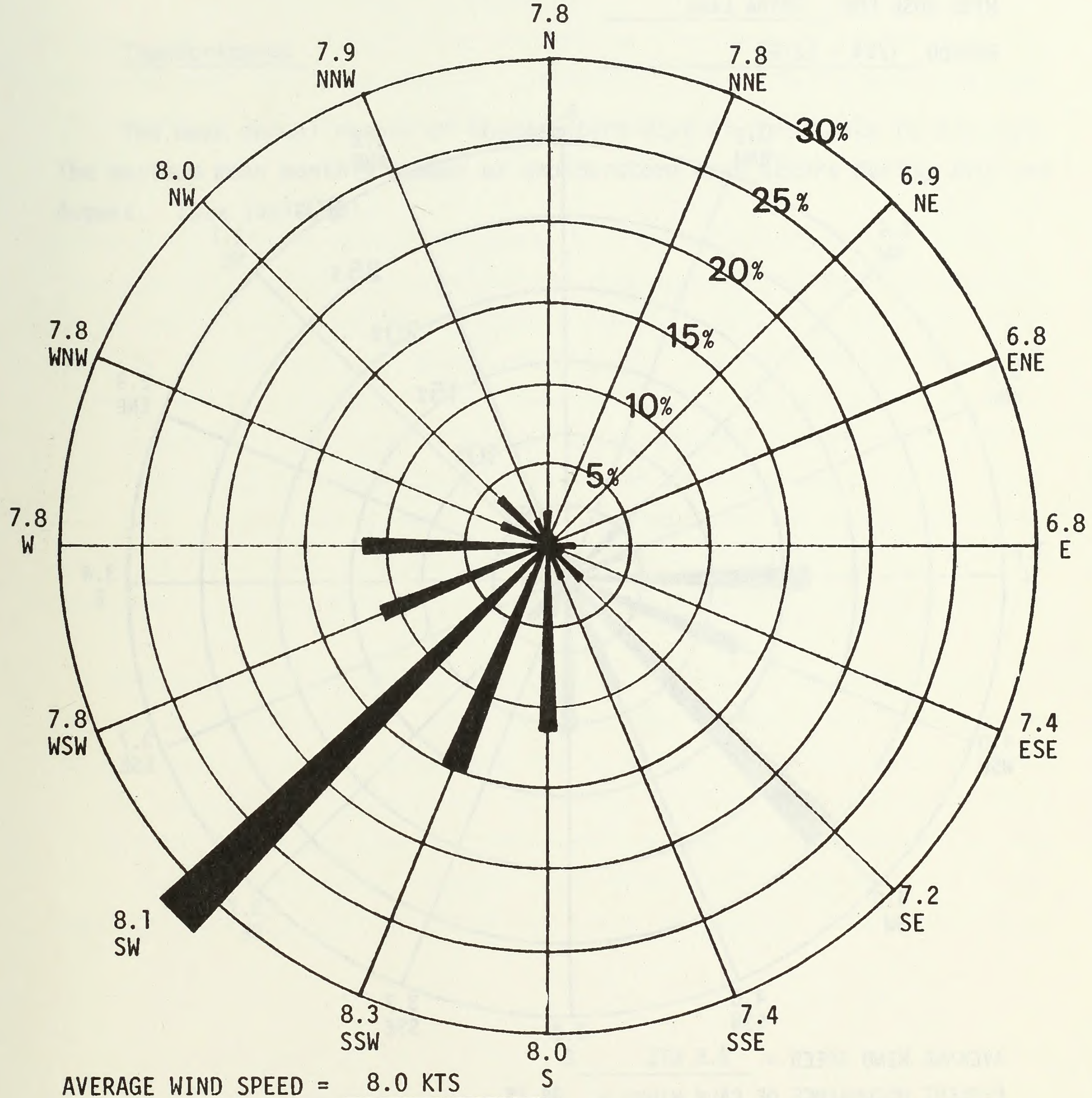

AVERAGE WIND SPEED = 8.0 KTS

PERCENT OCCURRENCE OF CALM WINDS = 0.0%

AVERAGE WIND SPEED BY SECTOR SHOWN AT END OF RADIAL (KTS)

DIRECTIONAL SECTOR INDICATES DIRECTION FROM WHICH WIND FLOWS

FIGURE 12f
ANNUAL WIND ROSE
STABILITY CLASS F

WIND ROSE FOR China Lake

PERIOD 1/54 - 12/63

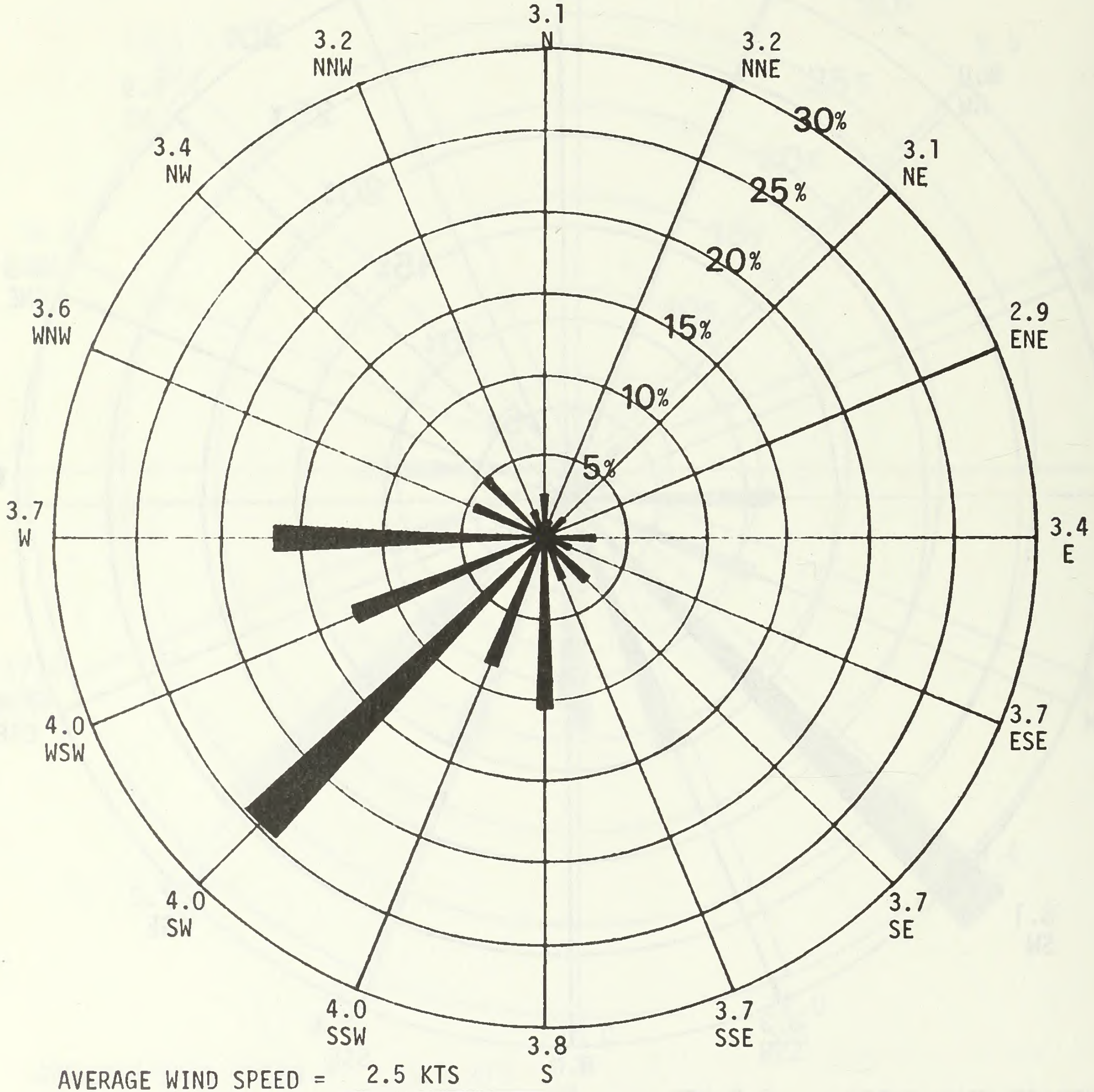

AVERAGE WIND SPEED = 2.5 KTS

PERCENT OCCURRENCE OF CALM WINDS = 34.7%

AVERAGE WIND SPEED BY SECTOR SHOWN AT END OF RADIAL (KTS)

DIRECTIONAL SECTOR INDICATES DIRECTION FROM WHICH WIND FLOWS

9.6 SEVERE STORMS

Thunderstorms

The mean annual number of thunderstorm days at China Lake is 2.8 days. The maximum mean monthly number of thunderstorm days occurs during July and August. (See Table 18).

FIGURE 12f
ANNUAL WIND ROSE
STABILITY CLASS F

WIND ROSE FOR China Lake

PERIOD 1/54 - 12/63

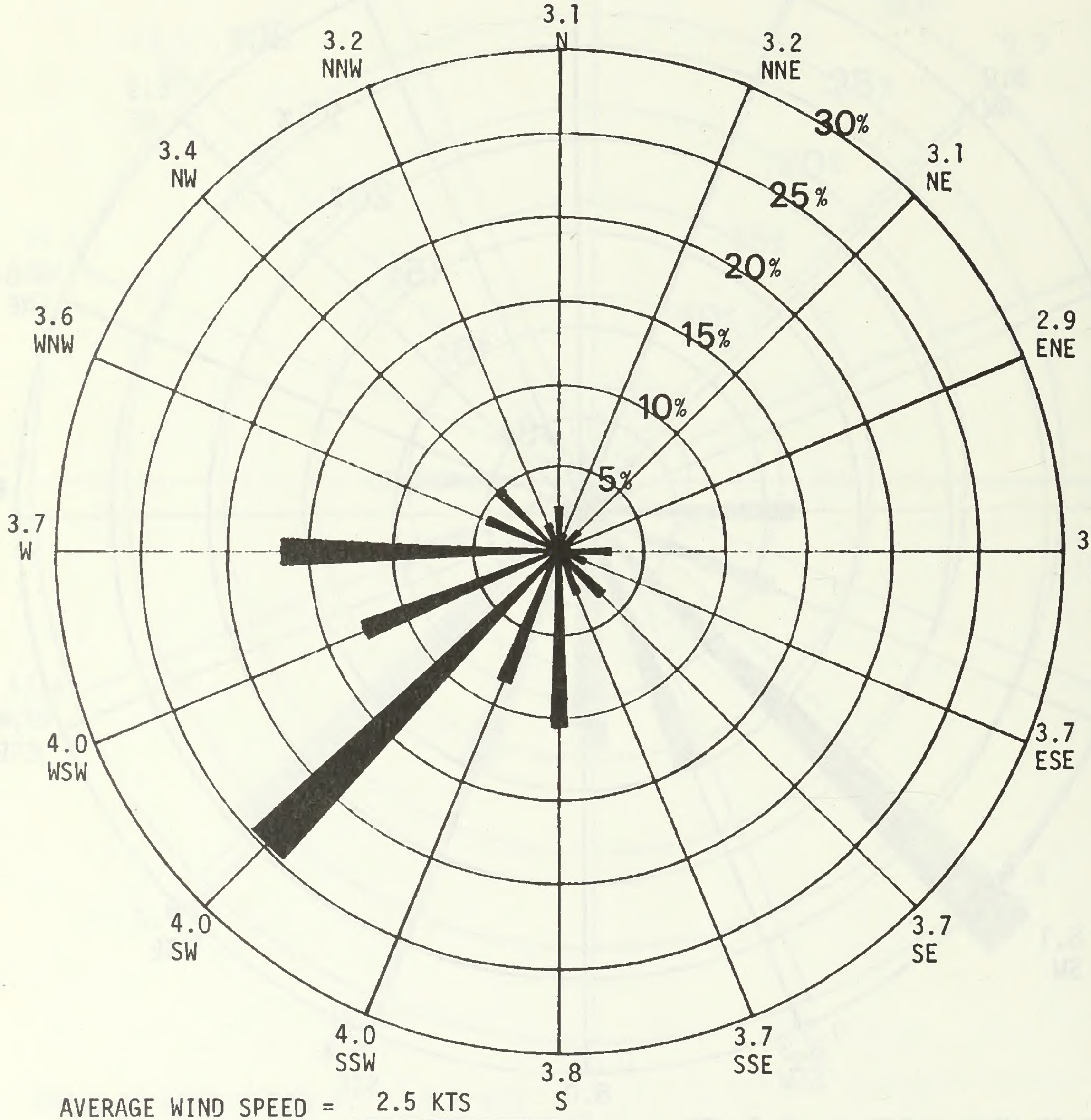

AVERAGE WIND SPEED = 2.5 KTS

PERCENT OCCURRENCE OF CALM WINDS = 34.7%

AVERAGE WIND SPEED BY SECTOR SHOWN AT END OF RADIAL (KTS)

DIRECTIONAL SECTOR INDICATES DIRECTION FROM WHICH WIND FLOWS

9.6 SEVERE STORMS

Thunderstorms

The mean annual number of thunderstorm days at China Lake is 2.8 days. The maximum mean monthly number of thunderstorm days occurs during July and August. (See Table 18).

9.7 CLIMATE IMPACTS

Any effects of geothermal development upon climate will be localized and should not affect regional patterns. The only potential impacts of any significance should be upon microclimatic variables, and can be expected to occur largely within the study area.

Local temperature patterns will change by several degrees due to waste heat emitted from the power plants, particularly from the cooling towers. There should be very little surface temperature effect because plume buoyancy will cause the heat to rise. The maximum impact should be in the atmospheric layer immediately above the cooling tower, with a radius of influence of up to several hundred feet depending upon local conditions. A related effect of waste heat could be the localized disturbance of low-lying inversions, which are most prevalant at night during the winter. The vertical mixing induced by plume buoyancy should cause more thorough dispersion of pollutants than would occur during undisturbed inversion conditions.

Water vapor is the primary gaseous species emitted from geothermal power plants; thus, ambient relative humidity will be increased, primarily within a radius of several miles of the power plant. This increase should normally be from less than one percent to ten percent. Considering the typical low humidity in the Coso area, this increase should not usually result in condensation (fog formation). However, under cold overcast conditions the excess humidity could add to the existing cloud or fog layer.

TABLE 18

MEAN NUMBER OF THUNDERSTORM DAYS - CHINA LAKE

January	0.0 days	July	0.7 days
February	0.0 days	August	0.7 days
March	0.1 days	September	0.4 days
April	0.1 days	October	0.2 days
May	0.3 days	November	0.1 days
June	0.2 days	December	0.0 days

Annual 2.8 days

GPO 694-690/151

Form 1279–3
(June 1984)

BORROWER'S

TD 195 .E4 C67 1980

Air quality technica
on the Coso geother

DATE LOANED	BORROWER
10/15/87	McClonahan

USDI – BLM